Modelling and Analysis of UAV-Assisted Cellular Networks

A THESIS

SUBMITTED IN PARTIAL FULFILLMENT OF THE REQUIREMENTS FOR THE DEGREE OF

Doctor of Philosophy

BY

Neetu R R

PhD19108

under the guidance of

Dr. Gourab Ghatak, Prof. Vivek Ashok Bohara and Prof. Anand Srivastava

Department of Electronics and Communication Engineering,

Indraprastha Institute of Information Technology-Delhi

New Delhi, India - 110020

December, 2025

Modelling and Analysis of UAV-Assisted Cellular Networks

A THESIS

SUBMITTED IN PARTIAL FULFILLMENT OF THE REQUIREMENTS FOR THE DEGREE OF

Doctor of Philosophy

BY

Neetu R R

PhD19108

under the guidance of

Dr. Gourab Ghatak, Prof. Vivek Ashok Bohara and Prof. Anand Srivastava

Department of Electronics and Communication Engineering,

Indraprastha Institute of Information Technology-Delhi

New Delhi, India - 110020

December, 2025

To my family...

Indraprastha Institute of Information Technology-Delhi
Okhla Industrial Estate, Phase III
New Delhi-110020, India
December-2025

Certificate

This is to certify that the thesis titled **Modelling and Analysis of UAV-Assisted Cellular Networks** being submitted by **Neetu R R** to the Indraprastha Institute of Information Technology-Delhi, for the award of the degree of **Doctor of Philosophy**, is an original research work carried out by her under our supervision. In our opinion, the thesis has reached the standards fulfilling the requirements of the regulations relating to the degree. The results contained in this thesis have not been submitted in part or full to any other university or institute for the award of any degree/diploma.

Dr. Gourab Ghatak
Assistant Professor
Dept. of Electrical
Electronics Engineering
IIT Delhi, 110016

Prof. Vivek Ashok Bohara
Professor
Dept. of Electronics &
Communication
IIIT Delhi, 110020

Prof. Anand Srivastava
Professor
Dept. of Electronics &
Communication
IIIT Delhi, 110020

Place: New Delhi
Date: December 2025

Indraprastha Institute of Information Technology-Delhi
Okhla Industrial Estate, Phase III
New Delhi-110020, India
December-2025

Declaration

This is to be certified that the dissertation entitled **Modelling and Analysis of UAV-Assisted Cellular Networks** being submitted by **Neetu R R** to the **Indraprastha Institute of Information Technology-Delhi**, for the award of degree of **Doctor of Philosophy**, is a bonafide work carried out by me. This research work has been carried out under the supervision of **Dr. Gourab Ghatak, Prof. Vivek Ashok Bohara and Prof. Anand Srivastava**.

The study pertains to this dissertation has not been submitted in part or in full, to any other University or Institution for the award of any other degree.

Neetu R R
PhD19108
Ph.D. student
IIIT-Delhi, India

Acknowledgement

I would like to express my sincere gratitude to my supervisors **Dr. Gourab Ghatak, Prof. Vivek Ashok Bohara**, and **Prof. Anand Srivastava** for giving me the opportunity to work on this thesis and for guiding my Ph.D. journey with continuous support, active monitoring, and timely feedback. They provided an ideal platform to showcase my abilities, offering unwavering encouragement at every stage. I feel extremely lucky to have such inspiring and supportive supervisors for my PhD research.

I am grateful to **Prof. Emil Bjõrnson** and **Prof. Cicek Cavdar** for offering me an internship at KTH Royal Institute of Technology, Sweden, which was an enriching experience. Their immense knowledge and thought-provoking approach are commendable. I thank my monitoring committee members, **Dr. Sanjit Kaul** and **Dr. Shamik Sarkar**, for their insightful feedback, cooperation and commitment to research throughout my Ph.D. I am also grateful to **IIIT-Delhi** for excellent infrastructure, research environment, and coursework. My thanks extend to colleagues from **Wirocomm Research Group** and **CoE Li-Fi** lab at IIIT-D, **Akshita Gupta, Saumya Chaturvedi, Priyanka Singh, Rahul, Saswati Paramita, Rana Kumar Jana, Dr. Mansi Peer, Dr. Anand Singh**, and **Hanshita Prabhakar** for our discussions, shepherding, and discussing necessary technicalities, which enhanced my deeper understanding of concepts. I also thank the technical and admin support staff of IIIT-D for being extremely helpful in the fast resolution of all technical and admin-related matters.

I am thankful to **my family** for their blessings and support throughout my life. My family's support, love, and cooperation provided me with enormous support throughout my journey.

Neetu R R

PhD19108

Abstract

Emerging as a transformative solution in next-generation wireless networks, unmanned-aerial vehicles (UAVs) provide unprecedented flexibility, rapid deployment, and enhanced connectivity. Their integration into conventional cellular networks presents numerous opportunities, such as dynamic coverage expansion, disaster relief and emergency response, and military and surveillance applications. However, it also brings challenges, including energy constraints, fronthaul and backhaul limitations, and mobility and handover management. This thesis explores three critical aspects of UAV-enabled networks: spectrum management in integrated access and backhaul (IAB) networks, mobility management for seamless handovers, and joint UAV activation control and power optimization in UAV-enabled cell-free massive multiple input multiple output (mMIMO) networks under fronthaul capacity limitations.

In the first part, we investigate spectrum management in UAV-enabled IAB networks, where the UAVs act as access points and relay data to the core network. We address the challenge of optimally allocating limited spectrum resources between access and backhaul links to maximize network efficiency. Our analysis includes disaster recovery scenarios, where optimal UAV positioning and resource partitioning are derived to sustain user connectivity and maximize throughput. Additionally, in urban environments, we introduce cache-enabled UAVs that reduce reliance on backhaul links, improving content delivery performance. Key metrics such as signal to interference noise ratio (SINR) coverage probability and successful content delivery probability are evaluated.

The second focus is on mobility management in UAV-enabled networks with mobile users. Frequent handovers (HOs) due to user mobility present significant challenges to network performance. To address this, we propose a caching-based handover management scheme that reduces handover occurrences by utilizing device caching, thereby enhancing quality of service (QoS). Using spatio-temporal analysis, we assess the scheme's effectiveness in minimizing handover frequency and ensuring seamless connectivity. Additionally, we examine network reliability by analyzing the conditional success probability (CSP) experienced by users in the presence of blockages. Furthermore, we derive the meta distribution (MD) of

SINR and mean local delay (MLD), offering deeper insights into network reliability.

The third aspect focuses on the joint optimization of UAV activation and power consumption in UAV-based cell-free mMIMO networks. These networks promise uniform service quality over large areas but are constrained by the limited capacity of wireless fronthaul links connecting UAVs to the central processing unit (CPU). We incorporate functional split options, specifically Options 8 and 7.2, to balance fronthaul capacity, computational complexity, and latency. By formulating and solving a joint placement and power optimization problem, we ensure efficient resource utilization while maintaining fair SINR coverage across users.

This thesis provides a structured framework for integrating UAVs into cellular networks, addressing key challenges in spectrum management, mobility, and resource optimization, paving the way for more reliable and efficient UAV-based wireless communication systems.

Contents

List of Figures

List of Abbreviations

3GPP 3rd Generation Partnership Project

BPP binomial point process

CCDF complementary cumulative distribution function

CPU central processing unit

CSI channel state information

CSP conditional success probability

CU centralized unit

DU distributed unit

HAP high altitude platform

HetNet heterogeneous network

HO handover

IAB integrated access and backhaul

LoS line-of-sight

MD meta distribution

MBS macro base station

MLD mean local delay

mmWave millimeter wave

mMIMO massive multiple input multiple output

MPPP marked-poisson point process

NLoS non-line-of-sight

PDF probability density function

PGFL probability generating functional

PPP poisson point process

QoS quality of service

RF radio frequency

RRH remote radio head

RSRP reference signal received power

RSS received signal strength

RSSI received signal strength indicator

SINR signal to interference noise ratio

TBS terrestrial base station

UAV unmanned-aerial vehicle

UAV-AP UAV-access point

UAV-BS UAV-base station

UE user equipment

URLLC ultra-reliable low-latency communications

ZF zero-forcing

Chapter 1

Introduction

In this chapter, we discuss the background, motivation, and objectives of this thesis.

1.1 Background and Motivation

Unmanned aerial vehicles (UAVs) have become an essential component of next-generation wireless communication systems due to their flexibility, mobility, and ability to provide on-demand coverage. Effective spectrum management in UAV networks is critical, especially when they serve as aerial base stations in IAB systems [1]–[3]. IAB leverages UAVs to simultaneously handle access links for user equipments (UEs) and backhaul links to the core network as given in Figure 1.1. In this architecture, access refers to the wireless connection between the users and the UAV-APs or TBSs, while backhaul refers to the connection between the UAVs and the core network, which may be established through either wired (via terrestrial base stations (TBSs)) or wireless links (via high altitude platforms (HAPs)). This dual functionality demands careful spectrum allocation to balance the needs of access and backhaul while minimizing interference. Advanced techniques such as frequency reuse, dynamic resource partitioning, and beamforming are employed to ensure optimal spectrum utilization in these scenarios.

n Release 15, 3rd Generation Partnership Project (3GPP), defined a new, flexible architecture for the fifth-generation (5G) random access network (RAN), where the base station or gNodeB (gNB) is split into three logical nodes: the centralized unit (CU), distributed unit (DU) and the radio unit (RU), each capable of hosting different functions of the 5G NR stack. 3GPP specifies eight functional split options for distributing the functionality of the 5G new-radio (NR) RAN protocol stack across different network elements, primarily to balance the trade-offs between fronthaul bandwidth, processing complexity, and latency as given in Figure 1.2. These options range from high-layer splits (Options 1–4), which separate

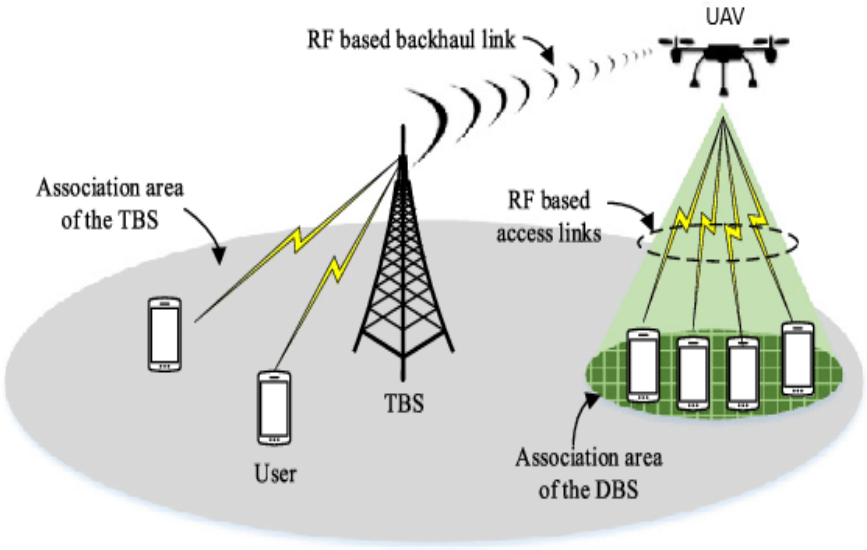

Figure 1.1. UAV-based HetNet [4].

functions at the packet data convergence protocol (PDCP) or radio link control (RLC) layers and are more tolerant to latency, to low-layer splits (Options 6–8), where more of the physical layer processing is centralized and fronthaul demands increase significantly. Among these, Option 8 represents a fully centralized approach where the UAV-APs act as remote radio heads (RRHs) and all baseband processing is handled by a central unit. This simplifies the UAV hardware but requires high-capacity and low-latency fronthaul links to transport raw I/Q samples. Option 7.2 offers a more balanced architecture by allowing partial PHY-layer processing (e.g., FFT/IFFT and precoding) at the UAV, while upper layers remain centralized. This reduces fronthaul bandwidth requirements and offers better latency performance, making it more suitable for wireless fronthaul in UAV-assisted networks.

UAV-IAB nodes following Option 7.2 functional split play a crucial role in this ecosystem [5]. Option 7.2 specifies that the radio functions, including the medium access control (MAC), RLC, and PDCP, are performed at the UAV base stations, while the higher layers, such as the radio resource control (RRC) and core network functions, are handled at the ground network. This split is important because it allows for efficient resource allocation and management directly at the UAVs, optimizing both access and backhaul links without the need for excessive signaling between the UAVs and the core network. Caching plays a pivotal role in improving spectrum efficiency in UAV-based IAB systems. By stor-

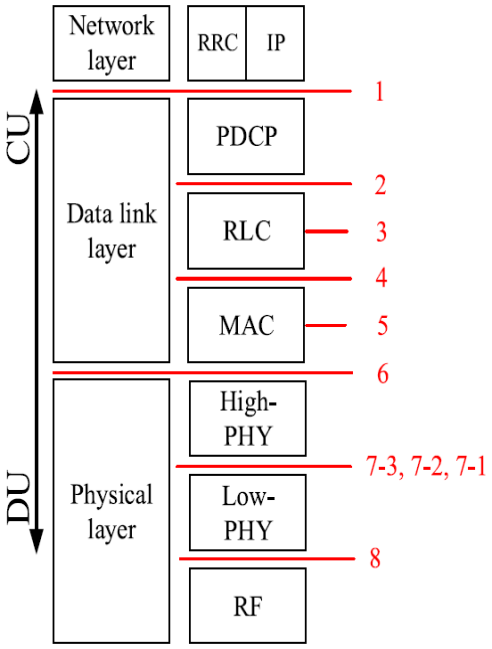

Figure 1.2. The LTE protocol stack with layers and sublayers, including the numbered functional split options proposed by 3GPP.

ing frequently accessed content locally at UAVs, backhaul traffic can be reduced, allowing more spectrum resources to be dedicated to access links. This approach is particularly effective when combined with dynamic spectrum allocation, which adjusts resource distribution based on real-time network demands. When cached content satisfies user requests, backhaul spectrum requirements are minimal, but when non-cached content is needed, the allocation shifts to prioritize backhaul links. This dynamic caching-integrated spectrum management significantly enhances overall network performance and ensures efficient utilization of limited bandwidth.

Handover management is a critical challenge in UAV networks due to the high mobility of both UAVs and users, often leading to frequent handovers and potential connection disruptions, as shown in Figure 1.3.

Effective handover strategies must balance reducing unnecessary HOs, minimizing delays, and ensuring seamless transitions between UAVs. Caching at user terminals can significantly aid this process by preloading popular content, thereby reducing reliance on real-time data during handovers. This approach helps mitigate service interruptions, especially in high-

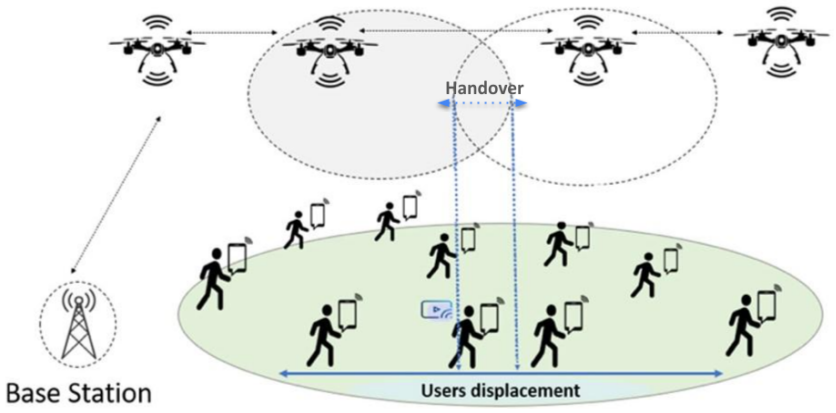

Figure 1.3. Handover mechanism in a UAV-based network [6].

demand scenarios where users frequently move between UAV coverage areas. Referring to what we discussed before, UAVs serving as access points follow the Option 8 functional split, where all baseband processing is centralized at the core network, and UAVs function primarily as RRHs as given in Figure 1.2. This functional split is crucial for HO management because it allows centralized coordination of handover decisions, reducing the computational burden on UAVs and ensuring efficient mobility management. By handling HO decisions centrally, Option 8 minimizes latency and ensures a more consistent QoS, especially in dense UAV deployments. Skipping unnecessary HOs is another key technique to enhance network stability. Predictive algorithms can analyze user mobility patterns and signal strength trends to determine whether a handover is required, reducing redundant transitions. Additionally, dynamic cell adjustments allow UAVs to modify their coverage areas, minimizing the need for frequent HOs. To improve QoS, multi-link handovers enable UEs to connect to multiple UAVs during transitions, ensuring uninterrupted communication. These strategies, combined with caching mechanisms, address the challenges posed by blockages, which can disrupt LoS communication. Pre-cached data at UEs or UAVs acts as a buffer, ensuring service continuity during temporary obstructions.

Joint optimization of power and placement in UAV-based cell-free mMIMO networks, as given in Figure 1.4, is critical for overcoming challenges such as limited fronthaul capacity and dynamic environments. Power optimization focuses on adjusting transmit power levels to

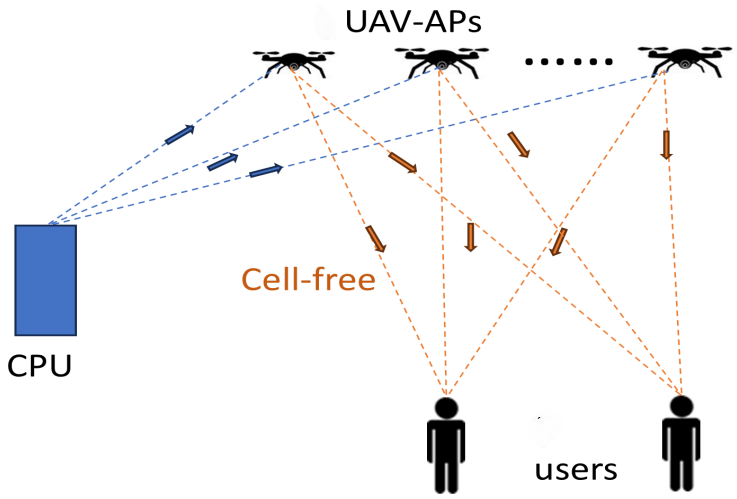

Figure 1.4. Cell-free mMIMO UAV-based network.

ensure energy-efficient operation while minimizing interference among UAVs. By balancing power levels across UAVs, networks can distribute load effectively, thereby enhancing capacity and coverage. Placement optimization complements this by strategically positioning UAVs to maximize LoS links with UEs, improving spectral efficiency and ensuring uniform coverage. Together, these optimization techniques provide a foundation for robust and efficient UAV-based mMIMO networks. Addressing fronthaul capacity limitations requires innovative solutions like functional splits, which distribute processing tasks between UAVs and central units. In UAV-based networks, two key functional split options, Option 8 and Option 7.2, offer different trade-offs in processing distribution and fronthaul requirements. Option 8, where all baseband processing is centralized at the core network, treats UAVs as RRHs. This approach simplifies UAV hardware and reduces energy consumption at the UAV level but increases fronthaul bandwidth demands, as radio signals must be transmitted to the CPU. In contrast, Option 7.2 allows UAVs to handle lower-layer processing, including functions like fast fourier transform (FFT) and precoding, while higher-layer operations remain centralized. This split reduces the fronthaul burden by transmitting pre-processed data instead of raw signals, making it more suitable for UAV deployments where fronthaul capacity is constrained. The choice between these functional splits significantly impacts network performance. Option 8 ensures centralized control and simplified UAV hardware, making it preferable when fronthaul capacity is abundant. Meanwhile, Option 7.2 provides

a more fronthaul-efficient approach, enabling better scalability in UAV-based networks with constrained backhaul links. These approaches enable UAV-based networks to adapt dynamically to user distributions and channel conditions, ensuring reliable connectivity and enhanced network performance.

1.1.1 Key Notations of Stochastic Geometry [7]

- **Point processes:** A point process is a measurable mapping Φ from a probability space to the space of locally finite counting measures on a measurable space ε. The process Φ can be denoted by the sum of Dirac measures of ε:

$$\Phi = \sum_i \delta_{X_i},$$

  where where δ_{X_i} denotes the Dirac measure centered at $X_i \in \varepsilon$ and $\{X_i\}$ are the points of Φ. In this thesis, the space ε is the Euclidean space $\mathbb{R}^d$ of dimension $d = \{1, 2, 3\}$.

- **Intensity measure:** The intensity measure Λ of Φ is defined as $\Lambda(B) = \mathbb{E}[\Phi(B)]$ for Borel B, where $\Phi(B)$ denotes the random variable representing the number of points of Φ falling within the set B. Thus, the intensity measure represents the average number of points expected to occur in a given Borel set B.

- **Poisson Point Process (PPP):** Let Λ be a locally finite measure on $\mathbb{R}^d$. A point process Φ is Poisson on $\mathbb{R}^d$ if the following conditions hold true:

  1. For all disjoint subsets, $A_1, \ldots A_n$ of ε, the random variables $\Phi(A_i)$ are independent.
  2. For all sets A of ε, the random variables $\Phi(A)$ are distributed according to a Poisson random variable with parameter Λ.

  An important property of the PPP used in this thesis is spatial independence: conditioning on the event $\Phi(A) = n$, the n points within the set A are independently and uniformly distributed over A.

- **Binomial Point Process (BPP):** Let $\Phi = \{x_1, \ldots, x_n\} \subset A$ be a point process with a fixed and finite number of points, denoted by n on the compact set A. Φ is a uniform binomial point process (BPP) if and only if Φ, viewed as a random vector, is uniformly distributed in A^n. In other words, the n points are independently and identically distributed (i.i.d.) according to the uniform distribution on A.

- **Marked Poisson Point Process (MPPP):** Let $\hat{\Phi} = (x_i, m_i)$ be a MPPP on $\mathbb{R}^d \times \mathbb{M}$, where each point $x_i \in \mathbb{R}^d$ is associated with a mark $m_i \in \mathbb{M}$. The process $\hat{\Phi}$ is defined on the product space $\mathbb{R}^d \times \mathbb{M}$, and the underlying point process $\Phi = x_i$ on $\mathbb{R}^d$ is referred to as the ground process. Then the following statements are equivalent:

  1. Φ is a poisson process on $\mathbb{R}^d$ with intensity measure Λ, and, given Φ, the marks m_x are independent with distribution M_x on $\mathbb{M}$.
  2. $\hat{\Phi}$ is a poisson process on $\mathbb{R}^d \times \mathbb{M}$ with intensity measure $\hat{\Lambda}$ for $A \subset \mathbb{R}^d \times \mathbb{M}$ given as,

$$\hat{\Lambda} = \iint_{(x,m)\in A} \Lambda(dx) M_x(dm).$$

- **Probability generating functional:** The probability generating functional (PGFL) of a point process Φ evaluated for a function ν is defined mathematically as the Laplace functional of $-\log \nu$, and is calculated as:

$$G_\Phi(\nu) = \mathbb{E}\Big[\prod_{x_i \in \Phi} \nu(x_i)\Big]$$

- **Palm probability:** The Palm probability refers to the probability of an event conditioned on a point of the process being located at a given position. Accordingly, the Palm distribution represents how the point process would look when viewed from one of its points.

- **Slivnyak's theorem:** Slivnyak's theorem for a PPP states that conditioning on the event that a point of Φ is located at the origin ($o \in \Phi$), equivalent to add a point at o

to the PPP Φ. Mathematically,

$$\mathbb{P}(\Phi \in Y|o) = \mathbb{P}(\Phi \cup \{o\} \in Y),$$

where Y is any point process property.

With these definitions explained, next we discuss a generalized network model in our thesis and how to characterize the downlink SINR of the network.

1.1.2 Generalized Network Model and SINR analysis:

We investigate a downlink UAV-based network designed for scenarios where conventional wireless access is limited or disrupted, such as during large-scale public events in under prepared areas or in disaster-stricken regions. UAVs are deployed as aerial base stations to restore connectivity for ground users. The UAV operations are subject to airspace regulations, and their altitude range follows the 3GPP specifications outlined in [8], [9], which support network-based 3D positioning for UAVs operating at altitudes up to $300\,\mathrm{m}$. Although current airspace regulations in most countries typically allow UAV operations up to 400 ft (122 meters) in uncontrolled airspace without waivers [10]–[12], there are specific contexts in which higher-altitude UAVs are operationally permitted. Moreover, these limitations can be lifted during the use of high-altitude UAVs as temporary aerial base stations, for emergency communications, public safety, especially for network overload and disaster recovery [13], [14]. Our network model aligns with 3GPP standards and is designed to model UAV deployments under diverse real-world scenarios. The locations of UAVs are modeled as a uniform distribution in the two-dimensional Euclidean space, $\mathbb{R}^2$. To characterize the spatial distribution of both UAVs and users, we employ stochastic geometry tools, enabling a systematic analysis of network performance. This approach facilitates efficient network deployment and resource allocation, ensuring reliable connectivity in critical situations where traditional infrastructure is unavailable or compromised.

In large-scale cellular networks, the received signal power at a typical user is inherently a random variable due to the uncertainty in the spatial distribution of both the serving BSs and the users, as well as the effects of wireless channel fading [15]. Furthermore, because

of simultaneous co-channel transmissions across the network, the interference power is influenced by multiple stochastic factors, such as the spatial distribution of interfering BSs, random shadowing, and small-scale fading. The received SINR experienced by the user placed at the origin is given as

$$\text{SINR} = \frac{P_t h_t d(||x_t||)}{N + \sum\limits_{i \in I} P_i h_i d(||x_i||)} \tag{1.1}$$

Here, subscript t represents the transmitter and I is the set of all interfering transmitters. P_t is the transmit power of transmitter, h_t is the small scale fading and d is the path-loss at a distance of $||x_t||$ from the origin. P_i, h_i and x_i are the corresponding transmit power, fading parameter and the locations of interfering transmitters. In general, I, h_t, h_i, x_t and x_i are random quantities. Thus, characterizing the average SINR is difficult to address. Therefore, using stochastic geometry, we derive SINR coverage probability $\mathcal{P}_{\text{suc}}(\gamma)$, which is the probability that an average user in the network receives an SINR above a certain threshold γ. In other words, it represents the fraction of the users under coverage in the network with respect to an SINR threshold γ.

$$\mathcal{P}_{\text{suc}}(\gamma) = \mathbb{P}\left(\frac{P_t h_t d(||x_t||)}{N + \sum\limits_{i \in I} P_i h_i d(||x_i||)} \geq \gamma \right) \tag{1.2}$$

Considering the locations of the set of interfering BSs are modeled as points of a PPP, the distribution of fading parameter, and the distribution of the distances of the user to associated and interfering transmitters, we solve the complementary cumulative distribution function (CCDF) of SINR, defined as SINR coverage probability or success probability $\mathcal{P}_{\text{suc}}(\gamma)$.

1.2 Goal and Objectives

This thesis addresses three distinct open challenges in conventional cellular networks and explores how UAV-based networks can serve as potential solutions. By leveraging the adaptability and caching capabilities, the proposed framework aims to enhance network perfor-

mance. Specifically, the study focuses on analyzing and characterizing the QoS experienced by users, optimizing resource allocation, minimizing handover delays, and evaluating power consumption in UAV-based networks. The main objectives of this thesis are as follows:

- We analyze joint resource allocation and coverage in an IAB UAV-based network. By utilizing content caching at the UAV-APs, we optimize resource allocation between access and backhaul links, evaluate the success probability, and establish dimensioning guidelines for the deployment of UAV-APs. In this setup, UAV-IAB nodes follow Option 7.2, ensuring efficient resource distribution between access and backhaul links and enhancing overall network performance.

- We analyze HOs in UAV-based networks, focusing on the impact of blockages and UAV density on user performance. By utilizing caching at mobile terminals, we propose a novel cache-based handover management strategy that dynamically selects the cell. In this setup, UAV-APs follow Option 8, enabling centralized handover decision-making and seamless mobility management, particularly in dense UAV deployments with frequent handovers. This approach reduces search time and delays the received signal strength (RSS)-based BS association.

- We investigate fronthaul capacity limitations in UAV-based wireless networks that provide cell-free access to users. By utilizing functional splits at the fronthaul, our approach focuses on maximizing the minimum SINR of users and minimizing power consumption at the UAV-APs. This is achieved by optimizing the transmit power of the UAV-APs and selectively activating them. We compare Option 8 and Option 7.2 functional splits to assess their impact on fronthaul efficiency, power consumption, and overall network performance.

1.3 Organization

The rest of the thesis is organized as follows:

Chapter 2 provides a comprehensive review of the state-of-the-art in UAV-assisted cellular networks, focusing on spectrum management, handover and mobility management, and

total power minimization. In Chapter 3, we investigate spectrum management and UAV placement in UAV-assisted IAB networks. We optimize resource allocation between access and backhaul links by caching frequently accessed content at UAVs to enhance the QoS for ground users. The success probability is maximized by jointly considering end-to-end SINR coverage across access, xhaul links, and cache hit event. In Chapter 4, we explore mobility management in UAV-based networks with mobile users in the presence of blockages. We utilize device caching to reduce frequent handovers by delaying the highest reference signal received power (RSRP) search time in a network where UAVs are modeled as an MPPP. The impact of blockages on UAV deployment density, UAV altitude, and UAV association is analyzed. In Chapter 5, we present a UAV-based cell-free mMIMO framework where distributed UAV-APs serve ground UEs while addressing wireless fronthaul capacity constraints. We evaluate functional split Options 7.2 and 8 for fronthaul links, aiming to maximize the minimum SINR among UEs and minimize power consumption by optimizing UAV-AP transmit powers and selectively activating UAV-APs. Chapter 6 discusses the conclusions derived from this thesis and the future directions.

Chapter 2

Literature Survey

In this section, we discuss the existing state-of-the-art in three broad areas:

- Spectrum Management in UAV Networks
- Handover Management in UAV Networks
- Joint UAV Activation and Power Optimization in UAV Networks

2.1 Spectrum Management in UAV Networks

Several studies have explored spectrum management in UAV networks, employing various tools such as optimization and stochastic geometry to analyze network performance [16]-[20]. In [21], the authors address deployment cost minimization in IAB networks with TBSs and tethered UAVs, considering multi-hop aerial-terrestrial networks under blockages. They aim to determine the optimal number of base stations, UAV positions, and routing paths. To achieve this, they propose the twin delayed deep deterministic policy gradient (TD3) framework, referred to as TD3-MB, a novel offline algorithm. TD3-MB integrates the max-Bellman optimality function into the TD3 reinforcement learning framework. This approach efficiently optimizes deployment and backhauling while minimizing costs. The work [22] proposes a deep reinforcement learning (DRL)-aided system to optimize UAV placement in 5G networks, aiming to maximize uplink and downlink data rates. It introduces a real-time, dynamic placement approach that adapts to user demands and network conditions. The framework addresses the trade-off between fronthaul and backhaul links for robust communication. UAVs act as dynamic DU nodes to improve coverage in critical areas. A decentralized DRL framework enhances scalability and responsiveness for large-scale networks with many users. The authors in [23] propose to maximize the sum rate for ground users (GUs) in a UAV-enabled wideband (WB) network by jointly optimizing UAV placement, power control,

and spectrum allocation. They consider an macro base station (MBS) communicating with a UAV via WB links, while the UAV serves GUs via wireless access (WA) links. To address the non-convex optimization problem, the authors propose an iterative algorithm using block coordinate descent and successive convex approximation. The algorithm alternates between solving spectrum allocation and the joint optimization of power control and UAV placement, ensuring efficient resource utilization and improved network performance.

However, the existing works do not consider caching to analyze the spectrum management in IAB UAV networks. The authors in [24] explored content distribution in hotspot areas by combining UAVs with edge caching to offload traffic. They evaluated the quality of experience (QoE) using the mean opinion score (MOS), considering user association, UAV placement, and caching placement. A joint optimization problem was then formulated to maximize the MOS. In [25], the authors addressed minimizing content delivery delay in UAV-enabled non-orthogonal multiple-access networks. They proposed a reinforcement learning algorithm to analyze the impact of cache capacity, the number of cached contents, and the number of users on content delivery delay. While existing literature focuses on efficient algorithms to optimize network parameters for specific network realizations, we employ stochastic geometry-based analysis to provide an expected view by spatially averaging across multiple realizations. In [26], the authors analyze the deployment of UAVs as aerial base stations (ABSs) in a hybrid heterogeneous network (HetNet) alongside TBSs using mmWave bands. They propose a non-orthogonal multiple access (NOMA)-based user association policy and employ stochastic geometry to derive analytical expressions for association probability, coverage probability, and spectrum efficiency. The study explores the trade-off between association probability and spectrum efficiency. The authors in [27] investigates cache-enabled UAV emergency communication networks in post-disaster scenarios using stochastic geometry. UAVs are distributed using a BPP at a fixed altitude. A probabilistic caching strategy is proposed to alleviate backhaul congestion, and analytical expressions for offloading probability and average rate are derived, considering LOS/NLOS path loss and Nakagami-m fading.

None of the above literature studies UAV-based IAB networks in a 3-D scenario to study the resource allocation between access and backhaul using stochastic geometry. Motivated by this, as discussed in Chapter 3, we model the location of UAVs using a 3-D spatial

stochastic process, which is challenging due to the need for distance distributions constrained to a three-dimensional (3-D) half-plane. Additionally, we propose a caching scheme where popular content is stored locally at UAVs while less popular files are probabilistically cached. We also analyze how caching affects access and backhaul resource allocation.

2.2 Handover Management in UAV Networks

Handover management in UAV networks ensures uninterrupted service continuity as UAVs transition across different network cells. Efficient handover schemes aim to minimize interruptions, optimize signal strength, and tackle challenges such as dynamic topology changes and varying wireless conditions [28]- [31].

In [32], the authors analyze a 3-D mobile communication network with UAVs serving ground UEs in the downlink, deriving handover probabilities for distance-based and RSS-based associations using stochastic geometry. The study evaluates handover and coverage probabilities in a multitier UAV network, considering mobility parameters like altitude, speed, and density. It compares mobility models like the 3GPP-based framework to set a performance benchmark. This work lays the foundation for future research on UAV network mobility and performance evaluation. The authors in [33] introduce an equivalent model for analyzing HO, handover failure (HOF), and ping-pong (PP) in k-tier UAV networks, using unified mapping rules to relate altitude and transmit power to UE-UAV horizontal distance. It models user path length as a random variable with a closed-form probability density function (PDF) and analyzes the relationship between cell residence time and time-to-trigger (TTT). The study derives HOF and PP trigger radii through equivalent geometric relations. Key design insights include optimal altitude and transmit power ratios for frequent HOs and tradeoffs between HOF and PP based on deployment and HO parameters. The authors in [15] propose a time-varying boundary model to analyze HO, HOF, and PP in UAV-assisted networks, distributed as a 2-D PPP, accounting for fast fading and dynamic trigger locations. They discuss a projection rule linking UAV altitude and transmit power to HO trigger boundaries, incorporating LoS and NLoS conditions and fast fading effects. Analytical expressions for HO, HOF, and PP events are derived based on the model and

timing relationships. They also analyze the joint distribution of UE-UAV distance and angle, comparing scenarios with and without fast fading.

In the existing literature, UAVs are typically modeled as a 2-D PPP with a fixed height, limiting their horizontal and vertical movement. In contrast, in our work discussed in Chapter 4, we model UAVs using a 2-D MPPP, enabling smooth vertical and horizontal movements for practical UAV deployment. Additionally, introducing caching in the network to reduce HOs and improve the performance is discussed in our work. In [34], the authors propose a cluster-centric and coded UAV-aided femtocaching (CCUF) framework to enhance content diversity and QoS in an integrated UAV and cluster-centric cellular network serving indoor and outdoor users. It introduces distinct caching strategies for indoor and outdoor areas, a two-phase clustering approach for femto access points (FAP) and UAV deployment, and a content placement strategy that categorizes content by popularity. The approach aims to optimize cache-hit ratios, SINR, and user access delay while improving cache diversity and reducing redundancy. The authors in [35] have studied the advantages of caching to address critical handover issues such as frequent handovers, handover failures, the load of target BSs, etc. They exploited the high-capacity mmWave connections of a dual-mode BS, allowing the UE to cache their requested content and avoid unnecessary HOs. They evaluated the expected rate of caching the data at the UE and studied the effect of the user's velocity on the caching rate and the average HO failure. They designed an optimization problem to reduce the load on the MBS by maximizing the possible HOs to small base station (SBS), thereby increasing the traffic offload from MBS. In Chapter 4, we propose a cache-enabled HO management algorithm that leverages caching capabilities at the UE to minimize unnecessary HOs, reduce HO delays, and improve QoS. This strategy dynamically adjusts cell search intervals and employs an HO skipping mechanism to enhance the user experience, particularly in dynamic and dense UAV urban networks with blockages.

2.3 Joint UAV Activation and Power Optimization in UAV Networks

In this section, we discuss activation and power optimization in UAV networks, focusing on strategically positioning UAVs and allocating transmit powers to improve coverage and capacity. A number of studies have so far investigated these aspects [36]-[39], aiming to maximize network performance while considering fronthaul constraints and energy efficiency.

In [40], the authors propose an efficient multi-UAV coverage scheme ensuring QoS guarantees while covering massive IoT devices and maximizing UAV data rates. It introduces the QoS demand-based power allocation (QDPA) algorithm to address diverse QoS requirements. The data rate maximization placement (DRMP) algorithm optimizes single UAV placement, and the joint power allocation and placement (JPAP) scheme extends this approach to multiple UAVs, serving all IDs with varying data rate demands. The authors in [41] address the sum capacity maximization problem in a 3-D placement scenario of flying base stations (FlyBSs) connected to the TBS either directly or through relaying FlyBSs. The problem involves optimizing user association, channel allocation, and transmission power, subject to practical constraints such as altitude and energy consumption. An iterative alternating optimization approach is proposed to handle nonconvexities, transforming user association and channel allocation into a linear programming problem. The work in [42] investigates UAV communication in cell-free mMIMO-enabled wireless power transfer (WPT) systems, focusing on downlink energy harvesting and uplink spectral efficiency (SE) while considering hardware impairments. Closed-form expressions for downlink harvested energy and uplink spectral efficiency are derived, showing superior performance for CF massive MIMO over cellular massive MIMO. The study identifies optimal UAV altitude and antenna configurations to enhance SE. Additionally, an angle search trajectory design scheme is proposed, outperforming access point (AP) search and line path schemes in CF massive MIMO. This scheme also effectively bypasses high-interference APs in both CF massive MIMO and SC systems but not in cellular massive MIMO.

The authors in [43] study uplink cell-free UAV network for maximizing the minimum

spectral efficiency for different fronthaul alternatives such as frequency division multiple access (FDMA) and spatial division multiple access (SDMA). They optimize the UAV deployment and UAV transmit power to maximize the minimum spectral efficiency. In [44], the authors present a holistic approach to resource orchestration for cell-free mMIMO and small-cell systems in the open-RAN (O-RAN) architecture, considering radio, optical fronthaul, and cloud processing resources. The authors incorporate intra-physical-layer functional splitting and adjust power consumption models accordingly. Based on performance targets, the study derives cloud processing requirements for a cell-free mMIMO orthogonal frequency division multiplexing (OFDM) system. The proposed framework addresses end-to-end network power consumption while meeting system performance requirements.

UAVs face power constraints due to limited battery capacity, making efficient resource allocation crucial. A lower-layer split, such as Option 8, is often preferred as it focuses on RF transmission, minimizing on-board processing. Higher-layer splits, like Option 7.2, better address fronthaul capacity limitations by offloading processing to the central unit. However, existing research lacks an analysis of fronthaul capacity constraints when jointly optimizing UAV selection and power allocation with functional split options. Motivated by this, in Chapter 5, we discuss a UAV-based cell-free mMIMO network in which two functional split options are considered in the wireless fronthaul between the CPU and UAV-APs, where UAVs function as base stations serving ground users while maintaining a reliable and efficient wireless fronthaul connection.

2.4 Contributions

The major contribution of this thesis can be summarized as follows:

- Optimal frequency resource allocation between access and backhaul in IAB UAV networks presents significant challenges due to the dynamic nature of UAV-BS locations, user locations, and user requirements. Modeling UAV locations as a 3-D spatial stochastic process offers a practical framework for analyzing such networks. However, studying spatial properties in a 3-D PPP is complex due to the anisotropic nature of the spatial process. To address this, we derive the distance distribution of the nearest

point on a 3-D half-plane from a tagged point on the same half-plane. We calculate the association probabilities for a typical user with a UAV-AP in the access link and for that tagged UAV-base station (UAV-BS) with a UAV-BS in the xHaul link. A key challenge in this analysis is the interdependence between xHaul link association probabilities and access link association events.

- We propose a caching scheme to optimize the distribution of frequency resources between access and xHaul, thereby maximizing the service success probability at the user end. By studying the effects of cache size, user density, and UAV density, we evaluate the success probability under various user associations with TBSs or UAV-BSs and caching configurations at the UAV-BSs. We optimize the service success probability by jointly considering the end-to-end SINR coverage of the access link, the xHaul link, and the cache hit event.

- Handover management in UAV-based networks involves dynamically coordinating UAV positions and resources to ensure seamless connectivity and minimize interruptions as the users move. This requires addressing challenges like frequent handovers due to dynamic user trajectories. To reduce the frequency of handovers, we propose a cache-enabled handover management scheme by leveraging device caching capabilities. Due to the mobility of users, a time-averaged analysis has to be performed, which leads to a spatio-temporal expectation to obtain the QoS experienced by the mobile users.

- The network topology plays a critical role in UAV-based analysis, where restricting UAV mobility to a fixed altitude is a significant limitation. We model UAV-BSs as a 2-D MPPP, representing their positions in 3-D space, with random distributions over $\mathbb{R}^2$ in the horizontal plane and along the vertical axis. Our analysis focuses on the impact of blockages on handovers experienced by mobile users in a cache-based handover scheme, as well as the network's reliability by evaluating the CSP, thereby obtaining the MD of SINR for a given reliability threshold.

- Wireless fronthaul capacity in UAV-based networks is constrained by bandwidth, dynamic channel conditions, and energy limitations, impacting data rates and latency. To

address these challenges, we implement functional split options, Option 8 and Option 7.2, at the fronthaul and analyze their trade-offs. Additionally, we investigate Sub-6 GHz and mmWave fronthaul links, comparing the power allocated by CPU to activate UAVs in these scenarios.

- Power consumption in UAVs is a critical challenge, driven by propulsion, communication, and processing demands, which limit flight time and efficiency. Additionally, UAV selection is a critical challenge, requiring optimization to balance coverage, connectivity, and energy efficiency in dynamic environments. To address this, we propose a joint UAV activation and power optimization algorithm, in order to minimize the total power consumption by optimizing UAV transmit power, fronthaul power allocation, and processing power for option 7.2, while ensuring fair SINR for all users in a cell-free mMIMO access network.

Chapter 3

Spectrum Management in UAV-Enabled Wireless Networks

In this chapter, we study spectrum management in a UAV-enabled network where UAV-APs function as IAB nodes. These UAV-APs simultaneously serve ground users and relay user data to the core network via a backhaul link. UAV-IAB nodes follow Option 7.2, ensuring efficient resource distribution between access and backhaul links to maximize network efficiency. Unlike prior work, we analyze UAV-based IAB networks in a 3-D scenario to study the resource allocation between access and backhaul using stochastic geometry. In Part I of this chapter, we examine the optimal placement and resource partitioning strategy between access and backhaul in a single-UAV network to maintain user connectivity in a disaster scenario. Specifically, we analyze a location-based optimal frequency partitioning scheme between access and backhaul links while considering a fixed number of ground users. Additionally, we optimize the UAV's position to maximize user coverage. In Part II, we extend our study to an urban scenario with TBSs, where UAV-APs are equipped with local storage capabilities. The cache-enabled UAV-APs can connect to the core network either via a backhaul-enabled UAV-BSs through an x-Haul link or via TBSs using wired optical fiber links. We derive the success probability of a typical user and optimize the distribution of frequency resources between the access and the xHaul links to maximize the successful content delivery to the users.

3.1 Network Model

We consider a downlink UAV-based network where the locations of UAVs and TBSs are modeled as points of PPP. The UAVs acting as IAB nodes provide access to the users on the ground, simultaneously connecting to the TBSs for a backhaul link. The UAV-IAB nodes

partition the total bandwidth B between the access and the xHaul links using a bandwidth allocation factor, β, which can take any value between 0 and 1, $\beta \in [0, 1]$. The allocated bandwidth to the access link is βB, and that to the xHaul link is $(1 - \beta)B$ [45]. Moreover, an orthogonal frequency allocation is considered to multiplex multiple users in the access link [46]. The TBSs transmissions always experience small-scale Rayleigh fading g_{M}, with a variance of 1. The UAV transmissions vary according to their visibility state. The UAVs can either be in LoS or NLoS state from the perspective of the ground user. Without loss of generality, utilizing the stationarity and isotropy properties of the PPP [7], we perform the analysis from the perspective of a typical user located at the origin of the 2-D Euclidean space.

3.2 Spectrum Management in Single UAV Network

Consider a disaster-affected area, modeled as a circle $A = \mathcal{B}(0, r_d)$ with the origin as the center and a radius r_{d} in the two-dimensional Euclidean plane. We assume that inside the circle, the users have lost cellular connectivity due to the breakdown of BSs. Thus, all terrestrial BSs are located in $\mathbb{R}^2 \backslash A$. In this scenario, we consider a downlink network consisting of a single UAV-IAB node, which is located in A, providing coverage to the users in the access link. Furthermore, the UAV is connected to the nearest BS for backhaul communication. The overall scenario is depicted in Figure 3.1. We analyze the performance of the downlink system with respect to a fixed number of users N_{u}, which are uniformly distributed in A and request critical information from the cellular network for emergency response. In particular, the location of the users is modeled as points of a BPP in A. The macro BSs are modelled as points of homogeneous PPP, Φ_{M} with intensity λ_{M}, in $\mathbb{R}^2 \backslash A$. The 2D position of the UAV is restricted inside A. The UAV is located at a position $\mathbf{r}_0$. Due to the rotation invariance of BPP, the x-axis is aligned along the direction of the UAV [47] such that $\mathbf{r}_0 = (u_0, 0)$, where $u_0 = ||\mathbf{r}_0|| \in [0, r_{\mathrm{d}}]$. The distance of the user i to the UAV at $\mathbf{r}_0$ is represented as w_{i}. The transmit powers of the TBSs and UAV are represented as P_{M} and P_{U}, respectively. The access and backhaul links are characterized by a small-scale Rayleigh fading h, the power of which follows an exponential distribution with unit mean. γ_{a} and

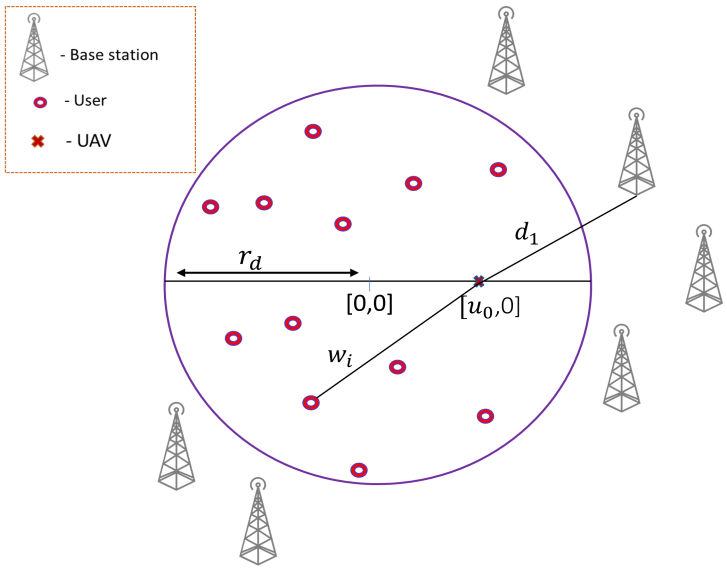

Figure 3.1. System model for a single UAV with IAB links

γ_{b} are the throughput thresholds defined for access and backhaul links, respectively. The metric of interest in our study is the overall success probability $\mathcal{P}_{\mathrm{suc}}$, defined as the product of the success probability of the access link and the backhaul link. The success probability represents the likelihood that a user is successfully served, i.e., the probability that the SINR experienced by the user exceeds a predefined threshold. Ergodically, it represents the fraction of successful transmissions from the BS to the user via the UAV.

3.2.1 Characterization of Success Probability

In the context of our study, a successful transmission to a user occurs only if both the access link and the backhaul link simultaneously meet their SINR requirements. For a transmission to be considered successful, the SINR on the access link (UAV to user link) must exceed a threshold γ_{a}, and the SINR on the backhaul link (UAV to core network link) must exceed a threshold γ_{b}. Therefore, the overall success probability $\mathcal{P}_{\mathrm{suc}}$ is defined as the joint probability that both of these conditions are satisfied.

Lemma 3.1. *The success probability of the access link is given as*

$$R_{\mathrm{a}}(\gamma_{\mathrm{a}}, u_0) = \int_0^{r_{\mathrm{d}}-u_0} R_{\mathrm{a1}}(\gamma_{\mathrm{a}}, w_{\mathrm{i}}) f_{1\mathrm{a}}(w_{\mathrm{i}}|u_0)\mathrm{d}(w_{\mathrm{i}}) + \int_{r_{\mathrm{d}}-u_0}^{r_{\mathrm{d}}+u_0} R_{\mathrm{a1}}(\gamma_{\mathrm{a}}, w_{\mathrm{i}}) f_{2\mathrm{a}}(w_{\mathrm{i}}|u_0)\mathrm{d}(w_{\mathrm{i}}), \quad (3.1)$$

where, $R_{\mathrm{a1}}(\gamma_{\mathrm{a}}, w_{\mathrm{i}}) = \exp\left[-\left\{\frac{N_0}{P_{\mathrm{U}} K w_{\mathrm{i}}^{-\alpha}}\left(2^{\frac{N_{\mathrm{u}}\gamma_{\mathrm{a}}}{B\beta}}-1\right)\right\}\right]$. *$K$ is the path-loss coefficient, i.e.,* $K = \left(\frac{\lambda_{\mathrm{c}}}{4\pi}\right)^2$, *where λ_{c} is the carrier wavelength and α is the path-loss exponent.*

The PDF of the distances of the users w_i from the UAV in the access link, which is given as

$$f_{\mathrm{a}}(w_{\mathrm{i}}|u_0) = \begin{cases} f_{1\mathrm{a}}(w_{\mathrm{i}}|u_0) & 0 \le w_{\mathrm{i}} \le r_{\mathrm{d}} - u_0 \\ f_{2\mathrm{a}}(w_{\mathrm{i}}|u_0) & r_{\mathrm{d}} - u_0 \le w_{\mathrm{i}} \le r_{\mathrm{d}} + u_0, \end{cases} \tag{3.2}$$

where,

$$f_{1\mathrm{a}}(w_{\mathrm{i}}|u_0) = 2w_{\mathrm{i}}/r_{\mathrm{d}}^2. \tag{3.3}$$

$$f_{2\mathrm{a}}(w_{\mathrm{i}}|u_0) = \frac{2w_{\mathrm{i}}}{\pi r_{\mathrm{d}}^2}\cos^{-1}\left(\frac{-r_{\mathrm{d}}^2 + w_{\mathrm{i}}^2 + u_0^2}{2u_0 w_{\mathrm{i}}}\right). \tag{3.4}$$

Proof. See Appendix A.1. □

Lemma 3.2. *The success probability for the backhaul link is given as*

$$R_{\mathrm{b}}(\gamma_{\mathrm{b}}, u_0) = \int_{r_{\mathrm{d}}-u_0}^{R_2} R_{\mathrm{b1}}(\gamma_{\mathrm{b}}, d_1) f_{\mathrm{b}}(d_1|u_0)\mathrm{d}(d_1), \tag{3.5}$$

where, $R_{\mathrm{b1}}(\gamma_{\mathrm{b}}, d_1) = \exp\left[-\left\{\frac{N_0}{P_{\mathrm{M}} K d_1^{-\alpha}}\left(2^{\frac{\gamma_{\mathrm{b}}}{B(1-\beta)}}-1\right)\right\}\right]$ *and R_2 is the upper limit for the area in which BSs are present.*

$f_{\mathrm{b}}(d_1|u_0)$ is distance distribution of the UAV to the nearest BS, which is given as

$$f_{\mathrm{b}}(d_1|u_0) = \begin{cases} f_{1\mathrm{b}}(d_1|u_0), & -r_{\mathrm{d}} < x_0 < r_{\mathrm{d}} \\ f_{2\mathrm{b}}(d_1|u_0), & x_0 \le -r_{\mathrm{d}}. \end{cases} \tag{3.6}$$

For $-r_{\mathrm{d}}<x_0<r_{\mathrm{d}}$,

$$f_{1\mathrm{b}}(d_1 \mid u_0) = \lambda_{\mathrm{M}} \exp\left(-\lambda_{\mathrm{M}}\left(d_1^2\left(\frac{\pi}{2}+y\sqrt{1-y^2}-\tan^{-1}\left(\frac{-y}{\sqrt{1-y^2}}\right)\right)\right.\right.$$
$$\left.\left.-r_{\mathrm{d}}^2\left(\frac{\pi}{2}-x\sqrt{1-x^2}-\tan^{-1}\left(\frac{x}{\sqrt{1-x^2}}\right)\right)\right)\right)$$
$$\times\left[\frac{-2d_1r_{\mathrm{d}}}{u_0}\sqrt{1-x^2}+2zd_1^2\sqrt{1-y^2}+2d_1\left(y\sqrt{1-y^2}+\frac{\pi}{2}-\tan^{-1}\left(\frac{-y}{\sqrt{1-y^2}}\right)\right)\right]. \quad (3.7)$$

where, $x=\frac{r_{\mathrm{d}}^2-d_1^2+u_0^2}{2u_0r_{\mathrm{d}}}$, $y=\frac{u_0^2-r_{\mathrm{d}}^2+d_1^2}{2u_0d_1}$, *and* $z=\frac{d_1^2+r_{\mathrm{d}}^2-u_0^2}{2u_0d_1^2}$.

For $x_0\le -r_{\mathrm{d}}$,

$$f_{2\mathrm{b}}(d_1|u_0)=2\pi d_1\lambda_{\mathrm{M}}\exp\left(-\lambda_{\mathrm{M}}\left(\pi d_1^2-\pi r_{\mathrm{d}}^2\right)\right). \quad (3.8)$$

Proof. See Appendix A.2. □

Therefore, the overall success probability of the whole system has a combined effect with the success probability of access and backhaul links and is calculated as follows

$$\mathcal{P}_{\mathrm{suc}}(\gamma_{\mathrm{a}},\gamma_{\mathrm{b}},u_0)\approx R_{\mathrm{a}}(\gamma_{\mathrm{a}},u_0)\cdot R_{\mathrm{b}}(\gamma_{\mathrm{b}},u_0). \quad (3.9)$$

The approximation in the above equation (3.9) is because it assumes that the SINR events on the access and backhaul links are statistically independent. The approximation is tight when the access and backhaul links are sufficiently spatially separated and the corresponding interference affecting the two links is independent or weakly correlated. Under such conditions, the joint success probability closely matches the product of the individual probabilities, making the approximation accurate.

3.2.2 Results and Discussions

In this section, we validate our analytical framework using Monte-Carlo simulations, providing a precise analysis equivalent to executing experiments and presenting some numerical results to discuss the salient features of the network.

3.2.2.1 Overall Success Probability $\mathcal{P}_{\text{suc}}$

Figs. 3.2(a) and 3.2(b) show the variation of success probability, $\mathcal{P}_{\text{suc}}$ with respect to β by varying access and backhaul system parameters. In Figure 3.2(a), since for smaller values

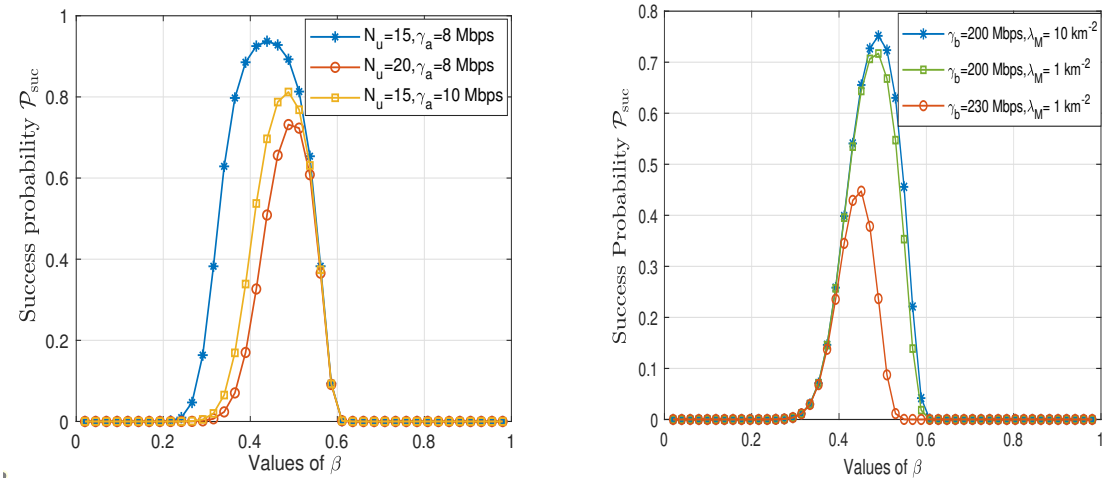

Figure 3.2. Trends in success probability with respect to (a) β for different values of N_u and γ_a (b) β for different values of γ_b and λ_t, for N_u=15.

of β, the bandwidth allocated to the access link is less compared to the backhaul link, the overall coverage is limited. On the contrary, for higher values of β, the bandwidth allocated to backhaul is decreases, which also limits the overall coverage. Thus, $\mathcal{P}_{\text{suc}}$ increases as β increases, reaches its peak for a particular value of β, and decreases after that. Furthermore, as γ_{a} increases, R_{a} increases, thus the optimal β increases. Similarly, as N_{u} increases, in order to meet the throughput requirements of more users, more fraction of bandwidth is allocated to the access link. We observe an opposite trend for β in Figure 3.2(b). In particular, when γ_{b} or λ_{M} increases, the throughput requirement for the backhaul link increases, and hence, the optimal value for β decreases to provide more bandwidth $(1-\beta)B$ to the backhaul link.

Figs. 3.3(a) and 3.3(b) show the variation of $\mathcal{P}_{\text{suc}}$ with respect to u_0 by varying access and backhaul system parameters, respectively. From Figure 3.3(a), for smaller values of u_0, R_{b} is less when compared to R_{a}. This is because UAV is located towards the center of the circle, and hence, R_{b} decreases. And for higher values of u_0, R_{a} is less when compared to

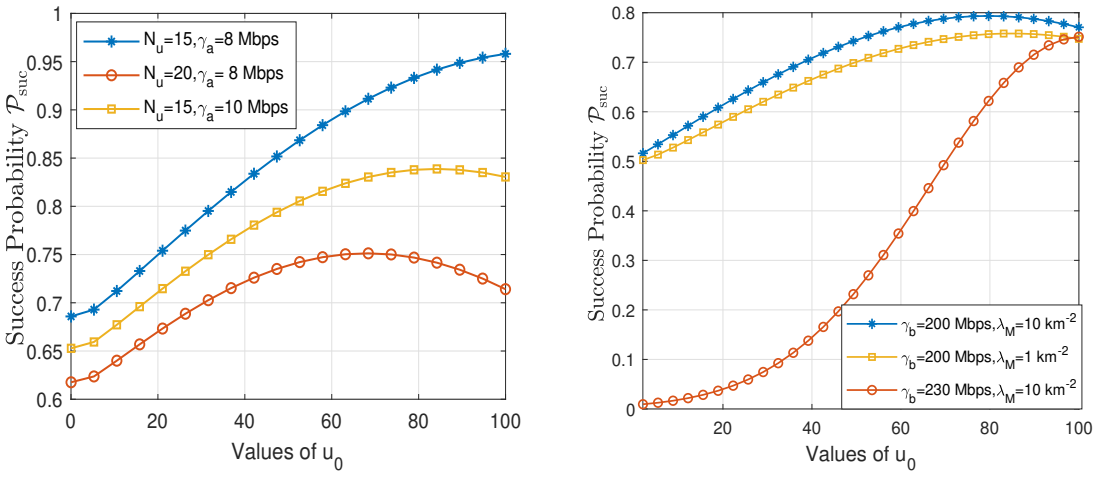

(a) (b)

Figure 3.3. Trends in success probability with respect to (a) u_0 for different values of N_{u} and γ_{a} (b) u_0 for different values of γ_{b} and λ_{M}, for N_{u}=15.

R_{b}. This is because UAV is located at the edge of the circle, and hence, R_{a} decreases. Thus, an optimal value of u_0 exists that maximizes $\mathcal{P}_{\mathrm{suc}}$.

3.2.2.2 Variation of optimal β

In Figure 3.4(a), the variation of optimal values of β and $\mathcal{P}_{\mathrm{suc}}$ with respect to γ_{a} for a fixed u_0, is plotted. As γ_{a} increases, in order to cater to the high throughput requirement of the access link, the optimal β also increases. Further, because of a decrease in R_{a}, optimal $\mathcal{P}_{\mathrm{suc}}$ also decreases as γ_{a} increases. Figure 3.4(b) shows the variation of optimal values of β and $\mathcal{P}_{\mathrm{suc}}$ with respect to γ_{b} for a fixed u_0. As γ_{b} increases to cater to the high throughput requirement of the backhaul link, the optimal β decreases. Further, optimal $\mathcal{P}_{\mathrm{suc}}$ decreases with the increase in γ_{b} because of a decrease in R_{b}. For a specific value of γ_{b}, as P_{M} increases, the throughput requirement for the backhaul link decreases, so the optimal values of β and $\mathcal{P}_{\mathrm{suc}}$ increase. Figure 3.4(c) shows the variation of optimal values of β and $\mathcal{P}_{\mathrm{suc}}$ with respect to N_{u} for a fixed u_0. As N_{u} increases, to cater for the increased throughput requirement of the access link, the optimal value of β also increases.

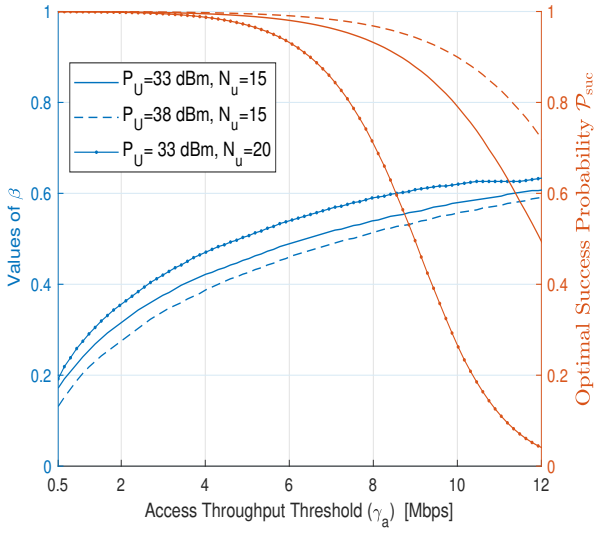
P_U=33 dBm, N_u=15
P_U=38 dBm, N_u=15
P_U= 33 dBm, N_u=20
Values of β
Optimal Success Probability P_suc
Access Throughput Threshold (γ_a) [Mbps]

(a)

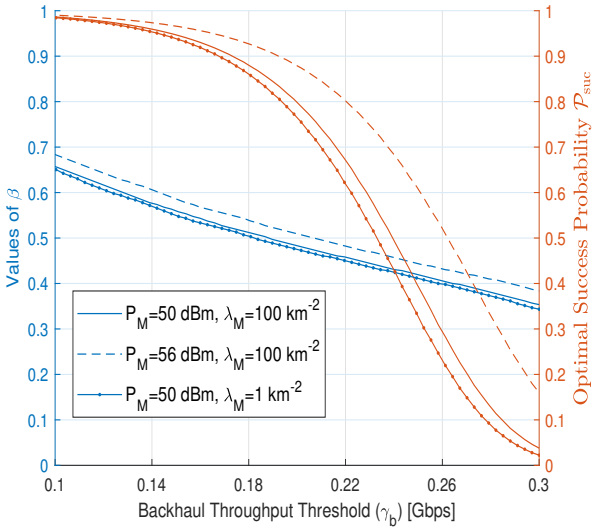
P_M=50 dBm, λ_M=100 km^-2
P_M=56 dBm, λ_M=100 km^-2
P_M=50 dBm, λ_M=1 km^-2
Values of β
Optimal Success Probability P_suc
Backhaul Throughput Threshold (γ_b) [Gbps]

(b)

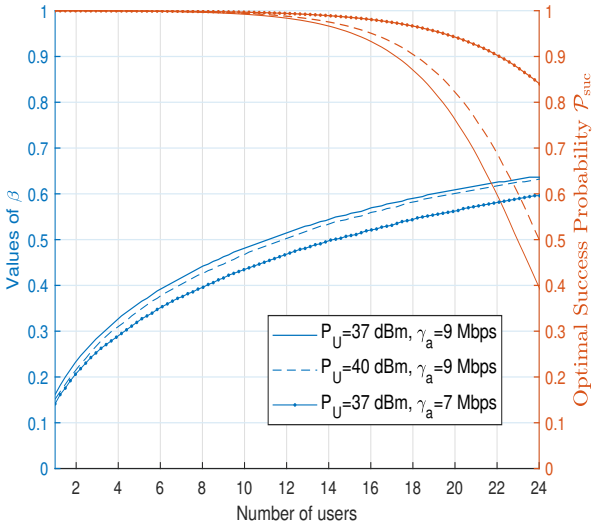
P_U=37 dBm, γ_a=9 Mbps
P_U=40 dBm, γ_a=9 Mbps
P_U=37 dBm, γ_a=7 Mbps
Values of β
Optimal Success Probability P_suc
Number of users

(c)

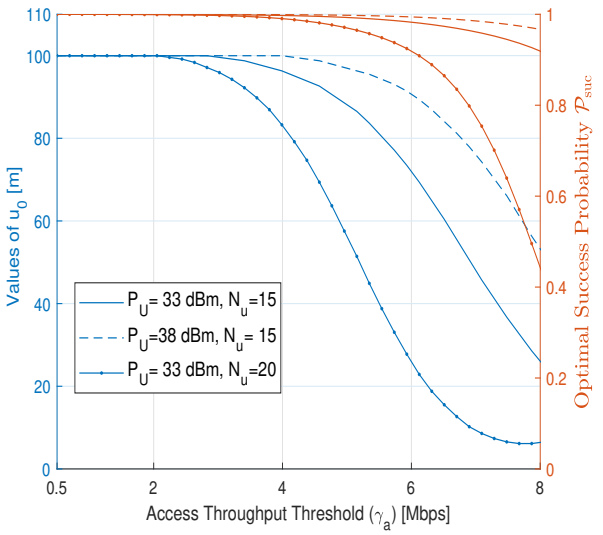
Values of u_0 [m]
Optimal Success Probability $\mathcal{P}_{\text{suc}}$
Access Throughput Threshold (γ_a) [Mbps]
P_U= 33 dBm, N_u=15
P_U=38 dBm, N_u= 15
P_U= 33 dBm, N_u=20

(a)

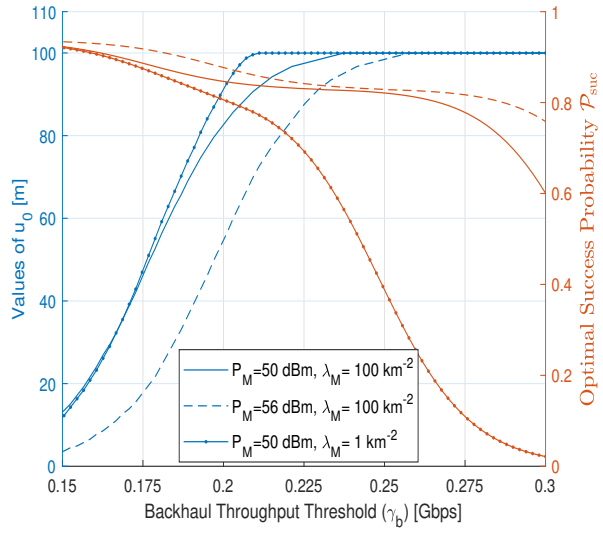
Values of u_0 [m]
Optimal Success Probability $\mathcal{P}_{\text{suc}}$
Backhaul Throughput Threshold (γ_b) [Gbps]
P_M=50 dBm, λ_M= 100 km^{-2}
P_M=56 dBm, λ_M= 100 km^{-2}
P_M=50 dBm, λ_M= 1 km^{-2}

(b)

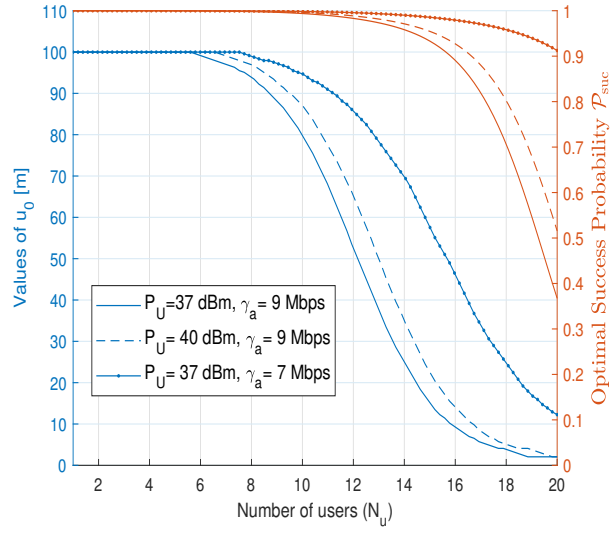
Values of u_0 [m]
Optimal Success Probability $\mathcal{P}_{\text{suc}}$
Number of users (N_u)
P_U=37 dBm, γ_a= 9 Mbps
P_U= 40 dBm, γ_a= 9 Mbps
P_U= 37 dBm, γ_a= 7 Mbps

(c)

3.2.2.3 Variation of Optimal u_0

In Figure 3.5(a), the variation of optimal values of u_0 and $\mathcal{P}_{\text{suc}}$ with respect to γ_{a} for a fixed β is discussed. As γ_{a} increases, the throughput requirement of the access link increases, and to meet the requirement of the access link, the UAV shifts towards the center of the circle of radius r_{d}. Further, as γ_{a} increases, $\mathcal{P}_{\text{suc}}$ decreases. Figure 3.5(b), shows the variation of optimal values of u_0 and R with respect to γ_{b} for a fixed β. As γ_{b} increases, the throughput requirement of the backhaul link increases, so the UAV shifts towards the edge of the circle. Further, as γ_{b} increases, R_{b} decreases, which leads to a decrease $\mathcal{P}_{\text{suc}}$. For a specific value of γ_{b}, as P_{M} increases, the throughput requirement for the backhaul link decreases and the UAV shifts towards the center in order to maintain $\mathcal{P}_{\text{suc}}$. Figure 3.5(c) shows the variation of optimal values of u_0 and $\mathcal{P}_{\text{suc}}$ with respect to N_{u} for a fixed β. As N_{u} increases, the throughput requirement of the access link increases, and the UAV shifts towards the center of the circle of radius r_{d} to meet the throughput demand. As N_{u} increases, there is a decrease in $\mathcal{P}_{\text{suc}}$.

3.3 Spectrum Management in Cache-Enabled UAV HetNets

In the previous section 3.2, we analyzed the optimal resource allocation between the access and backhaul links by considering the overall success probability at the user end in a single UAV-based IAB network. In this section, we extend the analysis to a 3-D HetNet comprising of cache-enabled UAV-IAB nodes.

Consider a downlink HetNet deployed for scenarios where the available wireless access infrastructure is insufficient, e.g., during mass events in areas not prepared for large crowds. The network consists of cache-enabled UAV-APs overlaid on top of a legacy TBSs consisting of MBSs and SBSs. The UAV-APs are small-sized low platform aerial vehicles, which connect to either the TBS or backhaul connected UAV-BS for xHaul support as given in Figure 3.6. The UAV-BSs are large-sized aerial vehicles with directional antennas for a good xHaul connection with the UAV-APs and core network. The users are assumed to be located co-planar with the TBS. The locations of the cached-enabled UAV-APs are modeled as a 3D PPP Φ_{U} defined on $\mathbb{R}^2 \times \mathbb{R}^+$, with intensity λ_{UA}. On the contrary, the locations of the TBSs are modeled as a 2D PPP, Φ_{M} on $\mathbb{R}^2$, with intensity λ_{M}. Additionally, the locations of UAV-BSs are modeled as a 3D PPP Φ_{B} in $\mathbb{R}^2 \times \mathbb{R}^+$, with intensity λ_{UB}. Further, it is assumed that Φ_B is independent of Φ_{U}. Therefore, $\Phi = \Phi_{\mathrm{M}} \cup \Phi_{\mathrm{U}} \cup \Phi_{\mathrm{B}}$.

The typical user associates with either the UAV-AP tier or the TBS tier using Uu interface [48], based on the strongest BS association scheme in the access link. The received signal strength indicator (RSSI) measurements in the downlink access channel are estimated for the association of the typical user to the UAV-AP tier or the TBS tier. Given a UAV-AP association, in case the file requested by the user is present in the UAV cache, only the access link is used [49]. Otherwise, the UAV-AP retrieves the file from either the TBS tier or the UAV-BS tier via an xHaul link. The local storage at the UAV-BS and the TBS tier is not considered due to the assumption of a reliable backhaul connection to the core network from these tiers. Thus, the UAV-AP associates with either the TBS tier or the UAV-BS tier for xHaul transport using Xn interface [48], based on RSSI measurements, sharing the same

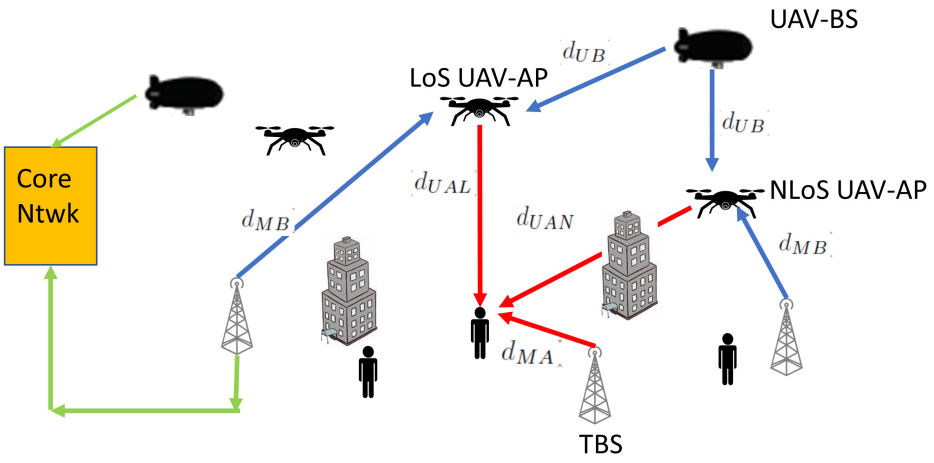

Figure 3.6. An illustration of the considered system model. The red and blue arrows are the access links and xHaul links, respectively. The green arrow is the wired/wireless link to the core network.

spectrum for xHaul. Restricting the heights of the UAV-APs or UAV-BSs to a finite range does not influence the association policy or subsequent analysis, since the considered 3-D PPP is defined over an unbounded spatial domain. The UAV-BS improves xHaul capacity by forming additional directional wireless links to multiple UAV-APs, leveraging spatial reuse over the shared xHaul spectrum. The UAV-APs and TBSs are equipped with down-tilted omnidirectional antennae for access link and directional antennas for backhaul link [50]. As discussed before, the UAV-BSs are equipped with only directional antennas to provide backhaul support to the UAV-APs. Therefore, the association of the typical user with the UAV-BS is limited.

Nomenclature: In what follows, based on the tier and the links, the subscript triplet ijk is used, where $j \in \{\mathrm{A}, \mathrm{B}\}$ refers to either the access or backhaul and $i \in \{\mathrm{M}, \mathrm{U}\}$ refers to either the TBS or the UAV tier (UAV-AP in case $j = \mathrm{A}$ and UAV-BS in case $j = \mathrm{B}$). Furthermore, when $i = \mathrm{U}$ and $j = \mathrm{A}$, we have $k \in \{\mathrm{L}, \mathrm{N}\}$ representing the visibility state, i.e., LoS or NLoS. For all other i and j, we drop the subscript k for ease of notation.

Next, we describe the channel modeling in the access and backhaul links and the caching strategy used to store data at the UAV-APs.

1. **Channel Model: Access link:** The access link propagation consists of small-scale fading and large-scale path loss. Let the locations of the UAV-APs in LoS and NLoS

be denoted as Φ_{L} and Φ_{N}, respectively, where $\Phi_{\mathrm{U}} = \Phi_{\mathrm{L}} \cup \Phi_{\mathrm{N}}$. The probability of LoS link between the UAV-AP and, the typical user is given as [51], [52]:

$$W_{\mathrm{L}}(\theta) = \frac{1}{1 + \eta \exp\left(-\mu\left(\frac{180}{\pi}\sin^{-1}\left(\frac{dcos(\theta)}{d}\right) - \eta\right)\right)}. \tag{3.10}$$

The height h can be written in terms of the distance between the LoS UAV-AP and the typical user d, and θ, which is the polar angle (angle between the polar axis and the line joining the typical user to the UAV-AP). Here, η and μ are the environment parameters for different visibility scenarios like suburban, urban, dense urban, and high-rise urban as given in Table 3.1. Consequently, the probability of NLoS transmissions are given as $W_{\mathrm{N}}(\theta) = 1 - W_{\mathrm{L}}(\theta)$. Due to the higher local scattering, the propagation model from an NLoS UAV to the typical user suffers from a Rayleigh fading g_{NL}. On the contrary, for the LoS UAV transmissions, Nakagami fading distribution, G_{L}, with shape parameter m is assumed.

Table 3.1: Visibility Scenarios

Scenarios	η	μ
Suburban	4.88	0.43
Urban	9.61	0.16
Dense Urban	11.95	0.136
High-rise Urban	24.23	0.08

The downlink transmit powers of the UAV-APs, the backhaul connected UAV-BSs, and the TBSs are P_{UA}, P_{UB}, and P_{M}, respectively. For the large-scale path loss, considering the classical power law where the received power at the typical user from a TBS at a distance of d_{MA}, an LoS UAV at a distance of d_{UAL}, and an NLoS UAV at a distance of d_{UAN} is given by $R_{\mathrm{MA}} = K_{\mathrm{M}} P_{\mathrm{M}} g_{\mathrm{M}} (d_{\mathrm{MA}})^{-\alpha_{\mathrm{N}}}$, $R_{\mathrm{UAL}} = K_{\mathrm{U}} P_{\mathrm{UA}} G_{\mathrm{L}} (d_{\mathrm{UAL}})^{-\alpha_{\mathrm{L}}}$, and $R_{\mathrm{UAN}} = K_{\mathrm{U}} P_{\mathrm{UA}} g_{\mathrm{NL}} (d_{\mathrm{UAN}})^{-\alpha_{\mathrm{N}}}$, respectively. Here K_{U} and K_{M} are the path loss coefficients given by $K_{\mathrm{U}} = K_{\mathrm{M}} = (\frac{\lambda_{\mathrm{c}}}{4\pi})^2$ where λ_{c} is the carrier wavelength. The path loss exponent are α_{L} and α_{N}.

2. **Channel Model- xHaul link:** Because of the high altitude of UAV-APs compared to the TBSs, and the directional antennas in the UAV-BSs guarantee an LoS visibil-

ity state for the UAV-APs in the xHaul link [50], [53]. It must be noted that due to this assumption of LoS connectivity, the locations of the UAV-APs may be more accurately modeled by doubly stochastic point patterns. However, due to its independent scattering property, the PP model encapsulates the impact of multi-objective location optimization of the UAVs across realizations and allows us to derive macro-level system design and dimensioning rules. For a UAV-AP to UAV-BS xHaul link, a Nakagami distributed fast-fading, J_{B}, with parameter m [54] is assumed. On the contrary, the fast-fading for the xHaul link between a TBS and an UAV-AP suffers from a Rayleigh distributed fast-fading, j_B with variance equal to 1, since Rayleigh fading and Nakagami-m fading offer the same network performance in the strongest BS association scheme for a LoS transmission. [55]. In [55], the authors have demonstrated that, when considering LoS propagation alone, the coverage probability shows the same performance for Nakagami-m fading and Rayleigh fading for the strongest BS association strategy. On the other hand, for the closest BS association strategy, the coverage probability monotonically increases with the shape parameter m. Similar to the access link, a power-law model for the large-scale path loss is assumed. Accordingly, the received power at a UAV-AP from a TBS located at a distance d_{MB} from it is $R_{\mathrm{MB}} = K_{\mathrm{M}} P_{\mathrm{M}} j_{\mathrm{B}} (d_{\mathrm{MB}})^{-\alpha_{\mathrm{L}}}$, where, α_{L} is the path loss exponent. The received power at a UAV-AP from a backhaul connected UAV-BS is $R_{\mathrm{UB}} = K_{\mathrm{U}} P_{\mathrm{UB}} J_{\mathrm{B}} (d_{\mathrm{UB}})^{-\alpha_{\mathrm{L}}}$, where, α_{L} is the path loss exponent.

3. **Caching Strategy:** The UAV-APs are equipped with a local storage capability so as to provide rapid access to popular files to the users. The typical user randomly requests contents from the finite content database stored in UAV-AP, $\mathcal{J} = \{f_1, f_2, f_3, ..., f_{\mathrm{L}}\}$, where the database size is L. Each file has the same size, which is normalized to one. A subset of the database is locally cached at the UAV-APs. The popularity of the files is modeled according to the Zipf law [56]. In particular, the popularity or the content request probability of the i^{th} file is given as: $z_{\mathrm{i}} = \frac{i^{-\upsilon}}{\sum_{j=1}^{L} j^{-\upsilon}}$, where $\upsilon \geq 0$ is the popularity factor. The cache size is split into two parts: the first part of the cache stores the most popular content (MPC), and the second part stores the less popular

content (LPC). In particular, consider that there are C_0 MPC files. Accordingly, all the MPC files are cached, i.e., setting $y_{\mathrm{i}} = 1, \forall 1 \leq i \leq C_0$. The remaining $C - C_0$ space of the cache is used to probabilistically cache the remaining $L - C_0$ files by setting:

$$y_{\mathrm{i}} = \min\left(\frac{z_{\mathrm{i}}\left(C - C_0\right)}{1 - \sum_{j=1}^{C_0} z_{\mathrm{j}}}, 1\right) \quad \forall C_0 + 1 \leq i \leq C. \tag{3.11}$$

In order to calculate the successful content delivery when the requested content by a user is cached in the nearest UAV-AP, we need to calculate the cache hit probability $\mathcal{P}_{\mathrm{hit}}$. The cache hit probability or the probability that the requested content by a user is cached in the nearest UAV-AP is [57]: $\mathcal{P}_{\mathrm{hit}} = \sum_{i=1}^{C} z_{\mathrm{i}} y_{\mathrm{i}}$. Consequently, the probability that the requested file is not stored in the cache and thus uses the backhaul link to deliver it to the user is referred to as $\mathcal{P}_{\mathrm{miss}}$, which is given as: $\mathcal{P}_{\mathrm{miss}} = \sum_{i=1}^{C} z_{\mathrm{i}}(1 - y_{\mathrm{i}})$.

3.3.1 Overall Success Probability

The overall success probability is defined as the likelihood that a user successfully receives the requested content. This can be achieved through one of the following possibilities:

1. The user is associated with the TBS tier, and the user is under coverage from the nearest TBS. This event is denoted by S_{t}.

2. The user is associated to the UAV-AP tier, and:

   (a) The requested file is cached at the nearest UAV-AP, and the user is under coverage from the nearest UAV-AP. In this case, the UAV-AP delivers the file without xHaul support. This event is denoted as S_{a}.

   (b) The requested file is not cached at the nearest UAV-AP; however, the user is under coverage from it, and the UAV-AP is under coverage from either the nearest TBS or the nearest backhaul-connected UAV BS via the xHaul link. This event is denoted as S_{x}.

The overall success probability $\mathcal{P}_{\mathrm{suc}}$ is given as

$$\mathcal{P}_{\mathrm{suc}} = \mathbb{P}\left(S_{\mathrm{t}}\right) + \mathbb{P}\left(S_{\mathrm{a}}\right) + \mathbb{P}\left(S_{\mathrm{x}}\right). \tag{3.12}$$

3.3.2 Distance Distribution and Association Probabilities

In this section, we discuss the distance distribution of the potential access and the xHaul links, and we derive the corresponding association probabilities. We start below with a preliminary result.

Lemma 3.3. *The PDF of the distance between the typical user and closest TBS in the access link, d_{MA}, is given by* $f_{d_{\mathrm{MA}}}(x) = 2\pi\lambda_{\mathrm{M}} x \exp\left(-\pi\lambda_{\mathrm{M}} x^2\right)$.

On the contrary, the UAV-APs can be categorized into having either an LoS or NLoS visibility state. The corresponding distance distributions are presented in the following lemma.

Lemma 3.4. *The PDF of the distances between the typical user and closest LoS and the closest NLoS UAV-AP, denoted by d_{UAL} and d_{UAN}, respectively, are given by*

$$f_{d_{\mathrm{UAL}}}(x) = 2\pi\lambda_{\mathrm{UA}} x^2 W'_{\mathrm{L}} \exp\left(-\frac{2}{3}\pi\lambda_{\mathrm{UA}} W'_{\mathrm{L}} x^3\right), \tag{3.13}$$

$$f_{d_{\mathrm{UAN}}}(x) = 2\pi\lambda_{\mathrm{UA}} x^2 W'_{\mathrm{N}} \exp\left(-\frac{2}{3}\pi\lambda_{\mathrm{UA}} W'_{\mathrm{N}} x^3\right), \tag{3.14}$$

where $W'_{\mathrm{L}} = \int_{-\pi/2}^{\frac{\pi}{2}} W_{\mathrm{L}}(\theta)\sin(\theta)d\theta$ *and* $W'_{\mathrm{N}} = \int_{-\pi/2}^{\frac{\pi}{2}} (1 - W_{\mathrm{L}}(\theta))\sin(\theta)d\theta$.

Proof. The distance distribution to the nearest LoS UAV is given as:

$$\begin{aligned} F_{d_{\mathrm{UAL}}}(x) = 1 - \mathbb{P}\left(d_{\mathrm{UAL}} > x\right) &= 1 - \exp\left(-2\pi\lambda_{\mathrm{UA}} \int_0^x \int_{-\pi/2}^{\frac{\pi}{2}} W_{\mathrm{L}}(\theta) y^2 \sin(\theta) d\theta dy\right). \\ &= 1 - \exp\left(-2\pi\lambda_{\mathrm{UA}} \int_0^x y^2 W'_{\mathrm{L}} dy\right). \end{aligned} \tag{3.15}$$

(3.15) follows the null probability of 3D PPP. $W_{\mathrm{L}}(\theta)$ denotes the probability of an LoS connection as a function of the polar angle θ. Finally, the PDF of the distance between the user and the LoS UAV-AP in (3.13), is derived by taking the derivative of (3.15), i.e., $f_{d_{\mathrm{UAL}}}(x) = \frac{d}{dx} F_{d_{\mathrm{UAL}}}(x)$. By following the same steps, $f_{d_{\mathrm{UAN}}}(x)$ can also be derived. □

Lemma 3.5. *The PDF of the distance between a tagged UAV-AP and its closest TBS on the ground is denoted by $f_{d_{\mathrm{MB}}}(x|d,\theta)$, while the PDF of the distance between the tagged UAV-AP*

and a UAV-BS for xHaul is denoted by $f_{d_{\mathrm{UB}}}(x|d,\theta)$*. These PDFs are given as:*

$$f_{d_{\mathrm{MB}}}(x|d,\theta) = 2x\pi\lambda_{\mathrm{M}} \exp\left(-\pi\lambda_{\mathrm{M}}(x^2-h^2)\right),\ x \geq h. \tag{3.16}$$

$$f_{d_{\mathrm{UB}}}(x|d,\theta) = \begin{cases} f'_{d_{\mathrm{UB}}}(x), & x \leq h \\ f''_{d_{\mathrm{UB}}}(x|d,\theta), & x>h, \end{cases} \tag{3.17}$$

where,

$$f'_{d_{\mathrm{UB}}}(x) = 4\pi\lambda_{\mathrm{UB}}x^2 \exp\left(-\lambda_{\mathrm{UB}}\frac{4}{3}\pi x^3\right). \tag{3.18}$$

$$f''_{d_{\mathrm{UB}}}(x|d,\theta) = 2\pi\lambda_{\mathrm{UB}}\left(x^2+xh\right)\exp\left[-\lambda_{\mathrm{UB}}\left(\frac{2}{3}\pi x^3+\pi x^2 h-\frac{1}{3}\pi h^3\right)\right]. \tag{3.19}$$

Proof. See Appendix A.3. □

In case of LoS UAV-AP association, $h = d_{\mathrm{UAL}}\cos(\theta)$ represents the projection of the LoS UAV-AP height onto the ground. Similarly, for NLoS UAV-AP association, $h = d_{\mathrm{UAN}}\cos(\theta)$. Here $\theta \sim \mathcal{U}\left[-\frac{\pi}{2},\frac{\pi}{2}\right]$ is the uniformly distributed random orientation of the tagged UAV-AP from the typical user [58]. We use the variable d_{a} to jointly refer to either d_{UAL} or d_{UAN}.

Next, we derive the association probabilities of the typical user in the access link. As discussed earlier, in the access link, the typical user can either associate with a TBSs or an LoS or an NLoS UAV-APs, based on the maximum power received at the user.

Lemma 3.6. *The probability that the typical user associates with the TBS tier in the access link, denoted by* A_{MA}*, is expressed as:*

$$A_{\mathrm{MA}} = A'_{\mathrm{MA}} + A''_{\mathrm{MA}}, \tag{3.20}$$

where the association occurs when the received power from the TBS exceeds that from both the LoS and NLoS UAV-AP tiers, which is represented as A'_{MA} *and* A''_{MA}*, respectively.*

$$A'_{\mathrm{MA}} = \int_0^\infty \int_{C_{\mathrm{M1}}}^\infty \left[\exp\left(-\frac{2}{3}\pi\lambda_{\mathrm{UA}}W'_{\mathrm{L}}\left(\left(\frac{P_{\mathrm{UA}}}{P_{\mathrm{M}}}\right)^{\frac{3}{\alpha_{\mathrm{L}}}} w^{\frac{3\alpha_{\mathrm{N}}}{\alpha_{\mathrm{L}}}}\right)\right) - \exp\left(-\frac{2}{3}\pi\lambda_{\mathrm{UA}}W'_{\mathrm{L}}x^{\frac{3\alpha_{\mathrm{N}}}{\alpha_{\mathrm{L}}}}\right)\right] \times$$
$$f_{d_{\mathrm{UAN}}}(x)\,\mathrm{d}x \exp\left(-\frac{2}{3}\pi\lambda_{\mathrm{UA}}W'_{\mathrm{N}}\left(\left(\frac{P_{\mathrm{UA}}}{P_{\mathrm{M}}}\right)^{\frac{3}{\alpha_{\mathrm{N}}}} w^{\frac{3\alpha_{\mathrm{N}}}{\alpha_{\mathrm{N}}}}\right)\right) f_{d_{\mathrm{MA}}}(w)\,\mathrm{d}w. \tag{3.21}$$

$$A''_{\mathrm{MA}} = \int_0^{\infty} \int_{C_{\mathrm{M2}}}^{\infty} \left[\exp\left(-\frac{2}{3}\pi\lambda_{\mathrm{UA}} W'_{\mathrm{N}} \left(\left(\frac{P_{\mathrm{UA}}}{P_{\mathrm{M}}} \right)^{\frac{3}{\alpha_{\mathrm{N}}}} w^{\frac{3\alpha_{\mathrm{N}}}{\alpha_{\mathrm{N}}}} \right) \right) - \exp\left(-\frac{2}{3}\pi\lambda_{\mathrm{UA}} W'_{\mathrm{N}} x^{\frac{3\alpha_{\mathrm{L}}}{\alpha_{\mathrm{N}}}} \right) \right] \times$$
$$f_{d_{\mathrm{UAL}}}(x)\,\mathrm{d}x \exp\left(-\frac{2}{3}\pi\lambda_{\mathrm{UA}} W'_{\mathrm{L}} \left(\left(\frac{P_{\mathrm{UA}}}{P_{\mathrm{M}}} \right)^{\frac{3}{\alpha_{\mathrm{L}}}} w^{\frac{3\alpha_{\mathrm{N}}}{\alpha_{\mathrm{L}}}} \right) \right) f_{d_{\mathrm{MA}}}(w)\,\mathrm{d}w, \quad (3.22)$$

where $C_{\mathrm{M1}} = \left(\frac{P_{\mathrm{UA}}}{P_{\mathrm{M}}}\right)^{\frac{1}{\alpha_{\mathrm{N}}}} w^{\frac{\alpha_{\mathrm{N}}}{\alpha_{\mathrm{N}}}}$, $C_{\mathrm{M2}} = \left(\frac{P_{\mathrm{UA}}}{P_{\mathrm{M}}}\right)^{\frac{1}{\alpha_{\mathrm{L}}}} w^{\frac{\alpha_{\mathrm{N}}}{\alpha_{\mathrm{L}}}}$,

Proof. See Appendix A.4. □

Special Case: In order to reduce the computational complexity, we simplify the above equations (3.21) and (3.22) by considering conditions such as

1. the transmit power of UAV-AP is the same as the transmit power of TBS, $P_{\mathrm{UA}} = P_{\mathrm{M}}$
2. the path-loss for LoS and NLoS links are the same, $\alpha_{\mathrm{N}} = \alpha_{\mathrm{L}}$.

The above equations (3.21) and (3.22) are simplified to

$$A'_{\mathrm{MA}} = \frac{W'_{\mathrm{L}}}{W'_{\mathrm{L}} + W'_{\mathrm{N}}} \int_0^{\infty} \exp\left(\frac{-2}{3}\pi\lambda_{\mathrm{UA}} \left(W'_{\mathrm{L}} + 2W'_{\mathrm{N}} \right) w^3 \right) f_{d_{\mathrm{MA}}}(w)\mathrm{dw}. \quad (3.23)$$

$$A''_{\mathrm{MA}} = \frac{W'_{\mathrm{N}}}{W'_{\mathrm{L}} + W'_{\mathrm{N}}} \int_0^{\infty} \exp\left(\frac{-2}{3}\pi\lambda_{\mathrm{UA}} \left(W'_{\mathrm{N}} + 2W'_{\mathrm{L}} \right) w^3 \right) f_{d_{\mathrm{MA}}}(w)\mathrm{dw}. \quad (3.24)$$

Note that we have averaged out the distance distribution of the nearest TBS from the typical user. However, for a UAV-AP, the association probabilities need to be derived conditioned on the respective access distances because of its impact on the backhaul association.

The association probabilities of the typical user getting associated with LoS and NLoS UAV-AP in the access link are discussed next.

Lemma 3.7. *For a given* d_{UAL}*, the probability that the typical user is associated with the LoS UAV-AP in the access link is:*

$$A_{\mathrm{UAL}}(d_{\mathrm{UAL}}) = A'_{\mathrm{UAL}}(d_{\mathrm{UAL}}) + A''_{\mathrm{UAL}}(d_{\mathrm{UAL}}), \quad (3.25)$$

where association occurs if the received power from the LoS UAV-AP exceeds that of the TBS

and NLoS UAV-AP, represented by $A'_{\mathrm{UAL}}(d_{\mathrm{UAL}})$ *and* $A''_{\mathrm{UAL}}(d_{\mathrm{UAL}})$*, respectively.*

$$A'_{\mathrm{UAL}}(d_{\mathrm{UAL}}) = \int_{C_{\mathrm{L1}}}^{\infty} \left[\exp\left(-\frac{2}{3}\pi\lambda_{\mathrm{UA}} W'_{\mathrm{N}} d_{\mathrm{UAL}}^{\frac{3\alpha_{\mathrm{L}}}{\alpha_{\mathrm{N}}}} \right) - \exp\left(-\frac{2}{3}\pi\lambda_{\mathrm{UA}} W'_{\mathrm{N}} \left(\frac{P_{\mathrm{UA}}}{P_{\mathrm{M}}}\right)^{\frac{3}{\alpha_{\mathrm{N}}}} x^3 \right) \right] \times \exp\left(-\pi\lambda_{\mathrm{M}} \left(\frac{P_{\mathrm{M}}}{P_{\mathrm{UA}}}\right)^{\frac{2}{\alpha_{\mathrm{N}}}} d_{\mathrm{UAL}}^{\frac{2\alpha_{\mathrm{L}}}{\alpha_{\mathrm{N}}}} \right) f_{d_{\mathrm{MA}}}(x)\,\mathrm{d}x. \quad (3.26)$$

$$A''_{\mathrm{UAL}}(d_{\mathrm{UAL}}) = \int_{d_{\mathrm{UAL}}^{\frac{\alpha_{\mathrm{L}}}{\alpha_{\mathrm{N}}}}}^{\infty} \left[\exp\left(-\pi\lambda_{\mathrm{M}} \left(\frac{P_{\mathrm{M}}}{P_{\mathrm{UA}}}\right)^{\frac{2}{\alpha_{\mathrm{N}}}} d_{\mathrm{UAL}}^{\frac{2\alpha_{\mathrm{L}}}{\alpha_{\mathrm{N}}}} \right) - \exp\left(-\pi\lambda_{\mathrm{M}} \left(\frac{P_{\mathrm{M}}}{P_{\mathrm{UA}}}\right)^{\frac{2}{\alpha_{\mathrm{N}}}} x^2 \right) \right] \times \exp\left(-\frac{2}{3}\pi\lambda_{\mathrm{UA}} W'_{\mathrm{N}} d_{\mathrm{UAL}}^{\frac{3\alpha_{\mathrm{L}}}{\alpha_{\mathrm{N}}}} \right) f_{d_{\mathrm{UAN}}}(x)\,\mathrm{d}x. \quad (3.27)$$

where $C_{\mathrm{L1}} = \left(\frac{P_{\mathrm{M}}}{P_{\mathrm{UA}}}\right)^{\frac{1}{\alpha_{\mathrm{N}}}} d_{\mathrm{UAL}}^{\frac{\alpha_{\mathrm{L}}}{\alpha_{\mathrm{N}}}}$.

Proof. See Appendix A.5. □

The probability of LoS UAV-AP association in the access link, de-conditioned on d_{UAL} is given by: $\bar{A}_{\mathrm{UAL}} = \int_0^{\infty} A_{\mathrm{UAL}}(x) f_{d_{\mathrm{UAL}}}(x)\mathrm{dx}$. The above expression prescribes required deployment densities of the UAV-APs.

Interestingly, in order to maximize the LoS UAV association, extreme densification can be detrimental as discussed below:

Proposition 1. *As* $\lambda_{\mathrm{UA}} \to \infty$, $\bar{A}_{\mathrm{UAL}} \to 0$ *and exhibits at least one maximum with respect to* λ_{UA}*. Therefore, there exists an optimal UAV density that maximizes the probability of association of a typical user with the LoS UAV-AP.*

Proof. See Appendix A.6. □

Next, we examine the effect of the height of UAV-APs on the LoS UAV-AP association probability:

Corollary 1. *The probability of association of a typical user with the LoS UAV-AP decreases as the height of the LoS UAV-AP increases.*

Proof. See Appendix A.7. □

Lemma 3.8. *For a given d_{UAN}, the probability that the typical user is associated with the NLoS UAV-AP in the access link is:*

$$A_{\mathrm{UAN}}(d_{\mathrm{UAN}}) = A'_{\mathrm{UAN}}(d_{\mathrm{UAN}}) + A''_{\mathrm{UAN}}(d_{\mathrm{UAN}}). \tag{3.28}$$

where association occurs if the received power from the NLoS UAV-AP exceeds that of the TBS and LoS UAV-AP, represented by $A'_{\mathrm{UAN}}(d_{\mathrm{UAN}})$ and $A''_{\mathrm{UAN}}(d_{\mathrm{UAN}})$, respectively.

$$A'_{\mathrm{UAN}}(d_{\mathrm{UAN}}) = \int_{C_{\mathrm{N1}}}^{\infty} \left[\exp\left(-\frac{2}{3}\pi\lambda_{\mathrm{UA}} W'_L \, d_{\mathrm{UAN}}^{\frac{3\alpha_{\mathrm{N}}}{\alpha_{\mathrm{L}}}} \right) - \exp\left(-\frac{2}{3}\pi\lambda_{\mathrm{UA}} W'_L \left(\frac{P_{\mathrm{UA}}}{P_{\mathrm{M}}}\right)^{\frac{3}{\alpha_{\mathrm{L}}}} x^{\frac{3\alpha_{\mathrm{N}}}{\alpha_{\mathrm{L}}}} \right) \right] \times \exp\left(-\pi\lambda_{\mathrm{M}}(C_{\mathrm{N1}})^2\right) f_{d_{\mathrm{MA}}}(x)\,\mathrm{d}x. \tag{3.29}$$

$$A''_{\mathrm{UAN}}(d_{\mathrm{UAN}}) = \int_{d_{\mathrm{UAN}}^{\frac{\alpha_{\mathrm{N}}}{\alpha_{\mathrm{L}}}}}^{\infty} \left[\exp\left(-\pi\lambda_{\mathrm{M}}(N_2)^2\right) - \exp\left(-\pi\lambda_{\mathrm{M}}(N_3)^2\right) \right] \times \exp\left(-\frac{2}{3}\pi\lambda_{\mathrm{UA}} W'_L \, d_{\mathrm{UAN}}^{\frac{3\alpha_{\mathrm{N}}}{\alpha_{\mathrm{L}}}} \right) f_{d_{\mathrm{UAL}}}(x)\,\mathrm{d}x. \tag{3.30}$$

where $C_{\mathrm{N1}} = (\frac{P_{\mathrm{M}}}{P_{\mathrm{UA}}})^{\frac{1}{\alpha_{\mathrm{N}}}} d_{\mathrm{UAN}}^{\frac{\alpha_{\mathrm{N}}}{\alpha_{\mathrm{N}}}}$, $N_2 = (\frac{P_{\mathrm{M}}}{P_{\mathrm{UA}}})^{\frac{1}{\alpha_{\mathrm{N}}}} d_{\mathrm{UAN}}^{\frac{\alpha_{\mathrm{N}}}{\alpha_{\mathrm{N}}}}$, $N_3 = (\frac{P_{\mathrm{M}}}{P_{\mathrm{UA}}})^{\frac{1}{\alpha_{\mathrm{N}}}} x^{\frac{\alpha_{\mathrm{L}}}{\alpha_{\mathrm{N}}}}$.

The probability of NLoS UAV-AP association in the access link, de-conditioned on d_{UAN} is given by: $\bar{A}_{\mathrm{UAN}} = \int_0^{\infty} A_{\mathrm{UAN}}(x) f_{d_{\mathrm{UAN}}}(x)\mathrm{dx}$.

The total association probability in the access link A_{AL} is expressed as

$$\mathbf{A}_{\mathrm{AL}} = \mathbf{A}_{\mathrm{MA}} + \bar{\mathbf{A}}_{\mathrm{UAL}} + \bar{\mathbf{A}}_{\mathrm{UAN}} = \mathbf{1} \tag{3.31}$$

Next, we consider the xHaul link in the case of a UAV-APs association in the access link. As discussed before, the xHaul association probabilities are dependent on the access link distance, d_{a} of the tagged UAV-AP from the typical user. Depending on the visibility state of the tagged UAV-AP from the typical user, the d_{a} can either be d_{UAL} or d_{UAN}. The tagged UAV-AP associates with either the TBS tier or a backhaul-connected UAV-BS tier for xHaul support. Similar to the access link, the xHaul association is also based on RSSI measurements. The backhaul association probabilities are given in the following lemma.

Lemma 3.9. *The probability, $A_{\mathrm{UB}}(d_{\mathrm{a}},\theta)$ that the tagged UAV-AP associates to the UAV-BS tier for xHaul support is*

$$A_{\mathrm{UB}}(d_{\mathrm{a}},\theta)=\int_{d_{\mathrm{a}}\cos(\theta)}^{\ell(d_{\mathrm{a}},\theta)}1-\exp\left(-\frac{4}{3}\pi\lambda_{\mathrm{UB}}\left(\frac{P_{\mathrm{M}}}{P_{\mathrm{UB}}}x^{-\alpha_{\mathrm{L}}}\right)^{-\frac{3}{\alpha_{\mathrm{L}}}}\right)f_{d_{\mathrm{MB}}}(x)\mathrm{dx}$$
$$+\int_{\ell(d_{\mathrm{a}},\theta)}^{\infty}F''_{d_{\mathrm{UB}}}\left(\left(\frac{P_{\mathrm{M}}}{P_{\mathrm{UB}}}d_{\mathrm{MB}}^{-\alpha_{\mathrm{L}}}\right)^{-\frac{1}{\alpha_{\mathrm{L}}}}\right)f_{d_{\mathrm{MB}}}(x)\mathrm{dx}. \quad (3.32)$$

$$\ell(d_{\mathrm{a}},\theta)=\left((d_{\mathrm{a}}\cos(\theta))^{-\alpha_{\mathrm{L}}}\frac{P_{\mathrm{UB}}}{P_{\mathrm{M}}}\right)^{-\frac{1}{\alpha_{\mathrm{L}}}}, \quad (3.33)$$

where, $F''_{d_{\mathrm{UB}}}(x)$ is the CDF corresponding to the PDF $f''_{d_{\mathrm{UB}}}(x)$ given in (3.19).

Proof. See Appendix A.8. □

Naturally, the probability that the tagged UAV-AP associates with the TBS tier for xHaul support is

$$A_{\mathrm{MB}}(d_{\mathrm{a}},\theta)=1-A_{\mathrm{UB}}(d_{\mathrm{a}},\theta). \quad (3.34)$$

3.3.3 Characterization of Success Probability

The success probability for the typical user, $\mathcal{P}_{\mathrm{suc}}$, is defined as the probability that the received SINR Γ at the typical user is greater than a SINR threshold T, i.e., $\mathcal{P}_{\mathrm{suc}}=\mathbb{P}(\Gamma>T)$. Ergodically, this represents the fraction of users that are under SINR coverage from the network. In the following, we adopt the same notation as above and denote the instantaneous SINR and the corresponding coverage probability by Γ_{ijk} and $\mathcal{P}_{\mathrm{ijk}}$, respectively.

Lemma 3.10. *The success probability of the typical user associated with the TBS in the access link is given as*

$$\mathcal{P}_{\mathrm{CM}}(s_{\mathrm{a}})=\int_{0}^{\infty}\left(\exp\left(\frac{-s_{\mathrm{a}}N_0}{K_{\mathrm{M}}P_{\mathrm{M}}q^{-\alpha_{\mathrm{N}}}}\right)I'_{\mathrm{M1}}I'_{\mathrm{L1}}I'_{\mathrm{NL1}}\right)f_{d_{\mathrm{MA}}}(q)\mathrm{dq}, \quad (3.35)$$

where I'_{L1}, I'_{NL1} and I'_{M1} are interference terms from the LoS UAV-APs, NLoSs UAV-APs and TBSs other than the associated TBS, respectively. s_{a} is the SINR threshold in the access

link and $f_{d_{\mathrm{MA}}}(q)$ *is the PDF of the distances between the user and the closest TBS.*

$$I'_{\mathrm{M1}} = \exp\left(-2\pi\lambda_{\mathrm{M}} \int_{d_{\mathrm{MA}}}^{\infty} \left(1 - \frac{1}{1 + \frac{s_{\mathrm{a}} t^{-\alpha_{\mathrm{N}}}}{q^{-\alpha_{\mathrm{N}}}}}\right) t\mathrm{d}t\right). \tag{3.36}$$

$$I'_{\mathrm{L1}} = \exp\left(-2\pi\lambda_{\mathrm{UA}} W'_{\mathrm{L}} \int_{J_{\mathrm{L}}}^{\infty} \left[x^2\mathrm{d}x - x^2\left(\frac{m}{m + \frac{\eta s_{\mathrm{a}} K_{\mathrm{U}} P_{\mathrm{UA}} x^{-\alpha_{\mathrm{L}}}}{K_{\mathrm{M}} P_{\mathrm{M}} q^{-\alpha_{\mathrm{N}}}}}\right)^{m} \mathrm{d}x\right]\right), \tag{3.37}$$

where $J_{\mathrm{L}} = (\frac{P_{\mathrm{UA}}}{P_{\mathrm{M}}})^{\frac{1}{\alpha_{\mathrm{L}}}} q^{\frac{\alpha_{\mathrm{N}}}{\alpha_{\mathrm{L}}}}$, $W'_{\mathrm{L}} = \int_{-\pi/2}^{\frac{\pi}{2}} W_{\mathrm{L}}(\theta)\sin(\theta)d\theta$ *and* $\eta = m(m!)^{\frac{-1}{m}}$.

$$I'_{\mathrm{NL1}} = \exp\left(-2\pi\lambda_{\mathrm{UA}} W'_{\mathrm{N}} \int_{(\frac{P_{\mathrm{UA}}}{P_{\mathrm{M}}})^{\frac{1}{\alpha_{\mathrm{N}}}} q^{\frac{\alpha_{\mathrm{N}}}{\alpha_{\mathrm{N}}}}}^{\infty} \left[y^2\mathrm{d}y - y^2\left(\frac{1}{1 + \frac{s_{\mathrm{a}} K_{\mathrm{U}} P_{\mathrm{UA}} y^{-\alpha_{\mathrm{N}}}}{K_{\mathrm{M}} P_{\mathrm{M}} q^{-\alpha_{\mathrm{N}}}}}\right)\mathrm{d}y\right]\right). \tag{3.38}$$

Proof. See Appendix A.9. □

Lemma 3.11. *Given that the typical user is associated with NLoS or LoS UAV-AP, the success probability of the typical user in the access link is given respectively as:*

- *NLoS UAV-AP*

$$\mathcal{P}_{\mathrm{CN}}(d_{\mathrm{UAN}}, s_{\mathrm{a}}) = \left(\exp\left(\frac{-s_{\mathrm{a}} N_0}{K_{\mathrm{U}} P_{\mathrm{UA}} d_{\mathrm{UAN}}^{-\alpha_{\mathrm{N}}}}\right) \cdot I'_{\mathrm{M2}} \cdot I'_{\mathrm{L2}} \cdot I'_{\mathrm{NL2}}\right), \tag{3.39}$$

I'_{L2}, I'_{M2} and I'_{NL2} are interference terms from LoS UAV-APs, TBSs and NLoS UAV-APs other than the associated NLoS UAV-AP, respectively.

$$I'_{\mathrm{M2}} = \exp\left(-2\pi\lambda_{\mathrm{M}} \int_{\frac{P_{\mathrm{M}}}{P_{\mathrm{UA}}}^{\frac{1}{\alpha_{\mathrm{N}}}} d_{\mathrm{UAN}}^{\frac{\alpha_{\mathrm{N}}}{\alpha_{\mathrm{N}}}}}^{\infty} \left(1 - \frac{1}{1 + \frac{s_{\mathrm{a}} K_{\mathrm{M}} P_{\mathrm{M}} t^{-\alpha_{\mathrm{N}}}}{K_{\mathrm{U}} P_{\mathrm{UA}} d_{\mathrm{UAN}}^{-\alpha_{\mathrm{N}}}}}\right) t\mathrm{d}t\right).$$

$$I'_{\mathrm{L2}} = \exp\left(-2\pi\lambda_{\mathrm{UA}} W'_{\mathrm{L}} \int_{d_{\mathrm{UAN}}^{\frac{\alpha_{\mathrm{N}}}{\alpha_{\mathrm{L}}}}}^{\infty} \left[y^2 dy - y^2\left(\frac{m}{m + \frac{\eta s_{\mathrm{a}} y^{-\alpha_{\mathrm{L}}}}{d_{\mathrm{UAN}}^{-\alpha_{\mathrm{N}}}}}\right)^{m} \mathrm{d}y\right]\right).$$

$$I'_{\mathrm{NL2}} = \exp\left(-2\pi\lambda_{\mathrm{UA}} W'_{\mathrm{N}} \int_{d_{\mathrm{UAN}}}^{\infty} \left(1 - \frac{1}{1 + \frac{s_{\mathrm{a}} x^{-\alpha_{\mathrm{N}}}}{d_{\mathrm{UAN}}^{-\alpha_{\mathrm{N}}}}}\right) x^2\mathrm{d}x\right).$$

- *LoS UAV-AP*

$$\mathcal{P}_{\mathrm{CL}}(d_{\mathrm{UAL}}, s_{\mathrm{a}}) = \sum_{n=1}^{m} (-1)^{n+1} \cdot {}^{m}C_{n} \exp\left(\frac{-n\eta s_{\mathrm{a}} N_0}{K_{\mathrm{U}} P_{\mathrm{UA}} d_{\mathrm{UAL}}^{-\alpha_{\mathrm{L}}}}\right) I'_{\mathrm{M3}} I'_{\mathrm{L3}} I'_{\mathrm{NL3}}. \tag{3.40}$$

I'_{L3}, I'_{NL3} and I'_{M3} are interference terms from other LoS, NLoS UAV-APs and TBSs respectively.

$$I'_{\mathrm{M3}} = \exp\left(-2\pi\lambda_{\mathrm{M}} \int_{\frac{P_{\mathrm{M}}}{P_{\mathrm{UA}}}^{\frac{1}{\alpha_{\mathrm{N}}}} d_{\mathrm{UAL}}^{\frac{\alpha_{\mathrm{L}}}{\alpha_{\mathrm{N}}}}}^{\infty} \left[t\mathrm{d}t - t\left(\frac{1}{1 + \frac{n\eta s_{\mathrm{a}} K_{\mathrm{M}} P_{\mathrm{M}} t^{-\alpha_{\mathrm{N}}}}{K_{\mathrm{U}} P_{\mathrm{UA}} d_{\mathrm{UAL}}^{-\alpha_{\mathrm{L}}}}}\right) \mathrm{d}t\right]\right).$$

$$I'_{\mathrm{L3}} = \exp\left(-2\pi\lambda_{\mathrm{UA}} W'_{\mathrm{L}} \int_{d_{\mathrm{UAL}}}^{\infty} \left[x^2 \mathrm{d}x - x^2\left(\frac{m}{m + \frac{n\eta s_{\mathrm{a}} x^{-\alpha_{\mathrm{L}}}}{d_{\mathrm{UAL}}^{-\alpha_{\mathrm{L}}}}}\right)^{m} \mathrm{d}x\right]\right).$$

$$I'_{\mathrm{NL3}} = \exp\left(-2\pi\lambda_{\mathrm{UA}} W'_{\mathrm{N}} \int_{d_{\mathrm{UAL}}^{\frac{\alpha_{\mathrm{L}}}{\alpha_{\mathrm{N}}}}}^{\infty} \left[y^2 \mathrm{d}y - y^2\left(\frac{1}{1 + \frac{n\eta s_{\mathrm{a}} y^{-\alpha_{\mathrm{N}}}}{d_{\mathrm{UAL}}^{-\alpha_{\mathrm{L}}}}}\right) \mathrm{d}y\right]\right).$$

Proof. See Appendix A.9. □

Lemma 3.12. *The success probability of the tagged UAV-AP associated with the TBS in the xHaul link is given as*

$$\mathcal{P}_{\mathrm{CMB}}(d_{\mathrm{MB}}, s_{\mathrm{b}}) = \exp\left(\frac{-s_{\mathrm{b}} N_0}{K_{\mathrm{M}} P_{\mathrm{M}} (d_{\mathrm{MB}})^{-\alpha_{\mathrm{L}}}}\right) \cdot I'_{\mathrm{M4}} \cdot I'_{\mathrm{U4}}. \tag{3.41}$$

I'_{M4} and I'_{U4} are interference terms from other TBSs and UAV-BSs respectively. s_b is the SINR threshold in the xHaul link.

$$I'_{\mathrm{M4}} = \exp\left(-2\pi\lambda_{\mathrm{M}} \int_{d_{\mathrm{MB}}}^{\infty} \left(1 - \frac{1}{1 + \frac{s_{\mathrm{b}} t^{-\alpha_{\mathrm{L}}}}{(d_{\mathrm{MB}})^{-\alpha_{\mathrm{L}}}}}\right) t,\ \mathrm{d}t\right).$$

$$I'_{\mathrm{U4}} = \exp\left(-2\pi\lambda_{\mathrm{UB}} W'_{\mathrm{L}} \int_{(\frac{P_{\mathrm{UB}}}{P_{\mathrm{M}}})^{\frac{1}{\alpha_{\mathrm{L}}}} d_{\mathrm{MB}}^{\frac{\alpha_{\mathrm{L}}}{\alpha_{\mathrm{L}}}}}^{\infty} \left[x^2 \mathrm{d}x - x^2\left(\frac{m}{m + \frac{s_{\mathrm{b}} K_{\mathrm{U}} P_{\mathrm{UB}} x^{-\alpha_{\mathrm{L}}}}{K_{\mathrm{M}} P_{\mathrm{M}} d_{\mathrm{MB}}^{-\alpha_{\mathrm{L}}}}}\right)^{m} \mathrm{d}x\right]\right).$$

Lemma 3.13. *The success probability of the typical UAV-AP associated with the UAV-BS*

in the xHaul link is:

$$\mathcal{P}_{\mathrm{CUB}}(d_{\mathrm{UB}}, s_{\mathrm{b}}) = \sum_{n=1}^{m} (-1)^{n+1} \cdot {}^{m}C_n \exp\left(\frac{-n\eta s_{\mathrm{b}} N_0}{K_{\mathrm{U}} P_{\mathrm{UB}} d_{\mathrm{UB}}^{-\alpha_{\mathrm{L}}}}\right) \cdot I'_{\mathrm{M5}} I'_{\mathrm{U5}}. \tag{3.42}$$

I'_{U5} and I'_{M5} are interference terms from other UAV-BSs and TBSs respectively.

$$I'_{\mathrm{M5}} = \exp\left(-2\pi\lambda_{\mathrm{M}} \int_{\frac{P_{\mathrm{M}}}{P_{\mathrm{UB}}}^{\frac{1}{\alpha_{\mathrm{L}}}} d_{\mathrm{UB}}^{\frac{\alpha_{\mathrm{L}}}{\alpha_{\mathrm{L}}}}}^{\infty} \left[tdt - t\left(\frac{1}{1 + \frac{n\eta s_{\mathrm{b}} K_{\mathrm{M}} P_{\mathrm{M}} t^{-\alpha_{\mathrm{L}}}}{K_{\mathrm{U}} P_{\mathrm{UB}} d_{\mathrm{UB}}^{-\alpha_{\mathrm{L}}}}}\right) \mathrm{d}t \right]\right).$$

$$I'_{\mathrm{U5}} = \exp\left(-2\pi\lambda_{\mathrm{UB}} W'_{\mathrm{L}} \int_{d_{\mathrm{UB}}}^{\infty} \left[x^2 dx - x^2 \left(\frac{m}{m + \frac{n\eta s_{\mathrm{b}} x^{-\alpha_{\mathrm{L}}}}{d_{\mathrm{UB}}^{-\alpha_{\mathrm{L}}}}}\right)^{m} \mathrm{d}x \right]\right).$$

Proof. The proof of the success probability of tagged UAV-AP associated to TBS or UAV-BS in the xHaul link follows in a similar way as Proof of Lemma 3.11. □

3.3.4 Rate Coverage and Content Delivery Success

The framework for success probability can be employed to derive the rate coverage probability, which is defined as the probability that the per-user rate at the typical user is greater than a given threshold r_0. Mathematically, for N_u simultaneous users in the access link with orthogonal channel allocation, we have:

$$\mathbb{P}\left(R \geq r_0\right) = \mathbb{P}\left(\frac{\beta B}{N_{\mathrm{u}}} \log_2\left(1 + \Gamma\right) \geq r_0\right) = \mathbb{P}\left(\Gamma \geq 2^{\frac{N_{\mathrm{u}} r_0}{\beta B}} - 1\right) = \mathcal{P}_{\mathrm{suc}}\left(2^{\frac{N_{\mathrm{u}} r_0}{\beta B}} - 1\right). \tag{3.43}$$

Let us assume that the minimum rate requirement in the access link to transfer a file requested by the user before the service deadline is given by r_a. Accordingly, for a successful transmission, the access link SINR threshold is given by: $s_{\mathrm{a}} = 2^{\frac{N_{\mathrm{u}} r_{\mathrm{a}}}{B\beta}} - 1$. Similarly, for an xHaul rate threshold of r_b, the xHaul SINR threshold: $s_{\mathrm{b}} = 2^{\frac{r_{\mathrm{b}}}{B(1-\beta)}} - 1$.

The successful content delivery of the user in (3.12) is defined as $\mathbb{P}(S_{\mathrm{t}}) = A_{\mathrm{MA}} \mathcal{P}_{\mathrm{CM}}\left(t_a\right)$

and

$$\mathbb{P}(S_{\mathrm{a}}) = \mathcal{P}_{\mathrm{hit}} \left(\underbrace{\int_0^{\infty} A_{\mathrm{UAL}}(x)\mathcal{P}_{\mathrm{CL}}(x, s_{\mathrm{a}}) f_{d_{\mathrm{UAL}}}(x)\mathrm{d}x}_{I} + \underbrace{\int_0^{\infty} A_{\mathrm{UAN}}(x)\mathcal{P}_{\mathrm{CN}}(x, s_{\mathrm{a}}) f_{d_{\mathrm{UAN}}}(x)\mathrm{d}x}_{II} \right). \tag{3.44}$$

$$\mathbb{P}(S_{\mathrm{x}}) = \mathcal{P}_{\mathrm{miss}} \Bigg[\int_{-\frac{\pi}{2}}^{\frac{\pi}{2}} \left(\int_0^{\infty} A_{\mathrm{UAL}}(x)\, \mathcal{P}_{\mathrm{CL}}(x, s_{\mathrm{a}})\, B_{\mathrm{l}}(x, \theta)\, f_{d_{\mathrm{UAL}}}(x)\, \mathrm{d}x \right) \mathrm{d}\theta + \int_{-\frac{\pi}{2}}^{\frac{\pi}{2}} \left(\int_0^{\infty} A_{\mathrm{UAN}}(x)\, \mathcal{P}_{\mathrm{CN}}(x, s_{\mathrm{a}})\, B_{\mathrm{l}}(x, \theta)\, f_{d_{\mathrm{UAN}}}(x)\, \mathrm{d}x \right) \mathrm{d}\theta \Bigg]. \tag{3.45}$$

$$B_{\mathrm{l}}(x, \theta) = \int_0^{\infty} A_{\mathrm{UB}}(x, \theta)\mathcal{P}_{\mathrm{CUB}}(y, s_{\mathrm{b}}) f_{d_{\mathrm{UB}}}(y|x, \theta)\mathrm{d}y + \int_{x\cos(\theta)}^{\infty} A_{\mathrm{MB}}(x, \theta)\mathcal{P}_{\mathrm{CMB}}(x, s_{\mathrm{b}}) f_{d_{\mathrm{MB}}}(y|x, \theta)\mathrm{d}y. \tag{3.46}$$

where $B_{\mathrm{l}}(x, \theta)$ is the total xHaul coverage probability. Here I is the success probability of the user associated to LoS UAV-AP and II is the success probability of the user associated to NLoS UAV-AP. Thus, we have characterized the different components of the expression (3.12), which characterize the content delivery success or the overall success probability $\mathcal{P}_{\mathrm{suc}}$.

Special Case: In order to reduce the computational complexity, we simplify the equations in Lemma 3.11, Lemma 3.12 and Lemma 3.13, by considering conditions such as (1) equal transmit powers for all the tiers $P_{\mathrm{M}} = P_{\mathrm{UA}} = P_{\mathrm{UB}}$ (2) Same path loss exponent $\alpha_{\mathrm{L}} = \alpha_{\mathrm{N}}$ (3) $m = 1$.

In Lemma 3.11, the success probability of a typical user in the access link for NLoS and LoS UAV-AP association is given as

$$\mathcal{P}_{\mathrm{CN}}(d_{\mathrm{UAN}}, s_{\mathrm{a}}) = \exp\left(\frac{-s_{\mathrm{a}} N_0}{K_{\mathrm{U}} P_{\mathrm{UA}} d_{\mathrm{UAN}}^{-\alpha_{\mathrm{N}}}} \right) \cdot I'_{\mathrm{M2}} \cdot I'_{\mathrm{L2}} \cdot I'_{\mathrm{NL2}}, \tag{3.47}$$

where $I'_{\mathrm{M2}} \cdot I'_{\mathrm{L2}} \cdot I'_{\mathrm{NL2}}$ can be simplified as

$$I'_{\mathrm{M2}} \cdot I'_{\mathrm{L2}} \cdot I'_{\mathrm{NL2}} = \exp\left(-2\pi \int_{d_{\mathrm{UAN}}}^{\infty} \left[\left(1 - \frac{1}{1 + \frac{s_{\mathrm{a}} t^{-\alpha_{\mathrm{N}}}}{d_{\mathrm{UAN}}^{-\alpha_{\mathrm{N}}}}}\right)\left(\lambda_M t + \lambda_{\mathrm{UA}} W_{\mathrm{L}}^{'} t^2 + \lambda_{\mathrm{UA}} W_{\mathrm{N}}^{'} t^2\right)\right] \mathrm{d}t\right).$$

Likewise, in Lemma 3.11, the success probability of the typical user for LoS association is given as

$$\mathcal{P}_{\mathrm{CL}}(d_{\mathrm{UAL}}, t_{\mathrm{a}}) = \sum_{n=1}^{m} (-1)^{n+1} \cdot {}^{m}C_n \exp\left(\frac{-n\eta s_{\mathrm{a}} N_0}{K_{\mathrm{U}} P_{\mathrm{UA}} d_{\mathrm{UAL}}^{-\alpha_{\mathrm{L}}}}\right) I'_{\mathrm{M3}} I'_{\mathrm{L3}} I'_{\mathrm{NL3}}, \tag{3.48}$$

where $I'_{\mathrm{M3}} \cdot I'_{\mathrm{L3}} \cdot I'_{\mathrm{NL3}}$ is simplified as

$$I'_{\mathrm{M3}} \cdot I'_{\mathrm{L3}} \cdot I'_{\mathrm{NL3}} = \exp\left(-2\pi \int_{d_{\mathrm{UAL}}}^{\infty} \left[\left(1 - \frac{1}{1 + \frac{n s_{\mathrm{a}} t^{-\alpha_{\mathrm{N}}}}{d_{\mathrm{UAL}}^{-\alpha_{\mathrm{N}}}}}\right)\left(\lambda_{\mathrm{M}} t + \lambda_{\mathrm{UA}} W_{\mathrm{L}}^{'} t^2 + \lambda_{\mathrm{UA}} W_{\mathrm{N}}^{'} t^2\right)\right] \mathrm{d}t\right). \tag{3.49}$$

Similarly, in Lemma 3.12 and Lemma 3.13, the total interference power experienced when analyzing the success probability of tagged UAV-AP to TBS and UAV-BS, respectively, is given as

$$I'_{\mathrm{M4}} \cdot I'_{\mathrm{U4}} = \exp\left(-2\pi \int_{d_{\mathrm{MB}}}^{\infty} \left[\left(1 - \frac{1}{1 + \frac{s_{\mathrm{b}} t^{-\alpha_{\mathrm{N}}}}{d_{\mathrm{MB}}^{-\alpha_{\mathrm{N}}}}}\right)\left(\lambda_{\mathrm{M}} t + \lambda_{\mathrm{UB}} W_{\mathrm{L}}^{'} t^2\right)\right] \mathrm{d}t\right). \tag{3.50}$$

$$I'_{\mathrm{M5}} \cdot I'_{\mathrm{U5}} = \exp\left(-2\pi \int_{d_{\mathrm{UB}}}^{\infty} \left[\left(1 - \frac{1}{1 + \frac{n s_{\mathrm{b}} t^{-\alpha_{\mathrm{N}}}}{d_{\mathrm{UB}}^{-\alpha_{\mathrm{N}}}}}\right)\left(\lambda_{\mathrm{M}} t + \lambda_{\mathrm{UB}} W_{\mathrm{L}}^{'} t^2\right)\right] \mathrm{d}t\right). \tag{3.51}$$

Consequently, the complexity of the rate coverage expression in (3.45) is reduced by three times, because the three interference components in each success probability expressions in Lemma 3.11, Lemma 3.12, and Lemma 3.13 are merged into a single compact integral. This reduces the number of integrals per link from three to one, resulting in a three times reduction in complexity. Since these integrals are evaluated repeatedly during numerical integrations, this simplification significantly reduces the computation time.

3.3.5 Results and Discussions

In this section, we validate our analytical framework using Monte-Carlo simulations, providing a precise analysis equivalent to executing experiments and presenting some numerical results to discuss the salient features of the network.

3.3.5.1 Trends in Association Probabilities

In Figure 3.7, we plot the association probabilities of a typical user in the access link versus the intensity of UAV-AP for urban and high-rise urban scenarios.The environment parameters chosen for urban and high-rise urban are $\eta = 9.61$, $\mu = 0.61$ and $\eta = 24.23$, $\mu = 0.08$ respectively. As discussed in Lemma 3.7, we note that the probability of LoS UAV-AP asso-

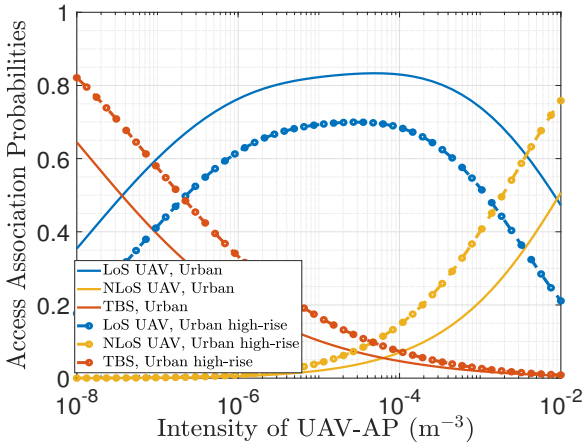

Figure 3.7. Access association probabilities versus intensity of UAV-APs for the typical user in the access link for $\lambda_M = 10^{-6}m^{-2}$.

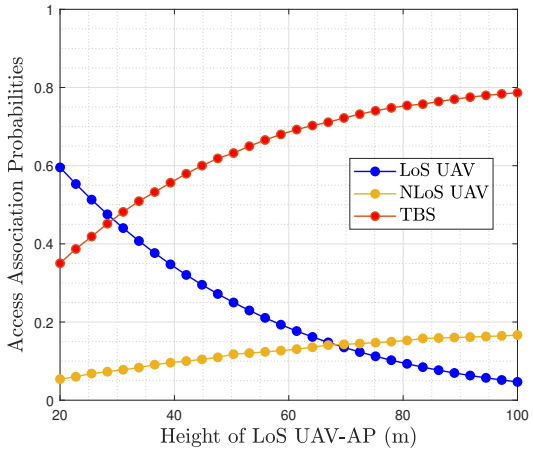

Figure 3.8. Access association probabilities versus height of LoS UAV-AP

ciation increases with λ_{UA}, reaches a maximum, and decreases with further increase in λ_{UA}. This is because a fractional increase in the density increases the number of LoS links for the very sparse deployment of UAVs. However, beyond a certain density, increasing the number of UAVs in the network further increases the potential of serving NLoS UAV-APs without substantially increasing the number of LoS links. Also, due to the RSSI-based association scheme, the access association probability does not depend on the intensity of users but only on the received powers from different tiers. Thus, this analysis equips the operator with an

essential insight: in order to maximize LoS connectivity, densification of the network does not help beyond a certain limit. Accordingly, our analysis prescribes the optimal deployment density to maximize the LoS association for a given blockage environment.

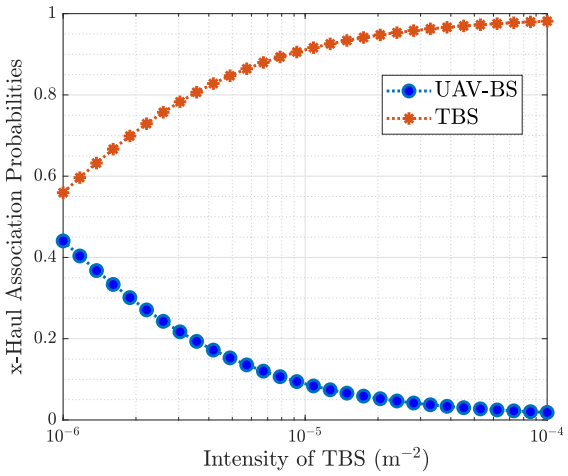

Figure 3.9. xHaul association probabilities versus intensity of TBS for a typical UAV-AP in the xHaul link for $\lambda_{\mathrm{UA}} = 10^{-5}m^{-3}$ and $\lambda_{\mathrm{UB}} = 10^{-7}m^{-3}$.

In Figure 3.8, we plot the association probabilities of a user in the access link versus the height of LoS UAV-AP. We observe that as the height of LoS UAV-AP increases, the LoS connection between the user and UAV-AP is interrupted, leading to a decrease in LoS UAV association probability. Moreover, as the height of LoS UAV-AP increases, the association probability of TBS and NLoS UAV-AP increases. The association of TBS is more than NLoS UAV-AP due to limited blockages during the TBS transmission. We can obtain a height for LoS UAV-AP, for which the LoS UAV-AP association probabilities are the same as TBS association probabilities. At this height of UAV-AP, there is more than 45% chance for the user to associate with LoS UAV-AP or TBS, and 10% chance to associate with NLoS UAV-AP to be under coverage.

On the contrary, Figure 3.9 shows that as the intensity of the TBSs tier increases, there is a monotonic increase and decrease of the TBS and UAV-BS association for xHaul support at a given UAV-AP.

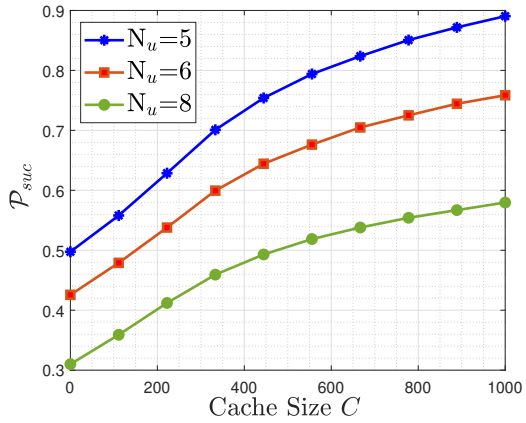

Figure 3.10. Success probability versus cache size for different values of N_{u} with $\lambda_{\mathrm{M}} = 10^{-6}m^{-2}$, $\lambda_{\mathrm{UA}} = 10^{-5}m^{-3}$, $\eta = 9.61$, $\mu = 0.16$.

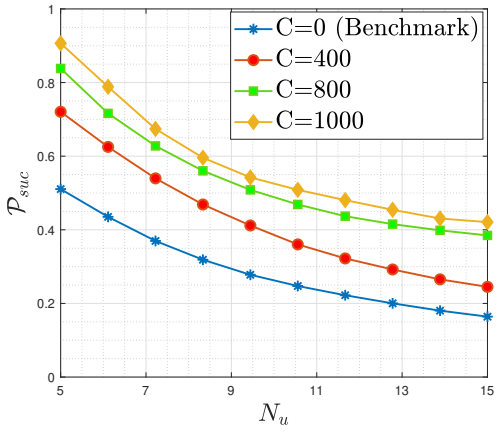

Figure 3.11. Success Probability versus Number of users in the access link

3.3.5.2 Trends in Overall Success Probability

Figure 3.10 shows the probability of successful content delivery for different numbers of simultaneously served users and cache sizes. Naturally, an increase in the cache size or a decrease in the number of users improves the per-user success probability. For the network operator, this reveals how our framework can be used to determine the number of simultaneously served users from one UAV-AP. For example, with $\lambda_{\mathrm{UA}} = 10^{-5}m^{-3}$, with a cache size of $C = 600$, the typical user observes about 80% success if 5 users are served simultaneously. At the same time, it drops to about 50% if 8 users are served simultaneously. In case the operator wants to sustain success of over 90%, the operator must necessarily facilitate admission control mechanisms so that no more than 5 users are served simultaneously. This is because with 5 users, even caching all the files in the local storage does not achieve a success probability greater than 0.9.

In Figure 3.11, we plot success probability versus the number of users in the access link by considering the benchmark scheme, i.e., the cache size is zero. Naturally, as the number of users increases, the success probability in the network decreases. For cache size, C=0 gives the lowest success probability as the requirement in the access link increases, and C=1000 gives the highest success probability. If the requirement in the access link is increased by three times, the success probability will decrease only by 22% if we cache more than 400 files

at the UAV-AP locally. If the files are not cached, the success probability is decreased by 35%. Although in general the success probability increases with an increase in the number of UAV-APs, extreme densification can be detrimental due to increased interference.

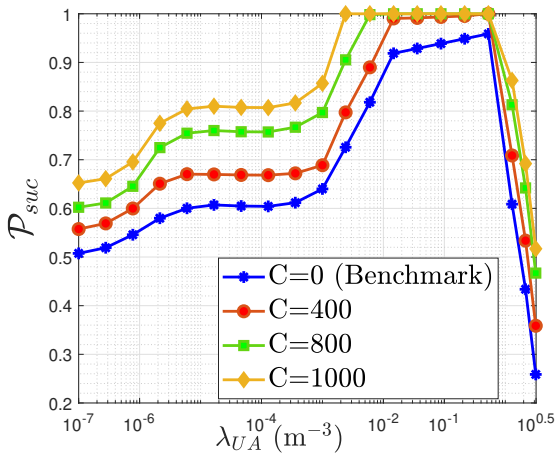

Figure 3.12. Success probability versus intensity of UAV-AP for different values of C for $\lambda_{\mathrm{M}} = 10^{-6}m^{-2}$.

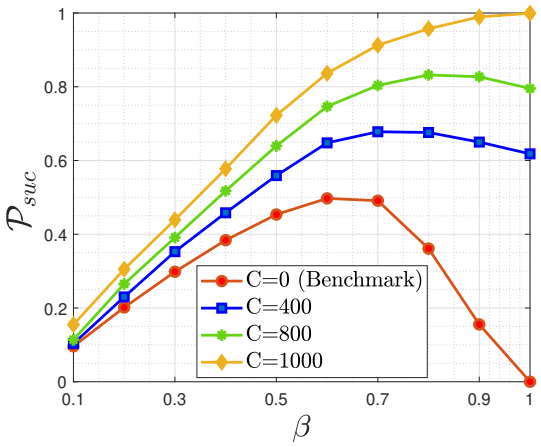

Figure 3.13. Success probability versus the resource partitioning factor for different values of C for C_0=$C/2$.

In Figure 3.12, we plot the success probability with respect to λ_{UA} for different cache sizes and a fixed resource partitioning factor $\beta = 0.5$. As a dimensioning rule, this prescribes the network operator with deployment densities given the storage capacity of the local cache of the UAV-APs. For example, when the UAV-APs do not cache any file locally, like in the benchmark scheme i.e., $C = 0$, a success probability of beyond 0.9 is obtained only beyond $\lambda_{\mathrm{UA}} = 0.01$ m^{-3}. On the contrary, with higher local storage, e.g., $C = 1000$, a success probability of 0.9 is achieved with 10 times fewer UAV-APs, i.e., $\lambda_{\mathrm{UA}} = 0.001$ m^{-3}. In both cases, however, the success probability falls rapidly after $\lambda_{\mathrm{UA}} = 0.5$ m^{-3} due to an increase in interference with densification. This effectively reduces the SINR and rate coverage probability.

Figure 3.13 shows the success probability with respect to the resource partitioning factor β for different values of cache sizes for the urban scenario. Indeed, $C = 0$ refers to the case when all the files requested by the user from the UAV-AP is retrieved from the backhaul connected UAV-BS, which in our work is the benchmark scheme. In this case, $\beta = 1$ i.e., when all the resources are allotted to the access link, results in a 0% success, although the

access link achieves a high coverage rate. We note the existence of an optimum value of β, which maximizes the success probability. When some of the files are stored at the local cache (e.g., $C = 400, 800$, etc.), the operator may provide all the resources to the access link (thereby reducing the xHaul load) without degrading the success probability. In contrast, when all the files are stored in the local cache $C = 1000$, all the frequency resources must necessarily be allotted to the access link. The optimal β thus increases with increasing cache size.

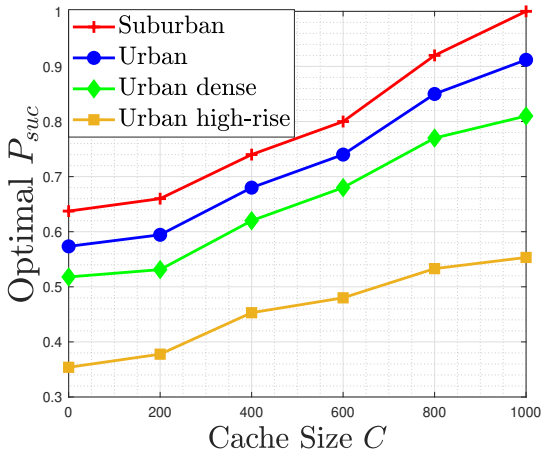

Figure 3.14. Variation of optimal P_{suc} with respect to C for different visibility scenarios

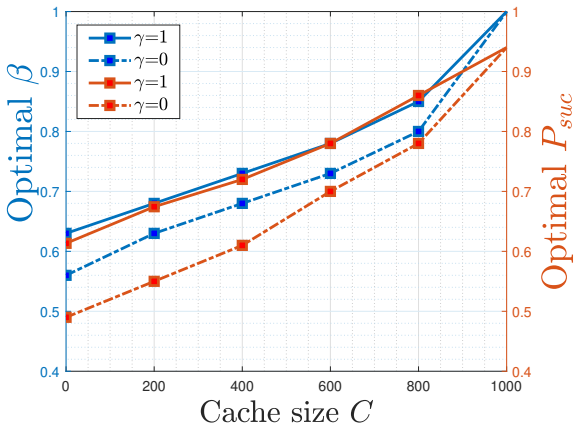

Figure 3.15. Variation of optimal β and optimal P_{suc} with respect to C for different values of γ.

3.3.5.3 Variation in Optimal $\mathcal{P}_{\text{suc}}$ and Optimal β

In Figure 3.14, we plot optimal success probability versus cache size for different visibility scenarios. As cache size increases, the probability of successful delivery of contents to the user increases. For the suburban scenario, where the success probability is high due to fewer blockages, for C=1000, the success in content delivery is 100%, i.e., all the users are delivered with the requested contents directly by the access link. On the contrary, for urban, urban high-rise, and dense-urban scenarios, even caching all the files locally at the UAV-APs results in lower success.

In Figure 3.15, we plot optimal β and success probability versus cache size C for the urban scenario. As the cache size increases, optimal β, along with the maximum success

probability, increases. In particular, let us consider two cases: $\gamma = 1$ and $\gamma = 0$. For $\gamma = 1$, i.e., when the files are of decreasing popularity, and the MPC are cached, the xHaul link is rarely accessed as compared to the case with $\gamma = 0$. Indeed, for $\gamma = 0$, for a given file request from the typical user, a $(1 - C)/1000$ fraction of the time the xHaul support is needed to deliver the file. Accordingly, we observe a higher value of optimal β, i.e., more resources allocated to the access link for $\gamma = 1$ as compared to $\gamma = 0$. Similarly, due to a more frequent xHaul requirement, the success probability for the case with $\gamma = 0$ is lower than that for $\gamma = 1$. This reveals that based on the popularity profile of the content, the network operator not only needs to design optimal access-xHaul split but also provision minimum local storage at the UAV-APs.

3.4 Chapter Conclusion

In UAV networks, the consideration of the xHaul link capacity and its joint optimization with the access link requirement been imperative. In this chapter, we analyzed a joint framework for the association and coverage of the access and xHaul links in a UAV-aided cellular network. First, we derived the expression for the success probability considering a single UAV-AP in a BPP network and then extended it to a UAV-assisted HetNet. We demonstrated that beyond a certain threshold density, deploying additional UAVs for network densification do not improve the LoS association probability. Instead, it degraded user performance due to increased interference and reduced spatial separation among UAVs. Accordingly, we prescribed optimal deployment densities to maximize the LoS coverage probability. Larger cache storage at the UAV-APs led to increased resource allocation on the access link, as the xHaul link been utilized less frequently compared to scenarios with smaller cache sizes. We proposed admission control strategies in terms of the maximum number of simultaneously served users to sustain a per-user throughput above a threshold.

Chapter 4

Mobility Management in UAV-Enabled Wireless Networks

In this chapter, we examine mobility management in UAV-enabled networks, focusing on the dynamic nature of ground user movement. Effective mobility management ensures seamless connectivity as users traverse the coverage area. The primary challenges include dynamically adjusting UAV positions, optimizing handover mechanisms, and efficiently allocating network resources in real-time to uphold the desired QoS. We consider a deployment where UAVs follow the Option 8 functional split, in which all baseband processing functions, including handover decisions, are centralized at the core network. To address these challenges, we propose leveraging caching mechanisms to minimize handover occurrences, thereby enhancing the QoS experienced by mobile users and improving overall network performance.

4.1 Statistical Analysis of Handover Management

In this section, we present a statistical analysis of handover management in aerial networks. This analysis evaluates key metrics such as handover rate and user-experienced throughput, both of which influence the overall QoS in a generalized system. In Part I, we examine the impact of caching capabilities in vehicles on the HO rate and the average data rate in a 1-D UAV-based network. Each vehicle is equipped with local storage and utilizes cached data to bypass frequent associations, thereby reducing the number of HOs. We incorporate the time overhead associated with each handover and derive the effective average rate experienced by vehicle terminals. In Part II, we analyze handover rate and user performance in a UAV-enabled network, where UAVs are deployed to provide connectivity for mobile users in a disaster scenario. We model the UAV distribution using a 2-D homogeneous MPPP, forming irregularly shaped voronoi cells. Furthermore, we derive expressions for the HO rate, success

probability, and the average rate experienced by mobile users.

4.1.1 Network Model

We consider a downlink UAV-based network characterized by mobile users and the location of UAV-APs are modeled as points of PPP. Each UAV-AP has a reliable backhaul connection to the core network. We assume an MT whose movement is uni-directional, i.e., an MT moves on a randomly oriented straight line with velocity v [59]. Due to the isotropy and stationarity of PPP [7], the MT moves only forward in a straight line along the x-axis and passes through the origin. At a given time $t = 0$, we consider that the MT is served by an UAV-AP located at x_0, where $x_0 \in \Phi$. This UAV-AP is referred to as reference UAV-AP. Averaging over the PPP Φ, this MT is referred to as typical MT. The typical MT is associated with a UAV-AP based on the maximum RSSI association scheme, i.e., the MT will get associated with the UAV-AP from which it receives maximum received power. The transmit power of UAV-APs is represented as P_{U}. Without loss of generality, we perform a downlink analysis from the perspective of this MT moving in a straight line passing through the origin.

4.1.2 Handover Management in 1-D UAV-Based Networks

We consider a highway scenario with moving vehicles, where multiple UAV-APs are deployed to ensure seamless connectivity. The locations of these UAV-APs are modeled as a homogeneous PPP Φ_{U} on $\mathbb{R}$ with intensity λ_{U}. Since all UAV-APs operate at the same altitude, we disregard the impact of the height of the UAVs in our analysis. Given the absence of blockages, each UAV-AP maintains an LoS link with mobile users. Consequently, we do not consider small-scale fading in our analysis, as the spatial and temporal dynamics of the network make it analytically intractable. A detailed illustration of the management architecture for cache-based HO is provided in Figure 4.1.

4.1.2.1 Cache-based HO Skipping

An HO management scheme by integrating device caching and thus reducing the frequency of HOs in the network while maintaining the QoS at the MT. As given in Figure 4.1, we

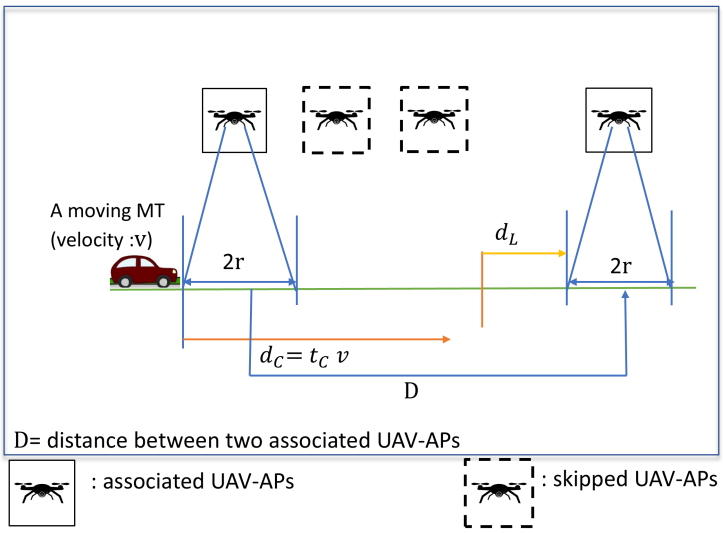

Figure 4.1. Illustration of typical MT moving with a velocity v

assume the MT is playing the video with a fixed play rate p. On that premise, we define a caching region of $2r$, referred to as C_{R}, across each UAV-AP, allowing the MT to cache a portion of the video segments. C_{R} is twice the distance of the MT from the UAV-AP, where it experiences a download rate equal to the play rate p. Hence, C_{R} distance depends on transmit power of UAV-AP, noise power, path loss coefficient, the sum of interference powers from the other UAV-APs, bandwidth, and path loss exponent. We refer r as the caching radius, which is evaluated as

$$r = \left(\frac{(N_0 + I)(2^{(\mathrm{p/B})} - 1)}{P_{\mathrm{U}} K} \right)^{-1/\alpha}, \tag{4.1}$$

p is the play rate. I is the total interference power, which is the sum of all the powers received by the MT from the UAV-AP other than the reference UAV-AP when the MT is located at a distance of r from the reference UAV-AP. Without loss of generality, we assume at time $t = 0$, the MT is at a distance of r from the reference UAV-AP at x_0.

The time travelled by typical MT by skipping the HOs and playing with a play rate p is referred to as cache time, t_{C}. When MT is outside C_{R} where the download rate is less than the play rate, the MT makes use of the data cached inside C_{R}. The MT moves forward, playing with play rate p utilizing the cached data, maintaining the connection with the associated

UAV-AP, and skips the consecutive HOs and makes the next HO when the cache data is fully exhausted. The distance traveled by the MT without initiating a HO until exhausting the cached data is referred to as cache distance as given in Figure 4.1, expressed as $d_{\mathrm{C}} = t_{\mathrm{C}} v$. From Figure 4.1, we can observe the distance d_{C} starts from the caching region of associated UAV-AP, which is at a distance of r from x_0 to the point where the MT exhausts all the cached data. The MT checks at the caching region of every UAV-AP it passes through that if there is enough cached data left at the MT to cover the caching region of that UAV-AP. If there is not enough cached data left, it makes the HO. We assume the next associated UAV-AP is at a distance of D from the associated UAV-AP at x_0. Therefore, d_{C} takes values less than or equal to D, where D depends on the no.of HOs skipped. If N HOs are skipped for a distance of d_{C}, D is the distance of the $(N+1)^{th}$ UAV-AP from the associated one. The number of HOs skipped for a distance of d_{C} is Poisson distributed, with parameter λ_U, and its average value is given by $\lambda_{\mathrm{U}} d_{\mathrm{C}}$. After moving for a distance of d_{C}, the MT moves for a distance of d_{L} before entering the caching region of the next associated UAV-AP at a distance of D, if $d_{\mathrm{C}} < D$. Throughout this distance of d_{L}, the MT plays the video at a rate equal to the download rate experienced by the MT from the associated UAV-AP. So, the distance d_{L} is referred to as a low play rate region or L_{R}. In this regard, we characterize the average rate, which is the expected rate experienced by the MT throughout its journey.

Frequency Reuse: We study the impact of frequency reuse on the average rate in our work. Frequency reuse is an inter-cell interference coordination technique. Each cell is allocated with resources so that interference in the network is minimized, which improves the network's performance. In our model, we consider a decentralized operation of the UAV-AP, i.e., the frequency band of operation for each UAV-AP is chosen probabilistically [60]. We assume that each UAV-AP transmits in a frequency sub-band randomly selected from the range of frequency indices {1,2,...Δ} [60]. As the value of Δ increases, the interference in the network decreases. We assume the UAV-AP's operations are not coordinated, and each UAV-AP independently and randomly chooses the frequency band with a probability of $\frac{1}{\Delta}$. We have compared the probabilistic scheme with the coordinated scheme, where each UAV-AP shares the channel with its $(\Delta+1)^{th}$ neighboring UAV-AP and operates on the corresponding frequency. However, analytical expressions are intractable as there is

dependent thinning of UAV-APs, i.e., the $(\Delta+1)^{th}$ UAV-APs are thinned.

4.1.2.2 Characterization of Average Rate

Let R' be the rate experienced by the MT at time t, taking into account the sum of the powers from all the interfering UAV-APs in PPP at time t, represented as I. The PDF of the total interference power experienced by the MT at time t is $f_{\mathrm{I}}(y,t)$. The distance between two associated UAV-APs is L. Therefore, the average rate experienced by the MT to move for a distance of L is given as

$$\bar{R} = \int_0^{\infty} \int_0^{\mathrm{L/v}} R'(t,y) f_{\mathrm{I}}(y,t) \mathrm{d}t \, \mathrm{d}y \tag{4.2}$$

In order to obtain the average rate, first, we derive the PDF of the total interference power experienced by the MT at time t.

Lemma 4.1. *The PDF of the total interference power experienced by the MT at time t, in a network across realizations, where the locations of UAV-APs are modeled as a 1-D PPP is given as*

$$f_{\mathrm{I}}(y,t) = \frac{1}{2\pi} \int_0^{\infty} \exp\left(-j\omega y\right) \psi_{\mathrm{I}}(\omega,t) \mathrm{d}\omega, \tag{4.3}$$

where,

$$\psi_{\mathrm{I}}(\omega,t) = \exp\left(-\frac{\lambda_{\mathrm{U}}}{\Delta} \int_{\mathrm{r}}^{\infty} 1 - \exp\left(j\omega P_{\mathrm{U}} K_{\mathrm{U}} g^{-\alpha}\right) \mathrm{d}g \right). \tag{4.4}$$

where $\psi_{\mathrm{I}}(\omega,t)$ is the characteristic function of the interference power at time t. The distance of the interfering UAV-APs from the MT at time t is represented as g.

Proof. See Appendix B.1. □

Corollary: From (4.4), we observe the distance of MT to the first interfering UAV-AP d_1 can take values $r \leq d_1 < \infty$. Therefore, for the calculation of the PDF of interference power, there is an impact of the caching radius r, which itself is a function of interference power I as seen in (4.1). Hence, for the analytical calculations, the impact of interference power on the caching radius r is neglected. This assumption is accurate for low interference scenarios, i.e., when the intensity of base stations is low. Also, for a lower play rate, the

assumption is accurate because, for higher play rates, the caching radius across the UAV-AP will be too large. Therefore, the impact of interference will reduce this caching radius but not as much to impact the HO rate and average experienced by the MT. Therefore, the caching radius r is written as

$$r = \left(\frac{N_0(2^{(\mathrm{p/B})} - 1)}{P_{\mathrm{U}} K_{\mathrm{U}}} \right)^{-1/\alpha}. \tag{4.5}$$

Figure 4.2 shows the CDF of the total interference power versus the power values in watts at a time instant for different values of Δ. When Δ=1, the MT experiences interference from all the UAV-APs in the point process Φ with intensity λ_{U}. When Δ increases, the interference power experienced by the MT decreases because the MT experiences interference from the UAV-APs in the point process Φ with the intensity of $\frac{\lambda_{\mathrm{U}}}{\Delta}$. The intensity of UAV-APs for the point process Φ is thinned by a factor of $\frac{1}{\Delta}$.

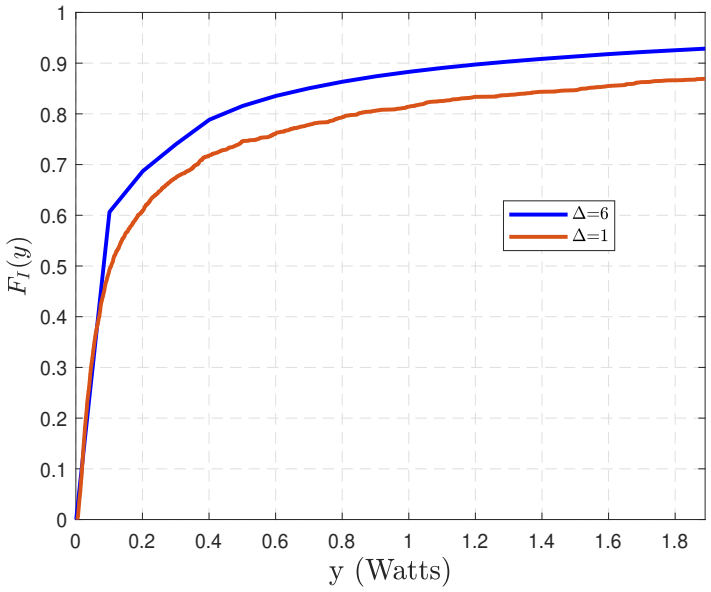

Figure 4.2. CDF of total interference power

Conventional HO scheme: We derive the average rate experienced by the MT in a conventional HO scheme. In a conventional HO scheme, at each cell boundary, a HO is initiated.

Lemma 4.2. *The average rate R_{co} experienced by the typical MT in a conventional HO*

scheme is given as

$$R_{\text{co}} = \int_0^\infty \int_0^\infty R_0(r_1, r_2) f_{l_1}(r_1) f_{l_2}(r_2) \mathrm{d}r_1 \mathrm{d}r_2, \tag{4.6}$$

where

$$R_0(l_1, l_2) = \int_0^\infty \frac{2v}{(l_1 + l_2)} \int_0^{\frac{(l_1+l_2)}{2v}} B \log_2 \left(1 + \frac{P_{\text{U}} K_{\text{U}} / (N_0 + L(t, l_1, l_2) + b)}{|(\frac{l_1}{2} - vt)^\alpha|}\right) f_{\text{S}}(t, l_1, l_2)\, \mathrm{d}t\, \mathrm{d}b. \tag{4.7}$$

where $b = S(t, l_1, l_2)$ i.e., the total interference power experienced by the MT from the UAV-APs, conditioned on l_1 and l_2, at time t. The PDF of total interference power $S(t, l_1, l_2)$, represented as $f_{\text{S}}(t, l_1, l_2)$, is given as

$$f_{\text{S}}(t, l_1, l_2) = \frac{1}{2\pi} \int_0^\infty \exp(-j\omega b) C_{\text{S}}(\omega, t, l_1, l_2) \mathrm{d}\omega \tag{4.8}$$

where $C_{\text{S}}(\omega, t, l_1, l_2)$ is the characteristic function given as

$$C_{\text{S}}(\omega, t, l_1, l_2) = \exp\left(-\frac{\lambda_{\text{U}}}{\Delta} \int_0^\infty \left[1 - \exp\left(j\omega P_{\text{U}} K_{\text{U}} (a + \frac{l_1}{2} + vt)^{-\alpha}\right)\right] \mathrm{d}a\right) \cdot \exp\left(-\frac{\lambda_{\text{U}}}{\Delta} \int_0^\infty \left[1 - \exp\left(j\omega P_{\text{U}} K_{\text{U}} (a + l_2 + \frac{l_1}{2} - vt)^{-\alpha}\right)\right] \mathrm{d}a\right) \tag{4.9}$$

N_0 is the noise power, B is the total bandwidth and v is the velocity.

Proof. See Appendix B.2. □

Cache-enabled HO Scheme: We derive the analytical expressions for cache time t_{C} and average rate R_{ca} for cache-enabled network, with the cache size of G bits. When the MT with limited local cache enters C_{R} and starts caching the data, the time at which the MT reaches its maximum caching capacity is denoted by t_{F}, i.e., the time at which the cache is full and the amount of bits cached is equal to G bits. As referred before, t_{C} is the time MT travels without initiating the HOs and making use of this cached data outside C_{R}. Let t_{R} be the time MT takes to move through the entire caching region C_{R} with a velocity v. Therefore, $t_{\text{R}} = \frac{2r}{v}$. The amount of data bits cached is the difference between the downloaded and played data bits. Therefore, it can be derived numerically as a solution to the following

equation.

$$\int_0^{t_{\mathrm{F}}} \left[B \log_2 \left(1 + \frac{P_{\mathrm{U}} K_{\mathrm{U}}}{(N_0 + I)(|r - vt|)^{\alpha}} \right) - p \right] dt = G. \tag{4.10}$$

- Limited Cache Size

  The cache time t_{C} for the cache-enabled network with limited cache is evaluated for two conditions such as:

  1. $t_{\mathrm{F}} < t_{\mathrm{R}}$.

     There is not enough cache memory left before the MT crosses the caching region C_{R}.

  2. $t_{\mathrm{F}} \geq t_{\mathrm{R}}$.

     There is enough cache memory left even after the MT crosses the caching region C_{R}.

  The cache time t_{C} for a cache-enabled network with a limited cache size of G bits at the MT is given as the solution to the given equation.

$$\begin{array}{ll} G + \int_{t_{\mathrm{R}}}^{t_{\mathrm{C}}} B \log_2 \left(1 + \frac{P_{\mathrm{U}} K_{\mathrm{U}} (|r - vt|)^{-\alpha}}{(N_0 + I(t))} \right) \mathrm{d}t = p(t_{\mathrm{C}} - t_{\mathrm{R}}) & t_{\mathrm{F}} < t_{\mathrm{R}}. \\ \int_0^{t_{\mathrm{C}}} B \log_2 \left(1 + \frac{P_{\mathrm{U}} K_{\mathrm{U}} (|r - vt|)^{-\alpha}}{(N_0 + I(t))} \right) \mathrm{d}t = p t_{\mathrm{C}} & t_{\mathrm{F}} \geq t_{\mathrm{R}}. \end{array} \tag{4.11}$$

  $I(t)$ is the sum of the received powers from the interferes experienced by the MT at time t for a given spatial realization. It is challenging to solve a closed-form expression for t_{C}. Hence, using numerical integration, we solve for the cache time t_{C} in (4.11), by rearranging the equation, substituting the parameter values, and performing the integration to compute t_{C} for each condition. We know the next associated UAV-AP is at a distance of D from the associated UAV-AP. Then, cache time t_{C} is given as

$$t'_{\mathrm{C}} = \min \left\{ t_{\mathrm{C}}, \frac{D}{v} \right\}. \tag{4.12}$$

  The caching distance, the distance at which the typical MT skips the unnecessary HOs, is represented as

$$d_{\mathrm{C}} = t'_{\mathrm{C}} v \tag{4.13}$$

Remark: From (4.11), it is observed that t_{C} depends on the interference and is spatially averaged later. Consequently, the cache distance d_{C} becomes interference-dependent and is denoted as $d_{\mathrm{C}}(I)$, with the constraint $d_{\mathrm{C}}(I) \leq D$.

- Unlimited Cache Size

  For unlimited cache size, i.e $G = \infty$, the time at which MT reaches its maximum capacity G is t_{F}, which in this case is infinite. Therefore, t_{F} is always greater than t_{R}. Therefore, t_{C} is given as

$$\int_0^{t_{\mathrm{C}}} B \log_2 \left(1 + \frac{P_{\mathrm{U}} K_{\mathrm{U}} (|r - vt|)^{-\alpha}}{(N_0 + I(t))}\right) \mathrm{d}t = p t_{\mathrm{C}}. \tag{4.14}$$

In order to derive the average rate experienced by the MT for a cache-enabled HO scheme, we divide the distance traveled by the MT into two:

1. The caching distance d_{C}
2. The distance d_L traveled by the MT after the caching distance, before entering the caching region of the next associated UAV-AP.

Throughout the caching distance d_{C}, the MT plays at the required play rate. Therefore, the average rate experienced by the MT throughout the caching distance is the required play rate. After the caching distance before entering the caching region of the next associated UAV-AP, the MT travels for a distance of d_{L}. The value of d_{L} depends on the location of the next associated UAV-AP, D, which is random. Therefore, d_{L} is also random, which is given as

$$d_{\mathrm{L}} = \begin{cases} D - d_{\mathrm{C}} & d_{\mathrm{C}} < D \\ 0 & d_{\mathrm{C}} = D. \end{cases} \tag{4.15}$$

Next, we derive the PDF of d_{L}.

Lemma 4.3. *The PDF of d_{L} conditioned on the interference power I is given by*

$$f_{d_{\mathrm{L}}|\mathrm{I}}(z \mid y) = \sum_{n=0}^{\infty} \exp\left(-2\frac{\lambda_{\mathrm{U}}}{\Delta}(z + d_{\mathrm{C}}(y))\right) \cdot \frac{\left(2\frac{\lambda_{\mathrm{U}}}{\Delta}(z + d_{\mathrm{C}}(y))\right)^{n+1}}{(z + d_{\mathrm{C}}(y))\,\Gamma(n+1)} \cdot \frac{\exp\left(-\frac{\lambda_{\mathrm{U}}}{\Delta} d_{\mathrm{C}}(y)\right)\left(\frac{\lambda_{\mathrm{U}}}{\Delta} d_{\mathrm{C}}(y)\right)^{n}}{n!}, \quad (4.16)$$

where n is assumed to be the number of HOs skipped for a distance of d_{C}, and it follows the distribution of the number of points in a PPP [61].

Proof. See Appendix B.3. □

Lemma 4.4. *The average rate experienced by the MT in a cache-enabled UAV-based network is given as*

$$R_{\mathrm{ca}} = \int_0^{\infty} R_2(y) f_{\mathrm{I}}(y) \mathrm{d}y, \quad (4.17)$$

$$R_2(y) \approx \int_0^{\infty} \frac{v}{(d_{\mathrm{C}}(y) + Z)} \left[\frac{p d_{\mathrm{C}}(y)}{v} + \int_0^{\mathrm{Z/v}} B \log_2\left(1 + \frac{P_{\mathrm{U}} K_{\mathrm{U}} / (N_0 + y)}{(Z + r - vt)^{\alpha}} f_{\mathrm{I}}(y,t) \mathrm{d}t\right)\right] f_{d_{\mathrm{L}}}(Z) \mathrm{d}Z. \quad (4.18)$$

where $Z = d_{\mathrm{L}}(y)$ is a function of the interference power y, experienced by the user at time t, $f_I(y,t)$ is the PDF of the total interference power at a given time t, p is the play rate and $f_{d_{\mathrm{L}}}(z)$ is derived in (4.16).

Proof. See Appendix B.4. □

4.1.2.3 Characterization of Handover Rate

In this section, we derive the handover rate experienced by the MT in a conventional and cache-enabled UAV-based network.

Lemma 4.5. *For a conventional HO scheme, expected number of HOs initiated by MT for 1D network is given as*

$$N_{\mathrm{co}} = \max\{\lambda_{\mathrm{U}} v T, 1\} - 1, \quad (4.19)$$

where T is the total time travelled by the MT and v is velocity.

Lemma 4.6. *For a cache-enabled HO scheme, the expected number of HOs initiated by the MT is given as*

$$N_{\mathrm{ca}} = N_{\mathrm{co}} - \lambda_{\mathrm{U}}(\max\{d_{\mathrm{C}}, r\} - r), \tag{4.20}$$

where r is half of caching region distance of the UAV-AP which MT is associated to.

Proof. See Appendix B.5. □

4.1.2.4 Handover Time Overhead

In this section, we discuss the time overheads corresponding to each operation during a BS handover.

1. We assume the MT initiates a cell search procedure every 20 ms, aligned with the periodic transmission interval of the synchronization signal block (SSB) bursts. An SSB burst consists of primary and secondary synchronization signals (PSS and SSS) along with the physical broadcast channel (PBCH), enabling the MT to achieve time/frequency synchronization and obtain essential cell information. This is one of the values specified by the 3GPP standard [62], [63].

2. The assumed RRC (radio resource control) processing delay is 3 ms.

3. The assumed handover processing delay for the Random Access Channel (RACH) procedure is 20 ms.

Therefore, the handover time overhead t_H for a UAV-AP handover is 43 ms [64].

4.1.2.5 Effective Average Rate

We derive the effective average rate considering the effect of HO rate and the time overhead for each HO on the average rate experienced by the MT.

Lemma 4.7. *The effective average rate of a conventional HO scheme is given as [64].*

$$R_{\mathrm{eco}} = R_{\mathrm{co}}(1 - \mu_{\mathrm{co}} t_{\mathrm{H}})^{+}, \tag{4.21}$$

where $(1-\mu_{\text{co}}t_H)^+ = \max(0,(1-\mu_{\text{co}}t_{\text{H}}))$, μ_{co} *is the HO rate for conventional HO scheme given as* $\mu_{\text{co}}=\frac{N_{\text{co}}}{T}$, t_{H} *is the handover time overhead and* R_{co} *is given in (4.6).*

Lemma 4.8. *The effective average rate of a cache-enabled HO scheme is given as*

$$R_{\text{eca}} = R_{\text{ca}}(1-\mu_{\text{ca}}t_{\text{H}})^+. \tag{4.22}$$

μ_{ca} *is the HO rate for cache-based HO scheme given as* $\mu_{\text{ca}}=\frac{N_{\text{ca}}}{T}$ *and* R_{ca} *is given in (4.17).*

4.1.2.6 Power Consumption Model

In our work, the total power consumption in the network consists of power consumption for caching, power consumption for frequent inter-frequency handovers, and transmit power required at the UAV-APs [65].

- **Power consumption for caching:** We consider a power-proportional model [66], where the total power consumed for caching depends on the amount of data being cached at the MT and the caching power efficiency w_{c}. Caching power efficiency is the power consumed for caching one bit of data. It depends on the caching technology employed at MT. In this work, we consider a high-speed solid state disk (SSD) will be employed for storing the cached data, whose power efficiency is given as $6.25\text{x}10^{-12}$ watt/bit [67]. Therefore, the total power consumed for caching is given as $P_{\text{C}} = Gw_{\text{c}}$, where G is the cache size and w_c is the power efficiency of caching.

- **Power consumption for Inter-frequency Measurements:** For every HO happening in the network, a certain amount of energy is consumed by the MT for inter-frequency measurements. The amount of energy consumed for one inter-frequency measurement is E_{I}=3 mJ [68]. Therefore, the total power consumed for inter-frequency measurements is given as $P_{\text{I}} = HE_{\text{I}}$, where H is the expected number of HOs initiated by the MT per unit time.

Hence, the total power consumed in the network is given as $P_{\text{TC}} = P_{\text{U}} + P_{\text{I}} + P_{\text{C}}$.

4.1.2.7 Results and Discussions

In this section, we validate our analytical framework using Monte-Carlo simulations, providing a precise analysis equivalent to executing experiments, and present some numerical results to discuss the salient features of the network. The conventional scheme is taken as the benchmark here. The simulation parameters are shown in Table 4.1.

Table 4.1: Simulation Parameters

Notation	Parameter	Value
P_{U}	Transmit power	35 dBm
λ_{U}	Intensity of UAV-AP	1 Km^{-1}
B	Bandwidth of the system	100 MHz
α	Path-loss Exponent	2
f_{c}	Carrier frequency	3.5 Ghz
σ^2	Noise density	-174 dBm/Hz.
p	Play rate	2 Gbps.
t_{H}	Handover time overhead	43 ms.
t_{S}	Search time	20 ms.

Trends in Handover Rate

Figure 4.3 shows that the analytical result on the HO rate closely matches the Monte-Carlo simulations. We observe that as the intensity of UAV-APs increases, HO rate increases. For lower intensity values, the expected number of handovers or the handover rate for the cache-enabled scheme and the conventional scheme is the same. However, for higher values of intensity, the cache-enabled scheme experiences less HOs compared to the benchmark scheme because unnecessary HOs are skipped in the proposed model.

Trends in Effective Average Rate

In Figure 4.4 and Figure 4.7, we plot the effective average rate versus intensity of UAV-APs for interference-dependent and noise-limited scenarios, respectively. In Figure 4.4, we plot the derived analytical expressions for the average rate considering the distribution of the total interference power at a given time instant. This serves as an upper bound, since the impact of interference within the caching region r is not accounted for. Here, we

show that the analytical result on the effective average rate closely matches the Monte-Carlo simulations.

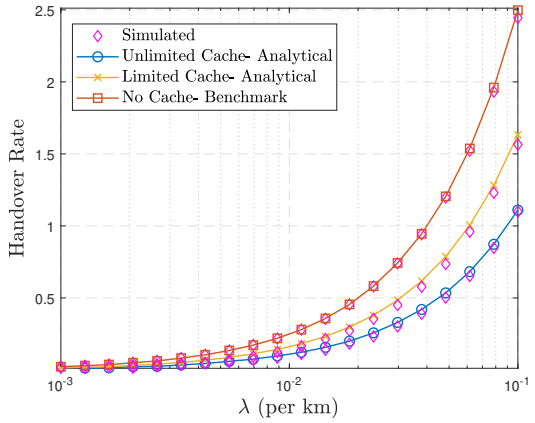

Figure 4.3. Handover rate versus Intensity of UAV-APs

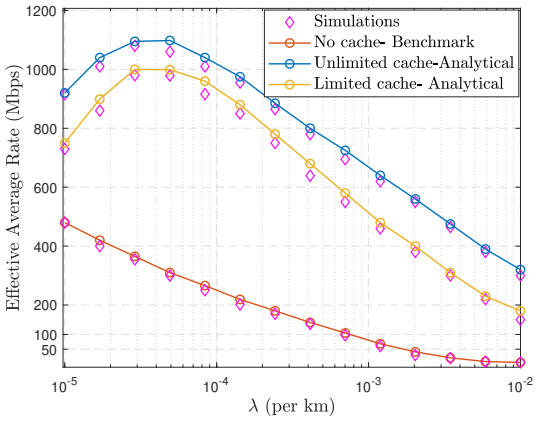

Figure 4.4. Effective average rate versus Intensity of UAV-APs for interference-dependent network for v=25 m/s

In both Figure 4.4 and Figure 4.7, we observe that for lower values of intensity, the effective average rate increases, and the intensity of UAV-APs increases. This is because there is less number of HOs for lower intensity values. After a particular value of intensity (defined as the optimal value), the effective average rate starts to decrease because of the increase in the number of HOs, leading to an increase in HO time overhead. This would help the network operator decide on the optimal deployment densities to obtain the maximum average rate for different cache sizes of the proposed scheme.

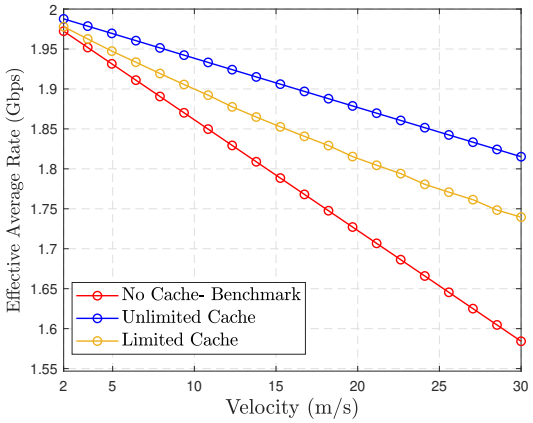

Figure 4.5. Effective average rate versus velocity of MT for $\lambda = 10^{-3}$

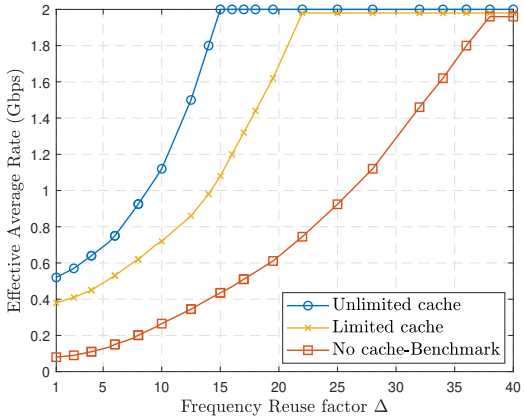

Figure 4.6. Effective average rate versus Frequency reuse factor Δ for λ=10^{-3} and v=25 for probabilistic scheme

In Fig. 4.5, we plot the effective average rate versus velocity of typical MT for the noise-limited network. As velocity increases, the effective average rate decreases because of the increase in HO rate with velocity. We observe that, for pedestrian users, e.g., the velocity of 5m/s, we obtain a high value of average rate compared to vehicular users, e.g., the velocity of 25 m/s, for a specific set of parameters. We also observe that skipping unnecessary HOs through the cache-enabled scheme is expendable for pedestrian users. This is because for a particular value of intensity and the lower values of velocity, the number of HOs skipped will be significantly less, indicating the performance is the same as that of the conventional scheme. However, for higher velocity values, the cache-enabled scheme performs better than the conventional scheme because of skipping more HOs.

In Fig. 4.6, we plot the effective average rate versus the frequency reuse factor Δ for the probabilistic frequency reuse scheme. Here, we observe that as Δ increases, the effective average rate increases. For an unlimited cache scenario, any values of Δ greater than 14 give the same performance as the noise-limited network for a fixed play rate. While for limited cache, the Δ value is 22, and for the benchmark scheme, it is 38. We obtain an optimal Δ for different cache sizes at the MT.

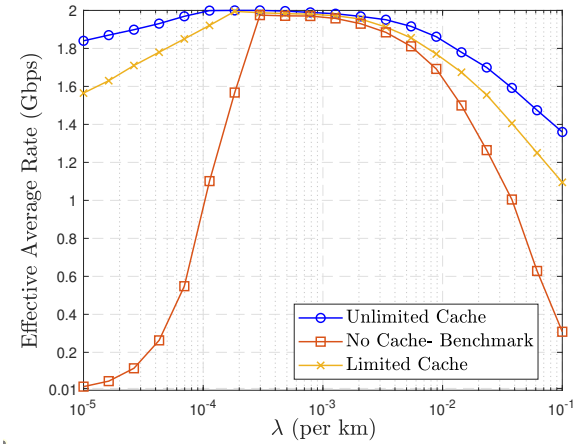

Figure 4.7. Effective average rate versus intensity of UAV-AP for noise-limited network for v=25 m/s

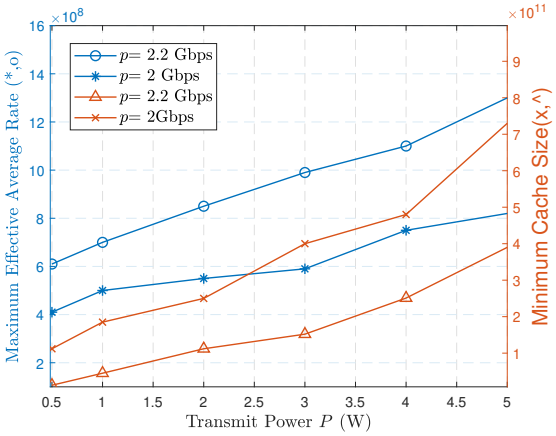

Figure 4.8. Maximum effective average rate for minimum cache size versus transmit power P for λ_U=10^{-3} and v=25 for interference-dependent network.

Figure 4.8 shows the minimum cache size required for obtaining the maximum effective average rate for different values of play rate p for an interference-dependent network, respectively. We observe that as the play rate increases, the cache size needed to obtain the maximum average rate decreases. This is because if the play rate is high, the amount of data stored in the cache reduces even though it experiences a high average rate. For the network operator, this reveals how our framework helps to decide the cache limit and transmit power of the UAV-APs for the MT to play the videos at a particular play rate. For instance, if the MT has a cache size of 32 GB and plays the video at the rate of 2.2 Gbps, the maximum average rate experienced by the MT will be 2.1 Gbps for a downlink transmit power of 3 W. In an interference-dependent network, we observe an increase in the cache size in order to include the effect of interference given in Figure 4.8. So, the minimum cache size for the network has increased to obtain the maximum average rate. This is because of a decreased downloaded data at the MT, which requires more cache to obtain the maximum rate.

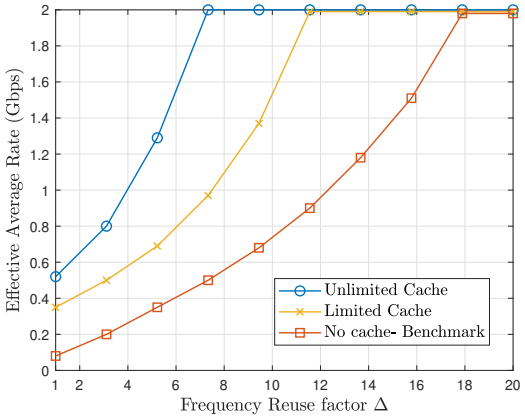

Figure 4.9. Effective Average Rate versus Frequency reuse factor Δ for coordinated scheme

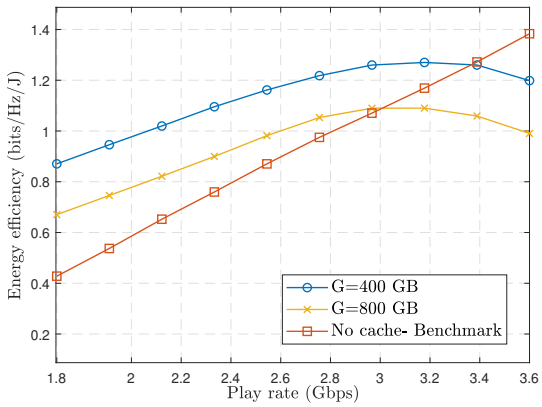

Figure 4.10. Energy Efficiency versus play rate for $\lambda_U = 10^{-3}$, v=25 for interference-dependent network

In Figure 4.9, we plot the effective average rate versus Δ for a coordinated operation between the UAV-AP. We observe that there is a significant decrease in the optimal value of Δ because of the reduction in the interference power experienced by the MT in the network. We conclude that coordinated transmission reduces interference in the network. However, because of analytical intractability, we implement the probabilistic frequency reuse scheme. This provides valuable insights to the network operator to determine the minimum number of frequency bands to be allocated to the UAV-APs.

Trends in Energy Efficiency

In Figure 4.10, we plot energy efficiency in the network, considering the total power consumption in the network, for different values of play rate p of the MT. We observe a preferred play rate for an improvement in the performance of the proposed network in an interference-dependent scenario. Also, we observe that for lower values of cache size, there is a maximum range of play rate the MT can experience in the proposed method, giving an improved performance compared to the benchmark scheme. As cache size increases, the maximum range of play rate reduces. In fact, for $G = 400$ GB, the MT can play at the rate from 1.8 Gbps to 3.3 Gbps for improved performance in terms of energy efficiency by a factor of almost 20%. But, for $G = 800$ GB, the play rate range is reduced to 1.8 Gbps-3 Gbps for this improved performance.

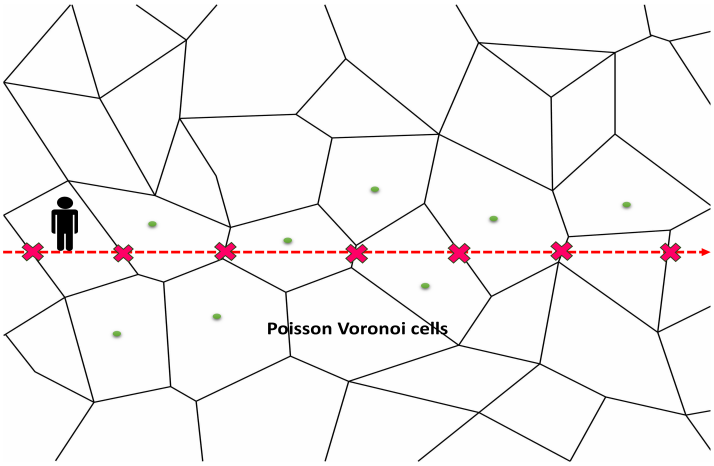

Figure 4.11. A snapshot of a Poisson cellular network with cell boundaries formed by the UAV-APs at bounded random heights. The red line is the trajectory of the user. Red Cross: BS handover locations, Green dot: 2-D locations of UAVs, which are modeled as 2-D PPP.

4.1.3 Handover Management in 2-D MPPP UAV Network

We consider a downlink UAV-based network deployed for scenarios where the users have lost cellular connectivity due to the breakdown of TBSs. The network consists of UAV-APs modelled as a 2-D homogeneous PPP, Φ_{U} on $\mathbb{R}^2$, with intensity λ_{U}. Each point of Φ_{U} has an associated mark representing the height of the UAVs. We assume the marks are uniformly distributed between $h_{\min}$ and $h_{\max}$. Each UAV-AP has a reliable backhaul connection to the core network. We assume the user moves on the ground along a randomly oriented straight line with speed v and performs a handover at every cell boundary is given in Figure 4.11. The downlink transmissions experience small-scale Rayleigh fading g, with a variance of 1. Since the UAV-APs are at random heights, the cell boundaries are formed by weighted Poisson Voronoi tessellation in the 2-D plane, and the HOs are inter-tier HOs. Let τ be the set of all cell boundaries between the UAV-APs. The number of HOs the user experiences is the number of intersections between the user trajectory $\mathcal{L}$ and τ.

4.1.3.1 Poisson Voronoi Tessellation

Poisson voronoi tessellation is a spatial partitioning method where a plane is divided into regions based on a PPP. In Poisson voronoi tessellation, each point from the PPP generates

a region called a Voronoi cell, which consists of all points in the plane closer to that specific point than to any other point in the process.

Given a homogeneous PPP Φ_{U} with intensity λ_{U} in $\mathbb{R}^2$, the Voronoi cell associated with a point $X \in \Phi_{\mathrm{U}}$ is:

$$V(x) = \{y \in \mathbb{R}^2 : ||y - X|| \leq ||y - X'||, \forall X' \in \Phi_{\mathrm{U}}, X' \neq X\} \tag{4.23}$$

Each Voronoi cell consists of all points closer to X than to any other point in Φ.

4.1.3.2 Characterization of HO rate

Let us assume that a typical user is at the origin $\mathbf{0} = (0, 0)$ and that it is associated with a UAV-AP at a location $\mathbf{z} = (b_0, 0, h_1)$. We consider a neighbouring UAV-AP to the serving UAV-AP, which is located at $\mathbf{x}_0 = (x_0, y_0, h_2)$. As mentioned earlier, τ is the set of cell boundaries of the BSs, i.e., it is the set of points on $\mathbb{R}^2$ where the same received power level is received from two neighboring UAV-APs. Therefore, τ is the trace of these cell boundaries satisfying the following,

$$\tau(\mathbf{z}, \mathbf{x}_0) = \left\{(x, y) \,\middle|\, (x - b_0)^2 + y^2 + h_1^2 = (x - x_0)^2 + (y - y_0)^2 + h_2^2\right\}. \tag{4.24}$$

Let the length intensity of the cell boundary be denoted by $\mu(\tau)$, which is the expected length of τ in a unit square [69]. From [70], the expected number of HOs per unit time is $H_{\mathrm{r}} = \frac{1}{\pi}\mu(\tau)v$. As it is difficult to quantify the 1-D measure $\mu(\tau)$, we consider a Δd extended version of 1-D measure, referred as the area intensity of the cell boundaries. Therefore, Δd extended cell boundary, denoted by $\tau^{\Delta \mathrm{d}}$ is the neighborhood of τ. A point is in $\tau^{\Delta \mathrm{d}}$ if the distance between the point and τ is less than Δd. Therefore, the area intensity of $\tau^{\Delta \mathrm{d}}$, denoted by $\mu(\tau^{\Delta \mathrm{d}})$ is the average area of $\tau^{\Delta \mathrm{d}}$ in a unit square. This is equivalent to the probability that the typical user at $\mathbf{0}$ is at the Δd extended cell boundary, $\mu(\tau^{\Delta \mathrm{d}}) = \mathbb{P}\left(\mathbf{0} \in \tau^{\Delta \mathrm{d}}\right)$.

To derive the area intensities of cell boundaries, we study the probability that the typical user at the origin is on $\tau^{\Delta \mathrm{d}}$, given that the associated UAV-AP is positioned at $\mathbf{b}_0$, where

the Euclidean distance from the user is b_0 and height h_1.

Lemma 4.9. *The conditional probability that the typical user is associated with a UAV-AP, which is at a distance of R and height H, is given as*

$$\mathbb{P}\left(0 \in \tau^{\Delta \mathrm{d}} | R = b_0, H = h_1\right) = \frac{2\lambda_{\mathrm{U}} \Delta d}{(h_{\max} - h_{\min})} \mathcal{F}(b_0, h_1), \tag{4.25}$$

$$\mathcal{F}(b_0, h_1) = \int_{h_{\min}}^{h_{\max}} \int_0^{2\pi} \left[2b_0^2 + h_1^2 + h_2^2 - 2b_0 \cos\theta \sqrt{b_0^2 + h_1^2 - h_2^2}\, \mathrm{d}\theta\, \mathrm{d}h_2\right]^{\frac{1}{2}}. \tag{4.26}$$

Proof. See Appendix B.6. □

Unconditioning (4.25), we obtain the unconditional probabilities that the typical user at **0** is in $\tau^{\Delta \mathrm{d}}$.

Lemma 4.10. *The area intensities of the cell boundaries.*

$$\mu(\tau^{\Delta \mathrm{d}}) = \int_{h_{\min}}^{h_{\max}} \int_0^{\infty} \frac{2\lambda_{\mathrm{U}} \Delta \mathrm{d}}{(h_{\max} - h_{\min})} \mathcal{F}(x, y) f_{\mathrm{b_0,h_1}}(x, y) \mathrm{d}x \mathrm{d}y, \tag{4.27}$$

where $f_{\mathrm{b_0,h_1}}(x, y)$ is the joint PDF of b_0 and h_1 which is obtained through simulations.

The length intensity of the cell boundaries is obtained by taking $\Delta \mathrm{d} \to 0$ in (4.27). From [70], $\mu(\tau) = \lim_{\Delta \mathrm{d} \to 0} \frac{\mu(\tau^{\Delta \mathrm{d}})}{2\Delta \mathrm{d}}$. Substituting this, we can obtain the expected number of HOs per unit time. Substituting $h_1 = h_2$ in (4.26) and following the same steps, we obtain the analytical expression of HO rate of fixed-h scenario.

4.1.3.3 Characterization of Success Probability

The success probability for the typical user, $\mathcal{P}_{\mathrm{suc}}$, is defined as the probability that the received SINR at the typical user is greater than a predefined SINR threshold. Without loss of generality, due to the ergodicity property of PPP [7], we perform the downlink analysis from the perspective of a typical user located at the origin. In order to evaluate the success probability, we find the distance distribution of the nearest UAV-AP from the typical user.

Lemma 4.11. *The PDF of the distance of the nearest UAV-AP from the typical user, where the UAV-AP are distributed as a marked PPP and marks uniformly distributed from $h_{\min}$ to*

$h_{\max}$, *is given as*

$$f_{\mathrm{Z}}(z)=\begin{cases}\frac{2\pi\lambda_{\mathrm{U}}(z^2-zh_{\min})}{(h_{\max}-h_{\min})}\exp\left(\frac{-\pi\lambda_{\mathrm{U}}\left(\frac{2}{3}z^3-z^2h_{\min}+\frac{h_{\min}^3}{3}\right)}{(h_{\max}-h_{\min})}\right); & h_{\min}\leq z<h_{\max}\\ 2\pi\lambda_{\mathrm{U}}z\exp\left(\frac{-\pi\lambda_{\mathrm{U}}\left(z^2(h_{\max}-h_{\min})+\frac{h_{\min}^3-h_{\max}^3}{3}\right)}{(h_{\max}-h_{\min})}\right); & z\geq h_{\max}.\end{cases} \tag{4.28}$$

Proof. See Appendix B.7. □

Leveraging this, we derive the success probability of the typical user as given in the following lemma.

Lemma 4.12. *The SINR coverage probability P_{C} of the typical user associated with the nearest UAV-AP at a height that is uniformly distributed between $h_{\min}$ and $h_{\max}$ and SINR threshold of γ is given as*

$$\mathcal{P}_{\mathrm{suc}}(\gamma)=\begin{cases}\int_{h_{\min}}^{h_{\max}}\exp\left(\frac{-\gamma N_0}{K_{\mathrm{U}}P_{\mathrm{U}}z^{-2}}-2\pi\lambda_{\mathrm{U}}(A+B)\right)\mathrm{d}z, & h_{\min}\leq z<h_{\max}\\ \int_{h_{\max}}^{\infty}\exp\left(\frac{-\gamma N_0}{K_{\mathrm{U}}P_{\mathrm{U}}z^{-2}}-2\pi\lambda_{\mathrm{U}}(C+D)\right)\mathrm{d}z, & z\geq h_{\max}\end{cases} \tag{4.29}$$

where,

$$A=\int_0^{\sqrt{z^2-h_{\min}^2}}\left(1-\left[\int_{\sqrt{z^2-x^2}}^{h_{\max}}\frac{1}{1+\frac{\gamma(\sqrt{x^2+t^2})^{-2}}{z^{-2}}}\cdot\frac{1}{(h_{\max}-\sqrt{z^2-x^2})}\mathrm{d}t\right]\right)x\mathrm{d}x. \tag{4.30}$$

$$B=\int_{\sqrt{z^2-h_{\min}^2}}^{\infty}\left(1-\left[\int_{h_{\min}}^{h_{\max}}\frac{1}{1+\frac{\gamma(\sqrt{x^2+t^2})^{-2}}{z^{-2}}}\cdot\frac{1}{(h_{\max}-h_{\min})}\mathrm{d}t\right]\right)x\mathrm{d}x. \tag{4.31}$$

$$C=\int_{\sqrt{z^2-h_{\max}^2}}^{\sqrt{z^2-h_{\min}^2}}\left(1-\left[\int_{\sqrt{z^2-x^2}}^{h_{\max}}\frac{1}{1+\frac{\gamma(\sqrt{x^2+t^2})^{-2}}{z^{-2}}}\cdot\frac{1}{(h_{\max}-\sqrt{z^2-x^2})}\mathrm{d}t\right]\right)x\mathrm{d}x. \tag{4.32}$$

$$D=\int_{\sqrt{z^2-h_{\min}^2}}^{\infty}\left(1-\left[\int_{h_{\min}}^{h_{\max}}\frac{1}{1+\frac{\gamma(\sqrt{x^2+t^2})^{-2}}{z^{-2}}}\cdot\frac{1}{(h_{\max}-h_{\min})}\mathrm{d}t\right]\right)x\mathrm{d}x. \tag{4.33}$$

Proof. See Appendix B.8. □

The average rate per user can be expressed in terms of the SINR coverage probability,

which is given as

$$R = \frac{B}{N_{\mathrm{u}}} \int_0^{\gamma_{\max}} \frac{\mathcal{P}_{\mathrm{suc}}(s)}{(s+1)} \mathrm{d}s, \tag{4.34}$$

where $\gamma_{\max}$ is the limit on the maximum achievable SINR defined [64], which depends on the modulation schemes and RF imperfections, $\mathcal{P}_{\mathrm{suc}}(\gamma)$ is given in (4.29), B is the total bandwidth and N_u is the number of ground users.

Proof.

$$R = \frac{B}{N_{\mathrm{u}}} \int_0^{\gamma_{\max}} \mathbb{P}\left(\ln\left(1 + \min(P_{\mathrm{suc}}, \gamma_{\max})\right) > s\right) \mathrm{d}s. \tag{4.35}$$

$$R = \frac{B}{N_{\mathrm{u}}} \int_0^{\gamma_{\max}} P_{\mathrm{suc}}(e^s - 1) \mathrm{d}s. \tag{4.36}$$

□

Next, we derive the effective average rate considering the HO rate and time overhead for each HO [71].

Lemma 4.13. *The effective average rate experienced by the user is given as*

$$R_{\mathrm{e}} = R(1 - H_{\mathrm{r}} t_{\mathrm{H}})^{+}, \tag{4.37}$$

where $(1 - H_{\mathrm{r}} t_{\mathrm{H}})^{+} = \max(0, (1 - H_{\mathrm{r}} t_{\mathrm{H}}))$ *and* t_{H} *is the BS handover time overhead.*

4.1.3.4 Results and Discussions

In this section, we validate our analytical framework and present numerical results to discuss the salient features of the network. The parameters are $P_{\mathrm{U}} = 33$ dBm [72], $\alpha = 2$, $v = 1$ m/s, $h_{\min} = 100$ m, $h_{\max} = 300$ m, B= 100 MHz.

In Figure 4.12(a), we plot the HO rate experienced by the user versus the intensity of BSs, λ_U for different values of the velocity of the user. We observe that as the intensity of UAV-APs increases, randomizing the heights within a bound experiences fewer HOs compared to fixing the height of BSs. Moreover, as the velocity of the user increases, the HO rate increases since more cell boundaries are crossed. We show that the derived analytical results closely match the Monte-Carlo simulations.

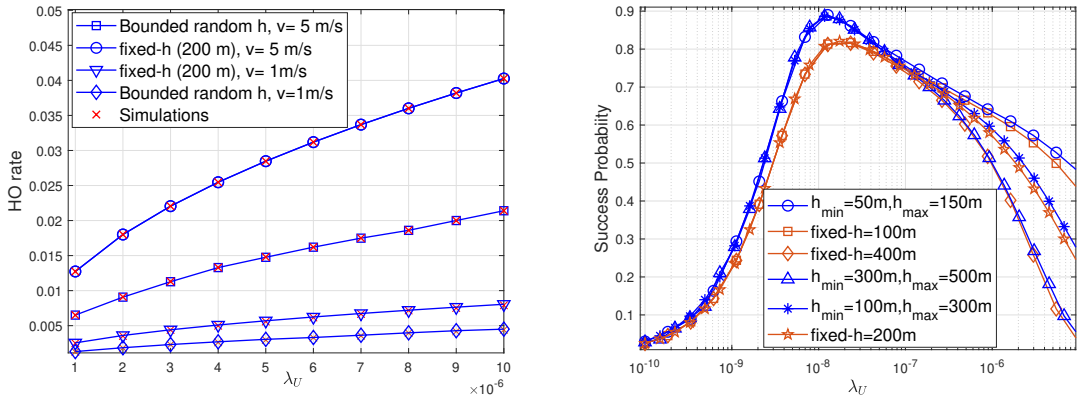

(a) (b)

Figure 4.12. Variation with intensity of UAV-APs a) Handover rate (b) SINR coverage probability

In Figure 4.12(b), we plot SINR coverage probability versus intensity of BSs. We observe that randomizing heights within a bound provides better results than the fixed-h scenario for all intensity values for a given set of parameters. For lower values of intensity, as the deployment height of the UAVs increases, the interference and signal power have the same impact on the SINR experienced by the user. Since the signal power experienced by the user when UAVs are distributed as bounded random heights is high, it ensures more coverage. Suppose the UAV-APs are at lower heights for higher values of intensity. In that case, signal power impacts the SINR more than the interference power since the associated UAV-AP is closer to the user.

In Figure 4.13(a), we plot the effect of the intensity of BSs on the effective average rate experienced by the user. As the intensity of BSs increases, because of the increase in interference power, QoS experienced by the user decreases. However, varying heights of UAV-APs give improved average rate because of the decrease in HO rate in the network. In the random height scenario, the average rate per user consistently exceeds that of the fixed height scenario by at least 15%, even with an increase in the number of users in the network.

In Figure 4.13(b), we plot the fraction of BSs not used in the network versus the intensity of BSs. For the fixed-h scenario, there is zero resource non-utilization since the users will be associated with at least one BS. However, for bounded random heights, the BSs deployed at higher heights have a chance of not getting associated.

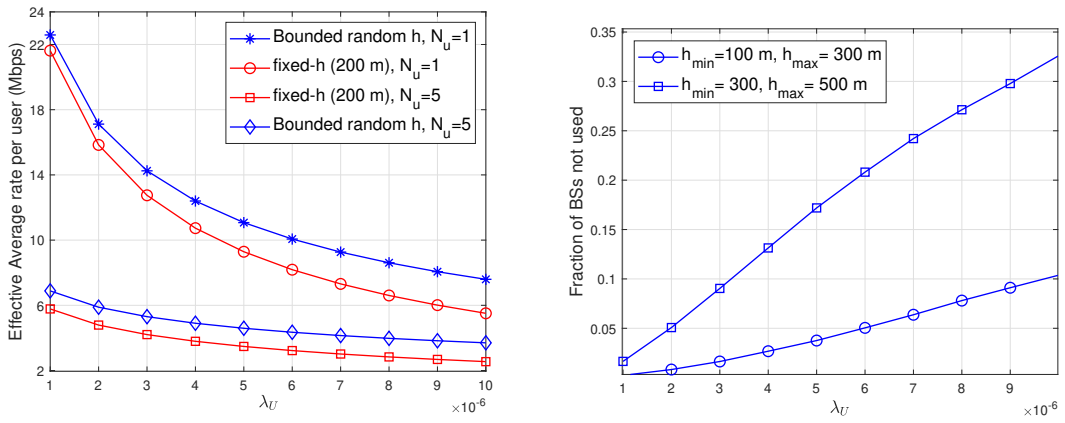

(a) (b)

Figure 4.13. (a) Effective average rate (b) Resource non-utilization

4.2 Fine Grained Analysis of Handover Management

In this section, we analyze the performance of mobile users in a UAV-based urban network with blockages. Specifically, we examine how deployment heights of UAV-APs, their spatial density, and the presence of blockages impact the reliability and latency experienced by ground users. This fine-grained analysis provides insights into the key factors that influence connectivity and service quality in urban UAV-enabled networks by maintaining the service demands of the users. We analyze the impact of blockages on network reliability by examining the MD of SINR, which is obtained from CSP. We propose a novel device caching method to skip unnecessary handovers and maintain the QoS at the user end.

The UAV-APs are modeled as a homogeneous 2-D (PPP), denoted by Φ_{U} on $\mathbb{R}^2$, with an intensity λ_{U}. Each point in Φ_{U} is associated with a mark representing the altitude of the corresponding UAV-AP, where the marks are uniformly distributed between $h_{\min}$ and $h_{\max}$, which forms an MPPP. Given that the altitudes of the UAV-APs are uniformly distributed between $h_{\min}$ and $h_{\max}$, the resulting cell boundaries in the 2-D plane are shaped by a weighted Poisson Voronoi tessellation. The illustration is given in Figure 4.14. Leveraging the stationarity and isotropy properties of the PPP [7], we focus on a single user moving in a straight line within a 2-D plane that intersects the origin, traveling at a constant velocity v.

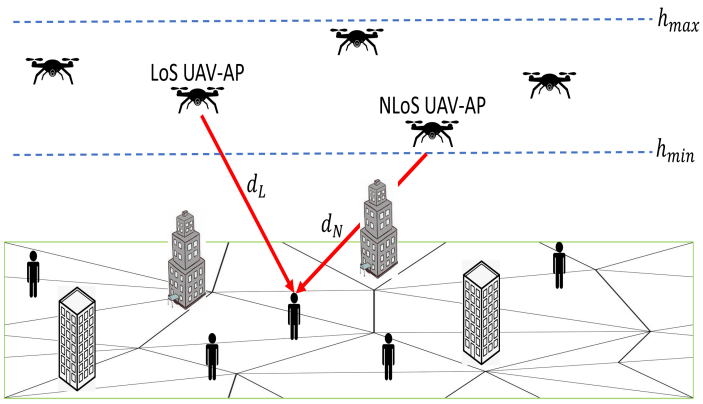

Figure 4.14. An illustration of the system model in which the user is served by either LoS or NLoS UAV-AP.

4.2.1 Blockage Process

The buildings are modeled as randomly positioned blockages using a Boolean scheme of random rectangles [73]. The centers of these blockages, denoted as C_{k}, form a homogeneous PPP Φ_{b} with intensity λ_{b}. By definition, the placement of blockages in the PPP is independent, ensuring that their geometries do not overlap. The lengths and widths of the blockages are assumed to be independent and identically distributed (iid), following the probability distributions $f_{\mathrm{L}}(l)$ and $f_{\mathrm{W}}(w)$, respectively. The intensity, length, and width of the blockages are selected such that a typical user moving in a straight line has zero probability of intersecting a blockage. The heights of the blockages are modeled by a Rayleigh distribution with a PDF $f_{\mathrm{H}}(h)$ [74].

The number of blockages, N, intersecting the 2-D LoS link between the user and the UAV-AP is a poisson-distributed random variable. From Figure 4.15, the parameter R_{b} represents the 2-D distance between the user and the UAV-AP, while y indicates the distance from the user to the point where a building intersects the link of length R_{b}. Given that N blockages intersect the link, their intersection points are uniformly distributed along the interval $[0, R_{\mathrm{b}}]$ [73], [69]. Consequently, y is a random variable following a uniform distribution over $[0, R_{\mathrm{b}}]$.

Lemma 4.14. *Given that a blockage intersects the 2-D link between the user and the UAV-*

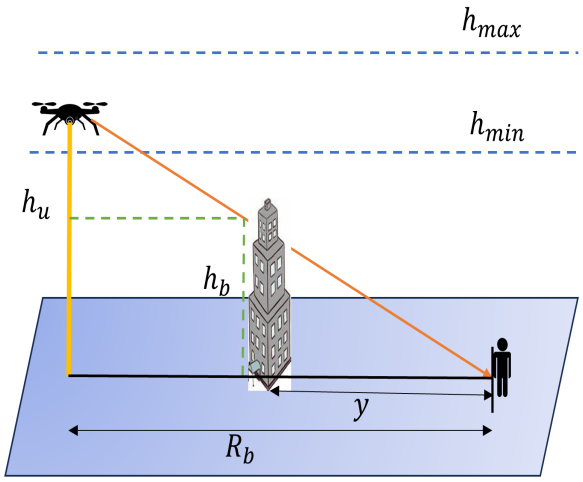

Figure 4.15. A building intersecting the 2-D link of length R_{b} between the user and UAV-AP intersects the 3-D link between user and UAV-AP at the altitude of h_{u} if and only if this altitude is greater than h_{b} as in the figure

AP of distance R_{b} at a height h_{u} as given in Figure 4.15, the conditional probability that it blocks the 3-D Euclidean link between the user and the UAV-AP is given as

$$\mathbb{P}(h > h_{\mathrm{b}} | y, h_{\mathrm{u}}) = 1 - \int_0^{\frac{yh_{\mathrm{u}}}{R_{\mathrm{b}}}} f_{\mathrm{H}}(h) dh, \tag{4.38}$$

where $h_{\mathrm{b}} = \frac{yh_{\mathrm{u}}}{R_{\mathrm{b}}}$. Marginalizing over y and h_{u},

$$\eta' = \frac{1}{(h_{\max} - h_{\min})} \int_{h_{\min}}^{h_{\max}} \int_0^1 \exp\left(-\frac{h^2 s^2}{2\sigma^2}\right) \mathrm{d}s\mathrm{d}h, \tag{4.39}$$

if and only if $R_{\mathrm{b}} > 0$.

Proof. See Appendix B.9. □

Remark: When $R_{\mathrm{b}} = 0$, the UAV-AP is located directly above the user. Substituting $R_{\mathrm{b}} = 0$ into (4.38), the conditional probability $\mathbb{P}(h > h_{\mathrm{b}} \mid y, h_{\mathrm{u}}) = 0$. Marginalizing over y and h_{u}, the unconditioned probability becomes $\eta' = 0$. The total number of blockages intersecting the 2-D link between the user and the UAV-AP is denoted by N. Since the blockages are modeled as a PPP, N is a Poisson random variable with a mean of $qR_{\mathrm{b}} + p$, where R_{b} represents the length of the 2-D link [73]. This can be expressed as:

$$\mathbb{E}[N] = qR_{\mathrm{b}} + p, \tag{4.40}$$

where $q = \frac{2\lambda_{\mathrm{b}}(\mathbb{E}[L_{\mathrm{b}}]+\mathbb{E}[W_{\mathrm{b}}])}{\pi}$ and $p = \lambda_{\mathrm{b}}\mathbb{E}[L_{\mathrm{b}}]\mathbb{E}[W_{\mathrm{b}}]$. Here, $\mathbb{E}[L_{\mathrm{b}}]$ and $\mathbb{E}[W_{\mathrm{b}}]$ are the average length and width of the blockages, respectively. The probability η' is independent of N, as the intersections form a PPP along the 2-D link of length R_{b}. Let $\bar{N}$ denote the number of blockages obstructing the 3-D link between the user and the UAV-AP. By applying independent thinning to N, the expected value of $\bar{N}$ is given by: $\mathbb{E}[\bar{N}] = \eta'\mathbb{E}[N]$.

4.2.2 Propagation Model

The UAV-APs can be either in LoS or NLoS state depending on visibility from the typical user. Let Φ_{L} represent the locations of LoS UAV-APs, and Φ_{N} represent the locations of NLoS UAV-APs. Therefore, the overall set of UAV-APs is given by $\Phi_{\mathrm{U}} = \Phi_{\mathrm{L}} \cup \Phi_{\mathrm{N}}$. LoS transmissions experience Nakagami-distributed fast-fading, denoted by G_{L}, with a shape parameter m [75]. In contrast, NLoS transmissions experience Rayleigh-distributed fast-fading, denoted by g_{N} with a unit variance. The downlink transmit power of the UAV-APs is P_{U}. Each UAV-AP can either be in an LoS or NLoS state relative to the typical user [16]. For large-scale path loss, the received power from the UAV-AP depends on its state (LoS or NLoS). For the large-scale path loss, we consider the received power at the typical user from the LoS UAV-AP which is at a distance of d_{L} is given by $R_{\mathrm{L}} = P_{\mathrm{U}}KG_{\mathrm{L}}d_{\mathrm{L}}^{-\alpha_{\mathrm{L}}}$ and the NLoS UAV-AP which is at a distance of d_{N} given as $R_{\mathrm{N}} = P_{\mathrm{U}}Kg_{\mathrm{N}}d_{\mathrm{N}}^{-\alpha_{\mathrm{N}}}$. α_{L} is the pathloss exponent for LoS links and α_{N} is the pathloss exponent for NLoS links.
Using (4.40) and the concept of void probability from stochastic geometry [7], the probability of establishing an LoS connection between the UAV-AP and the user is expressed as:

$$L_{\mathrm{S}}(d,h) = \exp\left(-\eta'(q\sqrt{d^2-h^2}+p)\right), \tag{4.41}$$

where h is the altitude of UAV-AP from the ground and d is the 3-D Euclidean distance between the UAV-AP and the user, according to the visibility state of the UAV-AP.

- LoS: $d = d_{\mathrm{L}}$, $\alpha = \alpha_{\mathrm{L}}$.

- NLoS: $d = d_{\mathrm{N}}$, $\alpha = \alpha_{\mathrm{N}}$.

Accordingly, the probability of NLoS transmissions is given as $N_{\mathrm{S}}(d,h) = 1 - L_{\mathrm{S}}(d,h)$. From (4.40), it is evident that the probability of establishing an LoS link between the UAV-AP and the user depends not only on the altitude and Euclidean distance but also on the intensity of blockages, the average length and width of the blockages, and their height.

4.2.3 Performance Metrics

The main factors driving 5G technology are reliability and latency, which form the foundation of ultra-reliable low-latency communications (URLLC) and support applications requiring real-time responsiveness and consistent performance. Considering this, we evaluate two critical performance metrics in a UAV network by analyzing the coverage probability or success probability experienced by the user. The first metric involves a fine-grained analysis of the SINR experienced by the user, offering detailed insights into the reliability of communication links. This approach transcends traditional average SINR evaluations by capturing link-level variability considering CSP. The second metric addresses handover management, leveraging caching capabilities at the user terminal to reduce unnecessary HOs leading to latency and QoS degradation during mobility.

- **MD of SINR:** To enable a detailed analysis of the SINR within a stationary and ergodic point process framework, we evaluate the MD of the SINR. The MD characterizes the distribution of the conditional success probability for a randomly selected user in the network. Unlike the mean SINR, which provides an aggregate measure, the MD offers a probabilistic perspective for assessing the reliability of communication links in a wireless network. It represents the CCDF of the success probability $\mathcal{P}_{\mathrm{suc}}(\gamma)$ is given as

$$\bar{F}_{P_{\mathrm{S}}}(\gamma, x_{\mathrm{r}}) = \mathbb{P}^{o}(\mathcal{P}_{\mathrm{suc}}(\gamma) \; > \; x_{\mathrm{r}}), \quad \gamma \in \mathbb{R}^{+}, \; x_{\mathrm{r}} \in [0,1], \tag{4.42}$$

  where $\mathbb{P}^{o}$ represents the reduced Palm probability conditioning the typical user at the origin o, x_{r} is the reliability threshold. The random variable $\mathcal{P}_{\mathrm{suc}}(\gamma)$ is given as

$$\mathcal{P}_{\mathrm{suc}}(\gamma) = \mathbb{P}(\mathrm{SINR} > \gamma | \Phi_{\mathrm{U}}, \Phi_{\mathrm{b}}). \tag{4.43}$$

- **Cache-enabled handover analysis:** Maintaining the required service rate is critical to ensuring continuous and uninterrupted QoS for users. However, when users are in motion, frequent handovers and potential handover failures can degrade QoS. In traditional cellular networks, handovers occur at every cell boundary, often causing excessive delays in communication. To address this, we propose a novel handover management strategy designed to minimize handovers and provide a seamless user experience, especially for applications such as autonomous driving, navigation, and video streaming. According to 3GPP standards [63], users perform a cell search every t_s seconds, and a handover is triggered when a neighboring UAV-AP offers a higher RSS than the currently associated UAV-AP. Measuring the RSS of neighboring cells requires ΔTseconds. To reduce latency, we dynamically adjust t_{s} by leveraging caching capabilities in the user equipment (UE) during motion. Each user is assumed to have a rate requirement of s_{r}, a cache size of G, and a velocity of v. Initially, the cache memory is empty. When the data downloaded by the user exceeds the required service rate s_r, the surplus data is stored in the cache. By utilizing this cached data, users can delay cell searches and avoid unnecessary handovers, thereby reducing latency and ensuring high QoS during mobility.

To evaluate these metrics, we derive the distance distribution of the associated UAV-AP relative to the typical user and analyze the success probability experienced by the user.

4.2.4 Distance Distribution and Association Probabilities

In this section, we obtain the distribution of the distance from a typical user to the nearest LoS or NLoS UAV-AP, where the locations of UAV-APs are distributed as a 2-D MPPP. The altitudes of the UAV-APs are uniformly distributed between $h_{\min}$ and $h_{\max}$.

Lemma 4.15. *Given that the typical user observes at least one LoS and one NLoS UAV-AP, the cumulative distribution function (CDF) for the distance distributions to the nearest LoS and NLoS UAV-AP distributed as a 2-D MPPP, defined as d_{L} and d_{N} respectively, are given*

as

$$F_{d_{\mathrm{L}}}(z) = \begin{cases} \left(1 - \exp\left(A \cdot \int_{h_{\min}}^{z} \mathcal{L}(z,h)\,\mathrm{d}h\right)\right)/B_{\mathrm{L}}; & h_{\min} \le z < h_{\max}. \\ \left(1 - \exp\left(A \cdot \int_{h_{\min}}^{h_{\max}} \mathcal{L}(z,h)\,\mathrm{d}h\right)\right)/B_{\mathrm{L}}; & z \ge h_{\max}. \end{cases} \tag{4.44}$$

$$F_{d_{\mathrm{N}}}(z) = \begin{cases} \left(1 - \exp\left(A \cdot \int_{h_{\min}}^{z} \mathcal{N}(z,h)\,\mathrm{d}h\right)\right); & h_{\min} \le z < h_{\max}. \\ \left(1 - \exp\left(A \cdot \int_{h_{\min}}^{h_{\max}} \mathcal{N}(z,h)\,\mathrm{d}h\right)\right); & z \ge h_{\max}. \end{cases} \tag{4.45}$$

Here $A = \frac{-2\lambda_{\mathrm{U}}\pi}{(h_{\max}-h_{\min})}$ *and* $\delta(z,h) = \sqrt{z^2-h^2}$*, if and only if* $R > 0$*.*

$$\mathcal{L}(z,h) = \frac{\exp\left(-p\eta\right) - L_{\mathrm{S}}(z,h)(q\eta\sqrt{z^2-h^2}+1)}{(q\eta)^2}. \tag{4.46a}$$

$$\mathcal{N}(z,h) = \frac{(z^2-h^2)}{2} - \mathcal{L}(z,h). \tag{4.46b}$$

Proof. See Appendix B.10. □

Remark: If $R_{\mathrm{b}} = 0$, when the UAV is exactly above the user, $L_{\mathrm{S}}(z,h) = 1$. Moreover, (4.46a) and (4.46b) will be replaced with $\mathcal{L}(z,h) = \frac{(z^2-h^2)}{2}$ and $\mathcal{N}(z,h) = 0$.

The functions of intensity and dimensions of blockages, p and q are defined in (4.40). B_{L} is the probability that there exists at least one LoS UAV-AP. Based on the blockage process considered in this paper, in high-blockage scenarios, The probability of having at least one LoS UAV-AP is not guaranteed to be one. Therefore, from [76], we derive the expression for B_{L} given as

$$B_{\mathrm{L}} = 1 - \exp\left(A \cdot \left[\int_{h_{\min}}^{h_{\max}} \int_{h_{\min}}^{z_1} \mathcal{L}(z_1,h_1)\mathrm{d}h_1\,\mathrm{d}z_1 + \int_{h_{\max}}^{\infty} \int_{h_{\min}}^{h_{\max}} \mathcal{L}(z_2,h_2)\mathrm{d}h_2\,\mathrm{d}z_2\right]\right). \tag{4.47}$$

However, given the blockage process, we observe that the probability of having at least one NLoS UAV-AP, considering they are distributed according to a PPP, is always one. Taking the derivative of (4.44) and (4.45) with respect to z, we obtain the PDF of the distance of the typical user from the nearest LoS and NLoS UAV-APs, given as, $f_{d_{\mathrm{L}}}(z)$ and $f_{d_{\mathrm{N}}}(z)$ respectively.

$$f_{d_{\mathrm{L}}}(z) = \begin{cases} f'_{d_{\mathrm{L}}}(z); & h_{\min} \le z < h_{\max} \\ f''_{d_{\mathrm{L}}}(z); & z \ge h_{\max} \end{cases} \tag{4.48}$$

Similar expressions are considered for $f_{d_{\mathrm{N}}}(z)$.

Next, we derive the association probabilities for LoS and NLoS UAV-APs. As previously mentioned, a typical user can connect to either a LoS or NLoS UAV-AP, depending on the maximum RSSI strategy.

Lemma 4.16. *The probability of association A_{N} of the typical user with an NLoS UAV-AP, when the UAV-APs are distributed as a 2-D MPPP, is given by:*

$$A_{\mathrm{N}} = \int_{h_{\min}}^{h_{\max}} \left[\exp\left(A \cdot \int_{h_{\min}}^{h_{\max}} \mathcal{L}(r_1^{\frac{\alpha_{\mathrm{N}}}{\alpha_{\mathrm{L}}}}, h_{\mathrm{a}})\, \mathrm{d}h_{\mathrm{a}} \right) \right] f'_{d_{\mathrm{N}}}(r_1)\mathrm{d}r_1 + \int_{h_{\max}}^{\infty} \left[\exp\left(A \cdot \int_{h_{\min}}^{h_{\max}} \mathcal{L}(r_2^{\frac{\alpha_{\mathrm{N}}}{\alpha_{\mathrm{L}}}}, h_{\mathrm{a}})\, \mathrm{d}h_{\mathrm{a}} \right) \right] f''_{d_{\mathrm{N}}}(r_2)\mathrm{d}r_2, \quad (4.49)$$

where $\mathcal{L}(z,h)$ can be obtained from (4.46a) and $A = \frac{-2\lambda_{\mathrm{U}}\pi}{(h_{\max}-h_{\min})}$.

Proof. See Appendix B.11. □

Naturally, the probability of LoS UAV-AP association $A_{\mathrm{L}} = 1 - A_{\mathrm{N}}$. This solution is valid when $\alpha_{\mathrm{N}} > \alpha_{\mathrm{L}}$ and $h_{\min} << h_{\max}$, which is feasible in practical scenarios. Otherwise, this analytical expression is intractable.

4.2.5 Meta Distribution of SINR

In this section, to obtain the MD of SINR, we derive the CSP experienced by the typical user associated with the LoS or NLoS UAV-AP, conditioned on the point processes Φ_{U} and Φ_{b}. Taking an expectation over the Φ_{U} and Φ_{b}, we calculate the b^{th} moment of the CSP, from which we can obtain the MD of SINR. Without loss of generality, leveraging the ergodicity property of the PPP [7], we conduct the downlink analysis from the perspective of a typical user situated at the origin.

4.2.5.1 Conditional Success Probability of LoS UAV-AP

The coverage probability or conditional success probability $P_{\mathrm{SL}}(\gamma)$ experienced by the user associated to an LoS UAV-AP, conditioning on Φ_U and Φ_{b}, is given as

$$P_{\mathrm{SL}}(\gamma) = \mathbb{P}\left(\frac{P_{\mathrm{U}} K_{\mathrm{U}} G_{\mathrm{L}} d_{\mathrm{L}}^{-\alpha_{\mathrm{L}}}}{\sigma_{\mathrm{N}} + I'_{\mathrm{L}} + I_{\mathrm{N}}} > \gamma | \Phi_{\mathrm{U}}, \Phi_{\mathrm{b}}\right), \tag{4.50}$$

where I'_{L} and I_{N} are the interfering strengths from the other LoS and NLoS UAV-APs respectively, where $I'_{\mathrm{L}} = \sum_{i:\mathbf{X}_i \in \Phi'_{\mathrm{L}}} P_{\mathrm{U}} K_{\mathrm{U}} G'_{\mathrm{L}} d'^{-\alpha_L}_{\mathrm{L}}$ and $I_{\mathrm{N}} = \sum_{i:\mathbf{X}_i \in \Phi_{\mathrm{N}}} P_{\mathrm{U}} K_{\mathrm{U}} g_{\mathrm{N}} d_{\mathrm{N}}^{-\alpha_{\mathrm{N}}}$. Φ'_{L} is the point process of LoS UAV-APs in which the associated LoS UAV-AP is omitted. Considering the Nakagami-m fading for LoS transmissions and Rayleigh fading for NLoS transmissions, we derive the b^{th} moment for LoS UAV-AP, which is given as

Theorem 1. *The b^{th} moment of $P_{SL}(\gamma)$ is given as*

$$M_{\mathrm{L}}(\gamma) = A_{\mathrm{L}} \int_{h_{\min}}^{h_{\max}} \left[\sum_{n=1}^{m} (-1)^{n+1} \cdot {}^{m}C_n \cdot U'(z,\gamma,b,n) \cdot A'(z,n) \cdot f_{d_{\mathrm{L}}}(z)\right] \mathrm{d}z + \int_{h_{\max}}^{\infty} \left[\sum_{n=1}^{m} (-1)^{n+1} \cdot {}^{m}C_n \cdot U'(z,\gamma,b,n) \cdot B'(z,n) \cdot f_{d_{\mathrm{L}}}(z)\right] \mathrm{d}z, \tag{4.51}$$

where

$$A'(z,n) = \exp\left(-2\pi\lambda_{\mathrm{U}} l'_1(z,n)\right) \cdot \exp\left(-2\pi\lambda_{\mathrm{U}} l'_2(z,n)\right). \tag{4.52}$$

$$B'(z,n) = \exp\left(-2\pi\lambda_{\mathrm{U}} l'_3(z,n)\right) \cdot \exp\left(-2\pi\lambda_{\mathrm{U}} l'_4(z,n)\right). \tag{4.53}$$

$$l'_1(z,n) = \int_0^{k(z)} \left(1 - \left[\int_{n(z,x)}^{h_{\max}} \frac{\rho'(t,x,n)}{(h_{\max} - w(z,x))} \mathrm{d}t\right]\right) x \mathrm{d}x + \int_{k(z)}^{\infty} \left(1 - \left[\int_{h_{\min}}^{h_{\max}} \frac{\rho'(t,x,n)}{(h_{\max} - h_{\min})} \mathrm{d}t\right]\right) x \mathrm{d}x. \tag{4.54}$$

$$l'_2(z,n) = \int_0^{k(z)} \left(1 - \left[\int_{n(z,x)}^{h_{\max}} \frac{\tau'(t,x,n)}{(h_{\max} - w(z,x))} \mathrm{d}t\right]\right) x \mathrm{d}x + \int_{k(z)}^{\infty} \left(1 - \left[\int_{h_{\min}}^{h_{\max}} \frac{\tau'(t,x,n)}{(h_{\max} - h_{\min})} \mathrm{d}t\right]\right) x \mathrm{d}x. \tag{4.55}$$

$$l_3'(z,n)=\int_{l(z)}^{k(z)}\left(1-\left[\int_{w(z,x)}^{h_{\max}}\frac{\rho'(t,x,n)}{(h_{\max}-w(z,x))}\mathrm{d}t\right]\right)x\mathrm{d}x+\int_{k(z)}^{\infty}\left(1-\left[\int_{h_{\min}}^{h_{\max}}\frac{\rho'(t,x,n)}{(h_{\max}-h_{\min})}\mathrm{d}t\right]\right)x\mathrm{d}x. \quad (4.56)$$

$$l_4'(z,n)=\int_{l(z)}^{k(z)}\left(1-\left[\int_{w(z,x)}^{h_{\max}}\frac{\tau'(t,x,n)}{(h_{max}-w(z,x))}\mathrm{d}t\right]\right)x\mathrm{d}x+\int_{k(z)}^{\infty}\left(1-\left[\int_{h_{\min}}^{h_{\max}}\frac{\tau'(t,x,n)}{(h_{\max}-h_{\min})}\mathrm{d}t\right]\right)x\mathrm{d}x. \quad (4.57)$$

$$U'(z,\gamma,b,n)=\exp\left(\tfrac{-n\varepsilon\gamma\sigma_{\mathrm{N}}b}{P_{\mathrm{U}}K_{\mathrm{U}}z^{-\alpha_{\mathrm{L}}}}\right),\ k(z)=\sqrt{z^2-h_{\min}^2},\ w(z,x)=\sqrt{z^2-x^2},\ l(z)=\sqrt{z^2-h_{\max}^2}.$$

$$\rho'(t,x,n)=L_S(\sqrt{x^2+t^2},t)\left(\frac{1}{1+\frac{n\varepsilon\gamma(\sqrt{x^2+t^2})^{-\alpha_{\mathrm{L}}}}{z^{-\alpha_{\mathrm{L}}}}}\right)^{b}+N_{\mathrm{S}}(\sqrt{x^2+t^2},t)\left(\frac{1}{1+\frac{n\varepsilon\gamma(\sqrt{x^2+t^2})^{-\alpha_{\mathrm{N}}}}{z^{-\alpha_{\mathrm{L}}}}}\right)^{b}. \quad (4.58)$$

$$\tau'(t,x,n)=L_S(\sqrt{x^2+t^2},t)\left(\frac{m}{m+\frac{n\varepsilon\gamma(\sqrt{x^2+t^2})^{-\alpha_{\mathrm{L}}}}{z^{-\alpha_{\mathrm{L}}}}}\right)^{mb}+N_{\mathrm{S}}(\sqrt{x^2+t^2},t)\left(\frac{m}{m+\frac{n\varepsilon\gamma(\sqrt{x^2+t^2})^{-\alpha_{\mathrm{N}}}}{z^{-\alpha_{\mathrm{L}}}}}\right)^{mb}. \quad (4.59)$$

where $\varepsilon=m(m!)^{\frac{-1}{m}}$.

Proof. See Appendix B.12. □

4.2.5.2 Conditional Success Probability of NLoS UAV-AP

Here, we derive the conditional success probability $P_{SN}(\gamma)$ of the typical user associated to an NLoS UAV-AP, i.e.,

$$P_{\mathrm{SN}}(\gamma)=\mathbb{P}\left(\frac{P_{\mathrm{U}}K_{\mathrm{U}}g_{\mathrm{N}}d_{\mathrm{N}}^{-\alpha_{\mathrm{N}}}}{\sigma_{\mathrm{N}}+I_{\mathrm{N}}'+I_{\mathrm{L}}}>\gamma|\Phi_{\mathrm{U}},\Phi_{\mathrm{b}}\right), \quad (4.60)$$

where I_{L} and I_{N}' are the interfering strengths from the LoS and the other NLoS UAV-APs respectively, where $I_{\mathrm{L}}=\sum_{i:\mathbf{X}_i\in\Phi_{\mathrm{L}}}P_{\mathrm{U}}K_{\mathrm{U}}G_{\mathrm{L}}d_{\mathrm{L}}^{-\alpha_{\mathrm{L}}}$ and $I_{\mathrm{N}}'=\sum_{i:\mathbf{X}_i\in\Phi_{\mathrm{N}}'}P_{\mathrm{U}}K_{\mathrm{U}}g_{\mathrm{N}}'d_{\mathrm{N}}'^{-\alpha_{\mathrm{N}}}$. Φ_{N}' is the

point process of NLoS UAV-APs in which the associated NLoS UAV-AP is omitted.

Theorem 2. *The b^{th} moment of $P_{\mathrm{SN}}(\gamma)$ is given as*

$$M_{\mathrm{N}}(\gamma) = A_{\mathrm{N}} \int_{h_{\min}}^{h_{\max}} \left[A''(z) \cdot U''(z,\gamma,b) \cdot f_{d_{\mathrm{N}}}(z)\right] \mathrm{d}z + \int_{h_{\max}}^{\infty} \left[B''(z) \cdot U''(z,\gamma,b) \cdot f_{d_{\mathrm{N}}}(z)\right] \mathrm{d}z, \quad (4.61)$$

where

$$A^{''}(z) = \exp\left(-2\pi\lambda_{\mathrm{U}} l_1^{''}(z)\right) \cdot \exp\left(-2\pi\lambda_{\mathrm{U}} l_2^{''}(z)\right). \quad (4.62)$$

$$B^{''}(z) = \exp\left(-2\pi\lambda_{\mathrm{U}} l_3^{''}(z)\right) \cdot \exp\left(-2\pi\lambda_{\mathrm{U}} l_4^{''}(z)\right). \quad (4.63)$$

$$l_1^{''}(z) = \int_0^{k(z)} \left(1 - \left[\int_{w(z,x)}^{h_{\max}} \frac{\rho^{''}(t,x)}{(h_{\max} - w(z,x))} \mathrm{d}t\right]\right) x \mathrm{d}x + \int_{k(z)}^{\infty} \left(1 - \left[\int_{h_{\min}}^{h_{\max}} \frac{\rho^{''}(t,x)}{(h_{\max} - h_{\min})} \mathrm{d}t\right]\right) x \mathrm{d}x. \quad (4.64)$$

$$l_2^{''}(z) = \int_0^{k(z)} \left(1 - \left[\int_{w(z,x)}^{h_{\max}} \frac{\tau^{''}(t,x)}{(h_{max} - w(z,x))} \mathrm{d}t\right]\right) x \mathrm{d}x + \int_{k(z)}^{\infty} \left(1 - \left[\int_{h_{\min}}^{h_{\max}} \frac{\tau^{''}(t,x)}{(h_{\max} - h_{\min})} \mathrm{d}t\right]\right) x \mathrm{d}x. \quad (4.65)$$

$$l_3^{''}(z) = \int_{l(z)}^{k(z)} \left(1 - \left[\int_{w(z,x)}^{h_{\max}} \frac{\rho^{''}(t,x)}{(h_{max} - w(z,x))} \mathrm{d}t\right]\right) x \mathrm{d}x + \int_{k(z)}^{\infty} \left(1 - \left[\int_{h_{\min}}^{h_{\max}} \frac{\rho^{''}(t,x)}{(h_{max} - h_{min})} \mathrm{d}t\right]\right) x \mathrm{d}x. \quad (4.66)$$

$$l_4^{''}(z) = \int_{l(z)}^{k(z)} \left(1 - \left[\int_{w(z,x)}^{h_{\max}} \frac{\tau^{''}(t,x)}{(h_{\max} - w(z,x))} \mathrm{d}t\right]\right) x \mathrm{d}x + \int_{k(z)}^{\infty} \left(1 - \left[\int_{h_{\min}}^{h_{\max}} \frac{\tau^{''}(t,x)}{(h_{\max} - h_{\min})} \mathrm{d}t\right]\right) x \mathrm{d}x. \quad (4.67)$$

$$U'(z,\gamma,b) = \exp\left(\frac{-\gamma\sigma_{\mathrm{N}}b}{P_{\mathrm{U}}K_{\mathrm{U}}z^{-\alpha_{\mathrm{N}}}}\right),\ k(z)=\sqrt{z^2-h_{\min}^2},\ w(z,x)=\sqrt{z^2-x^2},\ l(z)=\sqrt{z^2-h_{\max}^2}.$$

$$\rho^{''}(t,x) = L_{\mathrm{S}}(\sqrt{x^2+t^2},t)\left(\frac{1}{1+\frac{\gamma(\sqrt{x^2+t^2})^{-\alpha_{\mathrm{L}}}}{z^{-\alpha_{\mathrm{N}}}}}\right)^{b} + N_{\mathrm{S}}(\sqrt{x^2+t^2},t)\left(\frac{1}{1+\frac{\gamma(\sqrt{x^2+t^2})^{-\alpha_{\mathrm{N}}}}{z^{-\alpha_{\mathrm{N}}}}}\right)^{b}. \tag{4.68}$$

$$\tau'(t,x) = L_{\mathrm{S}}(\sqrt{x^2+t^2},t)\left(\frac{m}{m+\frac{\varepsilon\gamma(\sqrt{x^2+t^2})^{-\alpha_{\mathrm{L}}}}{z^{-\alpha_{\mathrm{N}}}}}\right)^{mb} + N_{\mathrm{S}}(\sqrt{x^2+t^2},t)\left(\frac{m}{m+\frac{\varepsilon\gamma(\sqrt{x^2+t^2})^{-\alpha_{\mathrm{N}}}}{z^{-\alpha_{\mathrm{N}}}}}\right)^{mb}. \tag{4.69}$$

The proof is the same as Theorem 1; therefore, we skip it for brevity.

The MD of SINR provides a probabilistic framework to analyze the reliability of communication links in a wireless network. For an ergodic point process in UAV networks, the MD $\bar{F}_{P_{\mathrm{suc}}}(\gamma, x_r)$ can be interpreted as the proportion of active links where the success probability $\mathcal{P}_{\mathrm{suc}}(\gamma)$ for a given value of threshold γ exceeds the reliability threshold x_{r}. The exact MD can be obtained from the Gil-Pelaez theorem [77] with b^{th} moment M_{b} of $\mathcal{P}_{\mathrm{suc}}(\gamma)$, $b \in \mathbb{R}$, $i=\sqrt{-1}$.

$$\bar{F}_{P_{\mathrm{suc}}}(\gamma, x_{\mathrm{r}}) = \frac{1}{2} + \frac{1}{\pi}\int_0^{\infty} \frac{\mathfrak{I}(e^{-it\log x_{\mathrm{r}}}M_{\mathrm{it}})}{t}\mathrm{d}t, \tag{4.70}$$

where $\mathfrak{I}(z)$ is the imaginary part of $z \in \mathbb{C}$. M_{it} is the it^{th} moment of $\mathcal{P}_{\mathrm{S}}(\gamma)$.

From (4.51) and (4.61), the b^{th} moment of the $\mathcal{P}_{\mathrm{suc}}(\gamma)$ is given as

$$M_{\mathrm{b}}(\gamma) = A_{\mathrm{L}}M_{\mathrm{L}}(\gamma) + A_{\mathrm{N}}M_{\mathrm{N}}(\gamma). \tag{4.71}$$

The SINR MD is obtained by substituting (4.71) in (4.70).

The first moment of $\mathcal{P}_{\mathrm{suc}}(\gamma)$, substituting $b=1$ in (4.71), gives the overall SINR coverage probability experienced by the user. The $(-1)^{th}$ moment of $\mathcal{P}_{\mathrm{suc}}(\gamma)$ is referred to as MLD $M_{-1}(\gamma)$, represents the average number of retransmission attempts required to successfully transmit a packet between the UAV-AP and the user.

4.2.5.3 Beta Approximation

Here, we provide an accurate approximation for SINR MD using beta approximation [78]. We calculate the MD of SINR $\bar{F}_{P_S}(\gamma, x_r)$ by matching the first moment M_1 and the second moment M_2. The MD of SINR can be approximated as

$$\bar{F}_{P_S}(\gamma, x_r) = 1 - I_{x_r}(\kappa, \beta) \tag{4.72}$$

where $\kappa = \frac{M_1 M_2 - M_1^2}{M_1^2 - M_2}$, $\beta = \frac{(1-M_1)(M_2-M_1)}{M_1^2 - M_2}$ and I_{x_r} is the regularized incomplete beta function.

4.2.6 Cache-Enabled HO Analysis

In this section, we present an efficient HO management scheme that leverages the caching capabilities of UEs. Building on our prior work in [71], where we examined HO management using caching in a 1-D network and analyzed its impact on network performance and delay, we extend this approach to a 2-D UAV network with blockages. The proposed HO management scheme aims to minimize handovers, thereby reducing transmission latency for mobile users. To evaluate its performance, we conduct a semi-analytical analysis to derive the average rate experienced by users under this cache-enabled HO scheme. For simplicity, the analysis focuses on the downlink scenario, considering a mobile user traveling in a straight line through the origin along the x-axis.

We consider a scenario where the user moves over a long period, denoted as T. At $t = 0$, the user will be associated with a UAV-AP at $(x_\mathrm{a}, y_\mathrm{a}, h_\mathrm{a})$ and experience a download rate of $R_\mathrm{r}(t)$ at every time t. The download rate experienced by the user associated with an LoS UAV-AP at time t is given as

$$R_\mathrm{r}(t) = B \log_2 \left(1 + \frac{P_\mathrm{U} K_\mathrm{U} G_\mathrm{L} d_\mathrm{mu}(t)^{-\alpha_\mathrm{L}}}{\sigma_\mathrm{N} + I'_\mathrm{L} + I_\mathrm{N}} \right), \tag{4.73}$$

where I'_L and I_N are the interfering strengths from the other LoS and NLoS UAV-APs respectively. The distance $d_\mathrm{mu}(t)$ between the associated BS and the user at time t, given as $d_\mathrm{mu}(t) = \sqrt{(x_\mathrm{a} - vt)^2 + (y_\mathrm{a} - y_u)^2 + h_\mathrm{a}^2}$. We assume the user is moving along the 2-D plane in a straight line with velocity v. G_L is the Nakagami-m fading factor, K is the pathloss

coefficient i.e., $K = (\frac{(\lambda_c)}{4\pi})^2$, where λ_c is the carrier wavelength. If it is NLoS UAV-AP, the path-loss and fading parameters change.

Consider the scenario where $R_r > s_r$. As the user moves forward, the user experiences a download rate greater than s_r. Consequently, the excess data (i.e., the difference between the downloaded data and the required data for the service) is cached in the UE memory of cache size G, with a complexity depending on UE velocity and preferences,which is of the order $\mathcal{O}(KG)$, where K denotes the number of users. This caching continues as long as the user's download rate exceeds or equal to the required service rate and the cache has available space. Let t_d denote the time at which the download rate reduces than the required rate for the service. Therefore, the downloaded data till time t_d is given as $C_D = \int_0^{t_d} R_r(t)\, dt$.

The amount of data used by the user to meet the service requirement till time t_n is given as $s_r t_n$. The user requires ΔT seconds to measure the RSSI from the neighboring cells. If there is sufficient data cached, i.e., more than $s_r \Delta T$, to skip HOs and perform RSS measurements, the cell search is muted, and HOs are skipped. The user remains associated with the previous UAV-AP until the next cell search is initiated. While utilizing cached data C_D, the user achieves the specified service rate s_r. Let the time be t_n, which the user can use the cached data to maintain the service requirement rate. If there is C_D data in the cache, the next cell search is triggered when the condition $C_D/s_r < \Delta T$ is met. The user maintains association with the current UAV-AP until this condition is satisfied or the download rate falls below the minimum threshold defined by 3GPP to sustain a connection. Once this occurs, the service rate drops to the current download rate R_r, prompting a cell search, RSS measurements, and the initiation of a handover. Using this methodology, the number of handovers experienced by the user in the cache-enabled HO scheme is given as H_N. By performing temporal and spatial averaging, the average HO rate is given as $\mu = \frac{H_N}{T}$. Performing spatial averaging, the average HO rate is given as μ'. The rate experienced by the user when utilizing the cached data is s_r. Considering the entire time of travel T, the average rate at the time of utilizing cached data is given as $\frac{s_r t_n}{T}$. Performing spatial averaging, the average rate experienced by the user when utilizing the cached data is given as R_s.

While the user experiences the download rate R_r less than the service rate, we derive the

average rate by utilizing the first moment of CSP $M_1(\gamma)$ derived in (4.71).

$$R_{\mathrm{d}} = B \int_0^{2^{\frac{s_{\mathrm{r}}}{B}}-1} \frac{M_1(k)}{k+1} \mathrm{d}k. \tag{4.74}$$

Here, the maximum SINR experienced by the user will be $2^{\frac{s_{\mathrm{r}}}{B}} - 1$ because this is the SINR experienced by the user when the cached data is fully exhausted before initiating the cell search. Therefore, the overall average rate experienced by the user is given as $R'_{\mathrm{a}} = R_{\mathrm{s}} + R_{\mathrm{d}}$.

The effective average rate experienced by the user is given as [71]

$$R_{\mathrm{eff}} = R'_{\mathrm{a}}(1 - \mu' t_{\mathrm{H}})^{+}, \tag{4.75}$$

where μ' is the average handover rate. The delay experienced by the user due to the HOs is expressed as $\mu' t_{\mathrm{H}}$.

4.2.7 Results and Discussions

In this section, we validate the proposed theoretical model using Monte Carlo simulations and present numerical results to analyze and discuss the key characteristics of the network. The simulation parameters are shown in Table 4.2.

4.2.7.1 Trends in MD of SINR

In Figure 4.16, we present the SINR MD as a function of the intensity of UAV-APs under various blockage scenarios, with a reliability threshold of x_r =0.9, representing the condition where 90% of the communication links are active. In low-blockage scenarios, at an intensity of $\lambda_U = 10^{-6}$ km^{-2}, the SINR MD value is 0.7, indicating that there is a 70% probability of achieving the reliability threshold. However, in high-blockage scenarios, users achieve the reliability threshold (90% active links) less than 55% of the time. Interestingly, deploying a large number of UAV-APs in low-blockage regions degrades network performance. Contrary to conventional expectations, regions with higher blockages benefit more from a denser deployment of UAV-APs, as the blockages help mitigate interference from neighboring UAV-APs. Moreover, we observe that increasing the network density does not enhance

Table 4.2: Simulation Parameters

Notation	Parameter	Value
P_{U}	Transmit power	10 W [78]
λ_{U}	Intensity of UAV-APs	10^{-5} km^{-2}
λ_{b}	Intensity of blockages	10^{-6} km^{-2}
$h_{\min}$	Minimum altitude	100 m
$h_{\max}$	Maximum altitude	300 m
H_{b}	Average blockage height	80 m
B	Bandwidth	100 MHz [79]
α_{L}	LoS Path-loss Exponent	2
α_{N}	NLoS Path-loss Exponent	4
f_{c}	Carrier frequency	3.5 GHz
σ^2	Noise density	-174 dBm/Hz
s_{r}	Service rate requirement	40 Mbps
v	Velocity	1 m/s
t_{H}	HO overhead time	43 ms
t_{s}	Search time	20 ms
T	Total time	5000 s

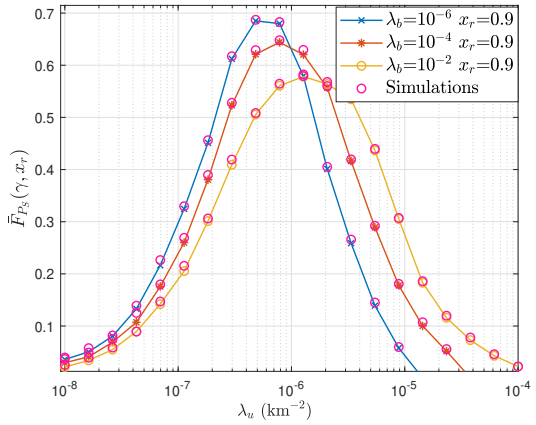

Figure 4.16. SINR MD as a function of the intensity of UAV-APs for different blockage intensities for $x_r = 0.9$, $\gamma = -10$ dB.

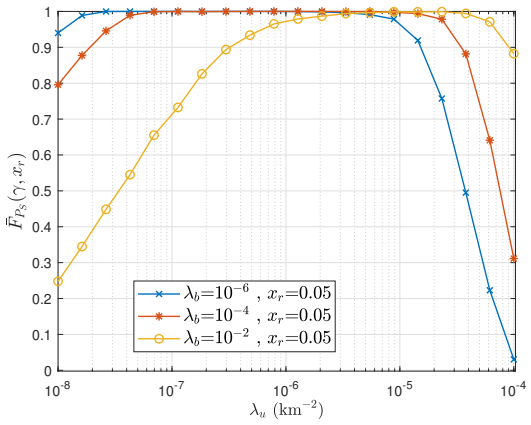

Figure 4.17. SINR MD as a function of the intensity of UAV-APs for different blockage intensities for $x_r = 0.05$.

performance beyond a certain threshold.

In Figure 4.17, we illustrate the SINR MD as a function of the intensity of UAV-APs, evaluated at a reliability threshold of 0.05. This threshold indicates that at least 5% of the communication links are active with SINR exceeding a specified value. The results demonstrate that in areas with low blockage, fewer UAV-APs are needed to maintain this level of active communication links, whereas areas with higher blockage require a denser deployment. For instance, in low-blockage scenarios with $\lambda_b = 10^{-6}$ km^{-2}, users consistently maintain at least 5% active communication links. Conversely, in high-blockage scenarios where $\lambda_b = 10^{-2}$ km^{-2}, increasing the UAV-AP density beyond 10 UAV-APs per km^2 ensures that all users sustain at least 5% of active communication links at all times.

In Figure 4.18, we present the MLD in the network for varying SINR requirements at the users. For a fixed UAV-AP intensity of 10^{-5} km^{-2}, we observe that an increase in blockage intensity results in a higher SINR threshold γ. This occurs because, to maintain a consistent mean local delay while satisfying the SINR constraints, the system must raise the SINR threshold. Conversely, for a fixed blockage intensity of 10^{-5} km^{-2}, increasing the UAV-AP intensity reduces γ. This reduction is attributed to improved coverage, allowing users to achieve the required communication quality more easily.

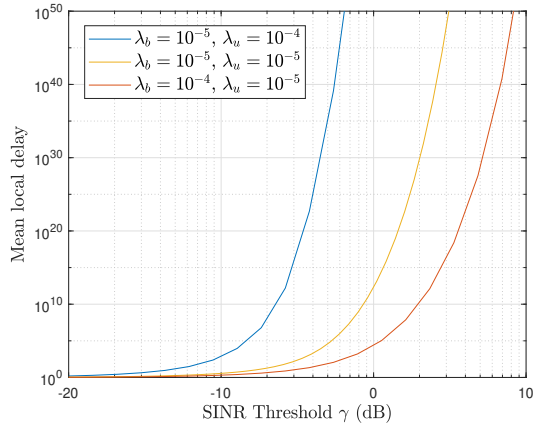

Figure 4.18. Mean local delay versus SINR threshold.

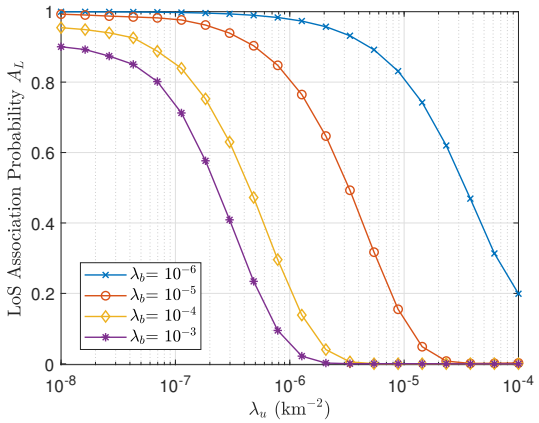

Figure 4.19. LoS Association Probabilities for different blockage intensities.

4.2.7.2 Association Probability

Figure 4.19 illustrates the LoS association probability of the network as a function of the intensity of UAV-APs. As the UAV-AP intensity increases, the LoS association probability decreases. In scenarios with sparse UAV-AP deployment, the LoS association probability is relatively high but diminishes as the density of UAV-APs grows. In the presence of TBSs, as discussed in [16], LoS associations are fewer at lower BS intensities. Further increases in UAV-AP intensity predominantly serve NLoS UAV-APs, with minimal impact on LoS links. In this study, we focus on the LoS association trends in the absence of TBSs. A key takeaway is that network densification alone is insufficient to improve LoS association probability or enhance overall coverage performance. Intuitively, as blockage intensity increases, the LoS association probability declines. However, a higher density of NLoS UAV-APs can mitigate interference, thereby improving the SINR, as highlighted in Figure 4.16 and Figure 4.17.

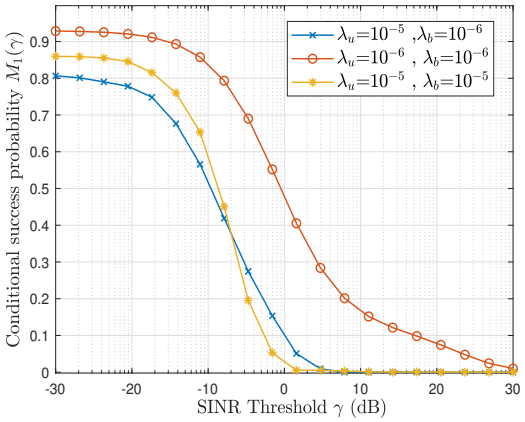

Figure 4.20. Conditional success probability versus SINR threshold γ.

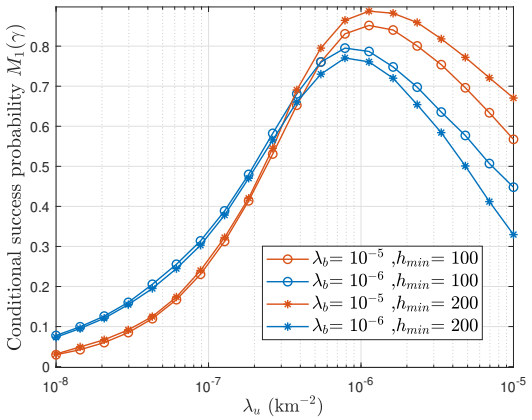

Figure 4.21. Conditional success probability of the network versus the intensity of UAV-APs for different blockage intensities and UAV altitudes.

4.2.7.3 Trends in Conditional Success Probability

Figure 4.20 shows the relationship between the SINR threshold and the CSP. As the SINR threshold increases, the CSP decreases. For a given blockage intensity, a higher deployment density of UAV-APs leads to degraded network performance due to increased interference.

When user requirements are low, blockages have a limited impact on network performance, as they effectively mitigate interference. However, when user requirements are high, blockages negatively affect performance by reducing LoS connections, thereby compromising network reliability.

Figure 4.21 depicts the CSP as a function of UAV-AP intensity for varying blockage intensities and minimum UAV-AP altitudes. As previously noted, in sparse UAV-AP deployments, scenarios with lower blockage intensity yield better performance. However, in denser deployments, higher blockage scenarios outperform due to the mitigation of interference from blocked UAV-APs in areas with significant blockages. Moreover, in regions with minimal blockages, deploying UAV-APs at lower altitudes enhances performance by increasing the number of LoS connections. Conversely, in regions with higher blockage intensity, deploying UAV-APs at greater altitudes improves performance by establishing more LoS links, which is crucial for overcoming the impact of large blockages.

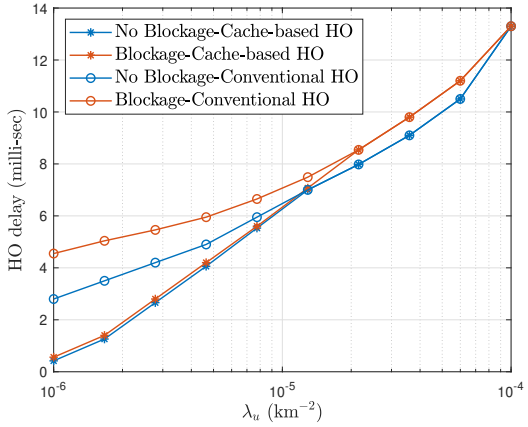

Figure 4.22. Handover Delay versus Intensity of UAV-AP.

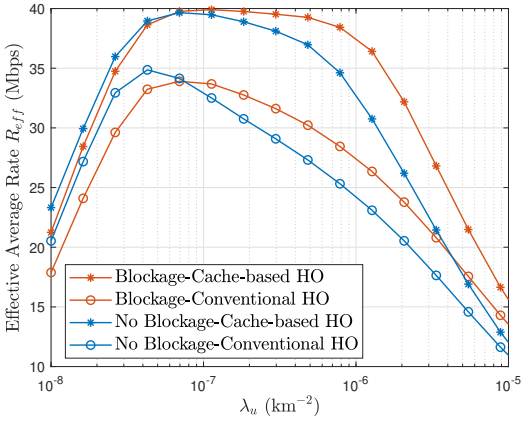

Figure 4.23. Effective Average Rate versus Intensity of UAV-AP.

4.2.7.4 Trends in HO delay and Average Rate

Figure 4.22 illustrates the HO delay as a function of the intensity of UAV-APs for different handover strategies. The conventional handover scheme exhibits higher handover rates compared to the cache-based scheme, as the latter skips unnecessary handovers by utilizing cached data at the UE. While this reduces the frequency of handovers, it can lead to

increased handover delay, resulting in transmission latency. However, as the intensity of UAV-APs increases beyond a certain threshold, the cache-based scheme begins to exhibit similar handover delays to the conventional scheme. This occurs due to a reduction in cached data at the UE, caused by higher interference in denser deployments, which lowers the user's download rate and diminishes the amount of cached data. Additionally, the cache-based handover strategy is less affected by blockages compared to the conventional scheme. In the conventional approach, blockages lead to frequent re-associations, thereby increasing the handover rate. In contrast, the cache-based strategy avoids initiating new associations by leveraging cached data at the UE, even in the presence of blockages. This effectively reduces the overall handover delay and decreases latency in the network.

Figure 4.23 shows the average rate experienced by the UE as a function of UAV-AP intensity. The cache-based scheme consistently outperforms the conventional scheme. In sparse UAV-AP deployments, both schemes are adversely affected by blockages. However, in dense UAV-AP deployments, blockages help mitigate interference, leading to improved network performance. Despite this improvement, blockage scenarios require a higher UAV-AP deployment density to achieve the same performance gains observed in no-blockage scenarios. Furthermore, at very high deployment densities, the average rate of the cache-based scheme converges with that of the conventional scheme. This convergence occurs due to increased interference, which reduces the user's download rate and depletes the cached data. As a result, at extremely high deployment densities, the cache-based scheme performs similarly to the conventional scheme.

4.2.7.5 Trends in Energy Efficiency

Figure 4.24 illustrates the system's energy efficiency as a function of UAV-AP intensity, comparing the conventional and cache-enabled handover (HO) schemes. The power consumption model used follows our previous work [71]. For a caching capacity of 100 GB, the cache-enabled HO scheme demonstrates superior energy efficiency compared to the conventional scheme up to a UAV-AP intensity of approximately 10 UAV-APs per km^2. This improvement is attributed to higher spectral efficiency and reduced inter-frequency HOs enabled by caching, even when accounting for the power consumption associated with caching. However,

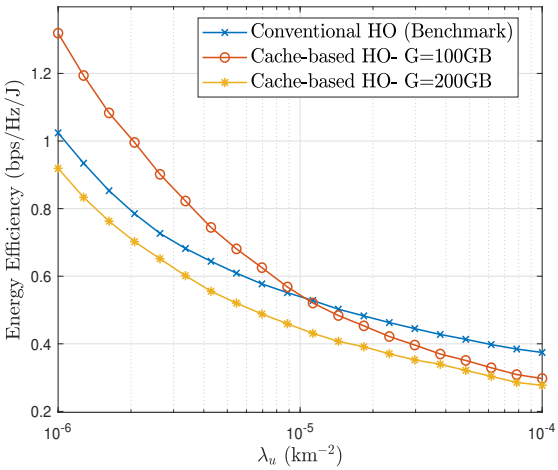

Figure 4.24. Energy Efficiency versus Intensity of UAV-APs for service rate $s_r = 40$ Mbps, $\lambda_b = 10^{-6}$.

as the UAV-AP intensity continues to increase, rising interference levels lead to a decline in spectral efficiency and an increase in the HO rate, ultimately reducing energy efficiency. For a larger cache size of 200 GB, the additional power consumption due to caching causes the cache-enabled scheme to perform worse than the conventional scheme in terms of energy efficiency.

4.3 Chapter Conclusion

In this chapter, we analyzed the performance of mobile users in UAV-based and 5G-enabled networks under various challenging scenarios, leveraging stochastic geometry and cache-enabled HO management. In vehicular and pedestrian environments, we demonstrated that caching at the mobile terminal had significantly improved network performance by reducing handover rates, increasing the average rate, and enhancing energy efficiency. We provided optimal deployment strategies considering factors such as cache size, deployment density, and power consumption. In disaster scenarios, we characterized the handover rate and average rate using a stochastic geometry framework, modeling UAV base stations as a 2-D MPPP. This approach highlighted the trade-offs between handover frequency and user throughput in networks with varying UAV deployment densities and heights. For urban environments with blockages, we analyzed the impact of blockages on reliability, association probabilities, and

interference management. Blockages, while reducing LoS associations, enhanced network reliability by mitigating interference. The proposed cache-enabled HO scheme minimized unnecessary handovers, reduced latency, and improved rate, especially in dense network deployments. Across all scenarios, we highlighted the importance of optimal network design to meet service rate requirements, ensure reliability, and enhance user experience.

Chapter 5

Power Optimization in UAV-Enabled Cell-Free Wireless Networks

In this chapter, we study placement and power optimization in UAV-based cell-free mMIMO networks. The concept of cell-free mMIMO networks has gained significant attention due to its ability to provide uniform service quality across large areas. Integrating UAVs with cell-free mMIMO leads to a transformative leap in network design by dynamically adjusting their positions to optimize network performance. One of the critical constraints in such networks is the limited capacity of the wireless fronthaul links connecting UAV-APs to the CPU. This limitation significantly impacts the performance of cell-free mMIMO networks, necessitating efficient strategies to manage both UAV placement and transmit power allocation. To address these fronthaul bandwidth limitations, we incorporate functional split options by dividing the baseband processing tasks between the central processing unit and the UAV-APs. We consider Option 8 and Option 7.2 functional splits to enable flexible trade-offs between fronthaul capacity, computational complexity, and latency, allowing the network to adapt to varying operational scenarios and resource constraints. This chapter explores the joint optimization of UAV placement and power allocation in cell-free mMIMO networks under fronthaul capacity constraints for different functional split options.

5.1 Network Model

We consider a downlink cell-free massive MIMO system consisting of L UAV-APs serving uniformly distributed K UEs on the ground, where $L \gg K$. Each UAV-AP is equipped with N_{a} antennas and serves single-antenna UEs in the access link. Each UAV-AP is connected to the CPU equipped with N_{c} antennas via a single fronthaul antenna as given in Figure 5.1.

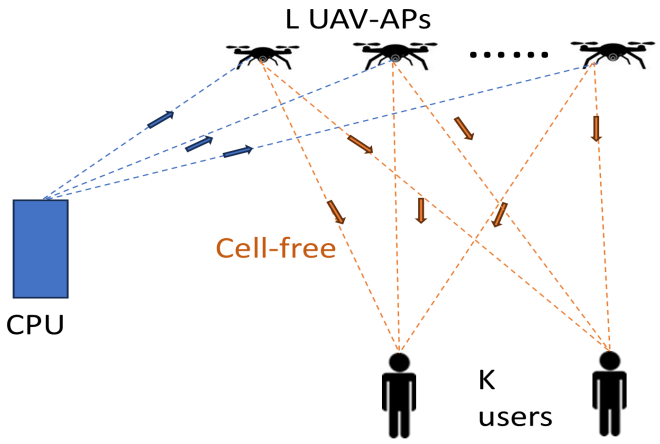

Figure 5.1. Wireless fronthaul UAV-based network with cell-free access. The blue lines represent the fronthaul links, and the red lines represent the access links.

5.1.1 Definition of Cell-free mMIMO

Cell-free massive MIMO as an ultra-dense network (i.e., many more APs than UEs) where the APs are cooperating to serve the UEs by joint coherent transmission and reception [80]. Consider a network with L APs, each equipped with N antennas, that are geographically distributed over the coverage area. The total number of AP antennas in the network is $M = NL$. The APs are jointly serving K single-antenna UEs. More precisely, each UE is communicating with a subset of the APs, which is selected based on the UE's needs. The APs are connected via fronthaul links to CPUs, which facilitate the AP coordination. The cellfree architecture can also handle multi-antenna UEs, where the extra antennas are utilized to suppress interference or spatially multiplex several signals per UE. The cell-free network will have sufficiently many spatial degrees of freedom so that the UEs can be separated in space by processing the transmitted and received signals.

5.2 Wireless Fronthaul

We consider a multi user-MIMO (MU-MIMO) setup in which a CPU equipped with N_c antennas transmits to a single antenna UAV-APs over a shared fronthaul channel with total bandwidth B_F Hz. A uniform planar array with antenna spacing δ is considered at the CPU.

All the fronthaul parameters are represented by the superscript f.

The received signal $\mathbf{y}^f = [y_1, y_2, ..., y_{\mathrm{L}}]^{\mathrm{T}}$ for all the UAV-APs are given as

$$\mathbf{y}^f = (\mathbf{H}^f)^{\mathrm{T}}\mathbf{P}\mathbf{x} + \mathbf{n}, \tag{5.1}$$

where $\mathbf{H}^f = [\mathbf{h}_1^f, \mathbf{h}_2^f, ..., \mathbf{h}_{\mathrm{L}}^f]$ is the channel matrix where $\mathbf{h}_l^f \in \mathbb{C}^{N_c}$ denote the frequency domain channel between CPU and UAV-AP l in the fronthaul link. The maximum transmit power at the CPU to be allocated to L UAV-APs is given as $P_{\max}^f$. We consider zero-forcing (ZF) precoding vector $\mathbf{P}^{\mathrm{ZF}}$ so that the interference at co-UAV-APs are nullified [81]. The ZF precoding vector is represented as

$$\mathbf{P}^{\mathrm{ZF}} = (\mathbf{H}^f)^*[(\mathbf{H}^f)^{\mathrm{T}}(\mathbf{H}^f)^*]^{-1}\mathbf{Z}^{\mathrm{ZF}}. \tag{5.2}$$

The ZF precoding has the property that $(\mathbf{H}^f)^{\mathrm{T}}\mathbf{P}^{\mathrm{ZF}} = (\mathbf{H}^f)^{\mathrm{T}}(\mathbf{H}^f)^*[(\mathbf{H}^f)^{\mathrm{T}}(\mathbf{H}^f)^*]^{-1}\mathbf{Z}^{\mathrm{ZF}} = \mathbf{Z}^{\mathrm{ZF}}$, so the impact of channel matrix nullifies from the received signal. However, the channel still impacts the selection of the matrix $\mathbf{Z}^{\mathrm{ZF}}$ that normalizes the columns of the precoding matrix. In order to obtain the one-valued diagonal entries, the matrix $(\mathbf{P}^{\mathrm{ZF}})^{\mathrm{H}}\mathbf{P}^{\mathrm{ZF}}$ can be expressed as

$$(\mathbf{P}^{\mathrm{ZF}})^{\mathrm{H}}\mathbf{P}^{\mathrm{ZF}} = \left[(\mathbf{H}^f)^*[(\mathbf{H}^f)^{\mathrm{T}}(\mathbf{H}^f)^*]^{-1}\mathbf{Z}^{\mathrm{ZF}}\right]^{\mathrm{H}}(\mathbf{H}^f)^*[(\mathbf{H}^f)^{\mathrm{T}}(\mathbf{H}^f)^*]^{-1}\mathbf{Z}^{\mathrm{ZF}} = (\mathbf{Z}^{\mathrm{ZF}})^{\mathrm{H}}[(\mathbf{H}^f)^{\mathrm{T}}(\mathbf{H}^f)^*]^{-1}\mathbf{Z}^{\mathrm{ZF}} \tag{5.3}$$

In order to make one-valued diagonal entries of $(\mathbf{P}^{\mathrm{ZF}})^{\mathrm{H}}\mathbf{P}^{\mathrm{ZF}}$, the $\mathbf{Z}^{\mathrm{ZF}}$ can be expressed a

$$\mathbf{Z}^{\mathrm{ZF}} = \mathrm{diag}\left(1/\sqrt{[[(\mathbf{H}^f)^{\mathrm{T}}(\mathbf{H}^f)^*]^{-1}]_{11}}, ...1/\sqrt{[[(\mathbf{H}^f)^{\mathrm{T}}(\mathbf{H}^f)^*]^{-1}]_{LL}}\right). \tag{5.4}$$

As discussed before, the channel impacts the precoding matrix; we compare the channel matrix for sub-6 GHz (mid-band) and mmWave channels in the wireless fronthaul to analyze their performance differences. We assume perfect channel state information (CSI) at the fronthaul link, justified by the quasi-static aerial environment and dominant LoS links, which allow accurate channel estimation using short pilots and parametric techniques despite minor

UAV-induced phase shifts.

5.2.1 Sub-6 GHz

The channel is modeled as correlated rician fading channels with phase shifts included in the array response vector at the CPU. The channel can be expressed as

$$\mathbf{h}_l^f = \bar{\mathbf{h}}_l^f + \tilde{\mathbf{h}}_l^f, \tag{5.5}$$

where $\bar{\mathbf{h}}_l^f$ represents the LoS component [82] and $\tilde{\mathbf{h}}_l^f$ represents the NLoS components. $\bar{\mathbf{h}}_l^f$ is given as $\bar{\mathbf{h}}_l^f = \sqrt{\bar{\beta}_l^f}\mathbf{a}_l^f(\varphi_l^f, \theta_l^f)$, where $\bar{\beta}_l^f$ is the LOS channel gain [83], and the array response vector at the CPU is given in [84].

$$\mathbf{a}_l^f(\varphi_l^f, \theta_l^f) = \left[1, e^{j\frac{2\pi\delta}{\lambda}[\sin(\varphi_l^f)\cos(\theta_l^f)+\sin(\theta_l^f)]}, \dots e^{j\frac{2\pi\delta}{\lambda}[(N_c-1)\sin(\varphi_l^f)\cos(\theta_l^f)+(N_c-1)\sin(\theta_l^f)]}\right]^{\mathrm{T}}, \tag{5.6}$$

where φ_l^f and θ_l^f are the azimuth and elevation angles of departure (AoD) towards the UAV-AP l. The NLoS channels are modeled as correlated rayleigh channels where the elements of the channel vector are modeled as complex gaussian distributed. The channel between the CPU and UAV-AP l is represented as $\tilde{\mathbf{h}}_l^f \sim \mathcal{N}_{\mathbb{C}}(\mathbf{0}_{N_c}, \tilde{\mathbf{R}}_l^f)$ where $\tilde{\mathbf{R}}_l^f \in \mathbb{C}^{N_c \times N_c}$ is the spatial correlation of the channel $\tilde{\mathbf{h}}_l^f$ between the N_c antenna of CPU connecting to the UAV-AP l. From the diagonal elements of $\tilde{\mathbf{R}}_l^f$, we define the average channel gain between an antenna at CPU and the UAV-AP l. The average channel gain $\beta_l^f = \frac{1}{N_c}\mathrm{tr}(\tilde{\mathbf{R}}_l^f)$, which depends on the large-scale effects such as path loss, geometric attenuation, and shadowing [83]. We assume a perfect fronthaul channel with perfect reliability and no need for channel estimation, thereby neglecting any signal degradation or latency, and the receiver noise $\mathbf{n}$ is defined as $n_l \sim \mathcal{N}_{\mathbb{C}}(0, B_{\mathrm{F}}N_0)$.

5.2.2 MmWave channel

We consider a downlink mmWave multi-user MIMO link with one scattering cluster i.e., $N_{\mathrm{cl}} = 1$. An extended Saleh-Valenzuela channel model is considered with one direct path between the CPU and the UAV-APs and a scattered path. As discussed before, the CPU is

equipped with N_c antennas, and UAV-APs are equipped with one antenna for the fronthaul link. The array response vector at the CPU is given in (5.6). The array response vector at the receiver $\mathbf{a}_r(\varphi, \epsilon)$ is always one. The frequency domain channel matrix for the l^{th} UAV-AP is given as

$$\mathbf{h}_l^f = \sum_{i=0}^{n} \alpha_i \mathbf{a}_{li}^f(\varphi_l^f, \theta_l^f)(\varphi_l^f, \theta_l^f)^{\mathrm{T}}, \tag{5.7}$$

where n denotes the number of paths. $\mathbf{a}_{li}^f(\varphi_l^f, \theta_l^f)$ is the array response vector given as in [84]. $\alpha_i \sim \mathcal{N}_{\mathbb{C}}(0, \beta_i)$ is the complex gain in the direct and scattered path. β_i is the average power of cluster i.

5.2.3 Fronthaul power constraint

Considering either of the channel models, we apply the ZF precoding vector given in (5.2) to suppress the interference at the fronthaul link, since ZF precoding leads to a beamformed transmission that creates nulls at all the co-users. The downlink rate experienced by the UAV-AP l is given as

$$R_l^f = B_{\mathrm{F}} \log_2 \left(1 + \frac{P_l^f}{B_{\mathrm{F}} N_0 \left[((\mathbf{H}^f)^{\mathrm{T}} (\mathbf{H}^f)^*)^{-1} \right]_{ll}} \right) \tag{5.8}$$

where P_l^f is the transmit power at the CPU allocated to the UAV-AP l and N_0 is the noise spectral density at the fronthaul. Rearranging the above equation, the transmit power allocated to UAV-AP l is given as

$$P_l^{f-\kappa} = \left(2^{\frac{R_l^{f-\kappa}}{B_{\mathrm{F}}}} - 1 \right) B_{\mathrm{F}} N_0 \left[\left((\mathbf{H}^f)^{\mathrm{T}} (\mathbf{H}^f)^* \right)^{-1} \right]_{ll}, \tag{5.9}$$

where κ represents the functional split options: Option 8 or Option 7.2. Therefore, κ can be represented as $\kappa \in 8, 7.2$

The maximum allowable transmit power at the CPU is

$$\sum_{i=1}^{L} P_i^{f-\kappa} \leq P_{\max}^f. \tag{5.10}$$

Functional Split: Due to the wireless fronthaul capacity limitation given in 5.10, we compare two low physical layer functional split options, Option 8 and Option 7.2 [5]. As discussed before, the 3GPP protocol stack is divided into two: RU and DU. In Option 8, only radio frequency (RF) sampler and upconverter are placed in RU, which are the UAV-APs, and the remaining functions are centralized. Therefore, the downlink fronthaul rate requirement for each UAV-AP for Option 8 is given as [85],[5]

$$R_l^{f\text{-}8} = 2 f_s N_{\text{bits}} N_a, \tag{5.11}$$

where f_s is the sampling frequency and N_{bits} is the total number of bits required to quantize the signal samples. In Option 7.2, the low-PHY functions, such as FFT operations which are relatively less complex, are included locally in the UAV-APs, and the high-PHY functions and the remaining higher-layer operations are centralized. Therefore, the downlink fronthaul rate requirement for each UAV-AP for Option 7.2 is given as [85],[5]

$$R_l^{f\text{-}7.2} = \frac{2 N_{\text{bits}} N_{\text{used}} N_a}{T_s}, \tag{5.12}$$

where N_{used} is the number of used sub-carriers neglecting those subcarriers used as a guard band, T_s is the OFDM symbol duration and factor 2 refers to the complex nature of signals.

5.3 Cell-free Access

We consider a cell-free mMIMO setup employing a time-division duplex, where UAV-APs are equipped with N_{a} antennas transmitting to single antenna users. The system utilizes orthogonal frequency-division multiplexing (OFDM), dividing the available bandwidth B_{A} into numerous sub-carriers. A block-fading channel model is considered [80], where time-frequency resources are divided into coherence blocks.

Without loss of generality, we consider the channel to be constant over time-frequency samples τ_c in each coherence block. We consider distributed cell-free operation, in which the channel estimation is performed at the UAV-APs for the local precoding during the data transmission. Each coherence block τ_c is divided into two phases: τ_u samples for uplink

channel estimation and τ_d samples for data transmission. All the UEs are served on the same time-frequency resources using spatial multiplexing. Moreover, channel estimation and precoding are implemented in each coherence block in the same way. All the access parameters are represented by the superscript a.

We consider the same channel modeling as the sub-6 GHz band in the fronthaul, with an additional phase shift of ϕ_l^a in the LoS component. The channel between AP l and UE k is given as

$$\mathbf{h}_{lk}^a = e^{-j\phi_l^a}\bar{\mathbf{h}}_{lk}^a + \tilde{\mathbf{h}}_{lk}^a, \tag{5.13}$$

where $\bar{\mathbf{h}}_{lk}^a$ represents the LoS component represented as $\bar{\mathbf{h}}_{lk}^a = \sqrt{\bar{\beta}_{lk}}\mathbf{a}_t^{lk}(\varphi_{lk}^a, \theta_{lk}^a)$. The phase shifts in the LoS components ϕ_l^a are uniformly distributed in the range of $[0, 2\pi)$. The array response vector $\mathbf{a}_t^{lk}(\varphi_{lk}^a, \theta_{lk}^a)$ is similar to (5.6). The NLoS component $\tilde{\mathbf{h}}_{lk}^a$ is correlated Rayleigh fading where $\tilde{\mathbf{h}}_{lk}^a \sim \mathcal{N}_{\mathbb{C}}(\mathbf{0}_{N_a}, \tilde{\mathbf{R}}_{lk}^a)$. The probability of LoS transmissions considering the elevation angle between the UAV-AP l and user k, $P_{\mathrm{L}}^a = \frac{1}{1+\eta_1^a \exp\left(-\eta_2^a(\theta_{lk}^a - \eta_1^a)\right)}$, where η_1^a and η_2^a are the environmental parameters on access link. The minimum mean-squared error channel estimation is performed by reusing a set of τ_u mutually orthogonal pilot sequences among multiple users, represented as $\phi_1, \phi_2, ...\phi_{\tau_u} \in \mathbb{C}^{\tau_u}$.

$$\phi_{p_1}^{\mathrm{H}}\phi_{p_2} = \begin{cases} \tau_u, & p_1 = p_2 \\ 0, & p_1 \neq p_2. \end{cases} \tag{5.14}$$

p_k is the index of the pilot assigned to user k where $p_k \in \{1, ..., \tau_u\}$. We assume imperfect CSI is available at the access link. Therefore, we apply the MMSE channel estimation [80], [85], the estimated channel is represented as $\hat{\mathbf{h}}_{lk}^a$ of the channel $\mathbf{h}_{lk}^a$ is given as

$$\hat{\mathbf{h}}_{lk}^a = \sqrt{\eta_k}\mathbf{R}_{lk}^a \left(\sum_{i\in\mathcal{P}_k} \eta_i \tau_u \mathbf{R}_{li}^a + \sigma_a^2 \mathbf{I}_{N_a}\right)^{-1} \mathbf{Y}_l^{\text{pilot}} \phi_{p_k}^*, \tag{5.15}$$

where η_k is the pilot power of user k and p_k is the index of the pilot assigned to user k. The received signal at the UAV-AP l at a conference block, which is given as $\mathbf{Y}_l^{\text{pilot}} = \sum_{i=1}^K \sqrt{\eta_i}\mathbf{h}_{li}^a \phi_{p_i}^{\mathrm{T}} + \mathbf{N}_l$. The correlation matrix is given as $\mathbf{R}_{lk} = \bar{\mathbf{h}}_{lk}^a \bar{\mathbf{h}}_{lk}^{a\mathrm{H}} + \tilde{\mathbf{R}}_{lk}$. $y_k^a = \sum_{l=1}^L \mathbf{h}_{lk}^{a\mathrm{T}} \mathbf{x}_l + n_k$ where n_k is the receiver noise where $n_k \sim \mathcal{N}_{\mathbb{C}}(0, \sigma^2)$. The transmitted

precoded signal from UAV-AP l is x_l which is given as $\mathbf{x}_l = \sum_{i=1}^{K} \sqrt{P_{li}^a}\mathbf{w}_{li}\zeta_i \in \mathbb{C}^{N_a}$ where ζ_i is the downlink data signal of user i, $\mathbb{E}(|\zeta_i|^2) = 1$. P_{lk}^a is the transmit power corresponding to user k from UAV-AP l in the access link. We consider the L-MMSE precoding technique in which the UAV-APs serve all the users in its vicinity to construct a good balance between maximizing the signal strength and canceling the interference. For a UAV-AP l that serves user k, the precoding vectors is given as $\mathbf{w}_{lk} = \frac{\bar{\mathbf{w}}_{lk}}{\sqrt{\mathbb{E}\{\|\bar{\mathbf{w}}_{lk}\|^2\}}}$. The error correlation matrix $\mathbf{M}_{lk} = \mathbb{E}\{(\mathbf{h}_{lk}^a - \hat{\mathbf{h}}_{lk}^a)(\mathbf{h}_{lk}^a - \hat{\mathbf{h}}_{lk}^a)^{\mathrm{H}}\}$. where ρ_{lk} is the transmit power from UAV-AP l to user k. $\bar{\mathbf{w}}_{lk}$ is the arbitrary scale vector pointing out the direction of the precoding vector $\mathbf{w}_{lk}$ [80]. Using L-MMSE precoding,

$$\bar{\mathbf{w}}_{lk} = \eta_k \left(\sum_{i=1}^{K} \eta_i \left(\hat{\mathbf{h}}_{li}^a (\hat{\mathbf{h}}_{li}^a)^{\mathrm{H}} + \mathbf{M}_{li} \right) + \sigma_a^2 \mathbf{I}_{N_a} \right)^{-1} \hat{\mathbf{h}}_{lk}. \tag{5.16}$$

SINR Analysis: Let $\mathcal{M}_k$ be the set of indices of the UAV-APs which are serving user k. The spectral efficiency experienced by the user k is given as

$$\mathcal{S}_k = \frac{\tau_d}{\tau_c} \log_2(1 + \gamma_k). \tag{5.17}$$

τ_d is the samples for data transmission and τ_c is the coherence time.

The effective downlink SINR experienced by user k is given as [80, Chs. 6, 7]

$$\gamma_k(\{\boldsymbol{\rho}_i\}) = \frac{|\mathbf{b}_k^{\mathrm{T}} \boldsymbol{\rho}_k|^2}{\sum_{i=1}^{K} \boldsymbol{\rho}_i^{\mathrm{T}} \mathbf{C}_{ki} \boldsymbol{\rho}_i - |\mathbf{b}_k^{\mathrm{T}} \boldsymbol{\rho}_k|^2 + \sigma_a^2}, \tag{5.18}$$

where, σ_a^2 is the noise power and

$$\boldsymbol{\rho}_k = [\sqrt{P_{k1}^a}, \ldots, \sqrt{P_{kL}^a}]^{\mathrm{T}} = [\rho_{k,1}, \ldots, \rho_{k,L}]^{\mathrm{T}}, \tag{5.19}$$

$$\mathbf{b}_k \in \mathbb{R}_{\geq 0}^{L}, [\mathbf{b}_k]_l = \mathbb{E}\{\mathbf{h}_{kl}^{a\mathrm{T}} \mathbf{w}_{kl}\}, \tag{5.20}$$

$$[\mathbf{C}_{ki}]_{lr} = \mathbb{E}\left\{ \mathbf{h}_{kl}^{a\mathrm{T}} \mathbf{w}_{il} \mathbf{w}_{ir}^{\mathrm{H}} \mathbf{h}_{kr}^{a*} \right\}. \tag{5.21}$$

Next, we perform a fairness and power optimization at the user by maximizing the minimum SINR and minimize the total power consumption at the UAV-APs.

5.4 Max-Min Fairness Optimization

The objective of max-min fairness in a network is to maximize the minimum downlink effective SINR among all users on the ground. This optimization problem is subject to two constraints: the total fronthaul transmit power, $P^f_{\max}$, and the maximum transmit power of each UAV-AP, P_{UAV}. The goal is to determine the transmit power allocated to users, denoted as P^a_{lk}, and to decide the activation status of the UAV-APs. The activation of UAV-APs is represented by the binary vector $\boldsymbol{\alpha} = [\alpha_1, \ldots, \alpha_L] \in \mathbb{B}^L$, where $\alpha_l = 1$ indicates that UAV-AP is active for the considered coherence block, where $\alpha_l = 0$ means that it is deactivated. To express the constraints and objective function in a mixed binary linear or conic form, the power coefficients are reformulated as follows:

$$\boldsymbol{\rho}_k = [\sqrt{P^a_{1k}}, \sqrt{P^a_{2k}}, ..., \sqrt{P^a_{Lk}}]^T, \tag{5.22}$$

representing the transmit power allocated to user k from all the L UAV-APs, and

$$\overline{\boldsymbol{\rho}}_l = [\sqrt{P^a_{l1}}, \sqrt{P^a_{l2}}, ..., \sqrt{P^a_{lK}}]^T, \tag{5.23}$$

representing the transmit power of UAV-AP l to all K users.

The optimization problem can be written as

$$\underset{\boldsymbol{\rho}_k, \alpha_l \forall k,l}{\text{maximize}} \quad \min_{k=1,\ldots,K} \quad \gamma_k(\{\boldsymbol{\rho}_i\}) \tag{5.24a}$$

$$\text{subject to} \quad \sum_{l=1}^{L} \alpha_l P^f_l \leq P^f_{\max}, \tag{5.24b}$$

$$||\overline{\boldsymbol{\rho}}_l|| \leq \alpha_l \sqrt{P_{\text{UAV}}}, \quad \forall l, \tag{5.24c}$$

$$\alpha_l \in \{0, 1\}, \quad \forall l. \tag{5.24d}$$

The constraint in (5.24b) ensures that the total fronthaul power assigned by the CPU to the active UAV-APs should be less than the total power allowable at the fronthaul. Accordingly, the UAV-APs are disabled or enabled to satisfy this constraint. (5.24c) refers to the maximum allowable transmit power per UAV-APs, and (5.24d) represents the transmit power

constraints for each UAV-AP.

This optimization problem can be solved using the bi-section search algorithm over t^c that corresponds to the minimum of the UE SINRs. For faster convergence, we replace the feasibility check problem with a total power minimization problem. Therefore, the optimization problem changes to a second-order cone problem with binary variables, where the following optimization problem is solved at each iteration.

$$\underset{\boldsymbol{\rho}_k, \alpha_l \forall k,l}{\text{minimize}} \quad \sum_{k=1}^{K} \|\boldsymbol{\rho}_k\|^2 \tag{5.25a}$$

$$\text{subject to} \quad (5.24b) - (5.24d), \tag{5.25b}$$

$$\left\| \begin{bmatrix} \mathbf{C}_{k1}^{\frac{1}{2}} \boldsymbol{\rho}_1 \\ \vdots \\ \mathbf{C}_{kK}^{\frac{1}{2}} \boldsymbol{\rho}_K \\ \sigma_a \end{bmatrix} \right\| \leq \sqrt{\frac{1+t^c}{t^c}} \mathbf{b}_k^{\mathrm{T}} \boldsymbol{\rho}_k, \quad \forall k. \tag{5.25c}$$

The constraints from (5.24b)-(5.24d) are the same. The solution is calculated over each value of t^c [80]. The value of t_c is updated based on the problem's feasibility, continuing until the largest feasible point is reached. By substituting the optimal values of transmit powers into (5.18) and taking a minimum SINR, we obtain the maximized minimum SINR of the UEs given as $\gamma_{\text{opt}} = \min_{k \in \{1,\ldots,K\}} \gamma_k(\{\boldsymbol{\rho}_i^{\text{opt}}\})$.

5.5 Total UAV-AP Power Minimization

When the fair SINR is obtained using the max-min fairness optimizing problem, we perform a power minimization at the UAV-APs. The total power consumption at the UAV-APs consists of processing powers and hardware requirements for a fixed-wing UAV. Considering the fronthaul power consumption in the network, the total power consumption of this UAV-based network consists of

- RF transmission power consumption

The RF transmission power consumption consists of the transmit power of a single UAV-AP, which is given as $||\overline{\boldsymbol{\rho}}_l||^2$. According to the load, it is multiplied by a factor Ψ. The total power consumption consists of the total number of UAV-APs selected. Each UAV-AP has static power consumption when no transmission occurs, which is combined in this term.

- Processing power consumption in Option 7.2

  The baseband processing is performed at the UAV-APs for Option 7.2. Based on a load-dependent power consumption model, $P_{\mathrm{RW},0}^{\mathrm{proc}} + \frac{\Psi_{\mathrm{RW}}^{\mathrm{proc}}\mathcal{P}}{C_{\mathrm{RW}}^{\max}}$ gives the total processing power consumption. Here, $P_{\mathrm{RW},0}^{\mathrm{proc}}$ is the processing power of each UAV-AP in idle mode. $\Psi_{\mathrm{RW}}^{\mathrm{proc}}$ is the slope of the load-dependent processing power consumption. $C_{\mathrm{RW}}^{\max}$ is the maximum processing capacity of each UAV-AP given in giga-operations per second (GOPS). After the RF operations, baseband filtering, which consists of polyphase filtering, is performed. The complexity to perform this filtering operation per UAV-AP is given as $C_{\mathrm{F}} = \frac{40N_{\mathrm{a}}f_s}{10^9}$ GOPS. Here N_a is the number of access link antennas, and f_s is the sampling frequency. After filtering, inverse DFT is performed with complexity given as $C_{\mathrm{D}} = \frac{8N_{\mathrm{a}}N_{\mathrm{DFT}}\log_2(N_{\mathrm{DFT}})}{T_s 10^9}$ GOPS. N_{DFT} is the total number of subcarriers and the dimension of the DFT, and T_s is the OFDM symbol rate. Therefore, the total GOPS in one UAV-AP for processing is given as $\mathcal{P} = C_{\mathrm{D}} + C_{\mathrm{F}}$.

- Fronthaul power consumption given in (5.9).

- Power amplifier power consumption P_{A}.

The input variable $\mathbb{I} \in \{0, 1\}$ indicates which functional split option is selected. If Option 8 is selected, $\mathbb{I} = 0$ and for Option 7.2, $\mathbb{I} = 1$.

The total power consumption at the UAV-AP is

$$\rho_{\mathrm{tot}}(\{\boldsymbol{\rho}_i, \alpha_l\}) = \mathbb{I}\left(P_{\mathrm{UAV},0}^{\mathrm{proc}} + \frac{\Psi_{\mathrm{UAV}}^{\mathrm{proc}}\mathcal{P}}{C_{\mathrm{UAV}}^{\max}}\right)\sum_{l=1}^{L}\alpha_l + \sum_{l=1}^{L}\alpha_l\left(\mathbb{I}P_l^{f\_7.2} + (1-\mathbb{I})P_l^{f\_8}\right) + \sum_{l=1}^{L}\alpha_l \cdot P_{\mathrm{A}} + \Psi_t\sum_{l=1}^{L}\sum_{k=1}^{K}\rho_{k,l}^2. \quad (5.26)$$

We minimize total power consumption in UAV-APs, considering the SINR requirement on the user end and the fronthaul power constraints. We formulate the optimization function as

$$\underset{\boldsymbol{\rho}_k, \alpha_l \forall k,l}{\text{minimize}} \quad \rho_{\text{tot}}(\{\boldsymbol{\rho}_i, \alpha_l\}) \tag{5.27a}$$

$$\text{subject to} \quad \left\| \begin{bmatrix} \mathbf{C}_{k1}^{\frac{1}{2}} \boldsymbol{\rho}_1 \\ \vdots \\ \mathbf{C}_{kK}^{\frac{1}{2}} \boldsymbol{\rho}_K \\ \sigma_a \end{bmatrix} \right\| \leq \sqrt{\frac{1+\Gamma_k}{\Gamma_k}} \mathbf{b}_k^{\mathrm{T}} \boldsymbol{\rho}_k, \quad \forall k, \tag{5.27b}$$

$$\sum_{l=1}^{L} \alpha_l \left(\mathbb{I} P_l^{f\text{-}7.2} + (1-\mathbb{I}) P_l^{f\text{-}8} \right) \leq P_{\max}^f, \tag{5.27c}$$

$$||\overline{\boldsymbol{\rho}}_l|| \leq \alpha_l \sqrt{P_{\text{UAV}}}, \quad \forall l, \tag{5.27d}$$

$$\alpha_l \in \{0, 1\}, \quad \forall l. \tag{5.27e}$$

The constraint in (5.27b) satisfies the minimum SINR requirement for each user, Γ_k, represented as a second-order-cone problem. The constraint (5.27c) limits the allocated fronthaul transmit powers for each UAV-AP according to the maximum allowable fronthaul power $P_{\max}^f$. The constraint in (5.27d) provides the transmit power constraint per UAV-AP. (5.27e) defines α_l as a binary variable. This is a mixed binary second-order cone problem in the convex form. However, it is non-convex and combinatorial due to the binary variables. Although the worst time complexity of the problem is exponential, the small number of binary variables makes the complexity of the problem manageable. As a result, we utilize the CVX-MOSEK solver [86] to solve this optimization problem effectively, with an algorithm runtime of 12.3 sec. By substituting the values of the variables, we can determine the minimized total power consumption of the UAV-APs while serving the users on the ground, all while adhering to the power constraints imposed on the fronthaul.

5.6 Results and Discussions

In this section, we discuss the impact of a number of antennas at the CPU on the fronthaul bandwidth allocated to activate at least one UAV-AP and the fair SINR obtained in the access link. We also analyze the total power consumption at the UAV-APs, considering the SINR requirement at the user end for sub-6 GHz and mmWave fronthaul channels.

The sub-6 GHz-band system simulation parameters are $L = 16$, $K = 8$, $N_{\mathrm{c}} = 64$, $N_{\mathrm{a}} = 4$, $f_c = 3.5$Ghz, $P^{f}_{\max} = 10$W, $P_{\mathrm{UAV}} = 1$W. The mmWave simulation parameters are $N_{\mathrm{c}} = 1024$, $f_c = 28$GHz, and number of paths $n = 2$ for the fronthaul link. The remote radio head (RRH) power and processing configurations are considered from [87], [88], [89]. The processing power parameters $P^{\mathrm{proc}}_{\mathrm{RW},0} = 20.8$W, $\Psi^{\mathrm{proc}}_{\mathrm{RW}} = 74$W, $C^{\max}_{\mathrm{RW}} = 180$GOPS [85]. The other parameters are $N_{\mathrm{DFT}} = 2048$, $N_{\mathrm{used}} = 1200$, $f_s = 30.72$MHz, $T_s = 71.4\mu$s, PilotPower = 100mW, $\tau_c = 192$, $\tau_u = 8$, $N_{\mathrm{bits}} = 8$. The users and the UAV-APs are distributed uniformly in an area of 1 km $\times$ 1 km. We consider a fixed-wing drone at a height $h_u = 200$m to serve the users on the ground, establishing a fronthaul for the CPU situated in the center at the height of $h_c = 50$m. We follow the same path loss model as [90] with the probability of LoS is defined as

$$P_{\mathrm{L}} = \frac{1}{1 + \eta \exp\left(-\mu(\theta_l - \eta)\right)}$$

, where η and μ are the environmental parameters and θ_l is the elevation angle. The environmental parameters in the fronthaul are represented as $\eta^f = 4.8$, $\mu^f = 0.43$, and in the access link are represented as $\eta^a = 9.61$ and $\mu^a = 0.16$. The mechanical power consumption for fixed-wing drones given in [91] is considered for the calculation of the service time of the fixed-wing UAV-APs. In Figure 5.2(a), we present the minimum fronthaul bandwidth required to activate a single UAV-AP in the network using the best fronthaul channel to serve the ground users. The results show a notable reduction in the fronthaul bandwidth requirement for Option 7.2 compared to Option 8. However, mmWave channels require 42% more bandwidth due to their higher path loss, though this remains feasible for real-time applications. Option 7.2 reduces the fronthaul bandwidth demand by approximately 55% compared to Option 8 due to the lower data rate requirements. In Figure 5.2(b), we plot

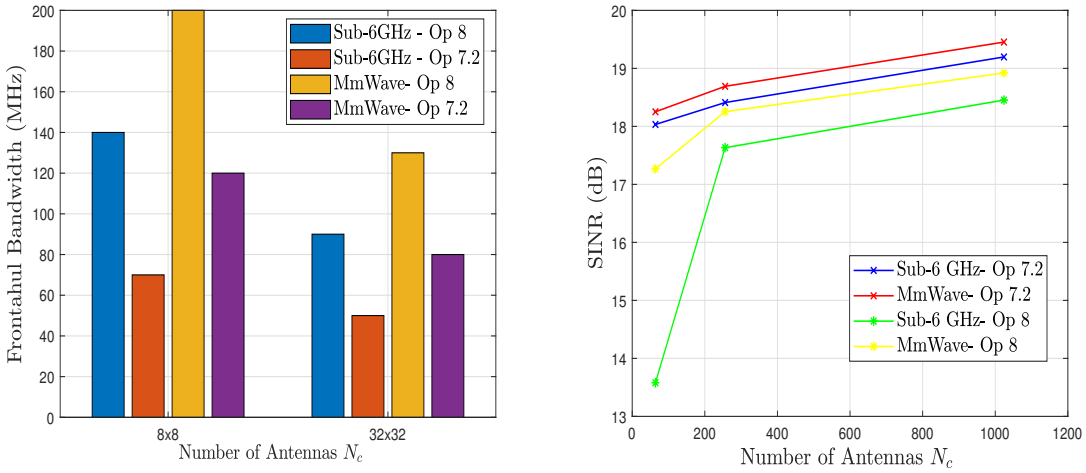

Figure 5.2. (a) Number of fronthaul antennas versus the fronthaul bandwidth to activate one UAV-AP for Option 8 and 7.2 (b) Number of fronthaul antennas versus the SINR at the user at the UAV-APs with fronthaul bandwidth B_{F} for mmWave= 500 MHz, B_{F} for sub-6 GHz = 150 MHz, for Option 8 and 7.2

the number of antennas at the CPU, N_{c}, against the SINR experienced by the users using the max-min fairness algorithm. The results indicate that Option 7.2 outperforms Option 8 as it enables a higher number of UAV-APs to remain active due to its reduced fronthaul bandwidth requirements, resulting in an overall increase in SINR in the network. Additionally, mmWave channels achieve higher SINR than sub-6 GHz channels, primarily due to their capacity to support the activation of more UAV-APs. Notably, the SINR performance for both Option 8 and Option 7.2 is nearly identical when using mmWave channels

In Figure 5.3(a), we illustrate the relationship between the SINR requirements at the user end and the total power consumption at the UAV-APs. The results show that Option 7.2 consumes 90% more power than Option 8 due to the additional processing functions performed at the UAV-APs, which significantly increase their power consumption. Additionally, mmWave channels demonstrate slightly lower power consumption than sub-6 GHz, owing to their higher fronthaul capacity, allowing them to achieve the same SINR more efficiently. Furthermore, mmWave channels combined with Option 8 deliver higher SINR while maintaining reduced power consumption. For SINR requirements exceeding 18 dB, the network's feasibility drops below 50%, which is beyond the scope of this analysis. A comparison of

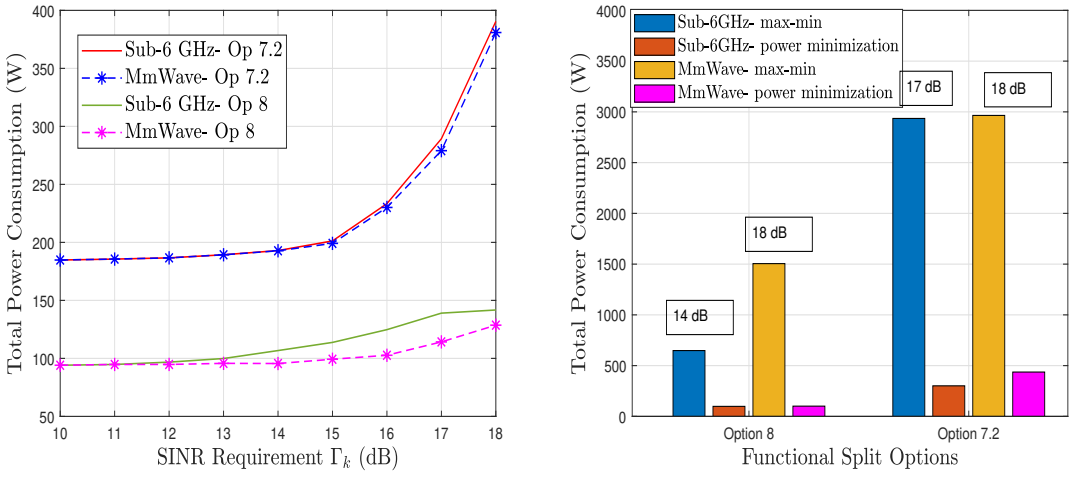

(a) (b)

Figure 5.3. (a) Total power consumption versus SINR requirement with B_F for mmWave= 500 MHz, $N_c = 1024$, B_F for Sub-6 GHz = 150 MHz, $N_c = 64$ for Option 8 and 7.2 (b) Comparison for min-max optimization and power minimization for different options with maximized SINR requirement

Figure 5.2(b) and Figure 5.3(a) reveals that the Option 8 split with a mmWave fronthaul channel not only consumes less power at the UAV-APs but also provides users with higher SINR. In Figure 5.3(b), we observe a substantial reduction in power consumption when transmit powers and UAV activation are optimized to meet a fair SINR requirement using the max-min fairness algorithm. Here, the optimal fair SINR obtained from the max-min fairness algorithm is used as the target SINR, Γ_k, in the power minimization problem. These optimal SINR values are highlighted in the figure, demonstrating that this approach leads to more energy-efficient UAV-APs while maintaining the required QoS for users.

Service time comparison: The service time for each UAV-AP depends on the battery mass and the total power consumed by the UAV-AP, which includes the mechanical power consumption and communication power consumption. Considering a fixed-wing UAV-AP, the mechanical power consumption consists of the weight of the battery and the weight of the aircraft [92]. The battery mass is varied from 5 kg to 9 kg, with 1 kg increment, and the specific energy (E_d) of the battery is changed to {50, 180, 350} Wh/kg according to battery technologies. Considering the total power consumption ρ_{tot} and battery energy per unit mass E_d, the service time is calculated as, $T_{sr} = \frac{E_d m_b}{\rho_{tot}}$, where m_b is the battery mass.

The results are shown in Table 5.1.

Table 5.1: Service Time

Option	Service Time (min)
Option 8	89
Option 7.2	82

5.7 Chapter Conclusion

In this chapter, the impact of fronthaul capacity limitations in a UAV-based wireless network with cell-free mMIMO providing the access link to users had been investigated. We analyzed the performance of different functional split options implemented in the fronthaul, focusing on their influence on user SINR and power consumption at the UAV-APs. Our findings highlighted that Option 7.2 achieved superior user performance by providing higher SINR compared to Option 8, owing to its reduced processing burden on the UAV-APs. This allowed more UAV-APs to remain active, thereby improving signal quality. However, in terms of power consumption, Option 8 had proven to be efficient, as it shifted significant processing functions to the central processing unit (CPU), reducing the energy demand on the UAV-APs. Despite its lower power consumption, Option 8 required higher fronthaul bandwidth to achieve the same SINR as Option 7.2, making the trade-off between fronthaul capacity and power efficiency a critical consideration in network design.

Chapter 6

Conclusions and Future Work

6.1 Main Conclusions

In this thesis, we focused on analyzing the fundamental limitations of conventional cellular networks and explored how UAV-based networks could serve as viable solutions. Traditional terrestrial networks suffered from challenges such as dynamic blockage effects, limited infrastructure flexibility, and inefficient handover management, particularly in highly mobile and disaster-prone environments. UAV-based networks, with their inherent adaptability and enhanced LoS capabilities, presented a promising alternative. We systematically investigated multiple aspects of UAV-enabled cellular networks, including access and fronthaul link management, caching-assisted mobility optimization, and cell-free mMIMO deployment strategies.

In Chapter 3, we analyzed a joint framework for access and xHaul link association in a UAV-aided cellular network. Unlike conventional networks, where fronthaul/backhaul infrastructure is largely static, UAV-based networks require a dynamic and adaptive approach to manage xHaul capacity efficiently. We derived analytical expressions for coverage probability, initially for a single UAV-AP scenario in a BPP network and then extended them to a UAV-assisted HetNet. Our results shown that, beyond a critical UAV deployment density, further network densification led to increased interference and diminished spatial separation, thereby degrading LoS association probability. This observation underscored the importance of optimized UAV placement strategies to balance coverage enhancement and interference mitigation. Additionally, we analyzed the impact of cache-enabled UAV-APs on access and xHaul link utilization. Our findings revealed that larger cache storage at UAV-APs significantly reduced reliance on xHaul links, freeing up network resources for access link transmissions. We also proposed admission control mechanisms to determine the optimal number of simultaneously served users per UAV-AP to ensure a per-user throughput

above a predefined threshold. These insights offered guidelines for effective UAV deployment, ensuring load balancing and maximizing network efficiency.

In Chapter 4, we investigated HO management in UAV-based networks, where frequent user mobility led to excessive handovers, increasing signaling overhead and degrading network performance. Using stochastic geometry and cache-enabled HO schemes, we evaluated network performance across different mobility scenarios, including vehicular and pedestrian environments. Our analysis demonstrated that terminal-side caching significantly reduced HO rates by enabling seamless content retrieval without frequent association switches. This approach not only enhanced average user throughput but also improved energy efficiency, particularly in dense urban deployments. In disaster-stricken areas where terrestrial infrastructure been damaged, UAV-assisted networks provided a crucial means of connectivity. We modeled UAV base stations as a 2-D MPPP to characterize handover rates, signal reliability, and user throughput under varying UAV densities and altitudes. Our findings indicated that, while increasing UAV density enhanced coverage, it also raised handover frequency, leading to trade-offs between mobility management and connectivity stability. For urban environments with blockages, we examined the role of obstacles in shaping network reliability and interference patterns. While blockages typically degraded LoS probability, they indirectly enhanced network reliability by mitigating interference in ultra-dense deployments. The proposed cache-enabled HO management scheme effectively reduced unnecessary handovers, lowered latency, and improved overall throughput, particularly in high-mobility environments.

In Chapter 5, we explored fronthaul capacity limitations in UAV-based cell-free mMIMO networks, where multiple distributed UAV-APs collaboratively served users without predefined cell boundaries. In such networks, functional split options in the fronthaul played a crucial role in determining user SINR, power consumption, and overall system efficiency. We analyzed the impact of Option 8 and Option 7.2 functional splits, comparing their effects on network performance. Our results revealed that Option 7.2 provided superior user performance by achieving higher SINR, as it reduced the computational burden on UAV-APs, allowing more APs to remain active. However, Option 8 proven to be more energy-efficient, as it offloaded significant processing to the CPU, thereby reducing power consumption at

the UAV-APs. Despite its lower power consumption, Option 8 required higher fronthaul bandwidth to achieve performance levels comparable to Option 7.2. This highlighted a critical trade-off between fronthaul capacity and power efficiency, emphasizing the need for optimized functional split selection based on network constraints. Additionally, we analyzed multi-user performance in the presence of limited fronthaul resources and proposed an adaptive UAV-AP activation strategy that dynamically adjusted the number of active UAVs based on real-time traffic demand. Our study provided key design insights for the deployment of cell-free mMIMO in UAV-based networks, ensuring seamless user connectivity while maintaining energy efficiency.

Overall, this thesis presented a comprehensive analysis of UAV-based cellular networks, addressing key challenges in access/fronthaul management, mobility optimization, and network reliability. Our findings provided theoretical and practical guidelines for designing efficient UAV-assisted 5G and beyond-5G networks, particularly in scenarios with mobile users, disaster recovery operations, and ultra-dense deployments. The integration of caching, stochastic geometry-based modeling, and advanced functional split options offered a pathway toward more scalable and energy-efficient UAV networks, ultimately enhancing QoS for users.

6.2 Future Work

This thesis will pave the way for some exciting future research work. The key research directions that can be explored are:

1. In our work, analyzed joint resource allocation and coverage in IAB UAV-based networks by leveraging content caching at the UAVs. A promising direction for future research is to explore distributed caching mechanisms among TBSs and UAV-BSs, and to evaluate their joint impact on system performance and resource partitioning. Such studies could be conducted in collaboration with research groups focusing on edge caching and aerial networks, such as Department of Science and Technology (DST), India, which fund projects on edge intelligence and network automation.

2. The current work focused on minimizing unnecessary handovers by incorporating caching capabilities at the user end, supported by a semi-analytical analysis of the cache-based scheme under blockage conditions. Future work could extend this model into a reinforcement learning (RL)-based framework to enhance the efficiency and adaptability of handover decisions. This extension opens opportunities for collaboration with research labs and industry partners developing AI-driven mobility management solutions, potentially under funding schemes such as the SERB Core Research Grant (CRG).

3. We also investigated fronthaul capacity limitations in UAV-based cell-free massive MIMO networks under different functional split options. This can be further extended to HetNet scenarios to analyze performance–energy trade-offs and optimize multi-tier architectures. Additionally, integrating reinforcement-based energy management techniques can enable UAVs to adapt their transmit power dynamically based on traffic or energy constraints. Future investigations could benefit from interdisciplinary collaborations between communication and computer science research groups, such as those at KTH Royal Institute of Technology, Sweden.

PUBLICATIONS

Journals

1. N. R. R, G. Ghatak, A. Srivastava and V. A. Bohara, "Cache Enabled UAV HetNets: Access - xHaul Coverage Analysis and Optimal Resource Partitioning," in IEEE Transactions on Cognitive Communications and Networking, vol. 10, no. 1, pp. 292-307, Feb. 2024, doi: 10.1109/TCCN.2023.3322985.

2. N. R.R., G. Ghatak, V. A. Bohara and A. Srivastava, "Performance Analysis of Cache-Enabled Handover Management for Vehicular Networks," in IEEE Transactions on Network Science and Engineering, vol. 11, no. 1, pp. 1151-1164, Jan.-Feb. 2024, doi: 10.1109/TNSE.2023.3321296.

3. N. R. R. et al., "UAV-Based Cell-Free Massive MIMO: Joint Activation and Power Optimization Under Fronthaul Capacity Limitations," in IEEE Wireless Communications Letters, vol. 14, no. 8, pp. 2496-2500, Aug. 2025, doi: 10.1109/LWC.2025.3574360.

4. N. R.R, G. Ghatak, and V. A. Bohara, "Handover Management in UAV Networks With Blockages," in IEEE Open Journal of the Communications Society, vol. 6, pp. 8209-8224, 2025, doi: 10.1109/OJCOMS.2025.3610952.

Conferences

1. N. R.R, A. Gupta, G. Ghatak, A. Srivastava and V. A. Bohara, "Joint Bandwidth and Position Optimization in UAV Networks Deployed for Disaster Scenarios," 2021 National Conference on Communications (NCC), Kanpur, India, 2021, pp. 1-6, doi: 10.1109/NCC52529.2021.9530185

2. N. R. R, G. Ghatak, V. A. Bohara and A. Srivastava, "Analysis of Handover Rate and Coverage Performance of Mobile Users in UAV Networks," 2024 IEEE 99th Vehicular

Technology Conference (VTC2024-Spring), Singapore, Singapore, 2024, pp. 1-5, doi: 10.1109/VTC2024-Spring 62846.2024.10683128.

Appendix A

Proofs of Chapter 3

A.1 Proof of Lemma 3.1

The throughput for the access link is given as

$$R_{\mathrm{u}} = \beta \sum_{i=1}^{N_{\mathrm{u}}} \left(\frac{B}{N_{\mathrm{u}}} \right) \log_2 \left(1 + \frac{P_{\mathrm{ra}}^{i}}{N_0} \right), \tag{A.1}$$

where P_{ra}^{i} is the power received at the i^{th} user from the UAV, N_0 is the additive white gaussian noise (AWGN) power and N_{u} is the total number of users. Since FDMA is assumed, each user is allocated $\frac{B}{N_{\mathrm{u}}}$ Hz of orthogonal bandwidth, and the total throughput is obtained by summing over the per-user rates. In order to characterize this, we first derive the distance distribution of the users from the UAV.

The conditional CDF of a typical user located at a distance of w_{i} from u_0 in the access link is given as [47]

$$F_{\mathrm{a}}(w_{\mathrm{i}}|u_0) = \begin{cases} F_{1\mathrm{a}}(w_{\mathrm{i}}|u_0), & 0 \leq w_{\mathrm{i}} \leq r_{\mathrm{d}} - u_0 \\ F_{2\mathrm{a}}(w_{\mathrm{i}}|u_0), & r_{\mathrm{d}} - u_0 \leq w_{\mathrm{i}} \leq r_{\mathrm{d}} + u_0. \end{cases} \tag{A.2}$$

Without loss of generality, let us assume that the UAV lies at the positive side of the x-axis. The CDF of w_{i} is derived using the geometric argument applied in [93, Th. 2.3.6]. There are two cases: i) $w_{\mathrm{i}} \leq r_{\mathrm{d}} - u_0$, i.e., when the circle with a radius joining the UAV and the user is completely inside the outer circle as in Figure A.1(a), and ii) $w_{\mathrm{i}} > r_{\mathrm{d}} - u_0$, i.e., when the users are far enough from the UAV position and the intersection area is not entirely inside the circle of radius r_{d} as in Figure A.1(b).

For the first case in Figure A.1(a), the CDF is simply: $F_{1\mathrm{a}}(w_{\mathrm{i}}|u_0) = w_{\mathrm{i}}^2/r_{\mathrm{d}}^2$.

For the second case, we compute the intersection area of the circles of radius r_{d} and w_{i}

to compute the CDF of a user at a distance of w_1 from u_0.

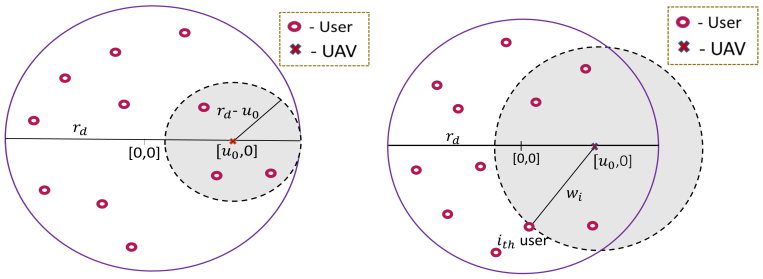

Figure A.1. (a) Access link- Users close to the UAV (b) Access link- Users far from the UAV

As the users are distributed as BPP, the CDF for a given user located outside the circle of radius $(r_\mathrm{d} - u_0)$ which is at a distance of w_1 from u_0 is given as

$$F_{2\mathrm{a}}(w_\mathrm{i}|u_0) = \frac{w_\mathrm{i}^2}{\pi r_\mathrm{d}^2}\left[w_\mathrm{i}^2\left(\theta - \frac{1}{2}\sin 2\theta\right) + r_\mathrm{d}^2\left(\phi - \frac{1}{2}\sin 2\phi\right)\right], \tag{A.3}$$

where, θ=$\cos^{-1}\left(\frac{-r_\mathrm{d}^2+w_\mathrm{i}^2+u_0^2}{2u_0 w_\mathrm{i}}\right)$ and ϕ=$\cos^{-1}\left(\frac{r_\mathrm{d}^2-w_\mathrm{i}^2+u_0^2}{2u_0 r_\mathrm{d}}\right)$.
The conditional PDF of w_i for a given u_0 is obtained by taking the derivative of CDF with respect to w_i as given in (3.2).

The throughput coverage probability of access link is obtained by comparing the rate throughput with γ_a, i.e., $\mathbb{P}\left(R_\mathrm{u} > \gamma_\mathrm{a}\right)$ where, γ_a is the throughput threshold defined for access link, which is given as

$$R_\mathrm{a}(\gamma_\mathrm{a}, u_0) = \int_{w_\mathrm{i}} \left(\exp\left[\left\{\frac{-N_0}{P_\mathrm{u} K w_\mathrm{i}^{-\alpha}}\left(2^{\frac{N_\mathrm{u}\gamma_\mathrm{a}}{B\beta}} - 1\right)\right\}\right]\right) f_\mathrm{a}(w_\mathrm{i}|u_0)\mathrm{d}w_\mathrm{i}. \tag{A.4}$$

$$R_\mathrm{a}(\gamma_\mathrm{a}, u_0) = \int_0^{r_\mathrm{d}-u_0} R_{\mathrm{a}1}(\gamma_\mathrm{a}, w_\mathrm{i}) f_{1\mathrm{a}}(w_\mathrm{i}|u_0)\mathrm{d}(w_\mathrm{i}) + \int_{r_\mathrm{d}-u_0}^{r_\mathrm{d}+u_0} R_{\mathrm{a}1}(\gamma_\mathrm{a}, w_\mathrm{i}) f_{2\mathrm{a}}(w_\mathrm{i}|u_0)\mathrm{d}(w_\mathrm{i}). \tag{A.5}$$

A.2 Proof of Lemma 3.2

The rate throughput for backhaul link is given as

$$R_\mathrm{t} = (1-\beta)B\log_2(1 + SNR_\mathrm{b}), \tag{A.6}$$

where, $SNR_{\mathrm{b}} = \frac{P_{\mathrm{rb}}}{N_0}$. P_{rb} is the received power at the UAV from the nearest BS.

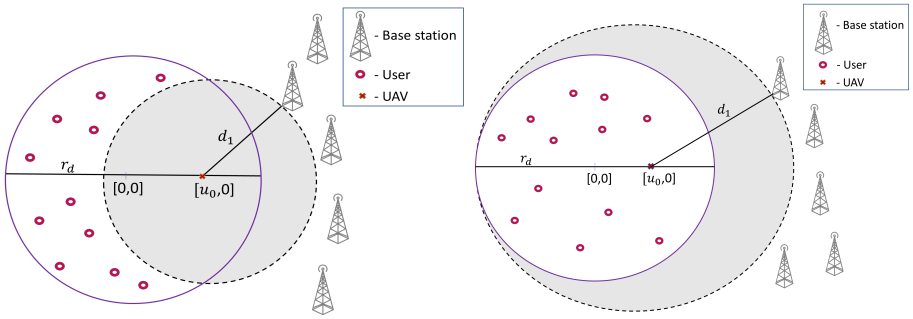

(a) (b)

Figure A.2. (a) Backhaul link- Nearest BS close to the circle of radius r_d (b) Backhaul link- Nearest BS far from the circle of radius r_d

In order to obtain R_t, we find the PDF of the distance of the UAV from the associated BS. Similar to the access, in order to find the PDF, there are two conditions which depends on x_0, which is the projection of the point of intersection of two circles on x-axis, as given in Figure A.2(a) and Figure A.2(b).

The conditions are i) $-r_{\mathrm{d}} < x_0 < r_{\mathrm{d}}$ and ii) $x_0 \leq -r_{\mathrm{d}}$.

1. $-r_{\mathrm{d}}<x_0<r_{\mathrm{d}}$

   We compute the intersection area of the circles in Figure A.2(a), in order to find the CDF of the nearest BS which is at a distance of d_1 from u_0. The intersection area represented as Y_1, which is to be considered for the calculation of CDF is

$$Y_1 = 2\left(\int_{u_0-d_1}^{x_0} \sqrt{d_1^2 - (a-u_0)^2}\mathrm{d}a + \int_{x_0}^{r_{\mathrm{d}}} \sqrt{r_{\mathrm{d}}^2 - a^2}\mathrm{d}a\right). \tag{A.7}$$

   Since, the BSs are outside the circle of radius r_{d} and they are distributed as PPP, the conditional CDF of the nearest BS located at a distance d_1 from u_0 is given as

$$F_{1\mathrm{b}}(d_1 \mid u_0) = 1 - \exp\left[-\lambda_{\mathrm{M}}\left(d_1^2\left(\frac{\pi}{2} + y\sqrt{1-y^2} - \tan^{-1}\frac{-y}{\sqrt{1-y^2}}\right) - r_{\mathrm{d}}^2\left(\frac{\pi}{2} - x\sqrt{1-x^2} - \tan^{-1}\frac{x}{\sqrt{1-x^2}}\right)\right)\right], \tag{A.8}$$

where, $x = \frac{r_{\mathrm{d}}^2 - d_1^2 + u_0^2}{2u_0 r_{\mathrm{d}}}$ and $y = \frac{u_0^2 - r_{\mathrm{d}}^2 + d_1^2}{2u_0 d_1}$.

To find the PDF of d_1, the derivative of CDF is computed. The conditional PDF of d_1 for a given u_0, $f_{1\mathrm{b}}(d_1|u_0)$ is given in (3.7), where, $z = \frac{d_1^2 + r_{\mathrm{d}}^2 - u_0^2}{2u_0 d_1^2}$.

2. $x_0 \leq -r_{\mathrm{d}}$

In Figure A.2(b), the intersection area of two circles is the area of the circle with radius r_{d} itself. So, the CDF of the distance of nearest BS d_1 from u_0 is

$$F_{2\mathrm{b}}(d_1|u_0) = 1 - \exp\left(-\lambda_{\mathrm{M}}\left(\pi d_1^2 - \pi r_{\mathrm{d}}^2\right)\right). \tag{A.9}$$

The conditional PDF of d_1 with respect to u_0, $f_{2\mathrm{b}}(d_1|u_0)$ is given in (3.8).

Using the PDF, we derive the throughput coverage probability of backhaul link is obtained by comparing the rate throughput with γ_{b} i.e., $\mathbb{P}\left(R_{\mathrm{t}} > \gamma_{\mathrm{b}}\right)$, where, γ_{b} is the throughput threshold for the backhaul link. Therefore, the throughput coverage probability for the backhaul link is given as

$$R_{\mathrm{b}}(\gamma_{\mathrm{b}}, u_0) = \int_{r_{\mathrm{d}} - u_0}^{R_2} R_{\mathrm{b1}}(\gamma_{\mathrm{b}}, d_1) f_{\mathrm{b}}(d_1|u_0)\mathrm{d}(d_1). \tag{A.10}$$

A.3 Proof of Lemma 3.5

In order to analyze the performance of backhaul links, first, we derive the CDF of the distance between the tagged UAV-AP and the closest TBS. The CDF of d_{MB} is evaluated as:

$$F_{d_{\mathrm{MB}}}(x) = 1 - \mathbb{P}\left(d_{\mathrm{MB}} > x\right) = 1 - \exp\left[-\pi\lambda_{\mathrm{M}}\left(x^2 - h^2\right)\right] \tag{A.11}$$

where h is the height of the tagged UAV-AP from the ground. In order to find the PDF of d_{MB}, we take the derivative of (A.11), and we can obtain $f_{d_{\mathrm{MB}}}(x)$ given in (3.16).

Next, we derive the distribution of the distance of the tagged UAV-AP to the closest UAV-BS as given in Fig. A.3. For the ease of presentation, the distance between the UAV-BS and UAV-AP is represented as t, which is the same as d_{UB}. From Figure A.4, we observe the two conditions to be considered when deriving the distribution of the distance d_{UB}.

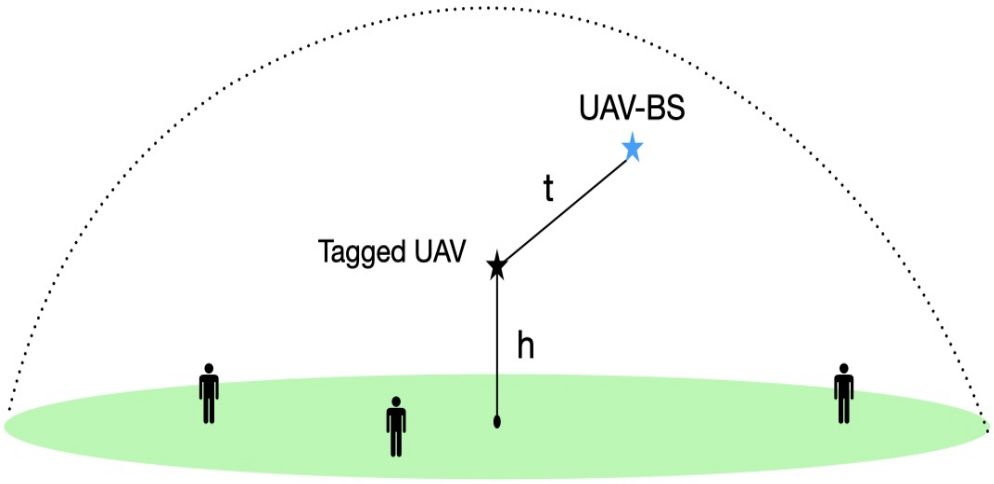

Figure A.3. Association of tagged UAV to the nearest UAV-BS

1. $t \leq h$

   The CDF of d_{UB} is obtained by leveraging the void probability of 3-D PPP. Conditioned on the height of the tagged UAV-AP as given in Figure A.4(a),

$$F'_{d_{\mathrm{UB}}}(x|h) = 1 - \mathbb{P}\left(d_{\mathrm{UB}} > x\right) = 1 - \exp\left(-\lambda_{\mathrm{UB}} \frac{4}{3}\pi x^3\right) \tag{A.12}$$

   Taking the derivative of (A.12), $f'_{d_{\mathrm{UB}}}(x|h)$ is obtained given in (3.18) .

2. $t > h$

   In order to find the CDF of the distance d_{UB} given in Figure A.4(b), we need to find the volume of the segment of height $t - h$ is given as

$$V_{\mathrm{t-h}} = \frac{1}{3}\pi\left(t-h\right)^2\left(3t - (t-h)\right) = \frac{1}{3}\pi\left[2t^3 - 3t^2h + h^3\right] \tag{A.13}$$

   The distance distribution is derived by considering the volume of the sphere from which the volume of the segment $V_{\mathrm{t-h}}$ is omitted. The CDF of d_{UB} is given as

$$F''_{d_{\mathrm{UB}}}(x) = 1 - \mathbb{P}\left(d_{\mathrm{UB}} > x\right) = 1 - \exp\left[-\lambda_{\mathrm{UB}}\left(\frac{2}{3}\pi x^3 + x^2\pi h - \frac{1}{3}\pi h^3\right)\right] \tag{A.14}$$

   The PDF of d_{UB} for $t > h$ is obtained by taking the derivative of (A.14), and we can

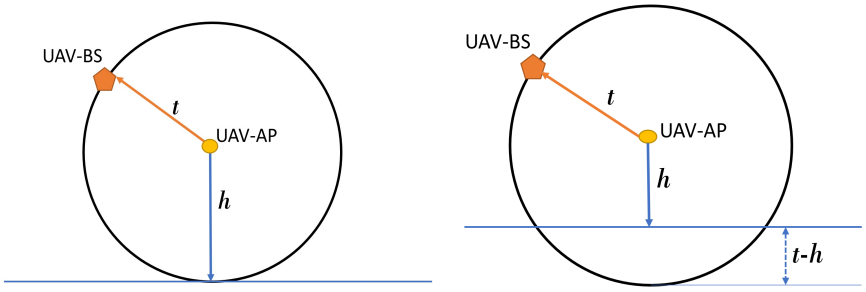

(a) (b)

Figure A.4. (a) $t \leq h$ (b) $t > h$

obtain $f''_{d_{\mathrm{UB}}}(x|h)$ as given in (3.19).

The PDF of the distance between the tagged UAV-AP and the closest UAV-BS at the backhaul link is given in (3.17).

A.4 Proof of Lemma 3.6

Comparing the received powers from all the TBS, LoS UAV-APs and NLoS UAV-APs, the typical user associates to the TBS tier when either of the following events are true:

1. $R_{\mathrm{MA}} > R_{\mathrm{UAL}} > R_{\mathrm{UAN}}$
2. $R_{\mathrm{MA}} > R_{\mathrm{UAN}} > R_{\mathrm{UAL}}$

The probability of the first event $R_{\mathrm{MA}} > R_{\mathrm{UAL}} > R_{\mathrm{UAN}}$ can be written as

$$\mathbb{P}\left(R_{\mathrm{MA}} > R_{\mathrm{UAL}} > R_{\mathrm{UAN}}\right) = \mathbb{P}\left(P_{\mathrm{M}} d_{\mathrm{MA}}^{-\alpha_{\mathrm{N}}} > P_{\mathrm{UA}} d_{\mathrm{UAL}}^{-\alpha_{\mathrm{L}}} > P_{\mathrm{UA}} d_{\mathrm{UAN}}^{-\alpha_{\mathrm{N}}} | d_{\mathrm{UAL}}\right). \tag{A.15}$$

Using the CDF of d_{UAL} from **Lemma** 3.4, for given instances of d_{UAN} and d_{MA}, (A.15) can be written as:

$$\begin{aligned}\mathbb{P}\left(P_{\mathrm{M}} d_{\mathrm{MA}}^{-\alpha_{\mathrm{N}}} > P_{\mathrm{UA}} d_{\mathrm{UAL}}^{-\alpha_{\mathrm{L}}} > P_{\mathrm{UA}} d_{\mathrm{UAN}}^{-\alpha_{\mathrm{N}}} \,\middle|\, d_{\mathrm{UAL}}\right) = \\ \left[F_{d_{\mathrm{UAL}}}\left(d_{\mathrm{UAN}}^{\frac{\alpha_{\mathrm{N}}}{\alpha_{\mathrm{L}}}}\right) - F_{d_{\mathrm{UAL}}}\left(C_{\mathrm{M}}\, d_{\mathrm{MA}}^{\frac{\alpha_{\mathrm{N}}}{\alpha_{\mathrm{L}}}}\right) \,\middle|\, d_{\mathrm{UAN}}, d_{\mathrm{MA}}\right] \\ \times \mathbb{P}\left(d_{\mathrm{UAN}}^{\frac{\alpha_{\mathrm{N}}}{\alpha_{\mathrm{L}}}} > C_{\mathrm{M}}\, d_{\mathrm{MA}}^{\frac{\alpha_{\mathrm{N}}}{\alpha_{\mathrm{L}}}}\right).\end{aligned} \tag{A.16}$$

Considering the CDF terms separately,

$$F_{d_{\mathrm{UAL}}}\left(d_{\mathrm{UAN}}^{\frac{\alpha_{\mathrm{N}}}{\alpha_{\mathrm{L}}}}\right)-F_{d_{\mathrm{UAL}}}\left(C_{\mathrm{M}}d_{\mathrm{MA}}^{\frac{\alpha_{\mathrm{N}}}{\alpha_{\mathrm{L}}}}\right)=\exp\left[-2\pi\lambda_{\mathrm{UA}}W_{\mathrm{L}}'\int_0^{\left(C_{\mathrm{M}}d_{\mathrm{MA}}^{\frac{\alpha_{\mathrm{N}}}{\alpha_{\mathrm{L}}}}\right)}z^2\,\mathrm{d}z\right]$$
$$-\exp\left[-2\pi\lambda_{\mathrm{UA}}W_{\mathrm{L}}'\int_0^{\left(d_{\mathrm{UAN}}^{\frac{\alpha_{\mathrm{N}}}{\alpha_{\mathrm{L}}}}\right)}y^2\,\mathrm{d}y\right]. \quad \text{(A.17)}$$

The outer term is given as

$$\mathbb{P}\left(d_{\mathrm{UAN}}^{\frac{\alpha_{\mathrm{N}}}{\alpha_{\mathrm{L}}}}>C_{\mathrm{M}}d_{\mathrm{MA}}^{\frac{\alpha_{\mathrm{N}}}{\alpha_{\mathrm{L}}}}\right)=\mathbb{E}_{d_{\mathrm{MA}}}\left[\exp\left(-2\pi\lambda_{\mathrm{UA}}W_{\mathrm{N}}'\int_0^{C_{\mathrm{M}}^{\frac{\alpha_{\mathrm{L}}}{\alpha_{\mathrm{N}}}}d_{\mathrm{MA}}}x^2\,\mathrm{d}x\right)\right]. \quad \text{(A.18)}$$

Taking the expectation with respect to d_{MA} and d_{UAN} over (A.17), and combine (A.17) and (A.18).

$$A_{\mathrm{MA}}^{'}=\int_0^{\infty}\int_{C_{\mathrm{M1}}}^{\infty}\left[\exp\left(-\frac{2}{3}\pi\lambda_{\mathrm{UA}}W_{\mathrm{L}}'\left(\left(\frac{P_{\mathrm{UA}}}{P_{\mathrm{M}}}\right)^{\frac{3}{\alpha_{\mathrm{L}}}}w^{\frac{3\alpha_{\mathrm{N}}}{\alpha_{\mathrm{L}}}}\right)\right)-\exp\left(-\frac{2}{3}\pi\lambda_{\mathrm{UA}}W_{\mathrm{L}}'x^{\frac{3\alpha_{\mathrm{N}}}{\alpha_{\mathrm{L}}}}\right)\right]\times$$
$$f_{d_{\mathrm{UAN}}}(x)\,\mathrm{d}x\exp\left(-\frac{2}{3}\pi\lambda_{\mathrm{UA}}W_{\mathrm{N}}'\left(\left(\frac{P_{\mathrm{UA}}}{P_{\mathrm{M}}}\right)^{\frac{3}{\alpha_{\mathrm{N}}}}w^{\frac{3\alpha_{\mathrm{N}}}{\alpha_{\mathrm{N}}}}\right)\right)f_{d_{\mathrm{MA}}}(w)\,\mathrm{d}w. \quad \text{(A.19)}$$

where $C_{\mathrm{M1}}=\left(\frac{P_{\mathrm{UA}}}{P_{\mathrm{M}}}\right)^{\frac{1}{\alpha_{\mathrm{N}}}}w$. Similarly, to compute $A_{\mathrm{MA}}^{''}$, we first evaluate the probability of the second event by using the CDF of d_{UAN} and then take the expectation with respect to d_{MA} and d_{UAL}. Finally, by summing $A_{\mathrm{MA}}^{'}$ and $A_{\mathrm{MA}}^{''}$, we obtain the overall probability of association with the TBS tier, A_{MA}. For a special case, this simplifies to the closed-form results given in (3.23) and (3.24).

A.5 Proof of Lemma 3.7

Comparing the received powers from all TBS, LoS UAV-AP and NLoS UAV-AP, where the recived power from the LoS UAV-AP is the highest, the typical user associates to the LoS UAV-AP tier when either of these events are true:

1. $R_{\mathrm{UAL}}>R_{\mathrm{UAN}}>R_{\mathrm{MA}}$

2. $R_{\mathrm{UAL}} > R_{\mathrm{MA}} > R_{\mathrm{UAN}}$

From (3.25), the first event $R_{\mathrm{UAL}} > R_{\mathrm{UAN}} > R_{\mathrm{MA}}$ can be written as $A'_{\mathrm{UAL}}(d_{\mathrm{UAL}})$, which is given as

$$A'_{\mathrm{UAL}}(d_{\mathrm{UAL}}) = \mathbb{P}\left(P_{\mathrm{UA}} d_{\mathrm{UAL}}^{-\alpha_{\mathrm{L}}} > P_{\mathrm{UA}} d_{\mathrm{UAN}}^{-\alpha_{\mathrm{N}}} > P_{\mathrm{M}} d_{\mathrm{MA}}^{-\alpha_{\mathrm{N}}}\right) = \mathbb{P}\left(C_{\mathrm{M1}} d_{\mathrm{MA}}^{\frac{\alpha_{\mathrm{N}}}{\alpha_{\mathrm{N}}}} > d_{\mathrm{UAN}} > d_{\mathrm{UAL}}^{\frac{\alpha_{\mathrm{N}}}{\alpha_{\mathrm{L}}}}\right) \tag{A.20}$$

where $C_{\mathrm{M1}} = \left(\frac{P_{\mathrm{UA}}}{P_{\mathrm{M}}}\right)^{\frac{1}{\alpha_{\mathrm{N}}}}$. For given instances of d_{UAL} and d_{MA}, considering the CDF of d_{UAN} from **Lemma** 3.4, the above probability (A.20) can be written as

$$A'_{\mathrm{UAL}}(d_{\mathrm{UAL}}) = \left[\exp\left(-2\pi\lambda_{\mathrm{UA}} W'_{\mathrm{N}} \int_0^{\left(d_{\mathrm{UAL}}^{\frac{\alpha_{\mathrm{L}}}{\alpha_{\mathrm{N}}}}\right)} z^2 \,\mathrm{d}z\right) - \exp\left(-2\pi\lambda_{\mathrm{UA}} W'_{\mathrm{N}} \int_0^{(C_{\mathrm{M1}} d_{\mathrm{MA}})} y^2 \,\mathrm{d}y\right)\right] \times \exp\left(-\pi\lambda_{\mathrm{M}} \left[\left(\frac{1}{C_{\mathrm{M1}}}\right) d_{\mathrm{UAL}}^{\frac{\alpha_{\mathrm{L}}}{\alpha_{\mathrm{N}}}}\right]^2\right). \tag{A.21}$$

Taking the expectation with respect to d_{MA}, we can obtain $A'_{\mathrm{UAL}}(d_{\mathrm{UAL}})$ as in (3.26).

Similarly, the probability of the second event $R_{\mathrm{UAL}} > R_{\mathrm{MA}} > R_{\mathrm{UAN}}$ is evaluated to obtain $A''_{\mathrm{UAL}}(d_{\mathrm{UAL}})$, where we first use the CDF of d_{MA} and then take the expectation over d_{UAN}. Furthermore, by combining A'_{UAL} and A''_{UAL}, we can obtain A_{UAL} as given in (3.25). Finally, by taking the expectation over d_{UAL}, the association probability at which the typical user to the LoS UAV-AP tier is obtained as:

$$\bar{A}_{\mathrm{UAL}} = \int_0^{\infty} A_{\mathrm{UAL}}(x)\, f_{d_{\mathrm{UAL}}}(x)\,\mathrm{d}x.$$

where, the PDF of d_{UAL}, which is represented as $f_{d_{\mathrm{UAL}}}$, can be obtained from (3.13).

A.6 Proof of Proposition 1

Recall the probability of LoS association in access link $\bar{A}_{\mathrm{UAL}}$, given in **Lemma** 3.7 is divided into two parts, which is represented as:

$$\bar{A}_{\mathrm{UAL}} = \int_0^{\infty} A'_{\mathrm{UAL}}(d_{\mathrm{UAL}}) f_{d_{\mathrm{UAL}}}(x)\mathrm{dx} + \int_0^{\infty} \mathrm{A}''_{\mathrm{UAL}}(\mathrm{d_{UAL}})\mathrm{f_{d_{UAL}}(x)dx} \tag{A.22}$$

Expanding the first part, which can be written as

$$\int_0^\infty A'_{\mathrm{UAL}}(d_{\mathrm{UAL}})\, f_{d_{\mathrm{UAL}}}(x)\,\mathrm{d}x = \int_0^\infty \int_{C_{\mathrm{L1}}}^\infty \left[\exp\left(-2\pi\lambda_{\mathrm{UA}} W'_{\mathrm{N}} \int_0^{d_{\mathrm{UAL}}^{\frac{\alpha_{\mathrm{L}}}{\alpha_{\mathrm{N}}}}} z^2\,\mathrm{d}z \right) - \exp\left(-2\pi\lambda_{\mathrm{UA}} W'_{\mathrm{N}} \int_0^{L_1} y^2\,\mathrm{d}y \right) \right] \cdot \exp\left(-\pi\lambda_{\mathrm{M}} \left(C_{\mathrm{L1}}\right)^2 \right) f_{d_{\mathrm{MA}}}(x)\, f_{d_{\mathrm{UAL}}}(y)\,\mathrm{d}x\,\mathrm{d}y \quad \text{(A.23)}$$

Splitting (A.23) into two parts by multiplying with the appropriate PDFs, represented as A_{P1} and A_{P2}, which can be written as,

$$\begin{aligned} \int_0^\infty A'_{\mathrm{UAL}}(d_{\mathrm{UAL}}) f_{d_{\mathrm{UAL}}}(x)\,\mathrm{d}x &= A_{\mathrm{P1}} - A_{\mathrm{P2}} \\ &= \underbrace{\int_0^\infty \int_{C_{\mathrm{L1}}}^\infty \exp\left(-2\pi\lambda_{\mathrm{UA}} W'_{\mathrm{N}} \int_0^{d_{\mathrm{UAL}}^{\frac{\alpha_{\mathrm{L}}}{\alpha_{\mathrm{N}}}}} z^2\,\mathrm{d}z \right) \exp\left(-\pi\lambda_{\mathrm{M}}(C_{\mathrm{L1}})^2\right) f_{d_{\mathrm{MA}}}(x) f_{d_{\mathrm{UAL}}}(y)\,\mathrm{d}x\,\mathrm{d}y}_{I} \\ &\underbrace{- \int_0^\infty \int_{C_{\mathrm{L1}}}^\infty \exp\left(-2\pi\lambda_{\mathrm{UA}} W'_{\mathrm{N}} \int_0^{L_1} y^2\,\mathrm{d}y \right) \exp\left(-\pi\lambda_{\mathrm{M}}(C_{\mathrm{L1}})^2\right) f_{d_{\mathrm{MA}}}(x) f_{d_{\mathrm{UAL}}}(y)\,\mathrm{d}x\,\mathrm{d}y}_{II}. \end{aligned} \quad \text{(A.24)}$$

where $C_{\mathrm{L1}} = (\frac{P_{\mathrm{M}}}{P_{\mathrm{UA}}})^{\frac{1}{\alpha_{\mathrm{N}}}} d_{\mathrm{UAL}}^{\frac{\alpha_{\mathrm{L}}}{\alpha_{\mathrm{N}}}}$, $L_1 = (\frac{P_{\mathrm{UA}}}{P_{\mathrm{M}}})^{\frac{1}{\alpha_{\mathrm{N}}}} d_{\mathrm{MA}}^{\frac{\alpha_{\mathrm{N}}}{\alpha_{\mathrm{N}}}}$.

In order to prove that there exists at least one maxima of the association probability with respect to λ_{UA}, let us observe the derivative of the first term of (A.24), represented as A_{P1}:

$$A_{\mathrm{P1}} = \frac{d}{d\lambda_{\mathrm{UA}}} \left[\int_0^\infty \int_{C_{\mathrm{L1}}}^\infty \exp\left(-\frac{2}{3}\pi\lambda_{\mathrm{UA}} W'_{\mathrm{N}} y^{\frac{3\alpha_{\mathrm{L}}}{\alpha_{\mathrm{N}}}} \right) \exp\left(-\pi\lambda_{\mathrm{M}} \left(\frac{P_{\mathrm{M}}}{P_{\mathrm{UA}}} \right)^{\frac{2}{\alpha_{\mathrm{N}}}} y^{\frac{2\alpha_{\mathrm{L}}}{\alpha_{\mathrm{N}}}} \right) \cdot 2\pi\lambda_{\mathrm{M}} x \exp\left(-\pi\lambda_{\mathrm{M}} x^2\right) 2\pi\lambda_{\mathrm{UA}} W'_{\mathrm{L}} y^2 \exp\left(-\frac{2}{3}\pi\lambda_{\mathrm{UA}} W'_{\mathrm{L}} y^3 \right) \mathrm{d}x\,\mathrm{d}y \right] \quad \text{(A.25)}$$

$$A_{\mathrm{P1}} = \frac{d}{d\lambda_{\mathrm{UA}}} \left[\int_0^\infty 2\pi\lambda_{\mathrm{UA}} y^2 W'_{\mathrm{L}} \exp\left(-2\pi\lambda_{\mathrm{M}} \left(\frac{P_{\mathrm{M}}}{P_{\mathrm{UA}}} \right)^{\frac{2}{\alpha_{\mathrm{N}}}} y^{\frac{2\alpha_{\mathrm{L}}}{\alpha_{\mathrm{N}}}} \right) \cdot \exp\left(-\frac{2}{3}\pi\lambda_{\mathrm{UA}} \left(W'_{\mathrm{N}} y^{\frac{3\alpha_{\mathrm{L}}}{\alpha_{\mathrm{N}}}} + W'_{\mathrm{L}} y^3 \right) \right) \mathrm{d}y \right] \quad \text{(A.26)}$$

Applying Leibniz Integral rule in (A.26),

$$A_{\mathrm{P1}} = \int_0^{\infty} \Bigg[-\frac{4}{3}\pi\lambda_{\mathrm{UA}} \left(W'_{\mathrm{N}}\, y^{\frac{3\alpha_{\mathrm{L}}}{\alpha_{\mathrm{N}}}} + W'_{\mathrm{L}}\, y^{3} \right) y^2 W'_{\mathrm{L}} \exp\left(-2\pi\lambda_{\mathrm{M}} \left(\frac{P_{\mathrm{M}}}{P_{\mathrm{UA}}} \right)^{\frac{2}{\alpha_{\mathrm{N}}}} y^{\frac{2\alpha_{\mathrm{L}}}{\alpha_{\mathrm{N}}}} \right) \times \exp\left(-\frac{2}{3}\pi\lambda_{\mathrm{UA}} \left(W'_{\mathrm{N}}\, y^{\frac{3\alpha_{\mathrm{L}}}{\alpha_{\mathrm{N}}}} + W'_{\mathrm{L}}\, y^{3} \right) \right) + 2\pi y^2 W'_{\mathrm{L}} \exp\left(-2\pi\lambda_{\mathrm{M}} \left(\frac{P_{\mathrm{M}}}{P_{\mathrm{UA}}} \right)^{\frac{2}{\alpha_{\mathrm{N}}}} y^{\frac{2\alpha_{\mathrm{L}}}{\alpha_{\mathrm{N}}}} \right) \times \exp\left(-\frac{2}{3}\pi\lambda_{\mathrm{UA}} \left(W'_{\mathrm{N}}\, y^{\frac{3\alpha_{\mathrm{L}}}{\alpha_{\mathrm{N}}}} + W'_{\mathrm{L}}\, y^{3} \right) \right) \Bigg] \mathrm{d}y \tag{A.27}$$

At $\lambda_{\mathrm{UA}} = 0$, (A.27) reduces to $\int_0^{\infty} 2\pi y^2 W'_{\mathrm{L}} \exp\left(-2\pi\lambda_{\mathrm{M}} \left[\left(\frac{P_{\mathrm{M}}}{P_{\mathrm{UA}}} \right)^{\frac{2}{\alpha_{\mathrm{N}}}} y^{\frac{2\alpha_{\mathrm{L}}}{\alpha_{\mathrm{N}}}} \right] \right) \mathrm{d}y$, which yields a positive value upon substitution and integration with respect to y. Similarly, the derivative of term II in (A.24), denoted as A_{P2}, is also positive when $\lambda_{\mathrm{UA}} = 0$. Furthermore, the derivative of $\int_0^{\infty} A''_{\mathrm{UAL}}(d_{\mathrm{UAL}}) f_{d_{\mathrm{UAL}}}(x)\, \mathrm{d}x$ in (A.22) with respect to λ_{UA} is likewise positive at $\lambda_{\mathrm{UA}} = 0$. Conversely, when $\lambda_{\mathrm{UA}} \to \infty$, direct substitution in (A.22) shows that both terms approach zero. Therefore, since $\bar{A}_{\mathrm{UAL}}$ increases with λ_{UA} near $\lambda_{\mathrm{UA}} = 0$ and converges to zero as $\lambda_{\mathrm{UA}} \to \infty$, it follows that there exists at least one optimal value of λ_{UA} that maximizes $\bar{A}_{\mathrm{UAL}}$. This indicates the existence of an optimal UAV density that maximizes the probability of association of a typical user with the LoS UAV-AP.

A.7 Proof of Corollary 1

According to the RSSI-based association scheme, the typical user connects to the LoS UAV-AP tier when either of the following events are true:

1. $R_{\mathrm{UAL}} > R_{\mathrm{UAN}} > R_{\mathrm{MA}}$
2. $R_{\mathrm{UAL}} > R_{\mathrm{MA}} > R_{\mathrm{UAN}}$

The probability of the first event $R_{\mathrm{UAL}} > R_{\mathrm{UAN}} > R_{\mathrm{MA}}$ can be written in terms of the height of the LoS UAV-AP h_{L} is given as:

$$\mathbb{P}\left(P_{\mathrm{UA}} d_{\mathrm{UAL}}^{-\alpha_{\mathrm{L}}} > P_{\mathrm{UA}} d_{\mathrm{UAN}}^{-\alpha_{\mathrm{N}}} > P_{\mathrm{M}} d_{\mathrm{MA}}^{-\alpha_{\mathrm{N}}} \right) = \mathbb{P}\left(P_{\mathrm{UA}} \left(\frac{h_{\mathrm{L}}}{\cos(\theta)} \right)^{-\alpha_{\mathrm{L}}} > P_{\mathrm{UA}} d_{\mathrm{UAN}}^{-\alpha_{\mathrm{N}}} > P_{\mathrm{M}} d_{\mathrm{MA}}^{-\alpha_{\mathrm{N}}} \right). \tag{A.28}$$

Taking expectation over d_{MA} conditioning on θ, the final expression for the first event $R_{\mathrm{UAL}} > R_{\mathrm{UAN}} > R_{\mathrm{MA}}$ can be written as

$$\mathbb{P}(R_{\mathrm{UAL}} > R_{\mathrm{UAN}} > R_{\mathrm{MA}} \,|\, \theta) = \int_{C_{\mathrm{L1}}}^{\infty} \left[\exp\left(-2\pi\lambda_{\mathrm{UA}} W'_{\mathrm{N}} \int_0^{\left(\frac{h_{\mathrm{L}}}{\cos(\theta)}\right)^{\frac{\alpha_{\mathrm{L}}}{\alpha_{\mathrm{N}}}}} z^2 \,\mathrm{d}z \right) - \exp\left(-2\pi\lambda_{\mathrm{UA}} W'_{\mathrm{N}} \int_0^{L_1} y^2 \,\mathrm{d}y \right) \right] \times \exp\left(-\pi\lambda_{\mathrm{M}} (C_{\mathrm{L1}})^2\right) f_{d_{\mathrm{MA}}}(x) \,\mathrm{d}x \quad \text{(A.29)}$$

where $C_{\mathrm{L1}} = \left(\frac{P_{\mathrm{M}}}{P_{\mathrm{UA}}}\right)^{\frac{1}{\alpha_{\mathrm{N}}}} \left(\frac{h_{\mathrm{L}}}{\cos(\theta)}\right)^{\frac{\alpha_{\mathrm{L}}}{\alpha_{\mathrm{N}}}}, L_1 = \left(\frac{P_{\mathrm{UA}}}{P_{\mathrm{M}}}\right)^{\frac{1}{\alpha_{\mathrm{N}}}} x^{\frac{\alpha_{\mathrm{N}}}{\alpha_{\mathrm{N}}}}$.

The second event $R_{\mathrm{UAL}} > R_{\mathrm{MA}} > R_{\mathrm{UAN}}$ by taking an expectation over d_{UAN} conditioning on θ is written as,

$$\mathbb{P}\left(R_{\mathrm{UAL}} > R_{\mathrm{MA}} > R_{\mathrm{UAN}} | \theta\right) = \int_{\left(\frac{h_{\mathrm{L}}}{\cos(\theta)}\right)^{\frac{\alpha_{\mathrm{L}}}{\alpha_{\mathrm{N}}}}}^{\infty} \left[\exp\left(-\pi\lambda_{\mathrm{M}} \left(L_2\right)^2\right) - \exp\left(-\pi\lambda_{\mathrm{M}} \left(L_3\right)^2\right)\right] \exp\left(-2\pi\lambda_{\mathrm{UA}} W'_{\mathrm{N}} \int_0^{\left(\frac{h_{\mathrm{L}}}{\cos(\theta)}\right)^{\frac{\alpha_{\mathrm{L}}}{\alpha_{\mathrm{N}}}}} x^2 \mathrm{d}x \right) f_{d_{\mathrm{UAN}}}(x) \mathrm{d}x, \quad \text{(A.30)}$$

where $L_2 = \left(\frac{P_{\mathrm{M}}}{P_{\mathrm{UA}}}\right)^{\frac{1}{\alpha_{\mathrm{N}}}} \left(\frac{h_{\mathrm{L}}}{\cos(\theta)}\right)^{\frac{\alpha_{\mathrm{L}}}{\alpha_{\mathrm{N}}}}, L_3 = \left(\frac{P_{\mathrm{M}}}{P_{\mathrm{UA}}}\right)^{\frac{1}{\alpha_{\mathrm{N}}}} x^{\frac{\alpha_{\mathrm{N}}}{\alpha_{\mathrm{N}}}}$.

Adding (A.29) and (A.30), we get the probability of LoS UAV-AP association in the access link A_{UAL}, de-conditioned on θ is given by: $\bar{A}_{\mathrm{UAL}}(h_{\mathrm{L}}) = \int_{-\pi/2}^{\pi/2} A_{\mathrm{UAL}}(\rho, h_{\mathrm{L}}) f_\theta(\rho) d(\rho)$, where $f_\theta(\rho) = \frac{1}{\pi}$. So, as we increase the height of LoS UAV-AP h_{L}, the LoS association probability $\bar{A}_{\mathrm{UAL}}(h_{\mathrm{L}})$ decreases. This is because, as h_{L} increases, the received power from the LoS UAV-AP at the typical user decreases. Thus the probability of associating to NLoS UAV-AP and TBS increases.

Further, we can derive the probability of associating to NLoS UAV-AP, $\bar{A}_{\mathrm{UAN}}$, by keeping the distance of LoS UAV-AP from the typical user in terms of h_{L} and θ. Furthermore, we can derive the probability of associating to TBS A_{MA}.

A.8 Proof of Lemma 3.9

Given an access link distance of d_{a}, the UAV-AP associates to a UAV-BS in case the received power from it is larger than the one received from a TBS. This probability is evaluated as:

$$A_{\mathrm{UB}}(d_{\mathrm{a}},\theta)=\mathbb{P}\left(P_{\mathrm{UB}}d_{\mathrm{UB}}^{-\alpha_{\mathrm{L}}}>P_{\mathrm{M}}d_{\mathrm{MB}}^{-\alpha_{\mathrm{L}}}|d_{\mathrm{a}}\right)=\mathbb{P}\left(d_{\mathrm{UB}}\leq\left(\frac{P_{\mathrm{M}}}{P_{\mathrm{UB}}}d_{\mathrm{MB}}^{-\alpha_{\mathrm{L}}}\right)^{-\frac{1}{\alpha_{\mathrm{L}}}}|d_{\mathrm{a}}\right)=\mathbb{E}_{d_{\mathrm{MB}}}\left[\mathcal{T}(d_{\mathrm{MB}})\right], \tag{A.31}$$

where,

$$\mathcal{T}(d_{\mathrm{MB}})=\begin{cases}1-\exp\left(-\frac{4}{3}\pi\lambda_{\mathrm{UB}}\left(\frac{P_{\mathrm{M}}}{P_{\mathrm{UB}}}d_{\mathrm{MB}}^{-\alpha_{\mathrm{L}}}\right)^{-\frac{3}{\alpha_{\mathrm{L}}}}\right); & d_{\mathrm{MB}}\leq\left((d_{\mathrm{a}}\cos(\theta))^{-\alpha_{\mathrm{L}}}\frac{P_{\mathrm{UB}}}{P_{\mathrm{M}}}\right)^{-\frac{1}{\alpha_{\mathrm{L}}}}\\ F''_{d_{\mathrm{UB}}}\left(\left(\frac{P_{\mathrm{M}}}{P_{\mathrm{UB}}}d_{\mathrm{MB}}^{-\alpha_{\mathrm{L}}}\right)^{-\frac{1}{\alpha_{\mathrm{L}}}}\right); & d_{\mathrm{MB}}>\left((d_{\mathrm{a}}\cos(\theta))^{-\alpha_{\mathrm{L}}}\frac{P_{\mathrm{UB}}}{P_{\mathrm{M}}}\right)^{-\frac{1}{\alpha_{\mathrm{L}}}}\end{cases} \tag{A.32}$$

The expectation is taken with respect to $f_{d_{\mathrm{MB}}}$, which is defined only for $x\geq h$ given in (3.16). Considering, $\ell(d_{\mathrm{a}},\theta)=\left((d_{\mathrm{a}}\cos(\theta))^{-\alpha_{\mathrm{L}}}\frac{P_{\mathrm{UB}}}{P_{\mathrm{M}}}\right)^{-\frac{1}{\alpha_{\mathrm{L}}}}$, we note that for $P_{\mathrm{UB}}\leq P_{\mathrm{M}}$, we have $\left(\frac{P_{\mathrm{UB}}}{P_{\mathrm{M}}}\right)^{-\frac{1}{\alpha_{\mathrm{L}}}}\geq 1$ and accordingly, $\left((d_{\mathrm{a}}\cos(\theta))^{-\alpha_{\mathrm{L}}}\frac{P_{\mathrm{UB}}}{P_{\mathrm{M}}}\right)^{-\frac{1}{\alpha_{\mathrm{L}}}}\geq d_{\mathrm{a}}\cos(\theta)$. Accordingly, the expectation with respect to d_{MB} evaluates to:

$$A_{\mathrm{UB}}(d_{\mathrm{a}},\theta)=\int_{d_{\mathrm{a}}\cos(\theta)}^{\ell(d_{\mathrm{a}},\theta)}1-\exp\left(-\frac{4}{3}\pi\lambda_{\mathrm{UB}}\left(\frac{P_{\mathrm{M}}}{P_{\mathrm{UB}}}x^{-\alpha_{\mathrm{L}}}\right)^{-\frac{3}{\alpha_{\mathrm{L}}}}\right)f_{d_{\mathrm{MB}}}(x)\mathrm{dx}+\int_{\ell(d_{\mathrm{a}},\theta)}^{\infty}F''_{d_{\mathrm{UB}}}\left(\left(\frac{P_{\mathrm{M}}}{P_{\mathrm{UB}}}d_{\mathrm{MB}}^{-\alpha_{\mathrm{L}}}\right)^{-\frac{1}{\alpha_{\mathrm{L}}}}\right)f_{d_{\mathrm{MB}}}(x)\mathrm{dx} \tag{A.33}$$

A.9 Proof of Lemma 3.10 and Lemma 3.11

Given that the typical user has associated to TBS, the SINR coverage probability is given as $\mathcal{P}_{\mathrm{CM}}=\mathbb{P}\left[\frac{K_{\mathrm{M}}P_{\mathrm{M}}d_{\mathrm{MA}}^{-\alpha_{\mathrm{N}}}g_{\mathrm{M}}}{N_0+I_{\mathrm{M1}}+I_{\mathrm{L1}}+I_{\mathrm{NL1}}}>s_{\mathrm{a}}\right]$, where I_{M1}, I_{L1} and I_{NL1} are the interference strength from the TBSs, LoS UAV-APs and NLoS UAV-BSs respectively, where $I_{\mathrm{M1}}=\sum_{\mathrm{l}:\mathrm{X_l}\in\Phi'_{\mathrm{M}}}K_{\mathrm{M}}P_{\mathrm{M}}d'^{-\alpha_{\mathrm{N}}}_{\mathrm{M,l}}\bar{g}'_{\mathrm{l}}$, $I_{\mathrm{L1}}=\sum_{\mathrm{l}:\mathrm{X_l}\in\Phi_{\mathrm{L}}}K_{\mathrm{U}}P_{\mathrm{UA}}d_{\mathrm{L,l}}^{-\alpha_{\mathrm{L}}}\bar{G}_{\mathrm{l}}$ and $I_{\mathrm{NL1}}=\sum_{\mathrm{l}:\mathrm{X_l}\in\Phi_{\mathrm{N}}}K_{\mathrm{U}}P_{\mathrm{UA}}d_{\mathrm{N,l}}^{-\alpha_{\mathrm{N}}}\hat{g}_{\mathrm{l}}$. Φ'_{M} is the tier of TBSs in which the associated TBS is omitted. d'_{M} is the distance of user from the TBSs other than the associated TBS. d_{L} is the distance of user from the interfering LoS UAV-APs. d_{N} is the

distance of user from the interfering NLoS UAV-APs. $\bar{g}$, $\bar{G}$ and $\hat{g}$ are the fast-fading coefficients from the interfering TBSs, LoS UAV-APs and NLoS UAV-APs respectively. Taking the expectation over the individually independent TBS, LoS/NLoS UAV-AP tiers of above equation, the interference terms are expressed as,

$$I'_{\mathrm{M1}} = \mathbb{E}_{\Phi'_{\mathrm{M}},\bar{g'}}\left[\exp\left(\frac{-s_{\mathrm{a}}I_{\mathrm{M1}}}{K_{\mathrm{M}}P_{\mathrm{M}}d_{\mathrm{MA}}^{-\alpha_{\mathrm{N}}}}\right)\right] = \mathbb{E}_{\Phi'_{\mathrm{M}}}\left[\prod_{\mathrm{l}:\mathrm{X_l}\in\Phi'_{\mathrm{M}}}\frac{1}{1+\frac{s_{\mathrm{a}}d_{\mathrm{M,l}}'^{-\alpha_{\mathrm{N}}}}{d_{\mathrm{MA}}^{-\alpha_{\mathrm{N}}}}}\right] \tag{A.34}$$

Computing the moment generating function of the exponential random variable $\bar{g}$, (3.36) is obtained.

$$I'_{\mathrm{L1}} = \mathbb{E}_{\Phi'_{\mathrm{L}},\bar{G_{\mathrm{l}}}}\left[\exp\left(\frac{-s_{\mathrm{a}}I_{\mathrm{L1}}}{K_{\mathrm{M}}P_{\mathrm{M}}d_{\mathrm{MA}}^{-\alpha_{\mathrm{N}}}}\right)\right] = \mathbb{E}_{\Phi'_{\mathrm{L}}}\left[\prod_{\mathrm{l}:\mathrm{X_l}\in\Phi'_{\mathrm{L}}}\left(\frac{m}{m+\frac{\eta s_{\mathrm{a}}K_{\mathrm{U}}P_{\mathrm{UA}}d_{\mathrm{L,l}}^{-\alpha_{\mathrm{L}}}}{K_{\mathrm{M}}P_{\mathrm{M}}d_{\mathrm{MA}}^{-\alpha_{\mathrm{N}}}}}\right)^{m}\right] \tag{A.35}$$

where $\eta = m(m!)^{\frac{-1}{m}}$. Noting that $|\bar{G}|^2$ is a normalized gamma random variable with parameter m. Computing the moment generating function of the gamma random variable $\bar{G}$, we can obtain (3.37).

$$I'_{\mathrm{NL1}} = \mathbb{E}_{\Phi'_{\mathrm{N}},\hat{g_{\mathrm{l}}}}\left[\exp\left(\frac{-s_{\mathrm{a}}I_{\mathrm{NL1}}}{K_{\mathrm{M}}P_{\mathrm{M}}d_{\mathrm{MA}}^{-\alpha_{\mathrm{N}}}}\right)\right] = \mathbb{E}_{\Phi'_{\mathrm{N}}}\left[\prod_{\mathrm{l}:\mathrm{X_l}\in\Phi'_{\mathrm{N}}}\frac{1}{1+\frac{s_{\mathrm{a}}K_{\mathrm{U}}P_{\mathrm{UA}}d_{\mathrm{N,l}}^{-\alpha_{\mathrm{N}}}}{K_{\mathrm{M}}P_{\mathrm{M}}d_{\mathrm{MA}}^{-\alpha_{\mathrm{N}}}}}\right] \tag{A.36}$$

Solving these equations and substituting in (3.35), we can obtain $\mathcal{P}_{\mathrm{CM}}$.

Similarly, the SINR coverage probability of a typical user associated with LoS UAV is given as $\mathcal{P}_{\mathrm{CL}} = \mathbb{P}\left[\frac{K_{\mathrm{U}}P_{\mathrm{UA}}d_{\mathrm{UAL}}^{-\alpha_{\mathrm{L}}}G_{\mathrm{L}}}{N_0+I_{\mathrm{M3}}+I_{\mathrm{L3}}+I_{\mathrm{NL3}}}>s_{\mathrm{a}}\right]$, where I_{M3}, I_{L3} and I_{NL3} are the interference strength from the TBSs, LoS UAV-APs and NLoS UAV-BSs respectively, where $I_{\mathrm{M3}} = \sum_{\mathrm{l}:\mathrm{X_l}\in\Phi_{\mathrm{M}}} K_{\mathrm{M}}P_{\mathrm{M}}d_{\mathrm{M,l}}^{-\alpha_{\mathrm{N}}}\bar{g}_{\mathrm{l}}$, $I_{\mathrm{L3}} = \sum_{\mathrm{l}:\mathrm{X_l}\in\Phi'_{\mathrm{L}}} K_{\mathrm{U}}P_{\mathrm{UA}}d_{\mathrm{L,l}}'^{-\alpha_{\mathrm{L}}}\bar{G}'_{\mathrm{l}}$ and $I_{\mathrm{NL3}} = \sum_{\mathrm{l}:\mathrm{X_l}\in\Phi_{\mathrm{N}}} K_{\mathrm{U}}P_{\mathrm{UA}}d_{\mathrm{N,l}}^{-\alpha_{\mathrm{N}}}\hat{g}_{\mathrm{l}}$. Φ'_{L} is the tier of LoS UAV-APs in which the associated LoS UAV-AP is omitted. d'_{L} is the distance of user from the LoS UAV-APs other than the associated LoS UAV-AP. $\bar{G}'$ is the fast-fading coefficient from the interfering LoS UAV-APs other than the associated LoS UAV-AP.

$\mathcal{P}_{\mathrm{CL}}$ can be written as,

$$\mathcal{P}_{\mathrm{CL}} = 1 - \mathbb{E}_{\Phi}\left[\left(1 - \exp\left(\frac{-\eta t_{\mathrm{a}}(N_0 + I_{\mathrm{M3}} + I_{\mathrm{NL3}} + I_{\mathrm{L3}})}{K_{\mathrm{U}} P_{\mathrm{UA}} d_{\mathrm{UAL}}^{-\alpha_{\mathrm{L}}}}\right)\right)^{m}\right] \tag{A.37}$$

where Φ is the union of the individual independent PPP. $\Phi = \Phi_{\mathrm{M}} \cup \Phi'_{\mathrm{L}} \cup \Phi_{\mathrm{N}}$.

The above equation, following the Binomial theorem, can be written as,

$$\mathcal{P}_{\mathrm{CL}} = \sum_{n=1}^{m} (-1)^{n+1} \cdot {}^{m}C_{n} \mathbb{E}_{\Phi}\left[\exp\left(\frac{-n\eta s_{\mathrm{a}}\left(N_0 + I_{\mathrm{M3}} + I_{\mathrm{NL3}} + I_{\mathrm{L3}}\right)}{K_{\mathrm{U}} P_{\mathrm{UA}} d_{\mathrm{UAL}}^{-\alpha_{\mathrm{L}}}}\right)\right] \tag{A.38}$$

Therefore, by applying expectation over the tiers in (A.38), and computing the moment generating function of gamma random variable $\bar{G}$, we can obtain (3.41) as derived before.

Solving these equations and substituting in (3.40), we can obtain P_{CL}. Similarly, we can obtain the SINR coverage probability of typical user associated to NLoS UAV, $\mathcal{P}_{CN}$ given in (3.39).

Appendix B

Proofs of Chapter 4

B.1 Proof of Lemma 4.1

We assume that all the UAV-APs are operating in the same frequency. Therefore, the typical MT experiences interference from all the other UAV-APs in the network, except the one with which it is associated. As we assume the MT moves along the positive x-axis, the location of the MT at time t is denoted as $\mathbf{u}(t) = (vt, 0)$. The total interference power experienced by the MT at time t is given by

$$I(t) = \sum_{j=1}^{\infty} P_{\mathrm{U}} K_{\mathrm{U}} a_j(t)^{-\alpha}, \tag{B.1}$$

where

$$a_j(t) = |x_j - \mathbf{u}(t)|, \quad \forall x_j \in \Phi \backslash x_0, \tag{B.2}$$

where $\mathbf{x}_j$ is the location of the j^{th} interfering UAV-AP, and $a_j(t)$ representing the corresponding distance to the MT. All UAV-APs are assumed to operate with the same transmit power P_{U}.

To find the PDF of total interference power experienced by the MT at time t, we derive the characteristic function, which is given as

$$\psi_I(\omega, t) = \mathbb{E}\left[\exp\left(j\omega I(t)\right)\right]. \tag{B.3}$$

Substituting (B.1) in (B.3),

$$\psi_I(\omega,t) = \mathbb{E}\left[\exp\left(j\omega\sum_{j=1}^{\infty} P_{\mathrm{U}} K_{\mathrm{U}} a_{\mathrm{j}}(t)^{-\alpha}\right)\right] \tag{B.4}$$

$$= \mathbb{E}\left[\prod_{j=1}^{\infty} \exp\left(j\omega P_{\mathrm{U}} K_{\mathrm{U}} a_{\mathrm{j}}(t)^{-\alpha}\right)\right] \tag{B.5}$$

Calculating the PGFL over the PPP ϕ in (B.5), we obtain the characteristic function in (4.4), where

$$g = a_{\mathrm{j}}(t) = |x_{\mathrm{j}} - u(t)| \quad \forall x_{\mathrm{j}} \in \Phi \backslash x_0 \tag{B.6}$$

which is given in (B.2).

Finally, applying the Gil-Pelaez inversion theorem [94], the PDF of total interference power I experienced by the MT at time t is given in (4.3).

B.2 Proof of Lemma 4.2

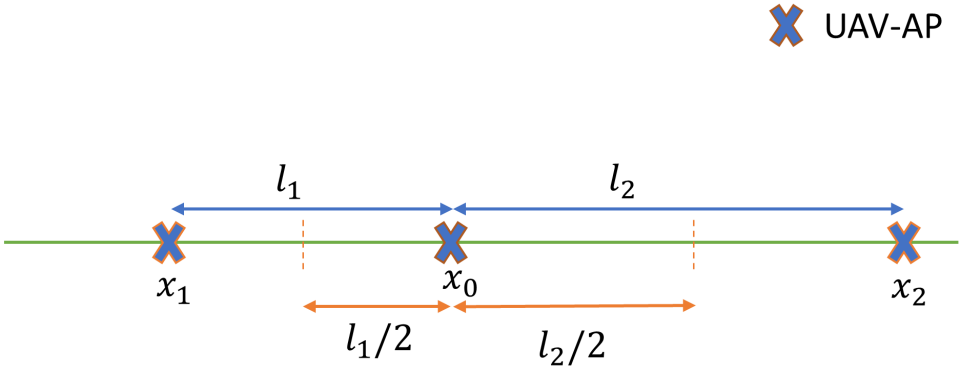

In the above figure, the first UAV-AP located at x_1 is at a distance of l_1 to the left of MT, and the second UAV-AP located at x_2 is at a distance of l_2 to the right of MT. At a given time, the location of the UAV-AP to which the user is associated, i.e., reference UAV-AP, is x_0. At $t = 0$, the MT is at a distance of $l_1/2$ to the left of the reference UAV-AP. At that point, the MT makes a HO from first to reference UAV-AP.

All the UAV-APs are distributed as a 1-D PPP, and we are conditioning on the distances of first and second UAV-AP from the reference UAV-AP at x_0, i.e., l_1 and l_2, where l_1 and l_2 takes random values.

The PDF of l_1, i.e., the distance between two UAV-APs in a 1D PPP, is given as

$$f_{l_1}(r) = \lambda_{\mathrm{U}} \exp(-\lambda r). \tag{B.7}$$

Similarly, the PDF of l_2 is given as,

$$f_{l_2}(r) = \lambda_{\mathrm{U}} \exp(-\lambda r). \tag{B.8}$$

In this regard, the total interference power experienced by the MT at time t is given as

$$M(t, l_1, l_2) = \underbrace{P_{\mathrm{U}} K_{\mathrm{U}} (l_1/2 + vt)^{-\alpha} + P_{\mathrm{U}} K_{\mathrm{U}} (l_2 + l_1/2 - vt)^{-\alpha}}_{I} + \underbrace{\sum_{j=3}^{\infty} P_{\mathrm{U}} K_{\mathrm{U}} a_{\mathrm{j}}(t, l_2, l_2)^{-\alpha}}_{II} \tag{B.9}$$

where a_{j} is the distance of the j^{th} interfering UAV-AP other than x_1 and x_2 from the MT at time t, which is conditioned on l_1 and l_2. I consists of the interference powers from the first and second UAV-APs, represented as

$$L(t, l_1, l_2) = P_{\mathrm{U}} K_{\mathrm{U}} (l_1/2 + vt)^{-\alpha} + P_{\mathrm{U}} K_{\mathrm{U}} (l_2 + l_1/2 - vt)^{-\alpha} \tag{B.10}$$

The total interference power from all the UAV-APs other than the UAV-APs at x_1 and x_2. It is represented as

$$S(t, l_1, l_2) = \sum_{j=3}^{\infty} P_{\mathrm{U}} K_{\mathrm{U}} a_j(t, l_2, l_2)^{-\alpha} \tag{B.11}$$

We evaluate the characteristic function of $S(t, l_1, l_2)$ which is given as

$$C_{\mathrm{S}}(\omega, t, l_1, l_2) = \mathbb{E}\left[\exp\left(j\omega \sum_{j=3}^{\infty} P_{\mathrm{U}} K_{\mathrm{U}} a_{\mathrm{j}}(t, l_1, l_2)^{-\alpha}\right)\right] \tag{B.12}$$

$$C_{\mathrm{S}}(\omega, t, l_1, l_2) = \mathbb{E}\left[\prod_{j=3}^{\infty} \exp\left(j\omega P_{\mathrm{U}} K_{\mathrm{U}} a_{\mathrm{j}}(t, l_1, l_2)^{-\alpha}\right)\right] \tag{B.13}$$

Applying PGFL,

$$C_{\mathrm{S}}(\omega,t,l_1,l_2)=\exp\left(-\frac{\lambda}{\Delta}\int_0^{\infty}1-\exp\left(j\omega P_{\mathrm{U}}K_{\mathrm{U}}(a+l_1/2+vt)^{-\alpha}\right)\mathrm{d}a\right)\cdot \exp\left(-\frac{\lambda}{\Delta}\int_0^{\infty}1-\exp\left(j\omega P_{\mathrm{U}}K_{\mathrm{U}}(a+l_2+l_1/2-vt)^{-\alpha}\right)\mathrm{d}a\right)$$

where t varies from $0\leq t\leq\frac{(l_1+l_2)}{2v}$ From the above equation, we can obtain the characteristic function $C_{\mathrm{S}}(\omega,t,l_1,l_2)$.

Therefore, the PDF of the total interference power from the UAV-APs other than the first and the second UAV-APs is given as

$$f_{\mathrm{S}}(t,l_1,l_2)=\frac{1}{2\pi}\int_0^{\infty}\exp\left(-j\omega b\right)C_{\mathrm{S}}(\omega,t,l_1,l_2)\mathrm{d}\omega \tag{B.14}$$

The average rate experienced by the MT moving from the cell region of first UAV-AP to second UAV-AP, conditioned over l_1 and l_2, is given as

$$R_0(l_1,l_2)=\int_0^{\infty}\frac{2v}{(l_1+l_2)}\int_0^{\frac{(l_1+l_2)}{2v}}B\log_2\left(1+\frac{P_{\mathrm{U}}K_{\mathrm{U}}/(N_0+L(t,l_1,l_2)+b)}{|(\frac{l_1}{2}-vt)^{\alpha}|}\right) f_{\mathrm{S}}(t,l_1,l_2),/\mathrm{d}t,/\mathrm{d}b. \tag{B.15}$$

where $b=S(t,l_1,l_2)$, given in (B.11) i.e., the total interference power experienced by the MT from the UAV-APs, conditioned on l_1 and l_2, at time t. Taking the expectation over l_1 and l_2, by multiplying the PDF given in (B.7), we obtain the average rate for conventional HO scheme in (4.6).

B.3 Proof of Lemma 4.3

From Figure 4.1, we observe that

$$d_{\mathrm{L}}=\begin{cases}D-d_{\mathrm{C}} & d_{\mathrm{C}}<D\\ 0 & d_{\mathrm{C}}=D.\end{cases} \tag{B.16}$$

where D is the distance between the UAV-AP to which the MT is associated, i.e., zeroth UAV-AP and the next associated UAV-AP, i.e., the UAV-AP with which the MT will get to associate after exhausting the cached data by playing at the rate p. The distance traveled by the MT by skipping the HOs until the cached data is exhausted is referred to as d_{C}. Therefore, $d_{\mathrm{C}} \leq D$.

Let N be the number of HOs skipped for a distance of d_{C}, where N can take random values 0,1,..∞ which is Poisson distributed. Then the MT gets associated to $(N+1)^{th}$ UAV-AP, which is at a distance of D from the zeroth UAV-AP. Therefore, D is the distance to the first UAV-AP from the zeroth UAV-AP when no HOs are skipped. Also, D can be the distance to the second UAV-AP from the zeroth UAV-AP when one HO is skipped, and so on. The CCDF of D is the probability that there are less than $(N+1)$ nodes closer than b [95, Th. 1]

$$P_N := \mathbb{P}(\text{At most N nodes within b}) = \sum_{k=0}^{N} \frac{\left(\frac{\lambda_U}{\Delta} 2b\right)^k}{k!} \exp\left(-\frac{\lambda_U}{\Delta} 2b\right). \tag{B.17}$$

where $2b$ is the standard Lesbegue measure or m-dimensional volume of the ball of radius b, where $b > 0$. We assume $m = 1$ since we consider a 1-D PPP. Δ is the frequency reuse factor. Finding the PDF of d_{L},

$$F_{d_{\mathrm{L}}}(z) = \mathbb{P}(d_{\mathrm{L}} \leq z) = \mathbb{P}(D \leq z + d_{\mathrm{C}}). \tag{B.18}$$

In a Poisson point process in $\mathbb{R}^1$ with intensity λ_{U}, the distance d_{L} between a point and its $(N+1)^{\text{th}}$ neighbor is distributed according to the generalized gamma distribution [95, Th. 1]. Therefore, the PDF of d_{L}, $f_{d_{\mathrm{L}}}(z)$= - $\frac{dP_{\mathrm{N}}}{db}$, where P_{N} is given in (B.17)

$$f_{d_{\mathrm{L}}}(z) = \frac{(N+1)}{(z+d_{\mathrm{C}})} \frac{\left(2\frac{\lambda_U}{\Delta}(z+d_{\mathrm{C}})\right)^{N+1}}{(N+1)!} \exp\left(-2\frac{\lambda_U}{\Delta}(z+d_{\mathrm{C}})\right); \quad z \geq 0. \tag{B.19}$$

Conditioning on the interference power considering the effect of d_{C}, the above equation can be represented as (4.16).

B.4 Proof of Lemma 4.4

We know that for a distance of d_{C}, the MT plays at the play rate. Further, for the distance d_{L}, it plays with a rate equal to the download rate, i.e., a lower play rate. The rate experienced by the MT for the proposed scheme is given as

$$R_2(y) = \frac{v}{d_{\mathrm{C}}(y) + d_{\mathrm{L}}(y)} \left[\frac{p d_{\mathrm{C}}(y)}{v} + \int_0^{d_{\mathrm{L}}/v} B \log_2 \left(1 + \frac{P_{\mathrm{U}} K_{\mathrm{U}} / (N_0 + y)}{(d_{\mathrm{L}}(y) - vt)^{\alpha}} \right) f_{\mathrm{I}}(y,t)\, \mathrm{dt} \right]. \quad \text{(B.20)}$$

Here, d_{L} is random. Therefore, taking the expectation over d_{L}, to obtain the average rate experienced by the MT in the network.

$$R_2(y) \approx \int_0^{\infty} \frac{v}{(d_{\mathrm{C}}(y) + Z)} \left[\frac{p d_{\mathrm{C}}(y)}{v} + \int_0^{Z/v} B \log_2 \left(1 + \frac{P_{\mathrm{U}} K_{\mathrm{U}} / (N_0 + y)}{(Z - vt)^{\alpha}} \right) f_{\mathrm{I}}(y,t) \mathrm{dt} \right] f_{d_{\mathrm{L}}}(Z)\, \mathrm{d}Z. \quad \text{(B.21)}$$

where $Z = d_{\mathrm{L}}(y)$, which is a function of interference I.

B.5 Proof of Lemma 4.6

The distance traveled by MT by utilizing the cached data is cache distance d_{C}. From Figure 4.1, we observe after associating to a UAV-AP, all the HOs after that are skipped. Therefore, the distance at which the HOs are skipped is $(d_{\mathrm{C}} - r)$. The number of HOs skipped for a distance of $d_{\mathrm{C}} - r$ is given as $\lambda_U(d_{\mathrm{C}} - r)$. Therefore, the number HOs initiated by the MT for cache-based HO scheme is given in (4.20).

B.6 Proof of Lemma 4.9

It is evident that $\mathbf{0} \in \tau^{\Delta d}$ is equivalent to the event that the distance of $\mathbf{0}$ to the trace $\tau(\mathbf{z}, \mathbf{x}_0)$ is less than Δd. Expanding (4.24), the trace of the cell boundaries can be expressed

as an equation of a line. Therefore, the distance of $\mathbf{0}$ to the trace is

$$d(\mathbf{z}, \mathbf{x}_0) = \frac{|b_0^2 + h_1^2 - h_2^2 - x_0^2 - y_0^2|}{2\sqrt{(b_0 - x_0)^2 + y_0^2}}. \tag{B.22}$$

We define a set of points of the neighboring UAV-BSs, $\mathcal{S}(\Delta d)$, such that $d(\mathbf{z}, \mathbf{x}_0)$ is less than Δd, i.e., $\mathcal{S}(\Delta d) = \left\{ \mathbf{x}_0 \middle| d(\mathbf{b}_0, \mathbf{x}_0) < \Delta d \right\}$. Since the heights of the UAV-BSs are considered as marks of the point process Φ, which are uniformly distributed, we convert (x_0, y_0, h_2) into cylindrical coordinates (r, θ, h_2).

- Finding the ranges of r: For the user at the cell boundary, the 3D distance Z between the user and the UAV-BSs are the same. Therefore, $\sqrt{b_0^2 + h_1^2} = \sqrt{r^2 + h_2^2}$.

  Note that there are no neighboring UAV-BSs located inside $\mathcal{B}(\mathbf{0}, \sqrt{a_0})$, where $a_0 = b_0^2 + h_1^2 - h_2^2$. Hence, $\mathcal{S}(\Delta d)$ represents a ring region with the lower bound of r and is given as $r_l \geq \sqrt{a_0}$. The upper bound of r can be obtained from (4.38), which is $r_u < \sqrt{a_0 + 2\Delta d\sqrt{b_0^2 + r^2 - 2rb_0 \cos\theta}}$.

  We can observe that $\forall (r, \theta, h_2) \in \mathcal{S}(\Delta d)$, $r = \sqrt{a_0} + \mathcal{O}(\Delta d)$. Substituting this in the above equation, $r < \left[a_0 + 2\Delta d\sqrt{2b_0^2 + h_1^2 - h_2^2 - 2b_0 \cos\theta\sqrt{a_0} + \mathcal{O}(\Delta d^2)}\right]^{\frac{1}{2}}$.

- Finding the void probability inside $\mathcal{S}(\Delta d)$: In order to find the probability that $\mathbf{0}$ is in the Δd extended cell boundary, we find the probability that there are no neighboring UAV-BSs inside $\mathcal{S}(\Delta d)$, which is $\mathcal{P}_{void}$, i.e., $\mathbb{P}\left(\mathbf{0} \in \tau^{\Delta d} | R = b_0, H = h_1\right) = 1 - \mathcal{P}_{void}$. As discussed before, the heights of UAV-BSs are uniformly distributed between h_{min} to h_{max}. Calculating void probability,

$$\mathcal{P}_{void} = \exp\left(\frac{-2\lambda_{\mathrm{U}}\Delta d}{(h_{\max} - h_{\min})}\mathcal{F}(b_0, h_1) + \mathcal{O}(\Delta d^2)\right), \tag{B.23}$$

  where $\mathcal{F}(b_0, h_1)$ is given in (4.26). Substituting (B.23), we obtain the probability that the typical user $\mathbf{0}$ is the Δd extended cell boundary, conditioned that the serving UAV-BS is at a location $\mathbf{b}_0$.

  Expanding (B.23) using Taylor series expansion and neglecting the higher orders of Δd, $\mathbb{P}\left(\mathbf{0} \in \tau^{\Delta d} | R = b_0, H = h_1\right) = \frac{2\lambda_{\mathrm{U}}\Delta d}{(h_{max} - h_{min})}\mathcal{F}(b_0, h_1)$. We observe as long as the

typical user is at the cell boundary, b_0 and h_1 are dependent random variables. As h_1 decreases, b_0 increases and vice versa.

B.7 Proof of Lemma 4.11

We know the heights of the UAV-BS are uniformly distributed from $h_{\min}$ to $h_{\max}$. For values of z less than $h_{\max}$, the thinned PPP where the heights of the points are between $h_{\min}$ and z is given as $\lambda_{\mathrm{p}} = \lambda_{\mathrm{U}} \frac{(z-h_{\min})}{(h_{\max}-h_{\min})}$. Therefore, for values of z less than $h_{\max}$ and greater than $h_{\min}$, the CDF is given as

$$F_{\mathrm{Z}}(z) = 1 - \exp\left(-\frac{\lambda_{\mathrm{p}}\pi}{(z-h_{\min})}\int_{h_{\min}}^{z}(z^2-h^2)\mathrm{d}h\right). \tag{B.24}$$

Taking a derivative with respect to z, the PDF is given as

$$f_{\mathrm{Z}}(z) = \frac{2\pi\lambda_{\mathrm{U}}(z^2 - z h_{\min})}{(h_{\max}-h_{\min})}\exp\left(\frac{-\pi\lambda_{\mathrm{U}}\left(\frac{2}{3}z^3 - z^2 h_{\min} + \frac{h_{\min}^3}{3}\right)}{(h_{\max}-h_{\min})}\right); h_{\min} \leq z < h_{\max} \tag{B.25}$$

Similarly, for values of z greater than $h_{\max}$, the thinned PPP is λ_{U} itself. Therefore, the CDF of z, where the values are greater than $h_{\max}$, is obtained by replacing z with $h_{\max}$ in (B.24). Taking the derivative with respect to z, we can obtain the PDF of z as given in (4.28).

B.8 Proof of Lemma 4.12

Given that the typical user is associated with the nearest UAV-BS, the success probability is given as

$$\mathcal{P}_{\mathrm{suc}} = \mathbb{P}\left[\frac{K_{\mathrm{U}}P_{\mathrm{U}}z^{-2}g}{N_0 + I_{\mathrm{U}}} > \gamma\right], \tag{B.26}$$

where I_{U} is the total interference strength from all the interfering UAV-BSs,where $I_{\mathrm{U}} = \sum_{X\in\Phi_{\mathrm{U}}'} K_{\mathrm{U}}P_{\mathrm{U}}g' z'^{-2}$. Φ' is the group of UAV-BSs where the associated BS is omitted. z' is the distance of the user from the UAV-BSs other than the associated BS. g' is the fast-fading coefficients from the interfering BSs. Taking an expectation over point process Φ_{U}' in (B.26) and taking an expectation over h' which is uniformly distributed from $h_{\min}$ to $h_{\max}$ and then

applying the PGFL over the point process, the interference term can be expressed for two ranges of z as in (4.29).

B.9 Proof of Lemma 4.14

As mentioned, the heights of the blockages are Rayleigh distributed with PDF given as

$$f_{\mathrm{H}}(x) = \frac{x}{\sigma^2} \exp\left(-\frac{x^2}{2\sigma^2}\right), \quad x \geq 0. \tag{B.27}$$

Leveraging the property of Rayleigh distribution, the average height of blockages $H_b = 1.253\sigma$. The probability that the 3-D link is blocked is given as

$$\mathbb{P}(h > h_{\mathrm{b}} | y, h_{\mathrm{u}}) = 1 - \int_0^{\frac{y h_{\mathrm{u}}}{R_{\mathrm{b}}}} f_{\mathrm{H}}(h) \mathrm{d}h = \exp\left(-\frac{h_{\mathrm{u}}^2 \left(\frac{y}{R}\right)^2}{2\sigma^2}\right). \tag{B.28}$$

Marginalizing (B.28) with respect y,

$$\mathbb{P}(h > h_{\mathrm{b}} | h_{\mathrm{u}}) = \frac{1}{R_{\mathrm{b}}} \int_0^R \exp\left(-\frac{h_{\mathrm{u}}^2 \left(\frac{t}{R_{\mathrm{b}}}\right)^2}{2\sigma^2}\right) \mathrm{d}t. \tag{B.29}$$

Substituting $\frac{t}{R} = s$, the above equation becomes,

$$\mathbb{P}(h > h_{\mathrm{b}} | h_{\mathrm{u}}) = \int_0^1 \exp\left(-\frac{h_{\mathrm{u}}^2 s^2}{2\sigma^2}\right) \mathrm{d}s. \tag{B.30}$$

Taking an expectation over h_{u}, which is uniformly distributed between $h_{\min}$ and $h_{\max}$, we obtain (4.39).

B.10 Proof of Lemma 4.15

The heights of the UAVs are uniformly distributed from $h_{\min}$ and $h_{\max}$. d_{L} and d_{N} are the 3-D Euclidean distance of the nearest LoS and NLoS UAV-BSs from the typical user,

respectively. The CDF of d_{L} between the typical user and nearest LoS UAV-BS is given as

$$F_{d_{\mathrm{L}}}(z) = \mathbb{P}(d_{\mathrm{L}} \leq z) = 1 - \mathbb{P}(d_{\mathrm{L}} > z) \tag{B.31}$$

There are two cases: (i) $h_{\min} \leq d_{\mathrm{L}} < h_{\max}$ (ii) $d_{\mathrm{L}} \geq h_{\max}$.

For case 1, we consider $h_{\min} \leq d_{\mathrm{L}} < h_{\max}$, hence the heights of the UAV-BS is constrained to $[h_{\min},\ d_{\mathrm{L}}]$. Consequently, we consider exclusively on those UAV-BSs whose heights fall within this specified range, leading to the formulation of a thinned PPP. The intensity of thinned PPP is given as $\lambda_{\mathrm{U}} \frac{d_{\mathrm{L}} - h_{\min}}{h_{\max} - h_{\min}}$, since the heights of UAV-BSs are uniformly distributed from $h_{\min}$ to $h_{\max}$. This models the spatial distribution of UAV-BSs within the specified height constraints.

The 3-D Euclidean distance d_{L} is represented as 2-D distance r_{L} and height h_{L}, where $d_{\mathrm{L}} = \sqrt{r^2 + h^2}$. Given that a UAV-BS is located at a 3-D distance d_{L} and height h, the probability that this UAV-BS is in LoS is denoted by $L_{\mathrm{S}}(d_{\mathrm{L}}, h)$. To determine the total probability of LoS with respect to the 2-D distance r between the user and the UAV-BS, the analysis requires integrating the dimensions of $L_{\mathrm{S}}(\sqrt{r^2 + h^2}, h)$ over the polar coordinates r and θ covering a circular region of radius r. This gives the 2-D area where the probability of a UAV-BS being in LoS is taken into account within the circular region. To account for the variations in h, which is uniformly distributed from $h_{\min}$ to $h_{\max}$, an expectation over h is taken. This provides the effective area within the 3-D space where there is a possibility of the UAV-BS being in LoS from the user. This quantifies the spatial region in which LoS conditions are likely to be met, considering both the 2-D distribution of locations of UAV-BSs and their random heights. Applying the proper limits for r, h and θ, the void probability is given as

$$\mathcal{V}(d_{\mathrm{L}}) \quad = \quad \exp\left(-2\pi\lambda_{\mathrm{U}} \frac{(d_{\mathrm{L}} - h_{\min})}{(h_{\max} - h_{\min})} \int_{h_{\min}}^{d_{\mathrm{L}}} \frac{1}{(d_{\mathrm{L}} - h_{\min})} \int_{0}^{\delta(d_{\mathrm{L}}, h)} L_{\mathrm{S}}(\sqrt{r^2 + h^2}, h) r \mathrm{d}r\ \mathrm{d}h\right) \tag{B.32}$$

where $\delta(d_{\mathrm{L}}, h) = \sqrt{d_{\mathrm{L}}^2 - h^2}$. The inner integral can be represented as

$$\mathcal{L}(d_{\mathrm{L}}, h) = \int_0^{\delta(d_{\mathrm{L}},h)} L_{\mathrm{S}}(\sqrt{r^2+h^2}, h) r \mathrm{d}r. \tag{B.33}$$

Therefore, the CDF $F_{d_{\mathrm{L}}}(z)$ is given as $F_{d_{\mathrm{L}}}(z) = (1 - \mathcal{V}(z))/B_{\mathrm{L}}$. B_{L} is the probability that there is at least one LoS UAV-BS given in (4.47). The derivation follows the same as in [76].

For case 2, where d_{L} is greater than or equal to $h_{\max}$, the heights of UAV-BSs can be anywhere between $h_{\min}$ and $h_{\max}$. Given that the altitudes of the UAVs are uniformly distributed from $h_{\min}$ to $h_{\max}$, $\mathbb{P}(h_{\min} \leq h \leq h_{\max}) = 1$. Consequently, the entire spatial distribution of UAV-BS within the height of $h_{\min}$ to $h_{\max}$ are considered. By calculating the effective area where there is a possibility of being in LoS from the user, considering the 2-D locations and random heights, the CDF $F_{d_{\mathrm{N}}}(z)$ can be represented as

$$F_{d_{\mathrm{N}}}(z) = \left[1 - \exp\left(-2\pi\lambda_{\mathrm{U}} \int_{h_{\min}}^{h_{\max}} \frac{1}{(h_{\max} - h_{\min})} \int_0^{\delta(z,h)} L_{\mathrm{S}}(\sqrt{r^2+h^2}, h) r \, \mathrm{d}r \, \mathrm{d}h\right)\right] / B_{\mathrm{L}} \tag{B.34}$$

Similarly, the distance distribution of nearest NLoS UAV-BS $F_{d_{\mathrm{N}}}(z)$ can be derived. If $R = 0$, then $\eta = 0$, and the inner integral $\int_0^{\delta(z,h)} L_{\mathrm{S}}(\sqrt{r^2+h^2}, h) r \, \mathrm{d}r \, \mathrm{d}h = \frac{(z^2-h^2)}{2}$.

B.11 Proof of Lemma 4.16

The probability of associating to an NLoS UAV-BS can be derived as

$$\mathbb{P}(P_{\mathrm{U}} d_{\mathrm{N}}^{-\alpha_{\mathrm{N}}} > P_{\mathrm{U}} d_{\mathrm{L}}^{-\alpha_{\mathrm{L}}}) = \mathbb{P}(d_{\mathrm{N}} < d_{\mathrm{L}}^{\frac{\alpha_{\mathrm{L}}}{\alpha_{\mathrm{N}}}}) = \mathbb{P}(d_{\mathrm{L}} > d_{\mathrm{N}}^{\frac{\alpha_{\mathrm{N}}}{\alpha_{\mathrm{L}}}}) \tag{B.35}$$

The event in which there is at least one LoS UAV-BS is given as E_1. The event that there are no LoS UAV-BSs is given as E_2. The event that there is atleast one NLoS UAV-BSs is given as E_3. Based on our blockage model, $\mathbb{P}(E_3) = 1$. The probability that the other events occur is given below: (i) $\mathbb{P}(E_1) = B_L$ (ii) $\mathbb{P}(E_2) = (1 - B_{\mathrm{L}})$. B_{L} is given in (4.47).

Therefore, the user getting associated with an NLoS UAV-BS can occur in two possible scenarios:

- The joint probability of having no LoS UAV-BSs and at least one NLoS UAV-BS, and under those conditions, the probability of associating to NLoS UAV-BS is given as $P = \mathbb{P}(E_3)\mathbb{P}(E_2)$.

- The joint probability of having at least one LoS UAV-BS and at least one NLoS UAV-BS, and under those conditions, the probability of associating to NLoS UAV-BS is given as

$$Q = \mathbb{P}(E_3)\mathbb{P}(E_1)\left[\mathbb{P}(d_{\mathrm{L}} > d_{\mathrm{N}}^{\frac{\alpha_{\mathrm{N}}}{\alpha_{\mathrm{L}}}} | E_3, E_1)\right] \tag{B.36}$$

The probability of associating to an NLoS UAV-BS for scenario 1 is given as $A_{\mathrm{N}}^1 = (1 - B_{\mathrm{L}})$. For scenario 2, we apply the CCDF for d_L from (4.44) and take an expectation over d_{N}.

We know the path loss in NLoS links is much higher than that of LoS links. Therefore, $\alpha_{\mathrm{N}} >> \alpha_{\mathrm{L}}$. The distance to the nearest NLoS UAV-BS d_{N} varies from $h_{\min}$ to ∞. Therefore, the values of d_{L} are always greater than $h_{\max}$. Hence, the height of LoS UAV-BS always vary from $h_{\min}$ to $h_{\max}$, since α_{N} is greater than α_{L}. Given that there exists at least one LoS UAV-BS and at least one NLoS UAV-BS, the distance to the LoS UAV-BS, d_{L} is greater than $d_{\mathrm{N}}^{\frac{\alpha_{\mathrm{N}}}{\alpha_{\mathrm{L}}}}$ if and only if there are no LoS UAV-BSs inside the 3-D region $\mathcal{B}$ with radius $\sqrt{d_{\mathrm{N}}^{\frac{2\alpha_{\mathrm{N}}}{\alpha_{\mathrm{L}}}} - h_{\mathrm{a}}^2}$ and height h_{a}.

Therefore, taking the CCDF of d_{L} from (4.44).

$$\mathbb{P}(d_{\mathrm{L}} > d_{\mathrm{N}}^{\frac{\alpha_{\mathrm{N}}}{\alpha_{\mathrm{L}}}} | E_3, E_1) = 1 - F_{d_{\mathrm{L}}}(d_{\mathrm{N}}^{\frac{\alpha_{\mathrm{N}}}{\alpha_{\mathrm{L}}}}) \tag{B.37}$$

$$= 1 - \left(\frac{1 - \exp\left(A \times \int_{h_{\min}}^{h_{\max}} \mathcal{L}(d_{\mathrm{N}}^{\frac{\alpha_{\mathrm{N}}}{\alpha_{\mathrm{L}}}}, h_{\mathrm{a}})\, \mathrm{d}h_{\mathrm{a}}\right)}{B_{\mathrm{L}}}\right) = \frac{\left[\exp\left(A \times \int_{h_{\min}}^{h_{\max}} \mathcal{L}(d_{\mathrm{N}}^{\frac{\alpha_{\mathrm{N}}}{\alpha_{\mathrm{L}}}}, h_{\mathrm{a}})\, \mathrm{d}h_{\mathrm{a}}\right) - (1 - B_{\mathrm{L}})\right]}{B_{\mathrm{L}}} \tag{B.38}$$

where $A = \frac{-2\lambda_{\mathrm{U}}\pi}{(h_{\max} - h_{\min})}$, $\mathcal{L}(z, h)$ is given in (4.46a). Therefore, the probability of associating

to an NLoS UAV-BS for scenario 2 is given as

$$A_{\mathrm{N}}^{2}(d_{\mathrm{N}}) = B_{\mathrm{L}} \frac{\left[\exp\left(A \times \int_{h_{\min}}^{h_{\max}} \mathcal{L}(d_{\mathrm{N}}^{\frac{\alpha_{\mathrm{N}}}{\alpha_{\mathrm{L}}}}, h_{\mathrm{a}})\, \mathrm{d}h_{\mathrm{a}}\right) - (1 - B_{\mathrm{L}})\right]}{B_{\mathrm{L}}} \tag{B.39}$$

Combining both scenarios, the probability of associating with an NLoS UAV-BS is given as

$$A'_{\mathrm{N}}(d_{\mathrm{N}}) = A_{\mathrm{N}}^{1} + A_{\mathrm{N}}^{2}(d_{\mathrm{N}}) \tag{B.40}$$

$$A'_{\mathrm{N}}(d_{\mathrm{N}}) = (1 - B_{\mathrm{L}}) + \exp\left(A \times \int_{h_{\min}}^{h_{\max}} \mathcal{L}(d_{\mathrm{N}}^{\frac{\alpha_{\mathrm{N}}}{\alpha_{\mathrm{L}}}}, h_{\mathrm{a}})\, \mathrm{d}h_{\mathrm{a}}\right) - 1 + B_{\mathrm{L}} \tag{B.41}$$

$$= \exp\left(A \times \int_{h_{\min}}^{h_{\max}} \mathcal{L}(d_{\mathrm{N}}^{\frac{\alpha_{\mathrm{N}}}{\alpha_{\mathrm{L}}}}, h_{\mathrm{a}})\, \mathrm{d}h_{\mathrm{a}}\right) \tag{B.42}$$

Further, taking an expectation over d_{N},

$$A_N = \int_{h_{\min}}^{h_{\max}} \left[\exp\left(A \times \int_{h_{\min}}^{h_{\max}} \mathcal{L}(r_1^{\frac{\alpha_{\mathrm{N}}}{\alpha_{\mathrm{L}}}}, h_{\mathrm{a}})\, \mathrm{d}h_{\mathrm{a}}\right)\right] f'_{d_{\mathrm{N}}}(r_1)\mathrm{d}r_1 + \int_{h_{\max}}^{\infty} \left[\exp\left(A \times \int_{h_{\min}}^{h_{\max}} \mathcal{L}(r_2^{\frac{\alpha_{\mathrm{N}}}{\alpha_{\mathrm{L}}}}, h_{\mathrm{a}})\, \mathrm{d}h_{\mathrm{a}}\right)\right] f''_{d_{\mathrm{N}}}(r_2)\mathrm{d}r_2 \tag{B.43}$$

where

$$f'_{d_{\mathrm{N}}}(r_1) = \frac{\mathrm{d}}{\mathrm{d}r_1} F_{d_{\mathrm{N}}}(r_1); \quad h_{\min} \leq r_1 < h_{\max} \tag{B.44}$$

$$f''_{d_{\mathrm{N}}}(r_2) = \frac{\mathrm{d}}{\mathrm{d}r_2} F_{d_{\mathrm{N}}}(r_2); \quad r_2 \geq h_{\max} \tag{B.45}$$

B.12 Proof of Theorem 1

The conditional success probability of associating to an LoS UAV-BS is given as

$$P_{\mathrm{SL}}(\gamma) = \mathbb{P}(\mathrm{SINR} > \gamma | \Phi_{\mathrm{U}}, \Phi_{\mathrm{b}}) = \mathbb{P}\left(\frac{P_{\mathrm{U}} K_{\mathrm{U}} G_{\mathrm{L}} d_{\mathrm{L}}^{-\alpha_{\mathrm{L}}}}{\sigma_{\mathrm{N}} + I'_{\mathrm{L}} + I_{\mathrm{N}}} > \gamma | \Phi_{\mathrm{U}}, \Phi_{\mathrm{b}}\right) \tag{B.46}$$

where I'_{L} and I_{N} are the interfering strengths from the other LoS and NLoS UAV-BSs respectively, where $I'_{\mathrm{L}} = \sum_{i:\mathbf{x}_i \in \Phi'_{\mathrm{L}}} P_{\mathrm{U}} K_{\mathrm{U}} G'_{\mathrm{L}} d'^{-\alpha_{\mathrm{L}}}_{\mathrm{L}}$ and $I_N = \sum_{i:\mathbf{x}_i \in \Phi_{\mathrm{N}}} P_{\mathrm{U}} K_{\mathrm{U}} g_{\mathrm{N}} d_{\mathrm{N}}^{-\alpha_{\mathrm{N}}}$.

Conditioning on Φ_{U} and Φ_{b}, we apply the CCDF of the gamma random variable G_{L} [16]

and take the expectation over G'_{L} and g_{N}.

$$P'_{\mathrm{SL}}(\gamma) = \sum_{n=1}^{m}(-1)^{n+1}.{}^{m}C_n \left[\exp\left(\frac{-n\varepsilon\gamma\sigma_{\mathrm{N}}}{P_{\mathrm{U}}K_{\mathrm{U}}d_{\mathrm{L}}^{-\alpha_{\mathrm{L}}}}\right)\prod_{i:\mathbf{X}_i\in\Phi_{\mathrm{N}}}\left(\frac{1}{1+\frac{n\varepsilon\gamma d_N^{-\alpha_{\mathrm{N}}}}{d_{\mathrm{L}}^{-\alpha_{\mathrm{L}}}}}\right)\prod_{i:\mathbf{X}_i\in\Phi'_{\mathrm{L}}}\left(\frac{m}{m+\frac{n\varepsilon\gamma d_{\mathrm{L}}'^{-\alpha_{\mathrm{L}}}}{d_{\mathrm{L}}^{-\alpha_{\mathrm{L}}}}}\right)^{m}\right] \tag{B.47}$$

The b^{th} moment can be given as $M_{\mathrm{bL}}{}''(d_{\mathrm{L}}) = \mathbb{E}_{\Phi_{\mathrm{b}},\Phi_{\mathrm{U}}}[(P'_{\mathrm{SL}}(\gamma))^b]$.

The product is taken over the points in the PPP Φ_{U}. Therefore, we first simplify the expression by taking the expectation over Φ_{b} inside the product and then taking the expectation over Φ_{U}. The final expression, which involves expectations over both Φ_{b} and Φ_{U} is given as

$$M''_{\mathrm{bL}}(d_{\mathrm{L}}) = \sum_{n=1}^{m}(-1)^{n+1}\cdot\binom{m}{n}\left[\exp\left(\frac{-n\varepsilon\gamma\sigma_{\mathrm{N}}}{P_{\mathrm{U}}K_{\mathrm{U}}d_{\mathrm{L}}^{-\alpha_{\mathrm{L}}}}\right)\mathbb{E}_{\Phi_{\mathrm{N}}}\left[\prod_{i:\mathbf{X}_i\in\Phi_{\mathrm{N}}}\mathbb{E}_{\Phi_{\mathrm{b}}}\left(\frac{1}{1+\frac{n\varepsilon\gamma\, d_{\mathrm{N}}^{-\alpha_{\mathrm{N}}}}{d_{\mathrm{L}}^{-\alpha_{\mathrm{L}}}}}\right)^{b}\right]\right.$$
$$\left.\times\,\mathbb{E}_{\Phi_{\mathrm{L}}}\left[\prod_{i:\mathbf{X}_i\in\Phi_{\mathrm{L}}}\mathbb{E}_{\Phi_{\mathrm{b}}}\left(\frac{m}{m+\frac{n\varepsilon\gamma\, d_{\mathrm{L}}'^{-\alpha_{\mathrm{L}}}}{d_{\mathrm{L}}^{-\alpha_{\mathrm{L}}}}}\right)^{mb}\right]\right] \tag{B.48}$$

Taking the inner expectation wrt to Φ_{b} for the NLoS case,

$$\mathbb{E}_{\Phi_{\mathrm{b}}}\left(\frac{1}{1+\frac{n\varepsilon\gamma\, d_{\mathrm{N}}^{-\alpha_{\mathrm{N}}}}{d_{\mathrm{L}}^{-\alpha_{\mathrm{L}}}}}\right)^{b} =$$
$$L_{\mathrm{S}}(\sqrt{x^2+t^2},t)\left(\frac{1}{1+\frac{n\varepsilon\gamma(\sqrt{x^2+t^2})^{-\alpha_{\mathrm{L}}}}{z^{-\alpha_{\mathrm{L}}}}}\right)^{b} + N_{\mathrm{S}}(\sqrt{x^2+t^2},t)\left(\frac{1}{1+\frac{n\varepsilon\gamma(\sqrt{x^2+t^2})^{-\alpha_{\mathrm{N}}}}{z^{-\alpha_{\mathrm{L}}}}}\right)^{b}. \tag{B.49}$$

Taking the inner expectation wrt to Φ_{b} for the LoS case,

$$\mathbb{E}_{\Phi_{\mathrm{b}}}\left(\frac{m}{m+\frac{n\varepsilon\gamma\, d_{\mathrm{L}}'^{-\alpha_{\mathrm{L}}}}{d_{\mathrm{L}}^{-\alpha_{\mathrm{L}}}}}\right)^{mb} =$$
$$L_{\mathrm{S}}(\sqrt{x^2+t^2},t)\left(\frac{m}{m+\frac{n\varepsilon\gamma(\sqrt{x^2+t^2})^{-\alpha_{\mathrm{L}}}}{z^{-\alpha_{\mathrm{L}}}}}\right)^{mb} + N_{\mathrm{S}}(\sqrt{x^2+t^2},t)\left(\frac{m}{m+\frac{n\varepsilon\gamma(\sqrt{x^2+t^2})^{-\alpha_{\mathrm{N}}}}{z^{-\alpha_{\mathrm{L}}}}}\right)^{mb}, \tag{B.50}$$

where $L_{\mathrm{S}}(x,y)$ is the probability that the UAV-BS at (x,y) is in LoS and $N_{\mathrm{S}}(x,y)$ is the probability that the UAV-BS at (x,y) is in NLoS. Taking an expectation over the height of the UAV-BSs for two cases of d_{L}.

For $h_{\min} \leq d_{\mathrm{L}} < h_{\max}$,

$$\mathbb{E}_{\Phi_{\mathrm{L}}}\left[\prod_{i:\mathbf{X}_i\in\Phi_{\mathrm{L}}} \mathbb{E}_{\Phi_{\mathrm{b}}}\left(\frac{m}{m+\frac{n\varepsilon\gamma\, {d'_{\mathrm{L}}}^{-\alpha_{\mathrm{L}}}}{d_{\mathrm{L}}^{-\alpha_{\mathrm{L}}}}}\right)^{mb}\right] = \int_{\sqrt{z^2-x^2}}^{h_{\max}} \left[L_S(\sqrt{x^2+t^2},t)\left(\frac{1}{1+\frac{n\varepsilon\gamma(\sqrt{x^2+t^2})^{-\alpha_{\mathrm{L}}}}{z^{-\alpha_{\mathrm{L}}}}}\right)^{b} + N_{\mathrm{S}}(\sqrt{x^2+t^2},t)\left(\frac{1}{1+\frac{n\varepsilon\gamma(\sqrt{x^2+t^2})^{-\alpha_{\mathrm{N}}}}{z^{-\alpha_{\mathrm{L}}}}}\right)^{b}\right] \frac{\mathrm{d}t}{(h_{\max}-\sqrt{z^2-x^2})} \quad \text{(B.51)}$$

For $d_{\mathrm{L}} \geq h_{\max}$,

$$\mathbb{E}_{\Phi_{\mathrm{L}}}\left[\prod_{i:\mathbf{X}_i\in\Phi_{\mathrm{L}}} \mathbb{E}_{\Phi_{\mathrm{b}}}\left(\frac{m}{m+\frac{n\varepsilon\gamma\, {d'_{\mathrm{L}}}^{-\alpha_{\mathrm{L}}}}{d_{\mathrm{L}}^{-\alpha_{\mathrm{L}}}}}\right)^{mb}\right] = \int_{h_{\min}}^{h_{\max}} \left[L_{\mathrm{S}}(\sqrt{x^2+t^2},t)\left(\frac{1}{1+\frac{n\varepsilon\gamma(\sqrt{x^2+t^2})^{-\alpha_{\mathrm{L}}}}{z^{-\alpha_{\mathrm{L}}}}}\right)^{b} + N_{\mathrm{S}}(\sqrt{x^2+t^2},t)\left(\frac{1}{1+\frac{n\varepsilon\gamma(\sqrt{x^2+t^2})^{-\alpha_{\mathrm{N}}}}{z^{-\alpha_{\mathrm{L}}}}}\right)^{b}\right] \frac{\mathrm{d}t}{(h_{\max}-h_{\min})} \quad \text{(B.52)}$$

Similarly, expectation over height is applied to the LoS case as well. Applying PGFL for the 2-D locations of the LoS UAV-BS and NLoS UAV-BSs of the PPP [16], the above equation can be written as (4.52) and (4.53). Taking an expectation over d_{L} and multiplying the probability of associating to LoS UAV-BS A_{L} gives the b^{th} moment of the CSP of associating to LoS UAV-BS as given in (4.51).

Bibliography

[1] Y. S. Chen, A. B. Rahman, and E. E. Tsiropoulou, "Aerial integrated access and backhaul networks," in *ICC 2025 - IEEE International Conference on Communications*, 2025, pp. 6579–6584.

[2] W. Shang, Y. Liao, V. Friderikos, and H. Yanikomeroglu, "Integrated robotic aerial base stations deployment and backhaul design in 6g multihop networks," in *2025 IEEE Wireless Communications and Networking Conference (WCNC)*, 2025, pp. 1–6.

[3] R. Ghasemi Alavicheh, S. M. Razavizadeh, and H. Yanikomeroglu, "Integrated access and backhaul (iab) in low altitude platforms," *IEEE Open Journal of the Communications Society*, vol. 5, pp. 5890–5904, 2024.

[4] N. Ansari, D. Wu, and X. Sun, "FSO as backhaul and energizer for drone-assisted mobile access networks," *ICT Express*, vol. 6, no. 2, pp. 139–144, 2020. DOI: 10.1016/j.icte.2019.12.002.

[5] L. M. P. Larsen, A. Checko, and H. L. Christiansen, "A Survey of the Functional Splits Proposed for 5G Mobile Crosshaul Networks," *IEEE Communications Surveys & Tutorials*, vol. 21, no. 1, pp. 146–172, 2019. DOI: 10.1109/COMST.2018.2868805.

[6] T. Ayass, C. T. Calafate, J.-C. Cano, and P. Manzoni, "Unmanned Aerial Vehicle with Handover Management Fuzzy System for 5G Networks: Challenges and Perspectives," *Intelligence & Robotics*, vol. 2, no. 1, pp. 20–36, 2022. DOI: 10.20517/ir.2021.07.

[7] M. Haenggi, *Stochastic Geometry for Wireless Networks* (Stochastic Geometry for Wireless Networks). Cambridge University Press, 2013, ISBN: 9781107014695. [Online]. Available: https://books.google.co.in/books?id=CLtDhblwWEgC.

[8] 3rd Generation Partnership Project (3GPP), "3GPP TS 22.125 V19.2.0: Uncrewed Aerial System (UAS) support in 3GPP; Stage 1; Release 19," 3rd Generation Partnership Project (3GPP), Technical Specification TS 22.125 V19.2.0, 2024.

[9] 3GPP, "Study on New Radio (NR) to support non-terrestrial networks (Release 15)," 3rd Generation Partnership Project (3GPP), 3GPP Technical Report 38.811, 2019. [Online]. Available: https://www.3gpp.org/DynaReport/38811.htm.

[10] Federal Aviation Administration, *Summary of small unmanned aircraft rule (part 107)*, https://www.faa.gov/uas/commercial_operators/part_107_summary, Accessed: 2025-07-07, 2016.

[11] European Union Aviation Safety Agency (EASA), *Eu drone rules: Overview*, https://www.easa.europa.eu/en/domains/civil-drones-rpas/easa-and-drone-operations, Accessed: 2025-07-07, 2021.

[12] Directorate General of Civil Aviation (India), *Drone rules, 2021*, https://digitalsky.dgca.gov.in/, Accessed: 2025-07-07, 2021.

[13] M. Nafees, J. Thompson, and M. Safari, "Multi-tier variable height uav networks: User coverage and throughput optimization," *IEEE Access*, vol. 9, pp. 119 684–119 699, 2021. DOI: 10.1109/ACCESS.2021.3108419.

[14] M. Ishigami and T. Sugiyama, "A novel drone's height control algorithm for throughput optimization in disaster resilient network," *IEEE Transactions on Vehicular Technology*, vol. 69, no. 12, pp. 16 188–16 190, 2020. DOI: 10.1109/TVT.2020.3032151.

[15] H. Wei and H. Zhang, "Time-varying boundary modeling and handover analysis of UAV-assisted networks with fading," *IEEE Transactions on Wireless Communications*, vol. 23, no. 7, pp. 7552–7565, 2024. DOI: 10.1109/TWC.2023.3342464.

[16] N. R. R, G. Ghatak, A. Srivastava, and V. A. Bohara, "Cache Enabled UAV HetNets: Access - xHaul Coverage Analysis and Optimal Resource Partitioning," *IEEE Transactions on Cognitive Communications and Networking*, vol. 10, no. 1, pp. 292–307, 2024. DOI: 10.1109/TCCN.2023.3322985.

[17] M. Matracia, M. A. Kishk, and M.-S. Alouini, "UAV-aided post-disaster cellular networks: A novel stochastic geometry approach," *IEEE Transactions on Vehicular Technology*, vol. 72, no. 7, pp. 9406–9418, 2023. DOI: 10.1109/TVT.2023.3247920.

[18] Y. Liu, H.-N. Dai, M. Imran, and N. Nasser, "Ground-to-UAV communication network: Stochastic geometry-based performance analysis," in *ICC 2021 - IEEE International Conference on Communications*, 2021, pp. 1–6. DOI: 10.1109/ICC42927.2021.9500746.

[19] M. A. Jasim, H. Shakhatreh, N. Siasi, A. H. Sawalmeh, A. Aldalbahi, and A. Al-Fuqaha, "A survey on spectrum management for unmanned aerial vehicles (UAVs)," *IEEE Access*, vol. 10, pp. 11 443–11 499, 2022. DOI: 10.1109/ACCESS.2021.3138048.

[20] Z. Yao, W. Cheng, W. Zhang, and H. Zhang, "Resource allocation for 5G-UAV-based emergency wireless communications," *IEEE Journal on Selected Areas in Communications*, vol. 39, no. 11, pp. 3395–3410, 2021. DOI: 10.1109/JSAC.2021.3088684.

[21] Y. Zhang, M. A. Kishk, and M.-S. Alouini, "Deployment optimization of tethered drone-assisted integrated access and backhaul networks," *IEEE Transactions on Wireless Communications*, vol. 23, no. 4, pp. 2668–2680, 2024. DOI: 10.1109/TWC.2023.3301880.

[22] Y. Wang and J. Farooq, "Deep-reinforcement-learning-based placement for integrated access backhauling in UAV-assisted wireless networks," *IEEE Internet of Things Journal*, vol. 11, no. 8, pp. 14 727–14 738, 2024. DOI: 10.1109/JIOT.2023.3344519.

[23] Q.-V. Pham, N. Iradukunda, N. H. Tran, W.-J. Hwang, and S.-H. Chung, "Joint placement, power control, and spectrum allocation for UAV wireless backhaul networks," *IEEE Networking Letters*, vol. 3, no. 2, pp. 56–60, 2021. DOI: 10.1109/LNET.2021.3065943.

[24] T. Zhang, Y. Wang, Y. Liu, W. Xu, and A. Nallanathan, "Cache-enabling UAV communications: Network deployment and resource allocation," *IEEE Transactions on Wireless Communications*, vol. 19, no. 11, pp. 7470–7483, 2020. DOI: 10.1109/TWC.2020.3011881.

[25] T. Zhang, Z. Wang, Y. Liu, W. Xu, and A. Nallanathan, "Caching placement and resource allocation for cache-enabling UAV NOMA networks," *IEEE Transactions on Vehicular Technology*, vol. 69, no. 11, pp. 12 897–12 911, 2020. DOI: 10.1109/TVT.2020.3015578.

[26] C. Zhao, Y. Liu, Y. Cai, M. Zhao, and Z. Ding, "Non-orthogonal multiple access for UAV-aided heterogeneous networks: A stochastic geometry model," *IEEE Transactions on Vehicular Technology*, vol. 72, no. 1, pp. 940–956, 2023. DOI: 10.1109/TVT.2022.3211201.

[27] C. Fan, X. Zhou, T. Zhang, W. Yi, and Y. Liu, "Cache-enabled UAV emergency communication networks: Performance analysis with stochastic geometry," *IEEE Transactions on Vehicular Technology*, vol. 72, no. 7, pp. 9308–9321, 2023. DOI: 10.1109/TVT.2023.3249283.

[28] R. Arshad, H. ElSawy, S. Sorour, T. Y. Al-Naffouri, and M.-S. Alouini, "Velocity-aware handover management in two-tier cellular networks," *IEEE Transactions on Wireless Communications*, vol. 16, no. 3, pp. 1851–1867, 2017. DOI: 10.1109/TWC.2017.2655517.

[29] J. Bai, S.-p. Yeh, F. Xue, and S. Talwar, "Route-aware handover enhancement for drones in cellular networks," in *2019 IEEE Global Communications Conference (GLOBECOM)*, 2019, pp. 1–6. DOI: 10.1109/GLOBECOM38437.2019.9013540.

[30] H. Muslih, S. M. A. Kazmi, M. Mazzara, and G. Baye, "Cache sharing in UAV-enabled cellular network: A deep reinforcement learning-based approach," *IEEE Access*, vol. 12, pp. 43 422–43 435, 2024. DOI: 10.1109/ACCESS.2024.3379323.

[31] F. H. Danufane and M. Di Renzo, "Analysis of the delay distribution in cellular networks by using stochastic geometry," *IEEE Open Journal of the Communications Society*, vol. 4, pp. 1728–1744, 2023. DOI: 10.1109/OJCOMS.2023.3294791.

[32] S. Zhou, X. Liu, B. Tang, and G. Tan, "Handover and coverage analysis in 3-D mobile UAV cellular networks," *IEEE Internet of Things Journal*, vol. 11, no. 18, pp. 29 911–29 925, 2024. DOI: 10.1109/JIOT.2024.3407161.

[33] H. Wei and H. Zhang, "Equivalent modeling and analysis of handover process in K-Tier UAV networks," *IEEE Transactions on Wireless Communications*, vol. 22, no. 12, pp. 9658–9671, 2023. DOI: 10.1109/TWC.2023.3272981.

[34] Z. Hajiakhondi-Meybodi, A. Mohammadi, J. Abouei, M. Hou, and K. N. Plataniotis, "Joint transmission scheme and coded content placement in cluster-centric UAV-aided cellular networks," *IEEE Internet of Things Journal*, vol. 9, no. 13, pp. 11 098–11 114, 2022. DOI: 10.1109/JIOT.2021.3127150.

[35] O. Semiari, W. Saad, M. Bennis, and B. Maham, "Caching meets millimeter wave communications for enhanced mobility management in 5G networks," *IEEE Transactions on Wireless Communications*, vol. 17, no. 2, pp. 779–793, 2018. DOI: 10.1109/TWC.2017.2771419.

[36] K. Heo, W. Lee, and K. Lee, "UAV-assisted wireless-powered secure communications: Integration of optimization and deep learning," *IEEE Transactions on Wireless Communications*, vol. 23, no. 9, pp. 10 530–10 545, 2024. DOI: 10.1109/TWC.2024.3372997.

[37] W. Feng, J. Tang, Q. Wu, *et al.*, "Resource allocation for power minimization in RIS-assisted multi-UAV networks with NOMA," *IEEE Transactions on Communications*, vol. 71, no. 11, pp. 6662–6676, 2023. DOI: 10.1109/TCOMM.2023.3298984.

[38] W. Tian, X. Ding, G. Liu, Y. Dai, and Z. Han, "A UAV-assisted secure communication system by jointly optimizing transmit power and trajectory in the internet of things," *IEEE Transactions on Green Communications and Networking*, vol. 7, no. 4, pp. 2025–2037, 2023. DOI: 10.1109/TGCN.2023.3235887.

[39] X. Yan, X. Fang, C. Deng, and X. Wang, "Joint optimization of resource allocation and trajectory control for mobile group users in fixed-wing UAV-enabled wireless network," *IEEE Transactions on Wireless Communications*, vol. 23, no. 2, pp. 1608–1621, 2024. DOI: 10.1109/TWC.2023.3290748.

[40] R. Chen, Y. Sun, L. Liang, and W. Cheng, "Joint power allocation and placement scheme for UAV-assisted IoT with QoS guarantee," *IEEE Transactions on Vehicular Technology*, vol. 71, no. 1, pp. 1066–1071, 2022. DOI: 10.1109/TVT.2021.3129880.

[41] M. Nikooroo, O. Esrafilian, Z. Becvar, and D. Gesbert, "Optimization of placement and resource allocation in UAV-aided multihop wireless networks," *IEEE Internet of Things Journal*, vol. 11, no. 11, pp. 20 051–20 071, 2024. DOI: 10.1109/JIOT.2024.3369174.

[42] J. Zheng, J. Zhang, and B. Ai, "UAV communications with WPT-aided cell-free massive MIMO systems," *IEEE Journal on Selected Areas in Communications*, vol. 39, no. 10, pp. 3114–3128, 2021. DOI: 10.1109/JSAC.2021.3088632.

[43] C. Diaz-Vilor, A. Lozano, and H. Jafarkhani, "Cell-free UAV networks with wireless fronthaul: Analysis and optimization," *IEEE Transactions on Wireless Communications*, vol. 23, no. 3, pp. 2054–2069, 2024. DOI: 10.1109/TWC.2023.3294908.

[44] Ö. T. Demir, M. Masoudi, E. Björnson, and Ç. Cavdar, "Cell-free massive MIMO in O-RAN: Energy-aware joint orchestration of cloud, fronthaul, and radio resources," *IEEE Journal on Selected Areas in Communications*, vol. 42, no. 2, pp. 356–372, 2024. DOI: 10.1109/JSAC.2023.3336187.

[45] C. Pan, J. Yi, C. Yin, J. Yu, and X. Li, "Joint 3D UAV Placement and Resource Allocation in Software-Defined Cellular Networks With Wireless Backhaul," *IEEE Access*, vol. 7, pp. 104 279–104 293, 2019. DOI: 10.1109/ACCESS.2019.2927521.

[46] A. Fouda, A. S. Ibrahim, I. Guvenc, and M. Ghosh, "UAV-Based In-Band Integrated Access and Backhaul for 5G Communications," in *2018 IEEE 88th Vehicular Technology Conference (VTC-Fall)*, 2018, pp. 1–5. DOI: 10.1109/VTCFall.2018.8690860.

[47] M. Afshang and H. S. Dhillon, "Fundamentals of Modeling Finite Wireless Networks Using Binomial Point Process," *IEEE Transactions on Wireless Communications*, vol. 16, no. 5, pp. 3355–3370, 2017. DOI: 10.1109/TWC.2017.2681659.

[48] R. G. Lazar, C. F. Caruntu, and C. Patachia-Sultanoiu, "Simulated and practical approach to assess the reliability of the 5G communications for the Uu interface," in *2022 14th International Conference on Communications (COMM)*, 2022, pp. 1–6. DOI: 10.1109/COMM54429.2022.9817312.

[49] W. Wang, N. Cheng, Y. Liu, H. Zhou, X. Lin, and X. Shen, "Content Delivery Analysis in Cellular Networks With Aerial Caching and mmWAVE Backhaul," *IEEE Transactions on Vehicular Technology*, vol. 70, no. 5, pp. 4809–4822, 2021. DOI: 10.1109/TVT.2021.3074991.

[50] M. Banagar and H. S. Dhillon, "3D Two-Hop Cellular Networks With Wireless Backhauled UAVs: Modeling and Fundamentals," *IEEE Transactions on Wireless Communications*, vol. 21, no. 8, pp. 6417–6433, 2022. DOI: 10.1109/TWC.2022.3149213.

[51] H. Sun, X. Wang, C. Xu, Y. Zhang, and T. Q. Quek, "Performance Analysis for Drone-Assisted HetNets with Flexible Cell Association," in *ICC 2020 - 2020 IEEE International Conference on Communications (ICC)*, 2020, pp. 1–6. DOI: 10.1109/ICC40277.2020.9149035.

[52] 3GPP, "Study on New Radio (NR) to Support Non-Terrestrial Networks," 3rd Generation Partnership Project (3GPP), Technical Report TR 38.811 V15.4.0, 2020.

[53] J. Zhang, H. Xu, L. Xiang, and J. Yang, "On the Application of Directional Antennas in Multi-Tier Unmanned Aerial Vehicle Networks," *IEEE Access*, vol. 7, pp. 132 095–132 110, 2019. DOI: 10.1109/ACCESS.2019.2940338.

[54] N. P. Le, L. C. Tran, X. Huang, *et al.*, "Energy-Harvesting Aided Unmanned Aerial Vehicles for Reliable Ground User Localization and Communications Under Lognormal-Nakagami-m Fading Channels," *IEEE Transactions on Vehicular Technology*, vol. 70, no. 2, pp. 1632–1647, 2021. DOI: 10.1109/TVT.2021.3054987.

[55] I. Atzeni, J. Arnau, and M. Kountouris, "Downlink Cellular Network Analysis With LOS/NLOS Propagation and Elevated Base Stations," *IEEE Transactions on Wireless Communications*, vol. 17, no. 1, pp. 142–156, 2018. DOI: 10.1109/TWC.2017.2763136.

[56] M. Furqan, Z. Ali, Q. Jan, S. Nazir, S. Iqbal, and Y. Huang, "An Efficient Load-Balancing Scheme for UAVs in 5G Infrastructure," *IEEE Systems Journal*, vol. 17, no. 1, pp. 780–791, 2023. DOI: 10.1109/JSYST.2022.3184838.

[57] X. Lin, J. Xia, and Z. Wang, "Probabilistic caching placement in UAV-assisted heterogeneous wireless networks," *Physical Communication*, vol. 33, pp. 54–61, 2019, ISSN: 1874-4907. DOI: https://doi.org/10.1016/j.phycom.2019.01.004. [Online]. Available: https://www.sciencedirect.com/science/article/pii/S1874490718304476.

[58] W. Yi, Y. Liu, and A. Nallanathan, "Modeling and Analysis of D2D Millimeter-Wave Networks With Poisson Cluster Processes," *IEEE Transactions on Communications*, vol. 65, no. 12, pp. 5574–5588, 2017. DOI: 10.1109/TCOMM.2017.2744644.

[59] M. Salehi and E. Hossain, "Stochastic Geometry Analysis of Sojourn Time in Multi-Tier Cellular Networks," *IEEE Transactions on Wireless Communications*, vol. 20, no. 3, pp. 1816–1830, 2021. DOI: 10.1109/TWC.2020.3036894.

[60] T. D. Novlan, R. K. Ganti, A. Ghosh, and J. G. Andrews, "Analytical Evaluation of Fractional Frequency Reuse for OFDMA Cellular Networks," *IEEE Transactions on Wireless Communications*, vol. 10, no. 12, pp. 4294–4305, 2011. DOI: 10.1109/TWC.2011.100611.110181.

[61] R. Arshad, L. Lampe, H. ElSawy, and M. J. Hossain, "Integrating UAVs into Existing Wireless Networks: A Stochastic Geometry Approach," in *2018 IEEE Globecom Workshops (GC Wkshps)*, 2018, pp. 1–6. DOI: 10.1109/GLOCOMW.2018.8644504.

[62] 3GPP, "Nr; user equipment (ue) radio transmission and reception; part 1: Range 1 standalone," *3rd Generation Partnership Project (3GPP), TS 38.101-1*, 2020.

[63] 3GPP, "Nr; user equipment (UE) radio transmission and reception; part 2: Range 2 standalone," *3rd Generation Partnership Project (3GPP), TS 38.101-2*, 2020.

[64] S. S. Kalamkar, F. Baccelli, F. M. Abinader, A. S. M. Fani, and L. G. U. Garcia, "Beam management in 5g: A stochastic geometry analysis," *IEEE Transactions on Wireless Communications*, vol. 21, no. 4, pp. 2275–2290, 2022. DOI: 10.1109/TWC.2021.3110785.

[65] Y. S. Soh, T. Q. S. Quek, M. Kountouris, and H. Shin, "Energy Efficient Heterogeneous Cellular Networks," *IEEE Journal on Selected Areas in Communications*, vol. 31, no. 5, pp. 840–850, 2013. DOI: 10.1109/JSAC.2013.130503.

[66] N. Choi, K. Guan, D. C. Kilper, and G. Atkinson, "In-network caching effect on optimal energy consumption in content-centric networking," in *2012 IEEE International Conference on Communications (ICC)*, 2012, pp. 2889–2894. DOI: 10.1109/ICC.2012.6364320.

[67] D. Perino and M. Varvello, "A reality check for content-centric networking," in *Proceedings of the ACM SIGCOMM Workshop on Information-Centric Networking*, ser. ICN '11, Toronto, Ontario, Canada: Association for Computing Machinery, 2011, 44–49, ISBN: 9781450308014. DOI: 10.1145/2018584.2018596. [Online]. Available: https://doi.org/10.1145/2018584.2018596.

[68] A. Prasad, O. Tirkkonen, P. Lundén, O. N. Yilmaz, L. Dalsgaard, and C. Wijting, "Energy-efficient inter-frequency small cell discovery techniques for LTE-advanced heterogeneous network deployments," *IEEE Communications Magazine*, vol. 51, no. 5, pp. 72–81, 2013. DOI: 10.1109/MCOM.2013.6515049.

[69] S. Chiu, D. Stoyan, W. Kendall, and J. Mecke, *Stochastic Geometry and Its Applications* (Wiley Series in Probability and Statistics). Wiley, 2013, ISBN: 9781118658253. [Online]. Available: https://books.google.co.in/books?id=825NfM6Nc-EC.

[70] W. Bao and B. Liang, "Stochastic Geometric Analysis of User Mobility in Heterogeneous Wireless Networks," *IEEE Journal on Selected Areas in Communications*, vol. 33, no. 10, pp. 2212–2225, 2015. DOI: 10.1109/JSAC.2015.2435451.

[71] N. R.R., G. Ghatak, V. A. Bohara, and A. Srivastava, "Performance Analysis of Cache-Enabled Handover Management for Vehicular Networks," *IEEE Transactions on Network Science and Engineering*, vol. 11, no. 1, pp. 1151–1164, 2024. DOI: 10.1109/TNSE.2023.3321296.

[72] P. Ji, X. Jia, Y. Lu, H. Hu, and Y. Ouyang, "Multi-UAV Assisted Multi-Tier Millimeter-Wave Cellular Networks for Hotspots With 2-Tier and 4-Tier Network Association," *IEEE Access*, vol. 8, pp. 158 972–158 995, 2020. DOI: 10.1109/ACCESS.2020.3019320.

[73] T. Bai, R. Vaze, and R. W. Heath, "Analysis of Blockage Effects on Urban Cellular Networks," *IEEE Transactions on Wireless Communications*, vol. 13, no. 9, pp. 5070–5083, 2014. DOI: 10.1109/TWC.2014.2331971.

[74] W. Tang, H. Zhang, and Y. He, "Performance Analysis of Power Control in Urban UAV Networks With 3D Blockage Effects," *IEEE Transactions on Vehicular Technology*, vol. 71, no. 1, pp. 626–638, 2022. DOI: 10.1109/TVT.2021.3130192.

[75] N. P. Le, L. C. Tran, X. Huang, *et al.*, "Energy-Harvesting Aided Unmanned Aerial Vehicles for Reliable Ground User Localization and Communications Under Lognormal-Nakagami-m Fading Channels," *IEEE Transactions on Vehicular Technology*, vol. 70, no. 2, pp. 1632–1647, 2021. DOI: 10.1109/TVT.2021.3054987.

[76] S. M. Azimi-Abarghouyi, B. Makki, M. Nasiri-Kenari, and T. Svensson, "Stochastic geometry modeling and analysis of finite millimeter wave wireless networks," *IEEE Transactions on Vehicular Technology*, vol. 68, no. 2, pp. 1378–1393, 2019. DOI: 10.1109/TVT.2018.2883891.

[77] M. Di Renzo and P. Guan, "Stochastic Geometry Modeling of Coverage and Rate of Cellular Networks Using the Gil-Pelaez Inversion Theorem," *IEEE Communications Letters*, vol. 18, no. 9, pp. 1575–1578, 2014. DOI: 10.1109/LCOMM.2014.2341251.

[78] M. Shi, K. Yang, D. Niyato, H. Yuan, H. Zhou, and Z. Xu, "The Meta Distribution of SINR in UAV-Assisted Cellular Networks," *IEEE Transactions on Communications*, vol. 71, no. 2, pp. 1193–1206, 2023. DOI: 10.1109/TCOMM.2022.3233064.

[79] E. Kalantari, M. Z. Shakir, H. Yanikomeroglu, and A. Yongacoglu, "Backhaul-aware robust 3D drone placement in 5G+ wireless networks," in *2017 IEEE International Conference on Communications Workshops (ICC Workshops)*, 2017, pp. 109–114. DOI: 10.1109/ICCW.2017.7962642.

[80] Ö. T. Demir, E. Björnson, and L. Sanguinetti, "Foundations of User-Centric Cell-Free Massive MIMO," *Foundations and Trends® in Signal Processing*, vol. 14, no. 3-4, pp. 162–472, 2021, ISSN: 1932-8346. DOI: 10.1561/2000000109. [Online]. Available: http://dx.doi.org/10.1561/2000000109.

[81] E. Björnson and Ö. T. Demir, "Introduction to multiple antenna communications and reconfigurable surfaces," *Boston-Delft: now publishers*, 2024. DOI: 10.1561/9781638283157.

[82] Ö. T. Demir and E. Björnson, "Max-Min Fair Wireless-Powered Cell-Free Massive MIMO for Uncorrelated Rician Fading Channels," in *2020 IEEE Wireless Communications and Networking Conference (WCNC)*, 2020, pp. 1–6. DOI: 10.1109/WCNC45663.2020.9120654.

[83] L. Sanguinetti, E. Björnson, and J. Hoydis, "Toward Massive MIMO 2.0: Understanding Spatial Correlation, Interference Suppression, and Pilot Contamination," *IEEE Transactions on Communications*, vol. 68, no. 1, pp. 232–257, 2020. DOI: 10.1109/TCOMM.2019.2945792.

[84] G. M. Zilli and W.-P. Zhu, "Constrained Tensor Decomposition-Based Hybrid Beamforming for Mmwave Massive MIMO-OFDM Communication Systems," *IEEE Transactions on Vehicular Technology*, vol. 70, no. 6, pp. 5775–5788, 2021. DOI: 10.1109/TVT.2021.3076691.

[85] Ö. T. Demir, M. Masoudi, E. Björnson, and C. Cavdar, "Cell-Free Massive MIMO in O-RAN: Energy-Aware Joint Orchestration of Cloud, Fronthaul, and Radio Resources," *IEEE Journal on Selected Areas in Communications*, vol. 42, no. 2, pp. 356–372, 2024. DOI: 10.1109/JSAC.2023.3336187.

[86] M. D. Nguyen, L. B. Le, and A. Girard, "Uav placement and resource allocation for intelligent reflecting surface assisted uav-based wireless networks," *IEEE Communications Letters*, vol. 26, no. 5, pp. 1106–1110, 2022. DOI: 10.1109/LCOMM.2022.3149467.

[87] N. Gkatzios, M. Anastasopoulos, A. Tzanakaki, and D. Simeonidou, "Dynamic softwarised ran function placement in optical data centre networks," in *Optical Network Design and Modeling*, A. Tzanakaki, M. Varvarigos, R. Muñoz, *et al.*, Eds., Cham: Springer International Publishing, 2020, pp. 108–117, ISBN: 978-3-030-38085-4.

[88] S. Malkowsky, J. Vieira, L. Liu, *et al.*, "The world's first real-time testbed for massive mimo: Design, implementation, and validation," *IEEE Access*, vol. 5, pp. 9073–9088, 2017. DOI: 10.1109/ACCESS.2017.2705561.

[89] G. Auer, V. Giannini, C. Desset, *et al.*, "How much energy is needed to run a wireless network?" *IEEE Wireless Communications*, vol. 18, no. 5, pp. 40–49, 2011. DOI: 10.1109/MWC.2011.6056691.

[90] A. Al-Hourani, S. Kandeepan, and S. Lardner, "Optimal LAP Altitude for Maximum Coverage," *IEEE Wireless Communications Letters*, vol. 3, no. 6, pp. 569–572, 2014. DOI: 10.1109/LWC.2014.2342736.

[91] Y. Zeng, J. Xu, and R. Zhang, "Energy Minimization for Wireless Communication With Rotary-Wing UAV," *IEEE Transactions on Wireless Communications*, vol. 18, no. 4, pp. 2329–2345, 2019. DOI: 10.1109/TWC.2019.2902559.

[92] S. S. Sri Ganesh Seeram, S. Zhang, M. Ozger, A. Grabs, J. Holis, and C. Cavdar, "Aerial Base Stations: Practical Considerations for Power Consumption and Service Time," in *GLOBECOM 2023 - 2023 IEEE Global Communications Conference*, 2023, pp. 5049–5054. DOI: 10.1109/GLOBECOM54140.2023.10437128.

[93] A. Mathai, *An Introduction to Geometrical Probability: Distributional Aspects with Applications* (Statistical distributions and models with applications). Taylor & Francis, 1999, ISBN: 9789056996819. [Online]. Available: https://books.google.co.in/books?id=FV6XncZgfcwC.

[94] M. Di Renzo and P. Guan, "Stochastic Geometry Modeling of Coverage and Rate of Cellular Networks Using the Gil-Pelaez Inversion Theorem," *IEEE Communications Letters*, vol. 18, no. 9, pp. 1575–1578, 2014. DOI: 10.1109/LCOMM.2014.2341251.

[95] M. Haenggi, "On distances in uniformly random networks," *IEEE Transactions on Information Theory*, vol. 51, no. 10, pp. 3584–3586, 2005. DOI: 10.1109/TIT.2005.855610.